October 2018

IEA Wind TCP Task 27

Compendium of IEA Wind TCP Task 27 Case Studies

iea wind

Technical Report

Compendium of IEA Wind TCP Task 27 Case Studies

Prepared for the
International Energy Agency Wind Implementing Agreement

Prepared by

Ignacio Cruz Cruz, CIEMAT, Spain
Trudy Forsyth, WAT, United States

October 2018

[Disclaimer text:]
IEA Wind TCP functions within a framework created by the International Energy Agency (IEA). Views, findings, and publications of IEA Wind do not necessarily represent the views or policies of the IEA Secretariat or of all its individual member countries. IEA Wind is part of IEA's Technology Collaboration Programme (TCP).

Compendium of IEA Wind TCP Task 27 Case Studies

October 2018

Contributions from:

Australia

Austria

Belgium

China

Denmark

Ireland

Japan

Poland

Republic of Korea

Spain

Sweden

United States

TABLE OF CONTENTS

INTRODUCTION 7

SCOPE AND FIELD OF APPLICATION 7

1.1 AUSTRALIA (active 2009 – 2014) 8

1.1.1 CFD models on wind flow results - Bunnings warehouse, Port Kennedy Perth, Australia 8

1.1.1.1 Relevant publication 8

1.1.1.2 Overview 8

1.1.1.3 Software used 9

1.1.1.4 Flow type 9

1.1.1.5 Governing equations 9

1.1.1.6 Turbulence model 10

1.1.1.7 Discretization 10

1.1.1.8 Velocity pressure coupling 10

1.1.1.9 Computational grid 10

1.1.1.10 Boundary Conditions for velocity and pressure 11

1.1.1.11 Reynolds number, time step and statistics 12

1.1.1.12 Inflow boundary condition assumptions 12

1.1.1.13 Conclusions 12

1.1.2 Rooftop turbine tests – Bunnings Warehouse, Port Kennedy Perth 16

1.1.2.1 Relevant Publications: 16

1.1.2.2 Overview 17

1.1.2.3 SWT Site Characterization 17

1.1.2.4 Data Acquisition Approach 19

1.1.2.5 Other instruments used: temperature, pressure, wind direction, humidity 19

1.1.2.6 Sampling rate 19

1.1.2.7 Data processing strategy, quality assurance methods 20

1.1.2.8 Conclusion of results 20

1.1.2.9 Wind Rose 21

1.1.2.10 Wind speed frequency distribution 21

1.1.2.11 Turbulent Kinetic Energy (TKE) and Turbulent Intensity (TI) 22

1.1.2.12 Power spectral density and corrected Kaimal Model 24

1.1.2.13 Conclusions 27

1.2 AUSTRIA (active 2015 – 2018) 29

1.2.1 Lichtenegg vibration measurements of a VAWT (Amperius) with and without oscilation decoupling element 29

1.2.1.1 SWT site characterization 29

1.2.1.2 Diagram and describe the surrounding obstacles with distances noted 29

1.2.1.3 Wind measurement description 30

1.2.1.4 Data acquisition approach 31

1.2.1.5 Duration and results of data collection efforts - highlight any maintenance or downtime issues 32

1.2.1.6 Data processing strategy 32

1.2.1.7 Conclusion of results 33

1.2.1.8 Summary of your findings and conclusions 35

1.2.1.9 References 35
1.3 BELGIUM (active 2017 – 2018) 36
1.4 CHINA (active 2009 – 2018) 36
1.4.1 *Validated CFD Models for Danish Fence Experiment Objects* 36
1.4.1.1 Project description 36
1.4.1.2 Software used 36
1.4.1.3 Compute Field 36
1.4.1.4 Fluid type 36
1.4.1.5 Governing equations 36
1.4.1.6 Turbulence model 36
1.4.1.7 Discretization methods 36
1.4.1.8 Computational grid 37
1.4.1.9 Boundary Conditions for velocity and pressure 37
1.4.1.10 Inflow boundary condition assumptions 37
1.4.1.11 CFD analysis results 38
1.4.2 CFD Case Study for Different Roof Types (Flat and Triangle) 42
1.4.2.1 Engineering and Technology Building on the IMUT campus project description 42
1.4.2.2 Numerical Model 42
1.4.2.3 Software used 42
1.4.2.4 Compute Field 42
1.4.2.5 Fluid type 42
1.4.2.6 Governing equations 43
1.4.2.7 Turbulence model 43
1.4.2.8 Discretization methods 43
1.4.2.9 Computational grid 43
1.4.2.10 Boundary Conditions for velocity and pressure 43
1.4.2.11 Inflow boundary condition assumptions 43
1.4.2.12 CFD analysis results 44
1.4.2.13 Findings 45
1.4.3 CFD Case Study a Storage Container in Zhang-bei 45
1.4.3.1 Project description 45
1.4.3.2 Numerical Model 45
1.4.3.3 Software used 45
1.4.3.4 Compute Field 45
1.4.3.5 Fluid type 45
1.4.3.6 Governing equations 46
1.4.3.7 Turbulence model 46
1.4.3.8 Discretization methods 46
1.4.3.9 Computational grid 46
1.4.3.10 Boundary Conditions for velocity and pressure 46
1.4.3.11 Inflow boundary condition assumptions 46
1.4.3.12 CFD analysis results 47
1.4.3.13 Findings 47
1.4.4 CFD Case Study for the U.S. Johnson Space Center/NASA Rooftop Test Facility 47

1.4.4.1 Project description 47
1.4.4.2 Numerical model 48
1.4.4.3 Computation Zone 48
1.4.4.4 Computation grid 49
1.4.4.5 Governing equations 49
1.4.4.6 Turbulence model 49
1.4.4.7 Time Integration 49
1.4.4.8 Boundary Condition 49
1.4.4.9 CFD analysis results 50
1.4.5 CFD Results for Flat Roof Building Cluster with Different Plan Densities 51
1.4.5.1 Project description 51
1.4.5.2 Software used 51
1.4.5.3 Compute field 51
1.4.5.4 Fluid type 51
1.4.5.5 Governing equations 52
1.4.5.6 Turbulence model 52
1.4.5.7 Discretization methods 52
1.4.5.8 Computational grid 52
1.4.5.9 Boundary conditions for velocity and pressure 52
1.4.5.10 Inflow boundary condition assumptions 52
1.4.5.11 CFD analysis results 52
1.5 DENMARK (active 2009 – 2016) 59
1.5.1 Fence experiment test and measurements 59
1.5.1.1 SWT site characterization 59
1.5.1.2 Diagram and describe the surrounding obstacles with distances noted 60
1.5.1.3 Off-site/reference wind measurement description 60
1.5.1.4 Data acquisition approach 60
1.5.1.5 Measurement location 61
1.5.1.6 Duration and results of data collection efforts - highlight any maintenance or downtime issues 61
1.5.1.7 Data processing strategy, quality assurance methods 61
1.5.1.8 Conclusion of results 63
1.5.1.9 Summary of your findings and conclusions 64
1.5.1.10 References 64
1.6 IRELAND (active 2009 – 2018) 64
1.6.1 Case Study 1 – Post installation operation assessment of 6 small wind turbines at consumer sites in Ireland 64
1.6.1.1 1.0 Introduction 64
1.6.1.2 Wind turbine systems and monitoring equipment 65
1.6.1.3 Monitoring equipment and data parameter measurements 65
1.6.1.4 Data quality checks 66
1.6.1.5 Conclusions 66
1.6.1.6 Some considerations when deciding to install a small wind turbine 67
1.6.1.7 Comparison of two Proven 6 wind turbines at different sites 68
1.6.1.8 Site A – Location 68
1.6.1.9 System description 69

1.6.1.10 Site A - Performance 70
1.6.1.11 Site B – Location 74
1.6.1.12 System description 75
1.6.1.13 Comparison of two Evance R9000 wind turbines at different sites..... 82
1.6.1.14 Comparison of two Skystream wind turbines at different sites 96
1.6.2 DKiT WW Comparison V52 measurements and energy production 109
1.6.2.1 Introduction 109
1.6.2.2 Measurement Sites 110
1.6.2.3 Data quality checks..... 110
1.6.2.4 Case Studies 110
1.6.2.5 Site M2..... 114
1.6.2.6 Key learning from case study 1 117
1.6.3 Case Study 2-Rural at low elevation..... 117
1.6.3.2 Key learning from case study 2 121
1.6.4 Case study 3 - DkIT Site – Peri-urban area 122
1.6.4.1 Results from Turbine data analysis 124
1.6.4.2 DkIT 10m mast measurements 126
1.6.4.3 Key learnings from case study 3..... 128
1.6.4.4 Summary conclusions 128
1.7 JAPAN (active 2009 – 2018) 129
1.7.1 CFD findings – rectangular building 129
1.7.2 Nasu Denki Tekko Rooftop Test Site 131
1.7.2.1 Measurement strategy: 131
1.7.2.2 1.1.3.2 Site photographs and layout drawings 132
1.7.2.3 Wind conditions: 133
1.7.2.4 Summary Turbulence Intensity Test Results Compared to NTM..... 134
1.7.2.5 EDC Results 135
1.7.2.6 Wind conditions (Compared with ultrasonic and 3-cup) 137
1.7.2.7 Characterize turbine and its power production 138
1.7.2.8 Field test site 139
1.7.2.9 Results..... 139
1.7.3 Ashikaga Institute of Technology Rooftop Test Site 141
1.7.3.1 Wind Resource Measurement Results 141
1.7.3.2 Characterize turbine and its power production 149
1.7.4 CFD model of V52 on campus of Dundalk Institute of Technology 162
1.7.4.1 Introduction 162
1.7.4.2 Computational Approach..... 163
1.7.4.3 Results and Discussions 164
1.7.4.4 Summary 165
1.7.5 Simplified Load Methodology for VAWTs 165
1.7.5.1 Main Features 166
1.8 POLAND 167
1.9 REPUBLIC OF KOREA (active 2009 – 2018) 2
1.9.1 Wind Profile Measurements on KIER Rooftop 2
1.9.1.1 Introduction 2
1.9.1.2 Measurement Site Characteristics 3

1.9.1.3 Measurement Setup 3
1.9.1.4 Measurement Results 4
1.10 SPAIN (active 2009 – present) 7
1.10.1 CFD model on Windflow results 7
1.10.1.1 Software used 7
1.10.1.2 Flow type 7
1.10.1.3 Governing Equations 7
1.10.1.4 Turbulence models 8
1.10.1.5 Spatial discretization of differential operators 8
1.10.1.6 Linear system solvers 8
1.10.1.7 Computational grid 8
1.10.1.8 Boundary conditions 8
1.10.1.9 Time dependent turbulent inflow data assumptions 8
1.10.1.10 Reynolds number 9
1.10.1.11 Conclusions 9
1.10.2 CEDER rooftop test site wind measurement and analysis results 10
1.11 SWEDEN (active 2009-2011) 20
1.11.1 Forest data 20
1.12 UNITED STATES (active 2009 – 2018) 22
1.12.1 Wind Resource Measurement Results – NASA Building 12 22
1.12.1.1 Overview 22
1.12.1.2 Project Work Packages: 23
1.12.1.3 SWT Site Characterization 24
1.12.1.4 Photos (360) 26
1.12.1.5 Wind Roses 27
1.12.1.6 Energy Roses 28
1.12.1.7 Wind speed frequency distribution 29
1.12.1.8 Off-site/reference wind measurement description 30
1.12.1.9 Data Acquisition Approach 32
1.12.1.10 Instrumentation 36
1.12.1.11 Dataloggers: 36
1.12.1.12 Duration and results of data collection efforts 37
1.12.1.13 Data processing strategy, quality assurance methods 39
1.12.1.14 Conclusion of results 39
1.12.1.15 Wind resource characterization 42
1.12.1.16 Summary of your findings 43
1.12.1.17 Conclusions 44
1.12.2 Deployment of Wind Turbines in Built Environment: Risks, Lessons, and Recommended Practices 44
Appendix A: Belgian Case Study 46

INTRODUCTION

There are a number of research questions the Task 27 group is hoping to shed light on:

- What are the range of I values that a SWT is likely to experience in the urban environment?
- How do the 3-D effects of turbulence impact design parameters including the normal turbulence model (NTM) and the load cases in IEC61400-2?
- How to capture effects of thermal instability on tools and models that typically assume thermal stability? The use of Richardson number for loads cases and other standard parameters.
- Why capturing preliminary measurements and model results for vertical velocity make offer guidance to future standards making organizations?

SCOPE AND FIELD OF APPLICATION

One of the tasks of the IEA Wind Implementing agreement is to develop Recommended Practices related to different aspects of wind energy. These documents summarize the best knowledge at the time of writing and shall be treated as recommendations and not as binding standards. IEA Wind endorses this work, but will not be held liable for the application of the information in those documents. These documents have served as important work for the development of international standards such as IEC.

Specific areas of research have been conducted under IEA Task 27 since 2009 when IEA experts held meetings back-to-back with IEC MT2, a team of experts convened to write the third revision of the IEC 61400-2. A number of areas of technical weakness were noted, one of which is the lack of realistic turbulence levels and models. Testing, analyzing and modelling work began in 2009 and is still ongoing, and different countries have been engaged in this work at different times.

This work took various activities to attempt to learn more about turbulence and it's impact on small wind turbine production. One activity was to take existing 3-D, 10Hz wind resource data and analyse it for preliminary understanding of turbulence parameters. Another activity was to use CFD models as tools to help understand the trends of windspeed and flow in a turbulent environment such as rooftops (Developed simplified models of cubes and fences). The last activity was gathering existing turbine production data and evaluating the effects of local micro- and meso-terrain affects turbine production.

A compendium of presentations exist on a CIEMAT ftp site and this document is only meant to highlight and summarize work done from the participating countries. As we began to share and compare data we realized we needed a way to loosely describe the setting of the turbine or test site so we have developed a formal description of Site Type. Another comparative variable includes z/h, where z is the height of the turbine rotor above the roof and h is the height of the building.

These and other findings are summarized below with specific references to sections within the IEC 61400-2 standard.

1.1 AUSTRALIA (active 2009 – 2014)

1.1.1 CFD models on wind flow results - Bunnings warehouse, Port Kennedy Perth, Australia

Murdoch University, Perth, Australia

PhD Student: Amir Bashirzadeh Tabrizi, Anup KC

Research Supervisors: Dr Jonathan Whale, Prof. Tom Lyons, Dr Tania Urmee

1.1.1.1 Relevant publication

Bashirzadeh Tabrizi, A. Whale, J., Lyons, T. Urmee, T. (2014) *Performance and safety of rooftop wind turbines: use of CFD to gain insight into inflow conditions*. Renewable Energy, 67, pp242-251.

1.1.1.2 Overview

Bunnings Ltd. is a chain of hardware stores throughout Australia and New Zealand. As part of a project to reduce the carbon footprint of the Bunnings hardware stores, 5 Swift turbines (1.5kW) were installed on each of two Bunnings warehouses in the Perth suburbs of Port Kennedy and Rockingham in March 2010. Murdoch University were involved in the wind resource assessment for the turbines and installed an ultrasonic anemometer at the Port Kennedy site in September 2009. The turbines failed to function properly due to continuing inverter problems and were removed in 2013. However the wind monitoring equipment remained on the roof of the Port Kennedy store until July 2016 and a large amount of wind data was recorded.

As part of the wind resource assessment, a CFD model of the Bunnings warehouse at Port Kennedy was created and buildings around the warehouse, up to 200 m radius, were added to the model domain. To predict the wind velocity at the inlet of the CFD domain, the wind atlas software WAsP was used; raw data from the Kwinana Industries Council (KIC) meteorological station located on Alcoa RDA Lake A, recorded between 12/08/2011 and 24/01/2012 were used as wind observations in WAsP. WAsP was used to generate a regional wind atlas for eight wind direction sectors N, NE, E, SE, S, SW and W at 200 metres above the ground. At 200 metres above the ground the wind characteristic for each sector is not affected by surface structures, and was used to predict the site-independent vertical wind profile for the region. This profile was then used as the inlet velocity profile at the outer boundary of the CFD model domain and the model was run for each sector to find the mean wind velocities on the roof of the warehouse. To allow for comparison the CFD results were extracted for the same period as the KIC measurements and ultrasonic measurements of wind flow on the roof of the Bunnings warehouse (12/08/2011 to 24/01/2012). The CFD results have been compared with neutrally stable measured wind data as well as with the whole set of measured data for the period to check the accuracy of using the combination of CFD and wind atlas software for rooftop wind

resource assessment. To isolate the neutrally stable data, the wind measurements above the Bunnings rooftop were filtered by application of Golder's curve of the Pasquill stability classes as functions of Monin-Obukhov length, and roughness length. The European Wind Atlas was consulted and the aerodynamic roughness of area around the Bunnings warehouse was estimated to be 50 cm.

1.1.1.3 Software used

The ANSYS CFX software package was used in this research to model wind flows over the Bunnings building.

1.1.1.4 Flow type

For this study the wind simulates steady-state, incompressible flow.

1.1.1.5 Governing equations

For modelling wind flow over complex terrain, the Reynolds-averaged Navier-Stokes approach (RANS) combined with a proper turbulence model was applied. Reynolds decomposition is employed to the variables of the governing equations, whereby each variable is divided into a time-averaged part and a fluctuating part, $\mathrm{u} = \bar{\mathrm{u}} + \acute{\mathrm{u}}$, resulting in the two following equations:

$$\rho\left(\frac{\partial \bar{u}_i}{\partial t} + \bar{u}_j \frac{\partial \bar{u}_i}{\partial x_j}\right) = -\frac{\partial \bar{P}}{\partial x_i} + \rho \bar{g}_i + \frac{\partial}{\partial x_j}\left[\mu\left(\frac{\partial \bar{u}_i}{\partial x_j} + \frac{\partial \bar{u}_j}{\partial x_i}\right)\right] - \frac{\partial}{\partial x_j}\rho\overline{\acute{u}_i \acute{u}_j} \qquad \text{eq. (1)}$$

$$\frac{\partial \bar{u}_k}{\partial x_k} = 0 \qquad \text{eq.(2)}$$

The terms $\overline{\acute{\mathrm{u}}_\mathrm{i}\acute{\mathrm{u}}_\mathrm{j}}$ are known as the Reynolds stresses and physically represent the additional stresses due to the fluctuating components of the flow. These Reynolds stresses have been modelled according to a 'Boussinesq' approximation, shown in the following equation as an analogy of Newton's friction law:

$$\tau_{ij} = -\rho\overline{\acute{u}_i \acute{u}_j} = \mu_t\left(\frac{\partial u_i}{\partial x_i} + \frac{\partial u_j}{\partial x_i}\right) + \frac{2}{3}\rho k \delta_{ij} \qquad \text{eq.(3)}$$

where μ_t is the turbulent viscosity and $\mathrm{k} = \frac{1}{2}\overline{\acute{\mathrm{u}}_\mathrm{i}\acute{\mathrm{u}}_\mathrm{j}}$ is the turbulent kinetic energy (TKE).
In this study, there was improved convergence of the CFX results using the Shear Stress Transport (SST) scheme. The SST scheme is a hybrid of two-equation models that combines the advantages of both k-epsilon $(\mathrm{k}-\varepsilon)$ and k-omega $(\mathrm{k}-\omega)$ models. The SST k- equations are:

$$\frac{\partial \rho k}{\partial t} + \frac{\partial}{\partial x_j}\left(\rho U_j k\right) = \frac{\partial}{\partial x_j}\left[\left(\mu + \frac{\mu_t}{\sigma_{k3}}\right)\frac{\partial k}{\partial x_j}\right] + P_k - \beta' \rho k \omega + P_{kb} \qquad \text{(eq. 4)}$$

$$\frac{\partial \rho\omega}{\partial t} + \frac{\partial \rho\omega}{\partial x_j}(\rho U_j k) = \frac{\partial}{\partial x_j}\left[\left(\mu + \frac{\mu_t}{\sigma_{\omega 3}}\right)\frac{\partial \omega}{\partial x_j}\right] + (1 - F_1)2\rho\frac{1}{\omega\sigma_{\omega 2}}\frac{\partial k}{\partial x_j}\frac{\partial \omega}{\partial x_j} - \alpha_3\frac{\omega}{k}P_k - \beta_3\rho\omega^2 + P_{wb} \quad \text{(eq. 5)}$$

where F_1 is a blending function, P_k is turbulence production due to viscous forces [kg/ms3], P_{kb} and P_{wb} are buoyancy production terms [kg/ms3], α is wind direction [°], β is a sheltering effect factor ,$\sigma_{\omega 2}$ and $\sigma_{\omega 3}$ are constants in the SST k-ω turbulence model and ω is the turbulent energy dissipation rate [1/s]. The SST k-ω model incorporates transport effects in the formulation of the eddy-viscosity terms and thus pays more attention to the transport of turbulence kinetic energy, and predicts the starting and the size of the separation of flow under adverse pressure gradients more accurately than the standard $(k - \varepsilon)$ model. This leads to improvement of prediction of the flow separation, which is important in the present study.

1.1.1.6 Turbulence model

In this study, the Shear Stress Transport (SST) scheme had been used as the turbulence model. The SST scheme is a hybrid of two-equation models that combines the advantages of both k-epsilon $(\mathrm{k} - \varepsilon)$ and k-omega $(\mathrm{k} - \omega)$ models.

1.1.1.7 Discretization

ANSYS CFX uses an element-based finite volume method, which first involves discretising the spatial domain using a mesh. The mesh is used to construct finite volumes, which are used to conserve relevant quantities such as mass, momentum, and energy.

1.1.1.8 Velocity pressure coupling

CFX is a fully coupled solver and so the pressure-velocity coupling is inherent in the solution procedure. Coupled solvers like CFX have all 3 momentum equations and the pressure equation in the same matrix so they are solved together.

1.1.1.9 Computational grid

An unstructured tetrahedral mesh was used with five inflation layers of 25 mm total thickness on the ground, roofs and walls of all buildings. The final mesh statistics in the modelling of wind flow from eight wind sectors are shown in Table 1. The domain of the CFX models for all simulated wind sectors was set up as a rectangular domain surrounding the urban grid.

Table 1- Final mesh statistics for all simulated wind sectors

Wind Sector	Number of Elements	Number of Nodes
North	2447170	649635
North East	3008735	795661

East	2848993	752701
South East	3053926	804307
South	2474711	657739
South West	3003951	793720
West	2848974	752528
North West	3052780	802437

1.1.1.10 Boundary Conditions for velocity and pressure

The following equation is used to model the wind profile at the inlet of CFD domain:

$$u = \frac{u_*}{k} \ln\left(\frac{y+z_0}{z_0}\right) \quad \text{(eq.6)}$$

where z_0 is the ground roughness of the area, u_* is the friction velocity, and k is von Karman's constant and is equal to 0.4. Since all the buildings within a radius of 200 metres around the target building have already been simulated in the CFD model, the ground roughness is set to 2 cm for all wind sector simulations. For each simulated sector, the mean wind speed at 200 metres above the ground (the output of the WAsP simulations) was used to find the friction velocity for the CFD simulation. Table 2 shows the results of the WAsP simulations in terms of mean wind speed for each sector.

Table 2- WAsP output: sector-wise mean wind speeds at 200 m

Wind Sector	**Mean wind speed (m/s)**
North	6.36
North East	5.33
East	8.01
South East	7.57
South	8.53
South West	8.36
West	6.19
North West	6.18

The downstream boundary was specified as an outlet with zero relative pressure and zero turbulence intensity gradients.

1.1.1.11 Reynolds number, time step and statistics

The Reynolds number was $2x10^5$, the maximum number of iterations was set to 150 and the residual target was 10^{-5}(residual type: RMS). For steady-state problems, the CFX-Solver applies a false time step as a means of under-relaxing the equations as they iterate towards the final solution. Because the solver formulation is robust and fully implicit, a relatively large time scale can typically be selected, so that the convergence to steady-state is as fast as possible.

1.1.1.12 Inflow boundary condition assumptions

For all wind sectors, the simulated buildings were placed in a rectangular domain of height equal to 200 meters and the lateral boundaries of the computational domain were placed at a distance of 5xHmax away from the closest part of the built area at each side, where Hmax is the height of the highest simulated building in the region of interest. A distance of 8xHmax between the inflow boundary and the built area was applied as a longitudinal extension of the domain in front of the simulated region, and 15xHmax behind the built area was employed to allow for flow re-development.

The turbulence level at the inlet boundary was adjusted to 5% as suggested by CFX guidelines. The downstream boundary was specified as an outlet with zero relative pressure and zero turbulence intensity gradients. Symmetric boundary conditions were employed for the side faces and top of the domain in all wind sectors. Solid boundaries, including the ground of the domain and roofs and walls of the buildings, have been set as no-slip walls with the CFX wall-function approach used to model flow near these surfaces. An automatic near-wall treatment method was deployed by CFX to treat the wall effects. The near-wall treatment method accounts for the rapid variation of flow variables that occur within the boundary layer region as well as viscous effects at the wall. This treatment provided a smooth shift from low-Reynolds number formulation to wall function formulation.

1.1.1.13 Conclusions

Table 3 shows the CFD simulated and measured results for the magnitude of the 10-minute averaged 3D velocity vectors on rooftop of Bunnings warehouse buildings over the period 12 Aug 2011 and 24 January 2012, for various atmospheric conditions. The percentage of error between numerical results and measured results has been presented in the table for all wind sectors. Also some figures that show the simulation results for the south-west wind sector have been provided (Figs. 1 -4).

Table 3- CFD simulation and measured results on rooftop of Bunnings warehouse for 10-minute averaged wind speeds

Wind Sector	CFD (m/s)	Measurement Neutrally Stable Condition(m/s)	Error (%)	No. of measured data- Neutrally Stable Data	Measurement Whole Data(m/s)	Error (%)	No. of measured - Whole Data
N	4.3429	4.1347	5.0	76	3.3665	29.0	182
NE	2.4954	3.5827	-30.3	250	2.8780	-13.3	1068
E	3.7422	4.5182	-17.2	520	3.8198	-2.0	1861
SE	4.5900	4.2027	9.2	451	3.4711	32.2	1697
S	5.6381	4.5000	25.3	718	3.9313	43.4	1430
SW	5.8489	5.6998	2.6	955	5.3290	9.8	1752
W	4.6927	5.2132	-10.0	345	4.7421	-1.0	862
NW	4.3355	6.1329	-29.3	229	5.5433	-21.8	674

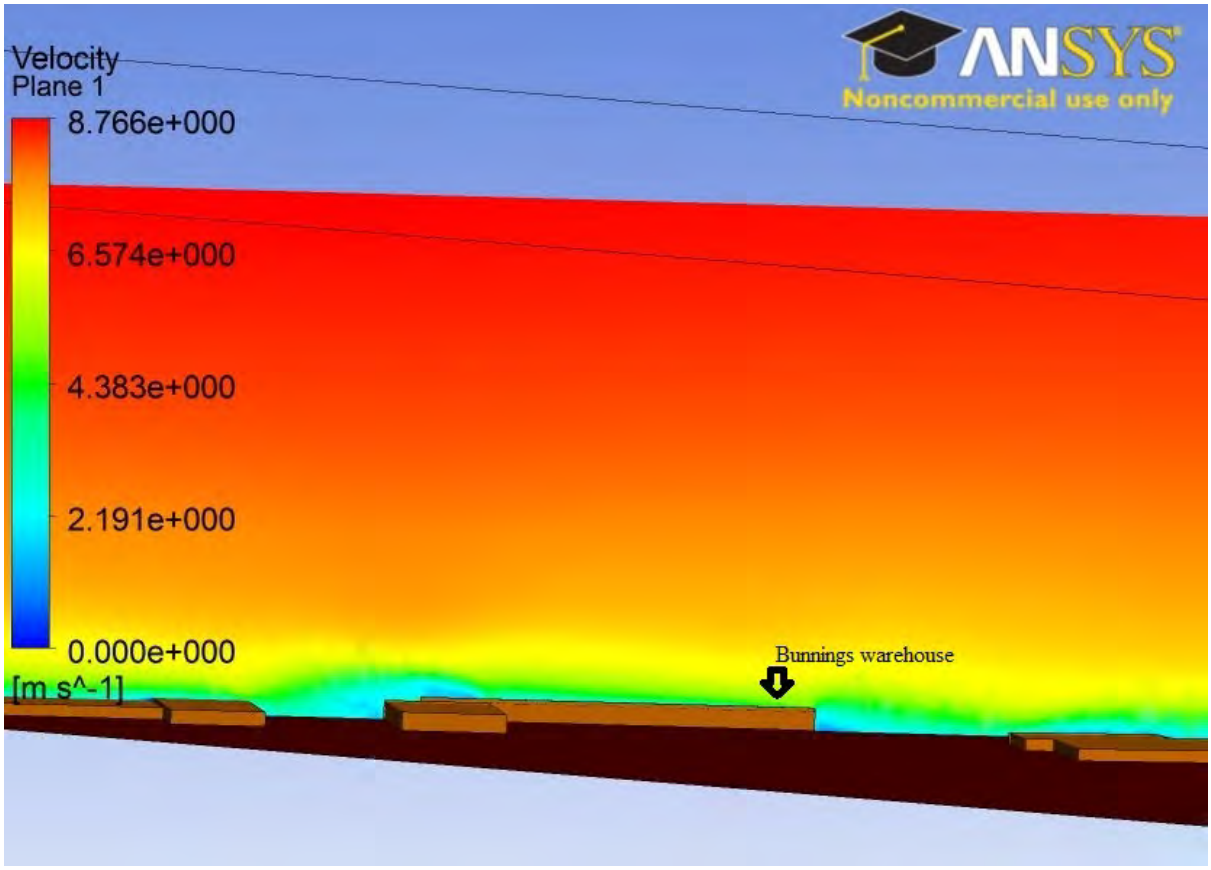

Fig. 1 Wind speed contours on the edge of the roof of the Bunnings warehouse building for the south-west wind sector simulation

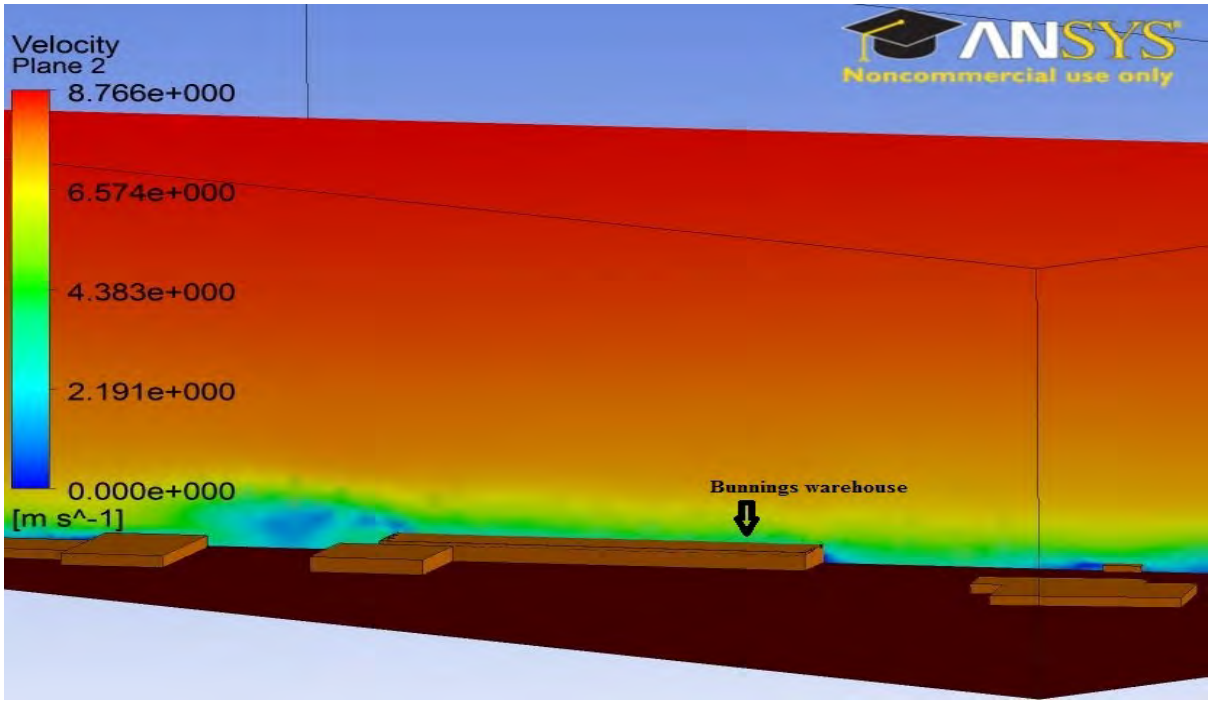

Fig. 2 Wind speed contours on the middle of the roof of the Bunnings warehouse building for the south-west wind sector simulation

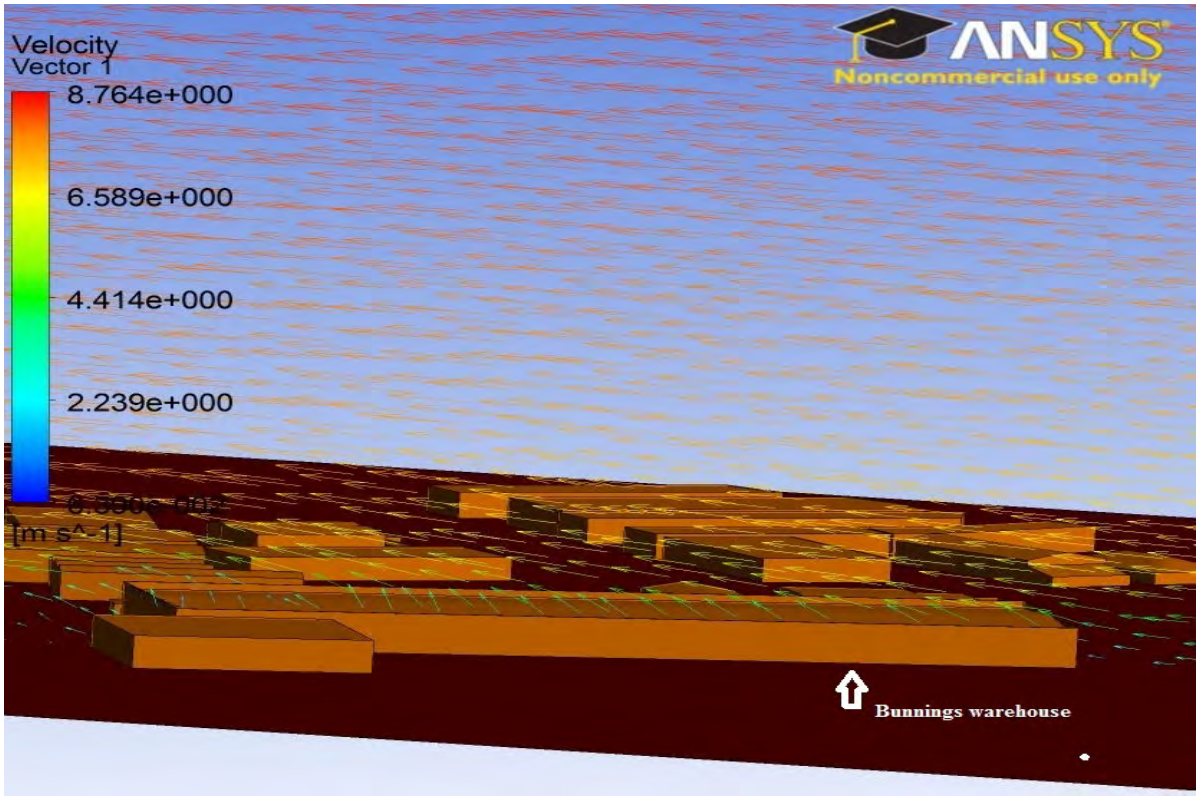

Fig. 3 Wind velocity vectors on the edge of the roof of the Bunnings warehouse for the south-west wind sector simulation

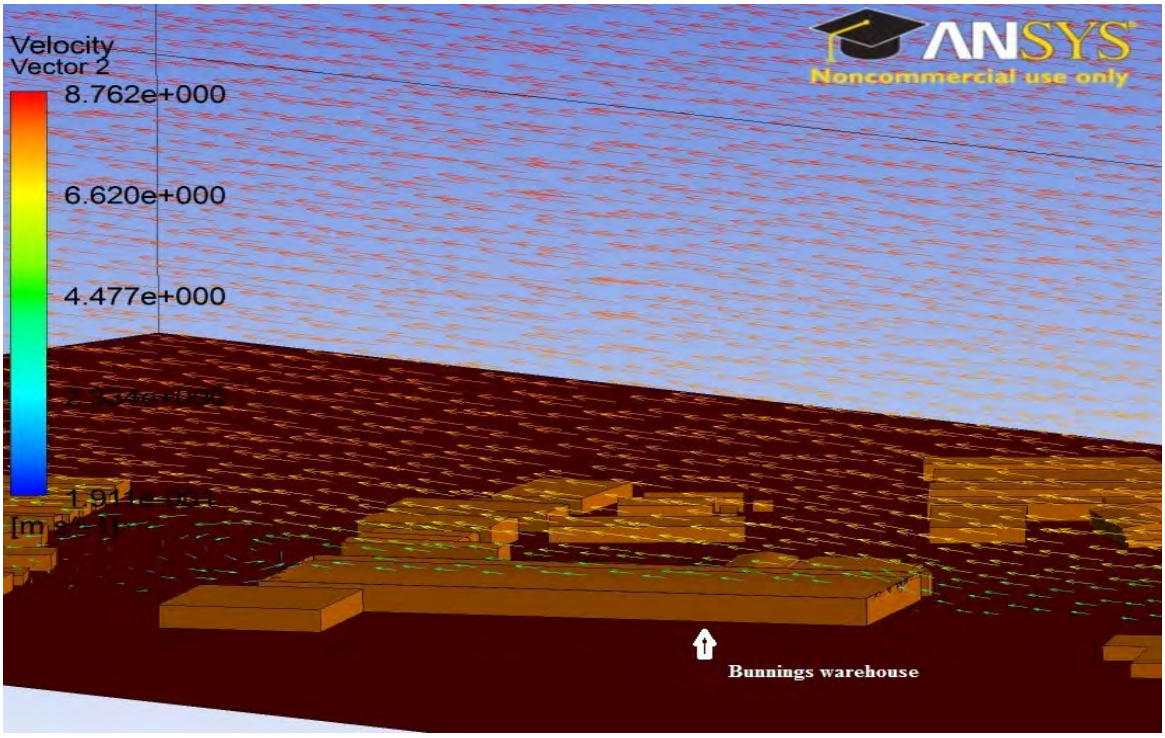

Fig. 4 Wind velocity vectors on the middle of the roof of the Bunnings warehouse building for south-east wind sector simulation (prevailing wind direction)

For further information please see:
Tabrizi, Amir, "Investigation of inflow wind conditions and load performance of small wind turbines in the built environment", PhD Thesis, Murdoch University Library Research Repository, 2016

1.1.2 **Rooftop turbine tests – Bunnings Warehouse, Port Kennedy Perth**

Murdoch University, Perth, Australia
PhD Students: Amir Bashirzadeh Tabrizi, Anup KC
Research Supervisors: Dr Jonathan Whale, Prof. Tom Lyons, Dr Tania Urmee

1.1.2.1 Relevant Publications:

Bashirzadeh Tabrizi, A., Whale, J., Lyons, T. and Urmee, T. (2015) Extent to which international wind turbine design standard, IEC61400-2 is valid for a rooftop wind installation. Journal of Wind Engineering & Industrial Aerodynamics, 139 . pp. 50-61.

Bashirzadeh Tabrizi, A. Whale, J., Lyons, T. Urmee, T. (2015) Rooftop wind monitoring campaigns for small wind turbine applications: Effect of sampling rate and averaging period, Renewable Energy, 77, pp. 320 - 330

1.1.2.2 Overview

Bunnings Ltd. is a chain of hardware stores throughout Australia and New Zealand. As part of a project to reduce the carbon footprint of the Bunnings hardware stores, 5 Swift turbines (1.5kW) were installed on each of two Bunnings warehouses in the Perth suburbs of Port Kennedy and Rockingham in March 2010. Murdoch University was involved in the wind resource assessment for the turbines and installed an ultrasonic anemometer at the Port Kennedy site in September 2009. The turbines failed to function properly due to continuing inverter problems and were removed in 2013. However the wind monitoring equipment remained on the roof of the Port Kennedy store until July 2016 and a large amount of wind data was recorded.

This work is in two parts. The first part investigates the characteristics of the wind conditions in the built environment of the Port Kennedy warehouse and compares the relevance of parameters associated with the longitudinal turbulence intensity, as defined in IEC61400-2, for the installation of small wind turbines in the built environment. The second part of this work investigates the extent to which the von Karman and Kaimal turbulence spectra models, as presented in IEC61400-2, are appropriate for use in the design of SWTs installed on the rooftop of a warehouse in the built environment. In particular the research attempts to gauge how different the turbulence spectra currently used for turbine design are from the actual inflow conditions experienced by the turbines on the roof. A sensitivity study was carried out to assess the influence of turbulence length scale on the results. The Kaimal spectral function was the better of the existing models in predicting the trends of all wind components and was used as a starting point in developing an approach to modelling turbulence power spectra for a rooftop site in the built environment by incorporating typical length scales at the site.

1.1.2.3 SWT Site Characterization

For this study, data is collected from a wind monitoring system on the roof of a large warehouse belonging to the hardware chain Bunnings Ltd. in the suburb of Port Kennedy, Perth, Western Australia. The warehouse is a rectangular building of height h = 8.5 m a.g.l, with its long-axis oriented NNE-SSW, and a very low pitched roof (almost flat) with a façade wall around the edge.

Fig. 1 Location of wind monitoring site (Port Kennedy) Pic Source Google Maps

The building lies approximately 5 km from the coast (Indian Ocean) with the prevailing winds from the south-west. The warehouse is situated in a commercial estate but has no larger buildings or large trees in the vicinity. Within a 1 km radius of the site there are mainly residential buildings to the north, commercial and industrial buildings to the east and a few buildings, low shrubs and low sand dunes to the south and west. The south-west front and the north-west side are comparatively open, though street furniture and a car park exist on these sides. The built-up area surrounding the warehouse is shown in following Fig. 1.

The wind monitoring system was installed in September 2009 as part of a wind resource assessment for the installation of five small wind turbines that were later commissioned in March 2010. A Gill WindMaster Pro 3D ultrasonic anemometer was installed on a boom on a 5.3 m mast attached to the front-façade in the south west corner of the warehouse (Refer Fig. 2). The boom had a sliding collar in order to position the ultrasonic anemometer at different heights above the roof. The mast could be tilted down in order to make adjustments or to replace sensors. The data analysed consists of 10 Hz data over a six month period from August 2011 to January 2012.

Fig. 2 Wind monitoring system at Bunnings, Port Kennedy (left) and view to the south-west prevailing winds from the Port Kennedy warehouse (right)

Despite the increased turbulence near the edge of the roof compared to the middle of the roof, it is not uncommon for SWTs to be installed close to the edge of the roof to ensure ease of access for maintenance. In addition the location of the turbines on the front façade of the building offered Bunnings maximum publicity from the project. Further, to reduce tower installation costs and comply with local government planning regulations, SWTs are usually installed close to the rooftop on short towers with a typical upper range of around 5m. Figure 2 show the position of the ultrasonic anemometer on the roof of the Bunnings warehouse with regards to the installed SWTs.

1.1.2.4 Data Acquisition Approach

For the characterization of urban wind and its comparison with the standard, the 6 months' worth of 10-min averaged data were utilized at a height (a.g.l) of 14.44 m (a 5.49 m tall mast placed above the façade of the building having a height of 8.5 m, with a normalized height of z/h = 1.70, where z is the height of the measurement a.g.l. and h is the height of the building to the top of the façade).

For the Kaimal power spectral study, smaller records of 10 days of data were extracted for each of 4 normalized heights studied; z/h = 1.35, 1.46, 1.58 and 1.70. The chosen positions for ultrasonic measurements are in the range of typical heights and situations that SWTs have previously been installed on rooftops. This data was analyzed to investigate the suitability of the turbulence models from the design standard for use at this site.

1.1.2.5 Other instruments used: temperature, pressure, wind direction, humidity

The monitoring system had an ultrasonic anemometer along with temperature and humidity sensors to record information related to wind speed, wind direction, relative humidity and temperature.

1.1.2.6 Sampling rate

For both the cases, the data were sampled at 10 Hz.

1.1.2.7 Data processing strategy, quality assurance methods

Custom Matlab code was used to analyse the data and compute the parameters of interest. Data were sorted and analyzed as per the conventions mentioned in the IEC 61400-2 and IEC 61400-12-1 standards. Different mathematical and statistical tools were used to compare and contrast the measured values with the values given in the standards.

Each data series, consisting of 10-minute averaged records of wind data at a known height from the rooftop of the warehouse, was analysed to investigate the suitability of the turbulence models from the design standard for use at this site. The most common atmospheric conditions experienced during the operation of an SWT in the built environment are either slightly unstable or neutral conditions. Thus the first step in processing the data was to filter each component of the raw three-dimensional wind speed measurements (longitudinal, lateral and vertical) using Pasquill stability classes in order to select only wind data recorded under slightly unstable or neutral conditions. Based on a table of roughness lengths, surface characteristics and roughness classes from the European wind atlas[1], the aerodynamic roughness of the Bunnings warehouse area was estimated to be 50 cm. The displacement height of the area, based on the equation presented by Panofsky & Dutton[2] has been calculated as 4.1 m. The curves presented by Golder[3] , were then used to find the range of Monin-Obukhov lengths corresponding to slightly unstable and neutral conditions on the roof of and these values were then used to filter the raw measurements.

The next part of the procedure was to rotate the filtered wind speed data from the reference frame of the ultrasonic anemometer to the reference frame of the mean three-dimensional wind speed (longitudinal, lateral and vertical) and direction, for each 10-minute averaged record.

To find the turbulence power spectral density data for each 10-minute averaged record the mean longitudinal, lateral and vertical wind components were separately subtracted from their respective measurements to leave the fluctuations for each component. The autocorrelation of the fluctuations was then computed and a Fast Fourier Transform of this autocorrelation provided the data for the power spectral density plots. The power spectra for different ten-minutes records at z/h = 1.35, 1.46, 1.58 and 1.70 in neutral and slightly unstable atmospheric conditions for longitudinal, lateral and vertical components were calculated, averaged over the 10 day period and compared with predictions from the von Karman and Kaimal spectra models.

1.1.2.8 Conclusion of results

The wind direction and wind speed distribution of 6 months' worth of 10-min average wind speeds as obtained from WAsP Climate Analyst is given in Figure 3 and 4, respectively. The results show that the site has prevailing winds from the South West (sea- breezes) as well as some

[1] I. Troen, E. L. Petersen, European Wind Atlas, RisØ National Laboratory, Roskilde, Denmark, 1989.

[2] H.A. Panofsky, J.A. Dutton, Atmospheric turbulence, John Wiley & Sons, Ltd, New York, 1984.

[3] D. Golder, Relations among stability parameters in the surface layer, Boundary Layer Meteorol. 3 (1972) 47-58.

significant winds from the East. The wind speed distribution is close to Rayleigh with a reasonable mean wind speed (for a roof site) of 4.2 m/s.

1.1.2.9 Wind Rose

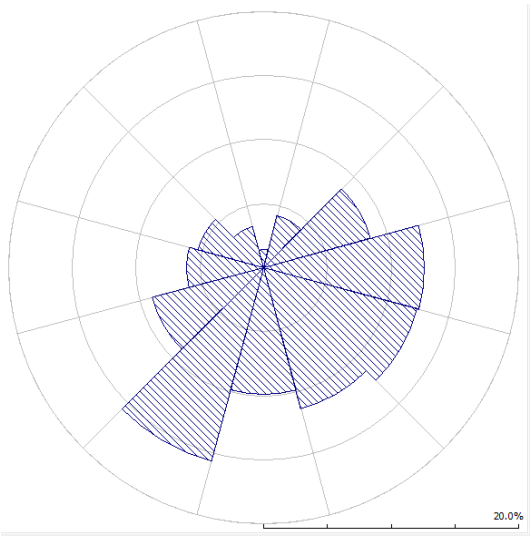

Fig. 3 Wind rose from Port Kennedy

1.1.2.10 Wind speed frequency distribution

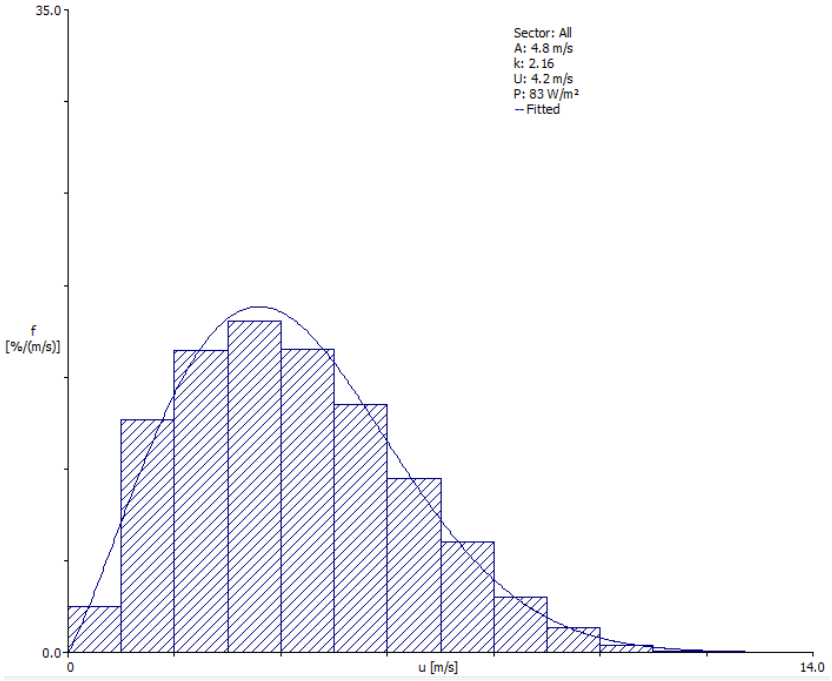

Fig. 4 Wind distribution of 10-min average wind velocities (U_bar)

1.1.2.11 Turbulent Kinetic Energy (TKE) and Turbulent Intensity (TI)

The raw data were sorted in 10-minute averaging as per the IEC 61400-2 standard and corresponding standard deviation of the average wind speed along the longitudinal direction (u-component of wind velocity) at each bin was calculated. The measured data, when compared with the IEC standard at 90th percentile of standard deviation, show deviations with the standard (see Fig. 5). For low wind speeds (<4 m/s), the standard overestimates the value while it underestimated the values for higher wind speeds. Also, there are several extreme wind events which are not accounted for in the standard.

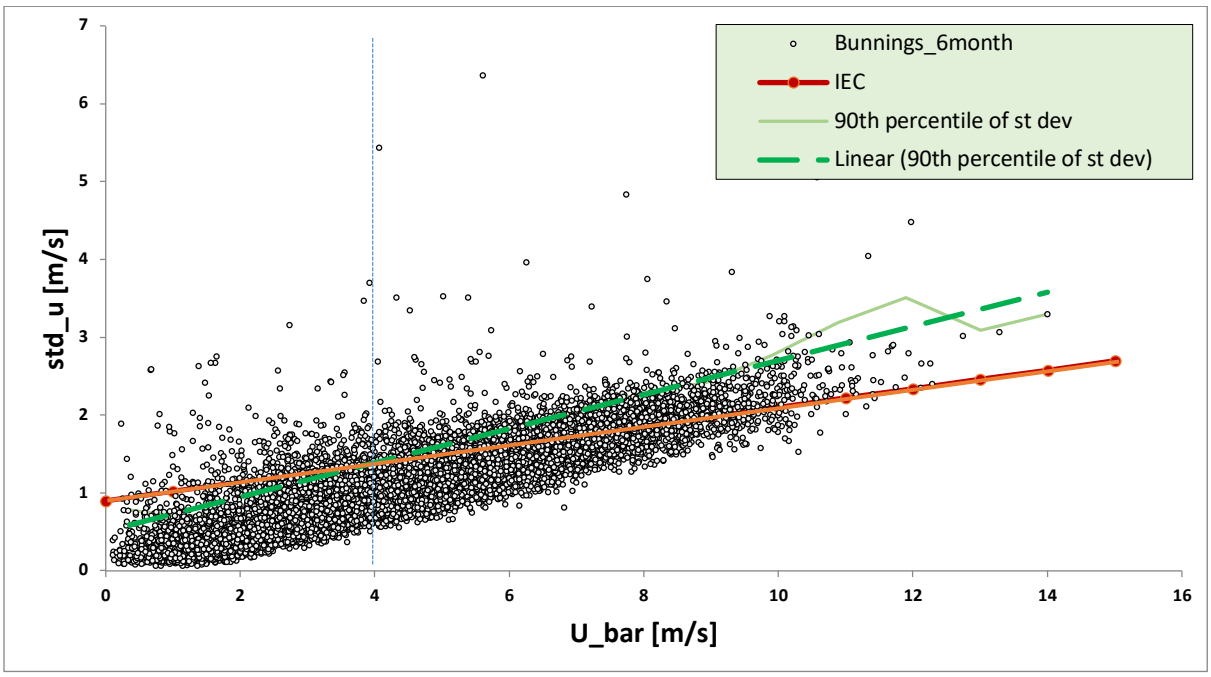

Fig. 5 $\overline{U}$ vs σ_u

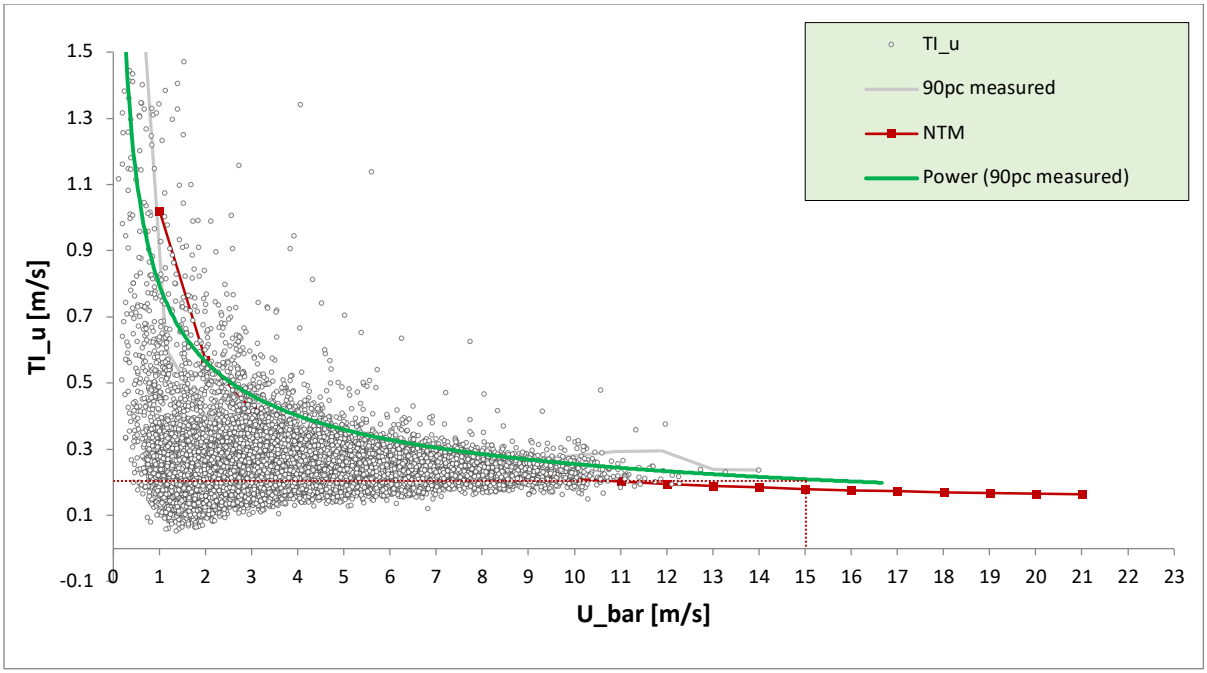

Fig. 6 Turbulence intensity in longitudinal direction vs mean wind speed (U_bar)

The standard IEC 61400-2 assumes a turbulence intensity of 18% at hub height wind speed of 15 m/s which is not reflected by the measured data (Refer Fig. 6). The measured data has a turbulence intensity of around 22% at 15 m/s hub height wind speed which is slightly larger than as predicted by the standard (Refer Fig. 6). Note that these values may be higher for some wind sectors, where there is particular interference with the wind by obstacles in that sector.

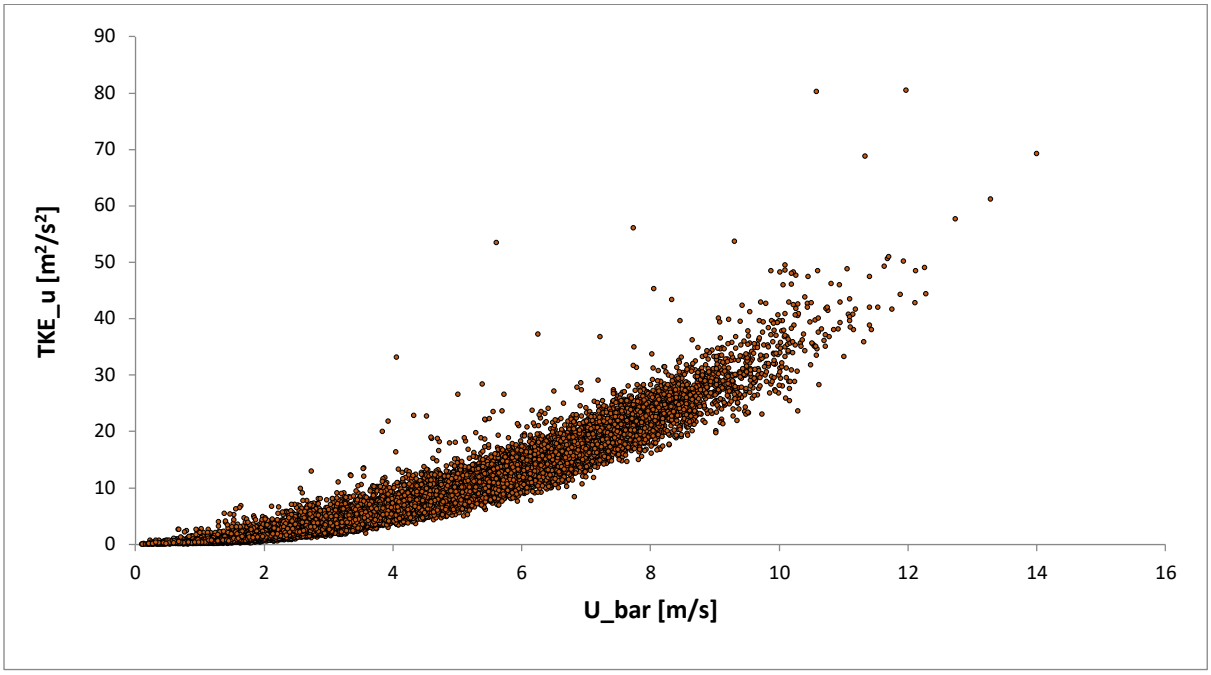

Fig. 7 Turbulent kinetic energy vs U_bar

The plot of TKE (Fig. 7) in the longitudinal direction shows some values with reasonably high magnitudes that may cause unexpected bending and loading on turbines. Such extreme events can be detrimental for both the turbine's components and power performance of the turbine.

1.1.2.12 Power spectral density and corrected Kaimal Model

Fig. 8 shows the average values of turbulence power spectral density, Sk, for longitudinal (k = 1) wind components plotted against normalized frequency ($\mathrm{fz_s'}/\mathrm{U}, \mathrm{z_s'} = \mathrm{z} - \mathrm{z_d}$) for neutral atmospheric conditions.

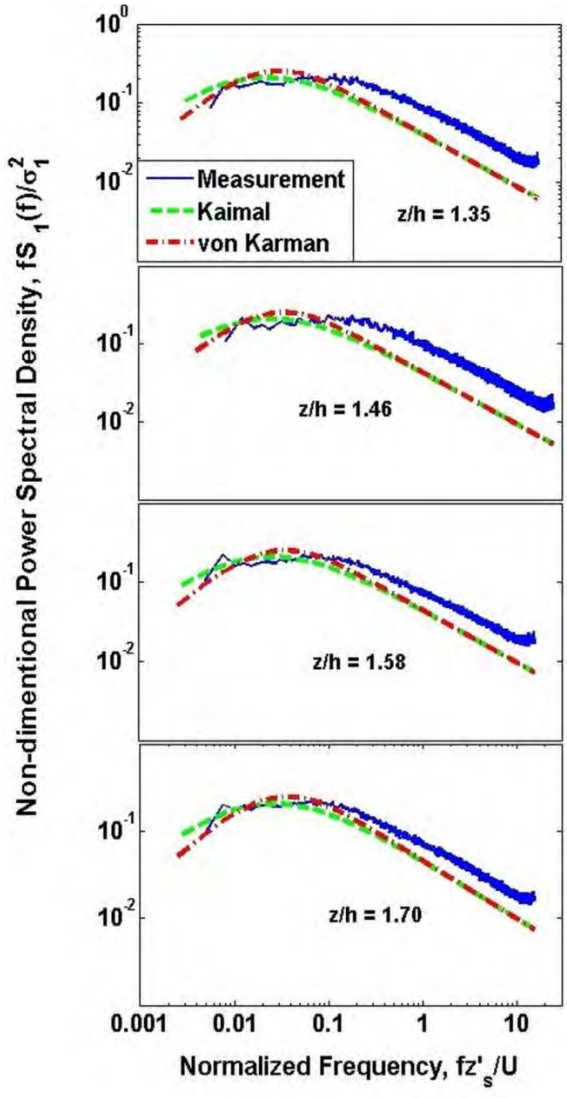

Fig. 8 Non-dimensional turbulence power spectral density of the longitudinal wind speed component for different heights above the rooftop of a warehouse in neutral atmospheric conditions

As is visually apparent from the figures, the longitudinal component of the spectra of the measured data is underestimated under both atmospheric conditions by both the von Karman and Kaimal models for normalized frequencies larger than around 0.1, although the Kaimal model appears closer to the measured values at lower frequencies.

At high frequencies, whilst the von Karman and Kaimal models as outlined in IEC61400-2 can predict the trend, if not the magnitude, of longitudinal turbulence spectra in the built-environment, only the Kaimal model provides a reasonable estimate of the trend of turbulence spectra for the lateral and vertical components. The suggested form of the Kaimal model in IEC61400-2, however, cannot predict the magnitude of the turbulence spectra with a high degree of agreement compared to the actual turbulence conditions especially close to building surfaces.

One likely reason for the inaccuracy of the Kaimal model in terms of predicting the magnitude of turbulence power spectra at the Port Kennedy rooftop site, is that the Kaimal model as defined in IEC61400-2, assumes length scales of turbulence that are characteristic of open terrain. The parameter of length scale represents the size of turbulent eddies[4] and in the built environment the scale of turbulence due to local inhomogeneties would be expected to be markedly different to the scales of turbulence in more uniform open terrain. Hence defining the length scale in terms of surface urban morphology may provide a more realistic estimation for use within the standard.

[4] B. S. Shiaua, Y. B. Chen, Observation on wind turbulence characteristics and velocity spectra near the ground at the coastal region, J. Wind Eng and Ind., 90 (2002) 1671–1681.

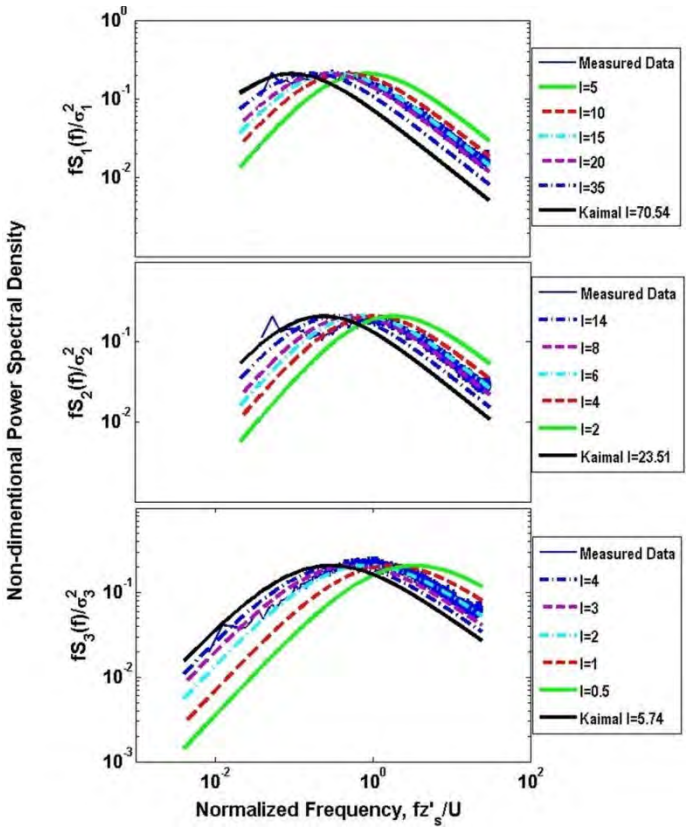

Fig. 9 Non-dimensional turbulence power spectral density on the rooftop of a warehouse at z/h = 1.46 for different length scales in neutral atmospheric conditions

Fig. 9 shows the impact of varying length scale on the Kaimal power spectral values model for longitudinal, lateral and vertical wind components at *z/h* = 1.46, under neutral atmospheric conditions. These graphs suggest that a more accurate prediction of the turbulence spectra at the Port Kennedy site could be obtained by persevering with the Kaimal model (since it predicts spectral trends reasonably well, particularly at higher frequencies) and using more appropriate length scales for the built environment in order to have agreement with the magnitude of measured spectral values.

A possible adaptive approach for the application of the Kaimal model in the built environment is proposed, where, the longitudinal integral length scale from IEC61400-2 is substituted by a more appropriate length scale derived from last figure.

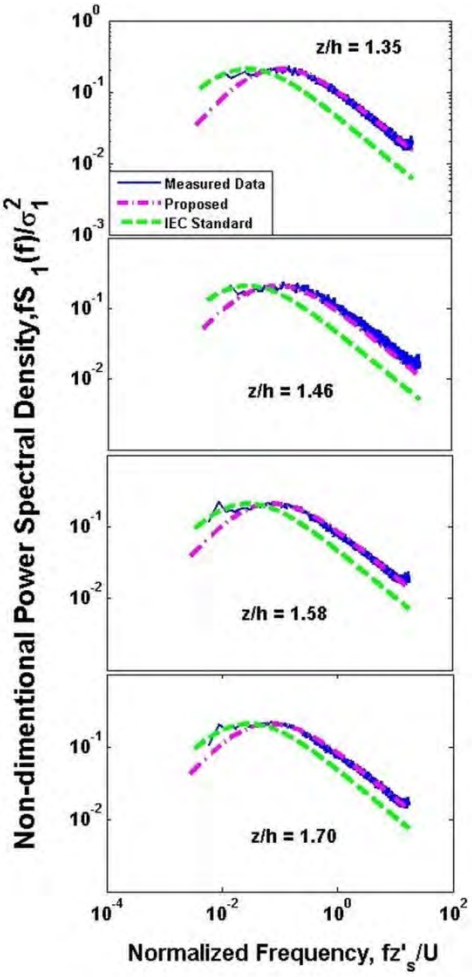

Fig. 10 Comparison of measured non-dimensional longitudinal turbulence power spectrum density and predicted values by Kaimal model via IEC standard approach and proposed approach for different heights above the rooftop of a warehouse in neutral atmospheric conditions

Figure 10 shows the results of comparing the new predictions from the suggested approach with the averaged values of the measured power spectra at the four different heights. The figure shows that the adaptive approach suggested above results in more accurate predictions by the Kaimal model over a large range of frequencies for longitudinal component, in neutral atmospheric conditions.

1.1.2.13 Conclusions

The results from the 6 months' wind data analysis infer that the wind model as used in IEC 61400-2 standard is not representative of the urban Port Kennedy site. Urban winds are comprised of elevated turbulence and extreme events due to interference of the wind with various obstacles. These wind conditions need to be addressed by the standard to ensure safety and reliable performance of small wind turbines in the built environment.

As for the wind model, the Kaimal spectra predicted the trends of all wind components better than the von Karman model over the rooftop of a building. This was particularly true at high frequencies which evidence suggests are the important frequencies when it comes to fatigue loading on wind turbines.

The results from this work suggest that there are some key parameters that influence the shape and scale of the turbulence power spectra over the rooftop of a building that need to be taken into account when considering the inflow of a SWT installed on the roof. **This study has focused on the influence of hub-height, atmospheric stability and turbulence length scales and wind direction.** The models have greater agreement with measured data for higher hub-heights (further from the roofline) and in neutral atmospheric conditions. In the built environment, wind direction is important and will determine whether the inflow will be influenced by obstacles on the roof (including other SWTs), the building itself or by surrounding trees and buildings. Further research is required to study the effect of wind direction on turbulence spectra for Port Kennedy, involving collection of more data.

A sensitivity study with respect to length scale showed that prediction of spectra at high frequencies could be improved by using smaller length scales in the current model. This reduction in length scale is consistent with the cascading effect that obstacles in the built environment have on atmospheric turbulence whereby smaller eddies are generated. This is significant for small wind turbines as small eddies of the same scale as the order of the rotor diameter and the blade chord will have the greatest impact in terms of fatigue loading on the turbine rotor.

As an approach to modelling turbulence power spectra for a rooftop site in the built environment, an adapted Kaimal approach has been proposed that incorporates typical length scale ratios for that environment. The approach showed good agreement with measured data from the Port Kennedy site for all heights where there was sufficient measured data. The approach appears promising as a step forward on the path towards upgrading the existing standard with a dedicated design model for wind turbine manufacturers who intend their turbines to be used in highly turbulent sites such as the built environment. However, as stated previously, this study was limited to one rooftop site and further research is needed as to whether the approach will be appropriate for different rooftop sites. In order to propose an alternative expression for turbulent power spectra for rooftop sites that can be incorporated in the IEC61400-2 standard, a more comprehensive measurement program is required. **Suggested future work includes a coordinated measurement campaign for various rooftop sites to accommodate changes in building geometry, turbine height, surrounding terrain and prevailing wind direction.**

For further information please see:
Tabrizi, Amir, “Investigation of inflow wind conditions and load performance of small wind turbines in the built environment”, PhD Thesis, Murdoch University Library Research Repository, 2016

1.2 AUSTRIA (active 2015 – 2018)

1.2.1 Lichtenegg vibration measurements of a VAWT (Amperius) with and without oscilation decoupling element

Fachhochschule Technikum Wien, Vienna, Austria
Energieforschungspark Lichtenegg
Mauro Peppoloni MSc., Alexander Hirschl MSc., Kurt Leonhartsberger MSc.

As for all rotating machinery, SWTs are subject to self-excited oscillation and vibrations which induce dynamic loads in various components of the turbine including its supporting structure. While static loads calculation is a common practice that is generally taken into consideration when dimensioning foundations and towers for SWT, the magnitude of dynamic loads are often underestimated when designing and planning a SWT and it's supportive structure. This has led to long term failures and fatigue damage of rotor components and towers in the past.
Oscillation assessments of a VAWT (Amperius VK58) in the Energy Research Park in Lichtenegg, were performed in order to identify the main source for increased oscillations and vibration.

1.2.1.1 SWT site characterization

The measurement campaign was conducted in the Energy Research Park Lichtenegg located at an elevation of 800 m asl. in the hilly area of lower austrian "Bucklige Welten". The GPS coordinates N 47°36' 32,4" E 16° 12' 16,2" were measured with an accuracy of +- 3 m at the location of the met mast.

Figure 1: Map of the site including elevation information (Source: AMap/BEV ÖK50)

1.2.1.2 Diagram and describe the surrounding obstacles with distances noted

The site is located on the ridge of a hill as can be seen in Figure 1. The nearest obstructions to undisturbed inflow are the forests north and south of the site, which run over to wheat fields in a distance of about 200 m from the turbine. The disturbance expected from these forests is

minimal as they are located mostly 20 to 30 m lower that the test site. Other obstructions (see Figure 2) are the barnyards located 400 m WNW and 500 m ESE from the test site

Figure 2: Site map of the Energy Research Park Lichtenegg (Source: Google maps)

1.2.1.3 Wind measurement description

A 19 m met mast with wind measurements at 16 m and 19 m above ground level was installed at the site. The measurement was set up according IEA Recommendation 11: Wind Speed Measurement and Use of Cup Anemometry, 1st Ed., 1999 and IEC 61400-12-1. All sensors were calibrated by a calibration body accredited to MEASNET, DKD and DAR standards. The distance between the turbine and the met mast was of 45 m.

1.2.1.4 Data acquisition approach

In order to identify the causes for increased oscillations and vibrations on the tested turbine, the following parameters were recorded during the measurement campaign:

- Oscillations (displacement, velocity, acceleration)
- Wind conditions (wind speed, wind direction, turbulence intensity)
- Turbine parameter (power, RPM)

The measurements were performed on a lattice tower with a height of 15 m. In an additional measurement campaign an oscillation decoupling element was installed between the tower and the turbine in order to determine the effect on oscillation of such a decoupling element.
The Oscillations were measured by means of 4 piezo-electric accelerometers. The location of the sensors is described in Figure 3. Reference wind conditions were measured by a 3D ultrasonic anemometer and a cup anemometer (see section 1.2.1.3). The turbine power output was measured with a 3-phase power transducer, the rpm was recorded by measuring the generator output frequency.

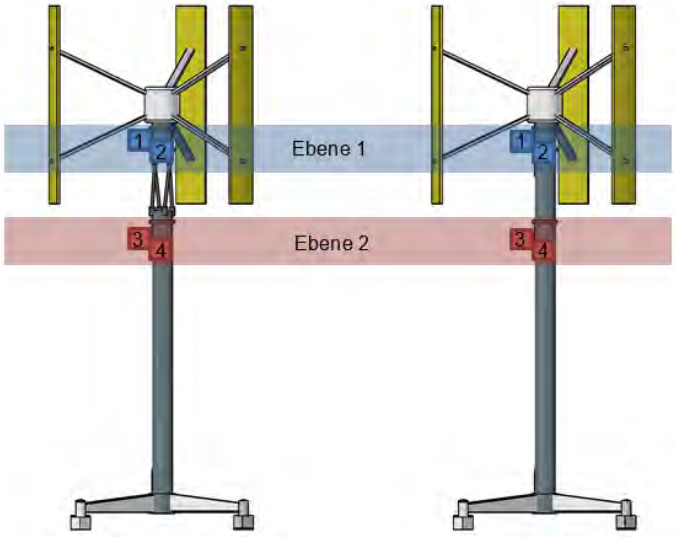

Figure 3: Location of the accelerometers on the turbine

1.2.1.5 Duration and results of data collection efforts - highlight any maintenance or downtime issues

The turbine was measured for a period of 10 without oscillation decoupling element and 12 days with the oscillation decoupling element to ensure that the turbine has performed at least 2 minutes of operation in each operation band up to nominal power. As the data volume was growing rapidly during the high-resolution oscillation measurements, data was recorded only while the turbine was operating and significant oscillation occurred. During the measurement campaigns, no downtime of the turbine was detected.

1.2.1.6 Data processing strategy

In order to identify the main causes for oscillations, a 3D frequency distribution of the oscillation data was plotted over the recorded parameters wind speed, turbulence intensity and RPM. This way, a correlation between the oscillation magnitude and specific conditions could be made. In a second step, sequences which showed particularly high oscillation magnitudes were examined further.

1.2.1.7 Conclusion of results

While the frequency distribution of oscillation over wind speed and turbulence intensity has shown no correlation, Figure 4: frequency distribution of oscillation velocity over RPM without decoupling elementFigure 4 shows a sharp correlation between oscillation velocity and the RPM of the turbine. Increased oscillations can be found at 55 RPM, 100 RPM and 175 RPM. This indicates that resonances occur at these RPM's.

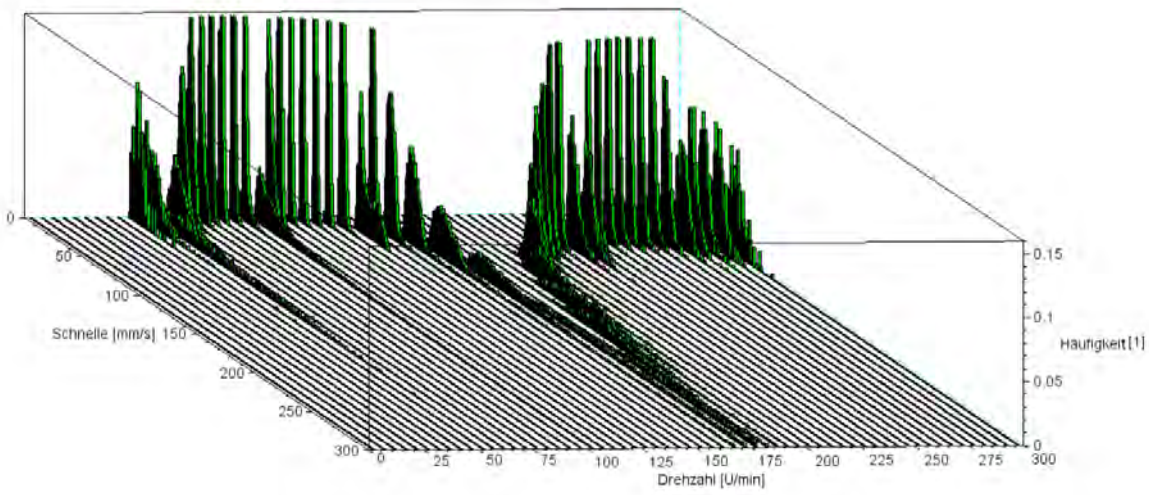

Figure 4: frequency distribution of oscillation velocity over RPM without decoupling element

After having identified that increased oscillations occur at specific RPM, a spectral analysis of the velocity signal is performed to determine the mechanical origins of the oscillations. Figure 5 shows that the major fraction of the overall magnitude can be found at a frequency of 2,93 Hz which is equivalent to the first order oscillation of the 175 RPM rotation which is caused by an imbalance of the rotor. Additional fractions can be found at 20th order and its multiples. These are caused by electromechanical effects in the 20 pole generator.

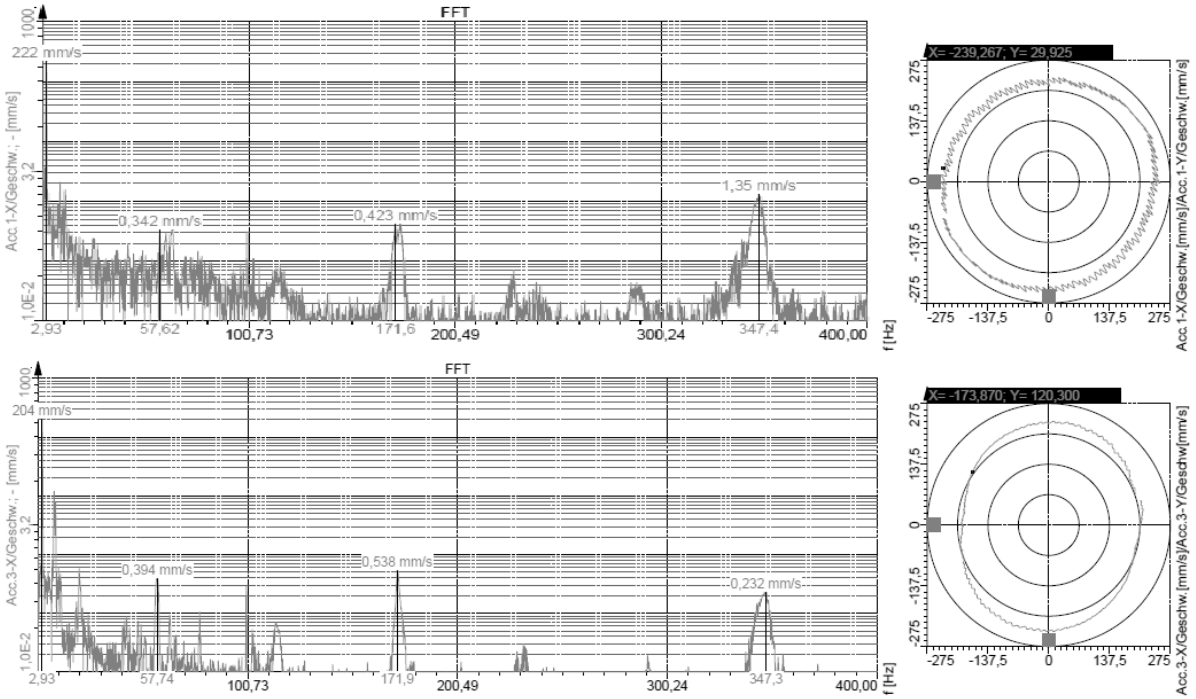

Figure 5: FFT-analysis (left) and shape (right) of the oscillation at level 1 (top) and level 2 (bottom) velocity at 175 RPM without decoupler

Compared to the results without decoupling element, the processed measurement results with decoupler in Figure 6 show that oscillations in particular those or higher frequencies are strongly damped. The first order oscillation however appears to have relatively high amplitudes under the decoupler. This can be explained by the fact that the dynamic masses are reduced by the decoupling element which leads to larger displacements at the top of the tower. As the dynamic oscillating masses were reduced by the decoupling element, the oscillation velocity can't be translated to forces and loads linearly. The fact that the local resonance occurs at a way higher RPM also makes it difficult to compare oscillation values as the driving forces at high wind speeds are higher

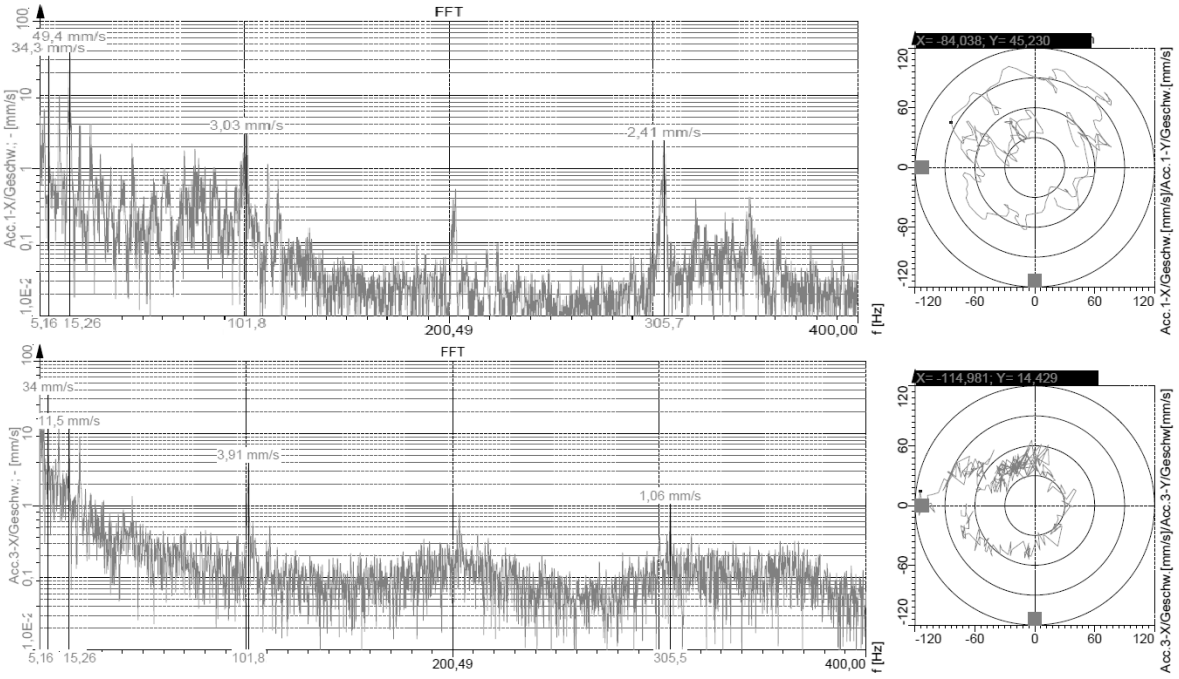

Figure 6: FFT-analysis (left) and shape (right) of the oscillation at level 1 (top) and level 2 (bottom) velocity at 304 RPM with decoupler

1.2.1.8 Summary of your findings and conclusions

The identified main cause for increased oscillations of SWT are intrinsic resonances which are stimulated at specific wind speeds. For the tested VAWT the major fraction of the oscillation magnitude was caused by an imbalance of the rotor.

With the installation of a decoupling element the higher frequency oscillations in the audible frequency range could be significantly reduced. Low frequency oscillations were not affected strongly by the decoupling element. With the deployed measurement setup it was not possible to determine the absolute loads therefore it is suggested to pursue the studies including dynamic simulation software to determine the dynamic loads.

1.2.1.9 References

[1] BAUA, 2016, Vibrationen, http://www.baua.de/de/Themen-von-A-Z/Vibration/Vibration_content.html, Letzter Zugriff: 21.04.2016

[2] Magnus, Popp, Sextro, 2008, Schwingungen – Eine Einführung in die physikalischen Grundlagen und die theoretische Behandlung von Schwingungsproblemen, 8. Auflage, Vieweg + Teubner Verlag, Wiesbaden.

[3] Twele, 2013, Empfehlungen zum Einsatz kleiner Windenergieanlagen im urbanen Raum – Ein Leitfaden, HTW Berlin, Berlin.

[4] Kuttner, 2015, Praxiswissen Schwingungsmesstechnik, Springer Vieweg, Wiesbaden.

VDI Wissensforum GmbH, 6. VDI-Fachtagung Schwingungen von Windenergieanlagen 2015, 2015, Bremen, VDI-Verlag Düsseldorf, ISBN 978-3-18-092242-3

1.3 BELGIUM (active 2017 – 2018)

The Belgian case study is included as an appendix at the end of this document.

1.4 CHINA (active 2009 – 2018)

1.4.1 *Validated CFD Models for Danish Fence Experiment Objects*

The rectangular solid fence vertical ground installation, wind direction and the fence surface into a 90 degree angle, interception of different height of the fence level, the study of the speed and turbulence characteristics of the fence. Comparison of experimental results and CFD simulation results are compared.

1.4.1.1 Project description

On the basis of experiments on the fence Denmark, turbulence characteristics of the wind blowing back in the direction of the French entity fence, under the fence and wind speed characteristics.

1.4.1.2 Software used

ANSYS 14.5 (DesignModeler, ICEM-CFD, FLUENT 14.5, CFD-POST), SOLIDERWORKES modeling, ORIGIN drawing.

1.4.1.3 Compute Field

fence height H = 3m, computational domain entry from the fence 3.3 H, exports from the fence 26.6H, where 16h is the slope ground, 10.6h flat ground, the computational domain of high 5H.

1.4.1.4 Fluid type

Incompressible fluid

1.4.1.5 Governing equations

Time averaged continuity equation

Time averaged Navier-Stokes equations

1.4.1.6 Turbulence model

Realizable k-ε turbulence model

1.4.1.7 Discretization methods

Second order schemes should be used for solving the equations

1.4.1.8 Computational grid

Use the ICEM - CFD grid, the grid size is related to the distance of the grid position from the fence, close to the grid density, distance away from the grid. The total number of meshes: 8,538,275, the total number of nodes: 8432041, hexahedral: 277748, Tetrahedron: 8,258,794, the minimum volume of 5.14 + e-7m3, the maximum volume is: 1.32m3.

1.4.1.9 Boundary Conditions for velocity and pressure

For the boundary conditions, the ground should be a non-slip wall with standard wall functions (Roughness Height=0.0016m), top and side should be symmetry, outlet should be pressure outlet and inflow would be a log law atmospheric boundary layer profile.

1.4.1.10 Inflow boundary condition assumptions

In this paper, inlet boundary condition was described using a UDF satisfying Eq(1) for the velocity Uy :

$$U_0(y)\frac{u_{est}}{k}ln\left(\frac{y}{z_0}\right)\text{----------(1)}$$

Where Uy is average speed at the height Z, Uest is the friction velocity, κ is von Karman's constant, κ=0.4.

Details

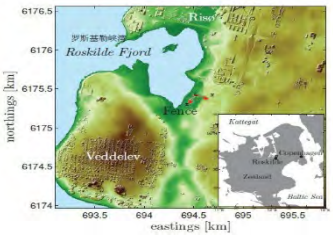

Fig. 1 Experimental sites

Fig. 2 Solid fence

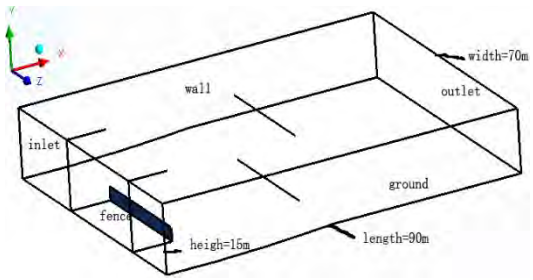

Fig. 3 Model parameters

1.4.1.11 CFD analysis results

1.4.1.11.1 Comparison of experimental and simulated values

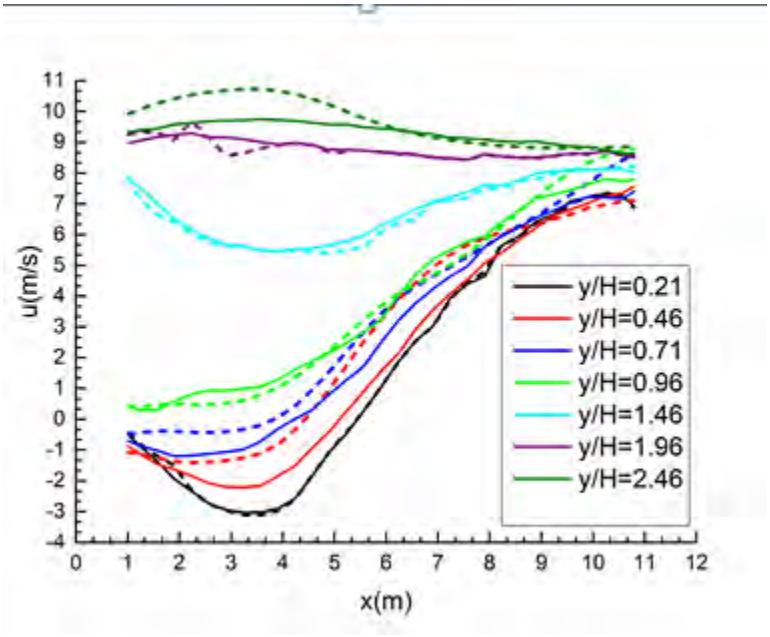

Fig. 4 Wind speed measurements a (solid lines) and CFD simulation results (dashed lines) for u

The solid line is the experimental value, the dotted line is simulated. The simulated value is higher than the experimental value.

(1)The velocity of different positions in the 10H tends to be stable.

(2)Y/H =[0.21,0.71] accelerated reflux effect.

1.4.1.11.2 Plane Turbulent Kinetic Energy

Taken in the direction along the height of the fence representative five different heights of the axial velocity u cloud. Plane Y=2.5m, plane Y=4m, plane Y=6m, plane Y=7.5m, plane Y=9m.

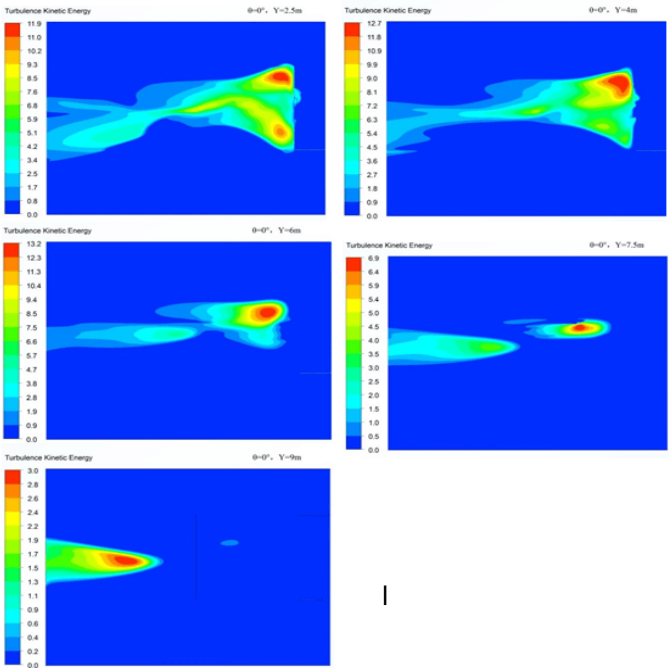

Fig. 5 The plane turbulent kinetic energy cloud

(1)As shown in Fig 5, after the wind flow around the fence, on the downstream side of the fence to form similar to the "goldfish" in the shape of a turbulent kinetic energy, turbulence kinetic energy is the rise of regional first increases with height after decreases, and by the "goldfish" region has shrunk into a circular region. Height at Y = 6 m, reach maximum turbulent kinetic energy, the value of 13.2.

(2)Along the flow direction of the wind, turbulence kinetic energy area gradually shrink. High fence at both ends of the formation of two turbulent kinetic energy circle area, along the direction of outer diameter diminishing turbulent kinetic energy.

(3) The fence that affect the downstream turbulence field: the range of the width of 11 H, the longest 27 H, up to 3H.

1.4.1.11.3 Velocity u

Taken in the direction along the height of the fence representative five different heights of the axial velocity u cloud. Plane Y=2.5m, plane Y=4m, plane Y=6m, plane Y=7.5m, plane Y=9m. Conclusion by analyzing the five surface: the hedge the impact of downstream speed u, its overall shape was "凸" .

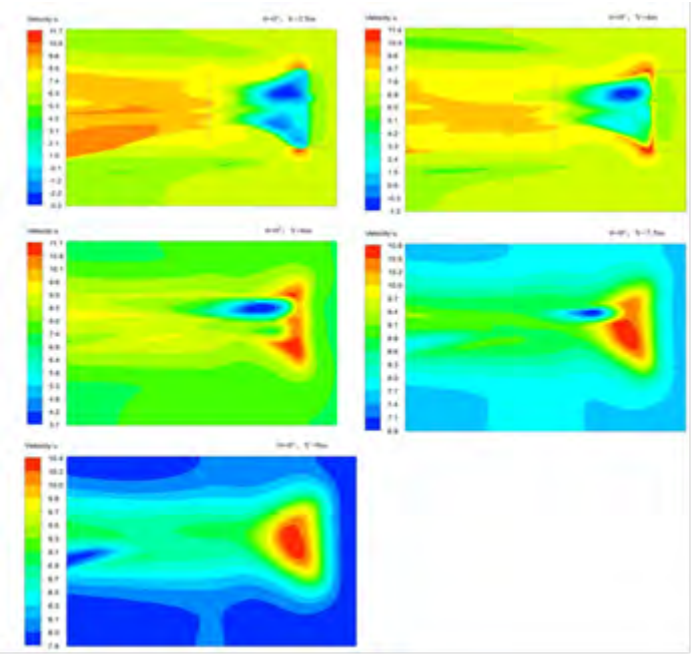

Fig 6. Fences of different height level downstream velocity profile u

(1)Long the height of the fence, with the increase of height range of impact speed of u fence is gradually enlarged and reduced, by plane Y=7.5m showed that the height of 7.5m, the effect on the wind speed of y=2.5H reaches the maximum value of the fence.

(2)Y=2.5m and Y=4m by plane velocity contours, can be clearly seen in the lateral ends of the fence, the formation of wind acceleration region similar to "half". The maximum wind speed is about 11m/s, the inflow wind speed is about 7m/s, the maximum acceleration effect can reach about 1.5 times. The plane Y=2.5m velocity image shows that the inside of the fence at both ends of the 1H, the height of the fence to form 2 circular flow area, a strong weak. As the height increases, the range of the 2 recirculation zones decreases, and the recirculation zone completely disappears when the height is 3H.

1.4.1.11.4 Turbulence intensity

Choose 1/2 fence length (15m), take the fence to cause obvious characteristics of the turbulent flow, both vertical and vertical ground and vertical fence of the 5 planes, respectively, A plane, B plane, C plane, D plane, E plane. The turbulence intensity of each plane from 9 **vertical** line, numbered 1 to 9, the number is larger, the distance from the location of the fence line farther, drawing 4.The 15m, the average is divided into 3 parts, the fence side 5m called the turning point, the fence center at 5m, known as the central area, located between the inflection point and the central area of the 5m called the transition zone. Where the D, E plane is located in the inflection point, B, C is located in the central area, A is located in the center area.

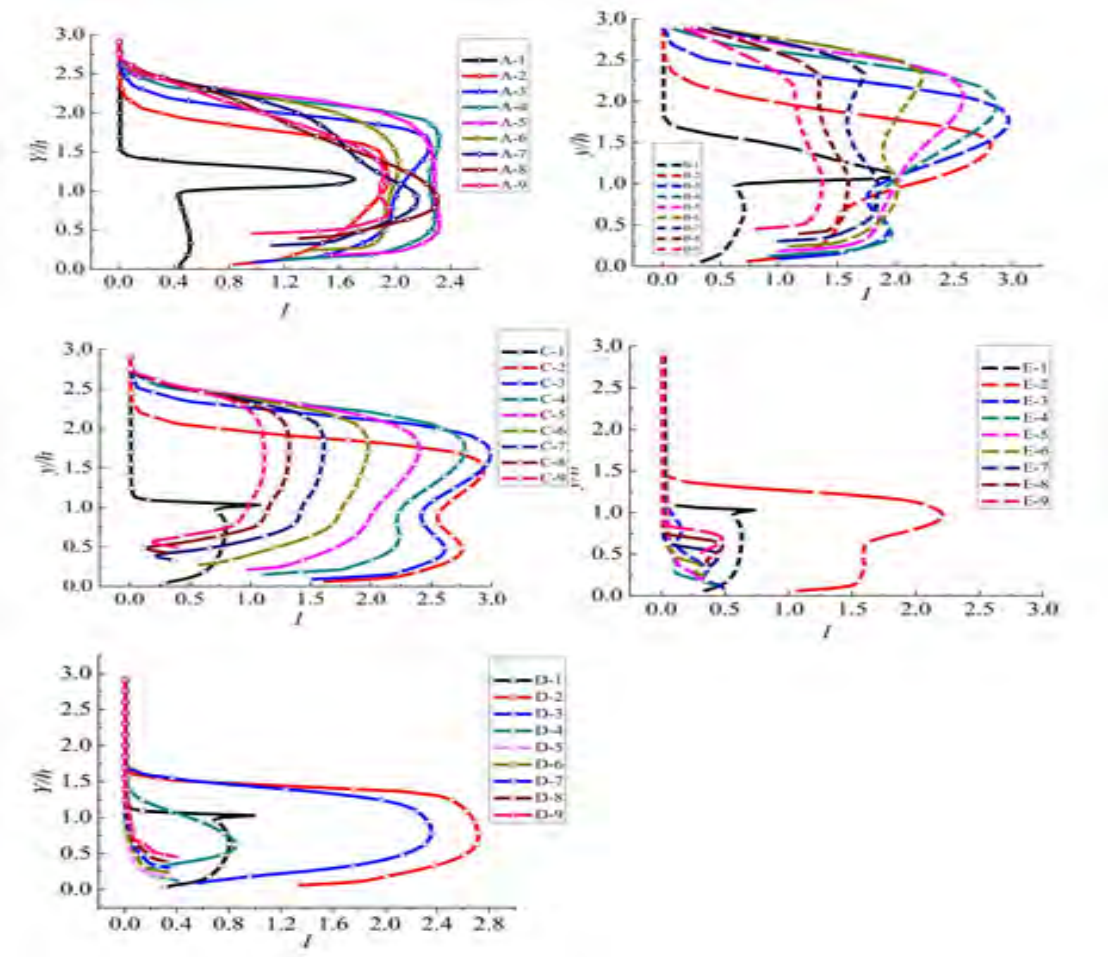

Fig. 7 Turbulence intensity at different heights

(1)The turbulence intensity is above the position of the fence, represented by the black line diagram position in Y=1H, mutations to the maximum.

(2)The turbulence intensity of the lower fence reaches the maximum value at the Y=[0.5,1]H of the turning point region, the maximum value is reached at the Y=[1,2]H of the transition region, and the maximum value is reached in the Y=[0.5,2]H range of the central region.

(3) The turning point region of the fence downstream, Y=1.5H, turbulence intensity sharply disappeared, transition area and center area when the turbulence intensity disappeared at Y=2.7H.

(4)In the lower reaches of the fence, the turbulence intensity is small, and conversely the turbulence intensity becomes larger. Near the end of the fence, this phenomenon is more obvious.

1.4.1.11.5 Conclusion

1.4.1.11.5.1 Velocity characteristics

1) The velocity u at different positions, convergence after x/H=10.

2) The acceleration reflux effect appears at y/H= [0.21,0.71] .

3) Outside the fence, the semi-circular region of speed-up. Inside the fence, 2 circular regions of back flow .Area decreases with height increase， y/H=3 disappear.

1.4.1.11.5.2 Turbulence characteristics

1) At both corner of the fence, 2 circular areas of high turbulent kinetic energy are formed, and the turbulent kinetic energy decreases along the outer diameter direction.

2) The range of turbulent kinetic energy in Downstream fence ： The most wide distance z:11H, the longest distance:27H, τhe highest :3H.

3) The turbulence intensity of downstream fence reaches the maximum value at the Y=[0.5,1]H of A corner zone, the maximum value is reached at the Y=[1,2]H Transition zone , and the maximum value is reached in the Y=[0.5,2]H range of the central zone.

1.4.2 CFD Case Study for Different Roof Types (Flat and Triangle)

1.4.2.1 *Engineering and Technology Building on the IMUT campus project description*

Based on the urban atmospheric boundary layer theory, more accurate and suitable inflow condition for the building environments has been introduced. A case named Engineering and Technology Building, ETB for short, in the campus of Inner Mongolia University of Technology was modeled. What's more, the wind turbulent characteristics of different zones at the top of the building were analyzed comprehensively, and the wind turbulent characteristics of three types of flat roofs were concluded initially. A new numerical micro-sting method of rooftop wind turbines was introduced, and it depends on the analyses of the wind turbulent characteristics of the rooftop using urban atmospheric boundary layer, U-ABL for short, which provided a new idea for the micro-sitting of the rooftop turbines in urban environment.

1.4.2.2 Numerical Model

Realizable k-ε turbulence model

1.4.2.3 Software used

Meshed by ICEM-CFD & Compute by FLUENT

1.4.2.4 Compute Field

If H is the height of the ETB, the Vertical direction dimension is 8H, the lateral dimension equals to 8H and flow direction dimension is 15H, while the blockage ratio is 3%.

1.4.2.5 Fluid type

Incompressible fluid

1.4.2.6 Governing equations

$$\frac{\partial(\rho k)}{\partial t}+\frac{\partial\left(\rho k\overline{u_j}\right)}{\partial x_j}=\frac{\partial}{\partial x_j}\left[\left(\mu+\frac{\mu_t}{\sigma_k}\right)\frac{\partial k}{\partial x_j}\right]+P_k+G_b-\rho\varepsilon-Y_M+S_k$$

$$\frac{\partial(\rho\varepsilon)}{\partial t}+\frac{\partial\left(\rho\varepsilon\overline{u_j}\right)}{\partial x_j}=\frac{\partial}{\partial x_j}\left[\left(\mu+\frac{\mu_t}{\sigma_\varepsilon}\right)\frac{\partial\varepsilon}{\partial x_j}\right]+\rho C_1\overline{S}\varepsilon-C_2\rho\frac{\varepsilon^2}{k+\sqrt{\nu\varepsilon}}+C_{\varepsilon1}\frac{\varepsilon}{k}C_{\varepsilon3}G_b$$

1.4.2.7 Turbulence model

Realizable k-ε turbulence model

1.4.2.8 Discretization methods

Second order schemes should be used for solving the equations

1.4.2.9 Computational grid

Meshed by ICEM-CFD

1.4.2.10 Boundary Conditions for velocity and pressure

The semi-log wind profile is used in this case as follows:

$$U(z)=\frac{U^*}{\kappa}\ln\left(\frac{z-d}{z_0}\right)\qquad z\geq z_{ref}$$

$$U(z)=U_{ref}\ \exp\left(\alpha\left(\frac{z}{z_{ref}}-1\right)\right)\qquad z\leq z_{ref}$$

Where the Uave=3.2m/s （10m） , z_{ref}=20m,U_{ref}=3.885m/s, U*=0.786m/s, d=8.739m and z_0=1.411m.

1.4.2.11 Inflow boundary condition assumptions

In this paper, inlet boundary condition was described using a UDF satisfying Esq. (1) ~ (4) for the velocity U_Z, turbulent kinetic energy k and turbulent diffusion rate ε which modified by semi-logarithmic law:

$$U(z)=\frac{0.786}{\kappa}\ln\left(\frac{z-8.739}{1.411}\right)\qquad z\geq 20m \qquad (1)$$

$$U(z)=3.885\times\exp\left(2.112\times\left(\frac{z}{20}-1\right)\right)\qquad z\leq 20m \qquad (2)$$

$$k=\frac{U^{*2}}{\sqrt{C_\mu}}\sqrt{C_1\ln\left(\frac{z+z_0}{z_0}\right)+C_2} \qquad (3)$$

$$\varepsilon=\frac{U_*^3}{\kappa(Z-Z_0)}\sqrt{C_1\ln\left(\frac{Z+Z_0}{Z_0}\right)+C_2} \qquad (4)$$

Where U_Z is average speed at the height Z, U_* is the friction velocity, κ is von Karman's constant. Z_0 is the surface roughness and C_μ is the turbulence model constant. C_1 and C_2 are constants equal to -0.17 and 1.62, which depend on the suggestion of Yang.

1.4.2.12 CFD analysis results

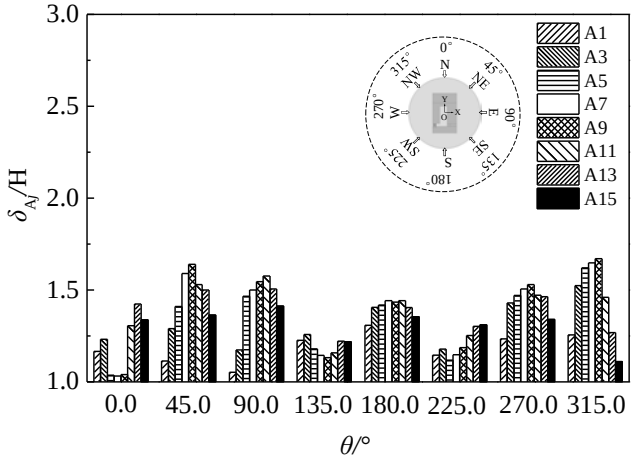

Fig. 1 Distribution of δ_{Aj} for each column at the top of the roof A

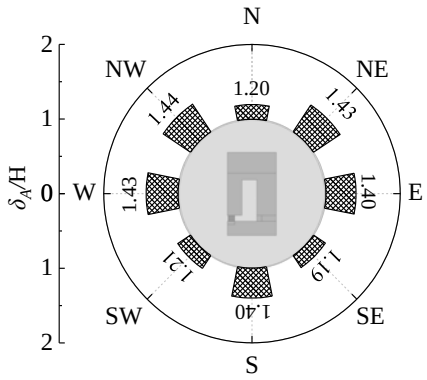

Fig. 2 Distribution of δ_A at the top of the roof A

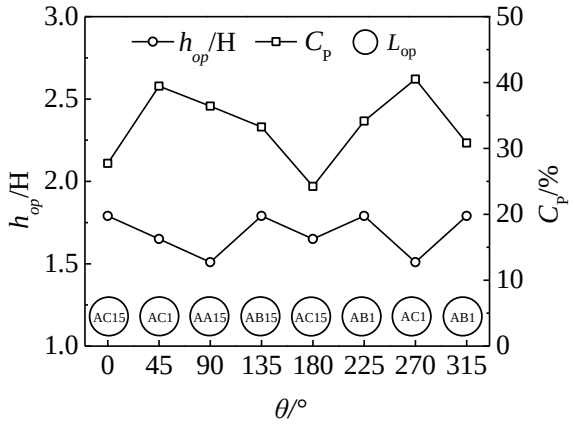

Fig. 3 Distribution of δ_{Aj} for each column at the top of the roof A

The wind profile in Hohhot was considered. Using the turbulent characteristic parameters, such as turbulent intensity and wind acceleration factor, wind turbulent characteristics of the zone A at the top of the ETB were analyzed. The suitable wind turbine installation height is up to 1.30 times the ETB's height from the ground and the suitable installation position is the frontier point. The average turbulent thickness was introduced originally, which plays a significant role on the precisely micro-sitting of a selected vertical axis wind turbine. Further, statistical analysis has been done about the turbulent parameters of the zone A under eight wind directions and the average wind speed in Hohhot. The most precise result has been found that the optimum installation height above ground interval 1.51 to 1.79 times the ETB's height and the best locations are the forefront points, which are edge points of Zone A under different wind directions. Also, the results show that the average turbulent thickness is about 1.34H, which will provide a reference for micro-sitting of wind turbine at top of the building.

1.4.2.13 Findings

According to the turbulent characteristic distribution of the different zones at the top of the ETB and based on the urban atmosphere boundary layer theory, a new numerical micro-sting method of rooftop wind turbine was introduced. It depends on the analyses of the wind turbulent characteristics of the rooftop using U-ABL. This provided a new idea and a new method for the micro-sitting of the rooftop turbines in urban environment.

1.4.3 CFD Case Study a Storage Container in Zhang-bei

1.4.3.1 Project description

Container placed in Zhangbei wind power construction base. The length and breadth of container is 12.4m×2.4m and the height is 3m. 270° , 292.5° , 315° , 335.5° and 360° are chose for the simulations.

1.4.3.2 Numerical Model

Standard k-ε turbulence model

1.4.3.3 Software used

Meshed by ICEM-CFD & Compute by FLUENT

1.4.3.4 Compute Field

If H is the height of the container, the Vertical direction dimension =5H, the lateral dimension=5H+container width and flow direction dimension = 15H, while the blockage ratio is 1%.

1.4.3.5 Fluid type

Incompressible fluid

1.4.3.6 Governing equations

$$u_j \frac{\partial u_i}{\partial x_j} = -\frac{\partial p}{\partial x_i} + \frac{\mu}{\rho}\frac{\partial^2 u_i}{\partial x_i \partial x_j} - \frac{\partial}{\partial x_j}(\overline{u_i' u_j'})$$

$$\frac{\partial u_j}{\partial x_j} = 0$$

1.4.3.7 Turbulence model

Standard k-ε turbulence model

1.4.3.8 Discretization methods

Second order schemes should be used for solving the equations

1.4.3.9 Computational grid

Meshed by ICEM-CFD

1.4.3.10 Boundary Conditions for velocity and pressure

For the boundary conditions, the ground should be a non-slip wall with standard wall functions (Roughness Height=0.20m), top and side should be symmetry, outlet should be pressure, outlet and inflow would be a log law atmospheric boundary layer profile.

1.4.3.11 Inflow boundary condition assumptions

In this paper, inlet boundary condition was described using a UDF satisfying Esq. (1) ~ (3) for the velocity UZ, turbulent kinetic energy k and turbulent diffusion rate ε which modified by logarithmic law:

$$U_Z = \frac{U_*}{\kappa}\ln\left(\frac{Z - Z_0}{Z_0}\right) \quad (1)$$

$$k = \frac{U_*^2}{\sqrt{C_\mu}}\sqrt{C_1 \ln\left(\frac{Z + Z_0}{Z_0}\right) + C_2} \quad (2)$$

$$\varepsilon = \frac{U_*^3}{\kappa(Z - Z_0)}\sqrt{C_1 \ln\left(\frac{Z + Z_0}{Z_0}\right) + C_2} \quad (3)$$

Where U_Z is average speed at the height Z, U_* is the friction velocity, κ is von Karman's constant. Z_0 is the surface roughness and C_μ is the turbulence model constant. C_1 and C_2 are constants equal to -0.17 and 1.62, which depend on the suggestion of Yang.

1.4.3.12 CFD analysis results

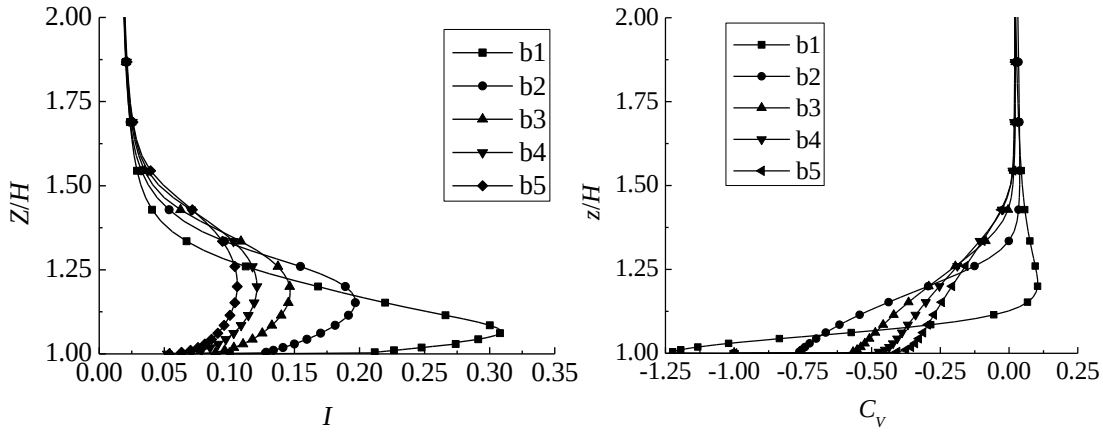

Fig. CFD analysis results

1.4.3.13 Findings

According to the International Electrotechnical Commission (IEC) Standard 61400-12, a turbine should not be exposed to wind with turbulence intensity greater than 0.25 and installed at the zone without high velocity gradient. Hence it is vital to estimate I and C_V at the turbine mounting locations. Fig.3(a) shows that the maximum value of turbulence intensity reaches up to 0.31 at location b1, and the zone where Z/H is greater than 1.17 doesn't belong to the high turbulence section. Fig.3(b) shows that the most pronounced speed up effect occurs at the frontier sites compared with other locations above the container, this significant phenomenon disappears when the height reach up to 1.60H. Therefore, the wind turbine should be installed at frontier points at the height of 1.17H~1.60H.

1.4.4 CFD Case Study for the U.S. Johnson Space Center/NASA Rooftop Test Facility

1.4.4.1 Project description

The flows around the NASA Building 12 would be simulated adopting a CFD code in order to investigate the acceleration and turbulence intensity on the roof.

The configuration of NASA Building is illustrated in Fig.1 a) and b). The size is 70.67 meters long, 45.29 meters wide and 9.14 meters high, provided by Prof. Charlie Dou.

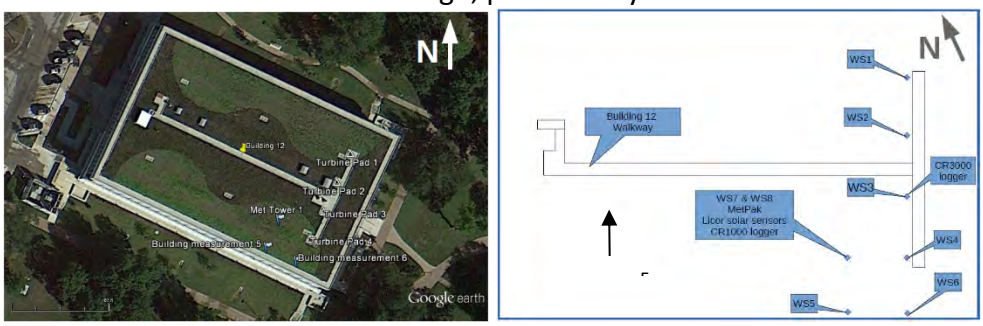

a) photo b) sketch

Fig. 1 configuration of the building

Flow conditions: the wind speed and direction are according to the 09:00, March 05, 2015 (Fig.2). That is, wind speed is about 7m/s, flow direction is about 200 degrees. Therefore, the flow is almost face to the building directly.

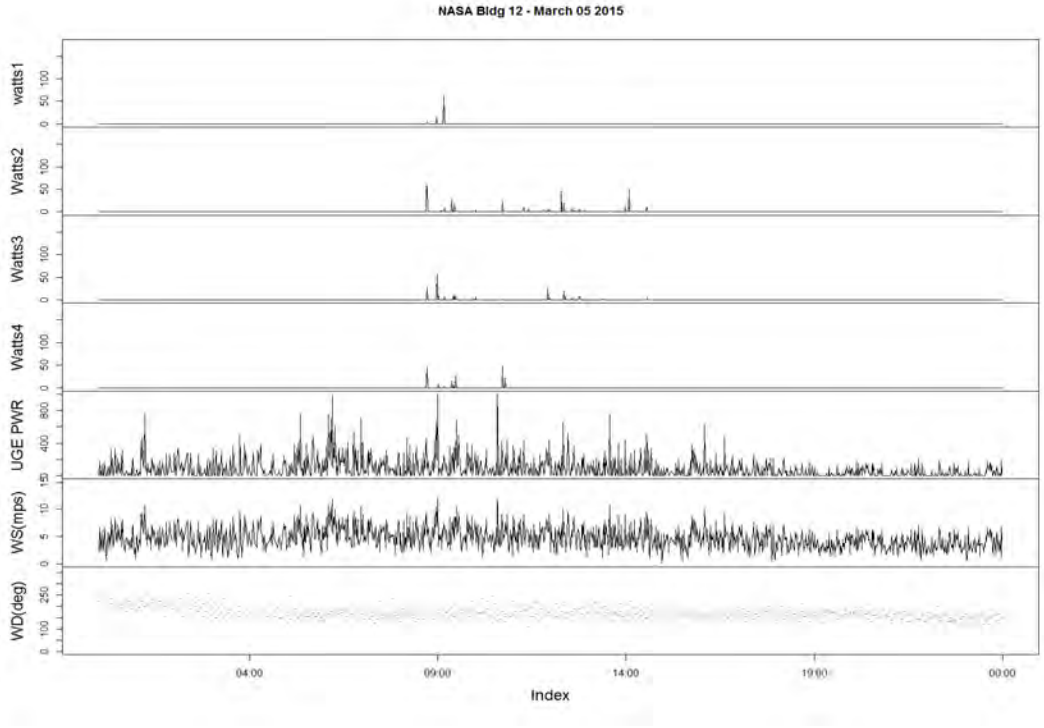

Fig. 2 Wind speed and direction

1.4.4.2 Numerical model

The code was developed in CFD Lab of Beihang University of China, for the application of aeronautics and astronautics. It is based on the cell-center finite volume method. A Godunov-type numerical scheme is used for the inviscid flux calculation and central scheme for viscous terms. The interpolation of flow variables from cell center to the cell interface is linear with the Van Leer limiter. Analytical 1-D Riemann Solver is used for the variable jumps on the both sides of the cell interface. LU-SGS iteration for the implicit time discretization is implemented until the steady flow is reached.

1.4.4.3 Computation Zone

Fig.3 illustrates the computation zone. It is a cylinder with radius 1000m and height 2000m, and the building is at the center of the bottom.

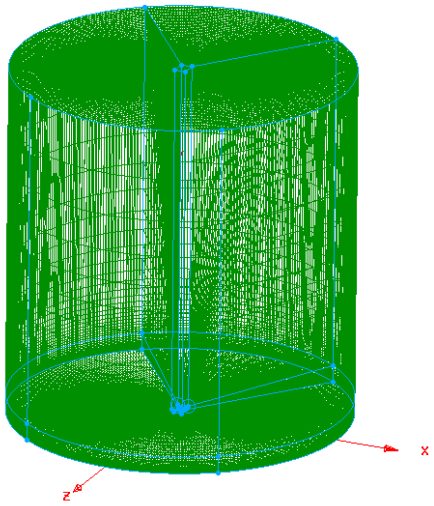

Fig. 3 Computation zone

1.4.4.4 Computation grid

The multi-block grid system is generated using the software Gridgen. The total grid number is about 2,300,000. The normal grid interval near solid walls (ground and the building) is 1mm.

1.4.4.5 Governing equations

The compressible Reynolds' averaged Navier-Stokes equations is used for the simulation, the viscosity coefficient is calculated with Sutherland's formula. The flow pressure is related to the density and temperature with the state equation: p= RT.

1.4.4.6 Turbulence model

A two-equation turbulence model called Menter's k- SST is used.

1.4.4.7 Time Integration

An iteration LU-SGS algorithm is applied for the steady flow computation.

1.4.4.8 Boundary Condition

The boundary conditions are set at the ghost cells. On the solid wall, the velocity is no-slip and the turbulence eddy viscosity coefficient is zero. The variables at the ghost cells near wall are set with linear extrapolation. The upstream boundary is set as the inflow, with the given velocity as in the boundary layer:

$$\frac{U}{U_e} = \left(\frac{y}{\delta}\right)^{1/7}$$

Where $U_e = 10\mathrm{m/s}$, $\delta = 500\mathrm{m}$.

For the downstream boundary, the out flow variables are set as zero gradient. On the top boundary, no reflection boundary is applied.

1.4.4.9 CFD analysis results

Fig.4 gives the u velocity contour at z=0m (center), 34m(near the corner) and 45m (no building) sections. At the center, severe separation flow on the top of the building. At z=34m, the separation zone is much smaller due to corner. The velocity at the plane 34m is shown in Fig.5. The red symbols represent the velocity at x=-100, where is the upstream flow. The velocity acceleration is 30% to 60%.

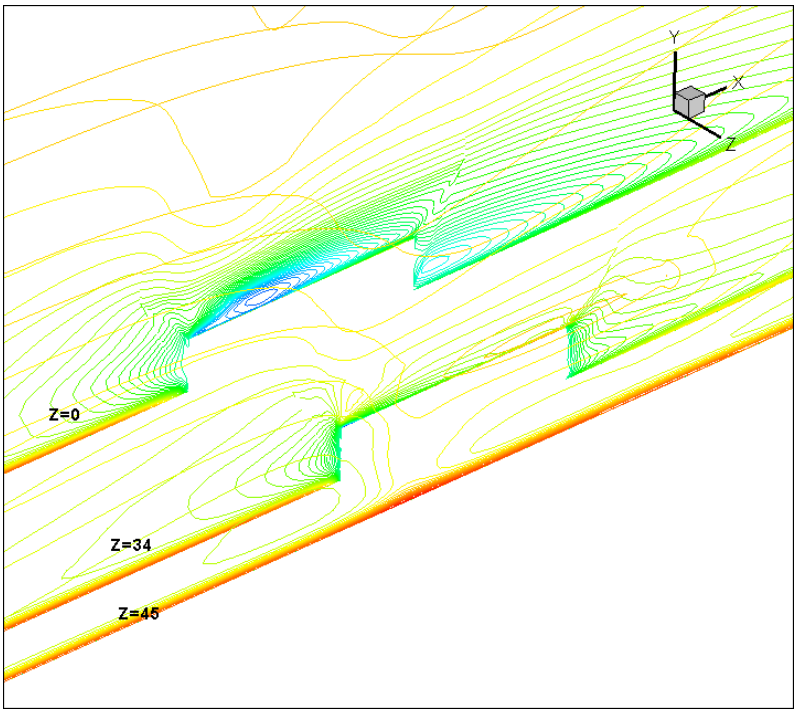

Fig. 4 U velocity contours

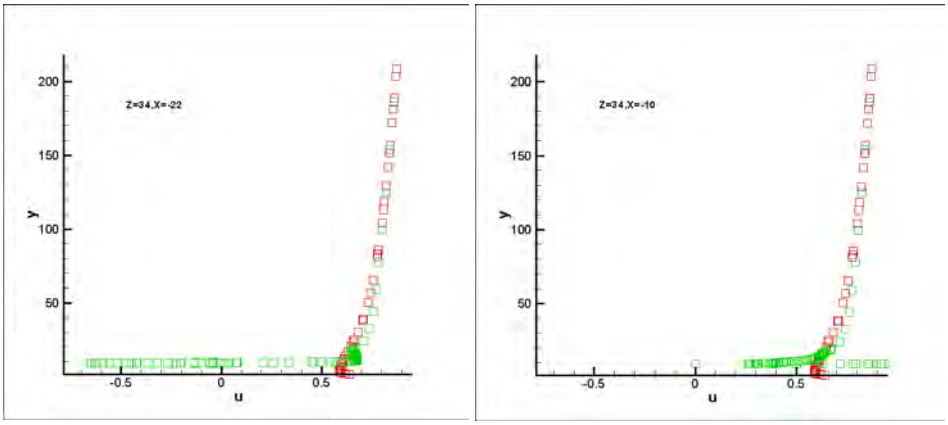

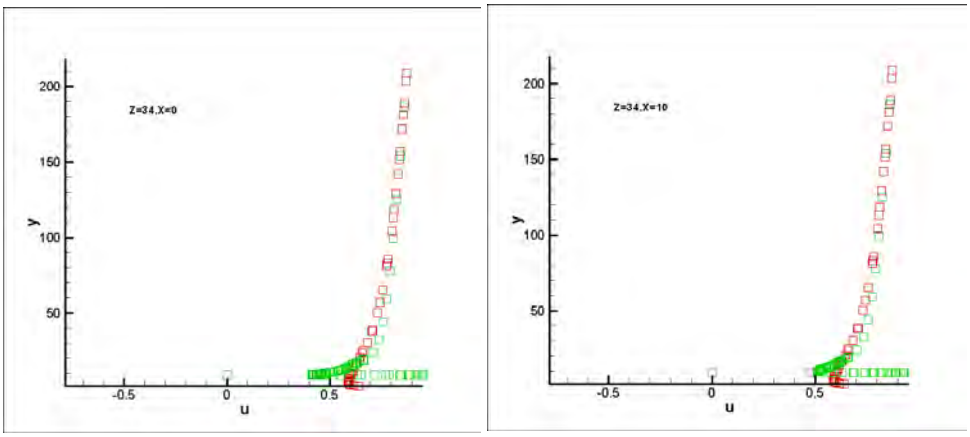

Fig. 5 Velocity distribution

Caution: the flow simulation was complemented preliminarily and not validated. The effect of the grid dependence and turbulence model should be investigated carefully in the near future.

1.4.5 CFD Results for Flat Roof Building Cluster with Different Plan Densities

1.4.5.1 Project description

The single building within the building cluster (included nine buildings), chose to the height of 3 meters, such as a ladder & two five-story building. The buildings have flat roofs and spaces between two buildings varied from 13.5m to 35m.

Based on the urban atmospheric boundary layer theory, more accurate and suitable inflow condition for the building environments has been introduced. The turbulence characteristics of building clusters with different λ_p are researched by the CFD. λ_p is the plan densities of the building cluster. Five kinds of the plan densities, such as λ_p=26%, λ_p=20%, λ_p=18%, λ_p=16%, λ_p=14%, are analyzed. The installation guides of roof wind turbine for building clusters with different plan densities are preliminarily established.

1.4.5.2 Software used

Meshed by ICEM-CFD & Compute by FLUENT

1.4.5.3 Compute field

If H is the average height of the building (H=15m), the distance from the front entrance to the windward side of the building is 10H, the distance from the side of the building to the boundary of the computational domain is 5H, the distance between the top surface and the boundary of the computational domain is 5H.The exit boundary is placed at the distance from the 20H of the building, while the blockage ratio is 3%.

1.4.5.4 Fluid type

Incompressible fluid

1.4.5.5 Governing equations

Time averaged continuity equation

Time averaged Navier-Stokes equations

1.4.5.6 Turbulence model

Realizable k-ε turbulence model

1.4.5.7 Discretization methods

Second order schemes should be used for solving the equations

1.4.5.8 Computational grid

ICEM-CFD is used to partition the unstructured tetrahedral meshes. The first layer height of grid is 0.025m & growth rate is 1.2 and about 6 layers. The quantity of grid is 5 million -7.5 million.

1.4.5.9 Boundary conditions for velocity and pressure

For the boundary conditions, the ground should be a non-slip wall with standard wall functions (Roughness Height=0.012m), top and side should be symmetry, outlet should be pressure outlet and inflow would be a log law atmospheric boundary layer profile.

1.4.5.10 Inflow boundary condition assumptions

In this paper, inlet boundary condition was described using a UDF satisfying Eq(1) for the velocity U_Z:

$$U(Z) = 6.7\exp\left[2.688\left(\frac{Z}{30}-1\right)\right](forZ \le 15m)$$
$$U(Z) = \frac{0.55}{\kappa}\ln\left(\frac{Z-12.28}{0.26}\right)(forZ > 15m) \quad (1)$$

Where U_Z is average speed at the height Z, U_* is the friction velocity, κ is von Karman's constant, κ=0.41.

The turbulence intensity of the inlet boundary condition is 10%.

1.4.5.11 CFD analysis results

1.4.5.11.1 Turbulence intensity

Contours of turbulence intensity above the roof level for λ_p=26% and λ_p=14% building array are listed.

For building cluster with λ_p=26%(Fig1), a wind turbine is not suitable to install below the height of 1.1H; When the height is higher than 1.2H, all the positions of buildings in the group, expect B(2-2) and B(3-3), may consider the installation of wind turbines on the roof; When the installation height is above 1.4H, it can be installed in any position in all buildings.

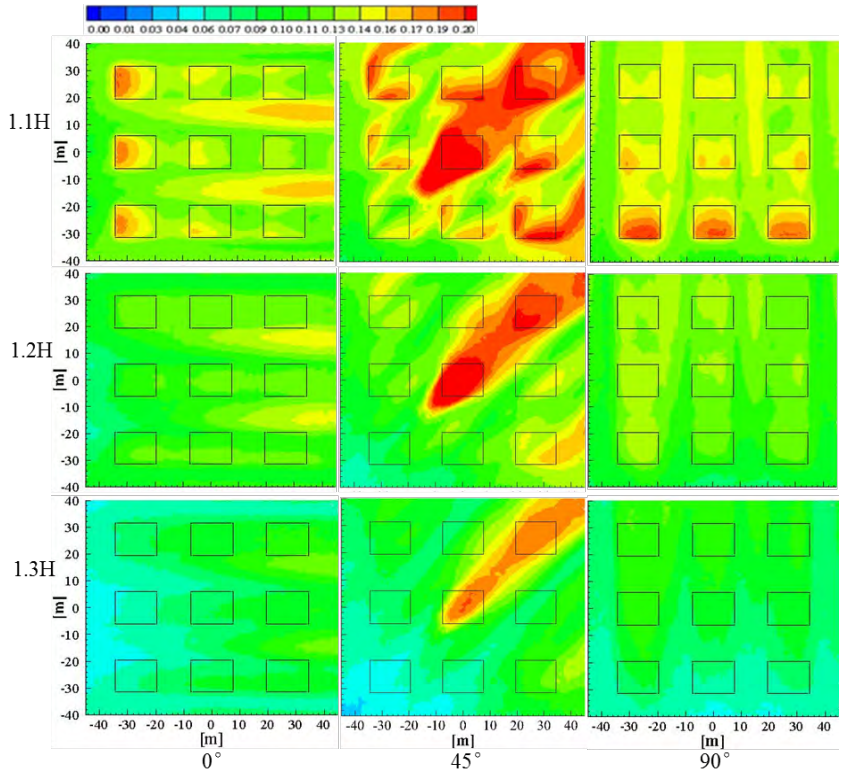

Fig. 1 Turbulence intensity above the roof level for λ_p=26% building array

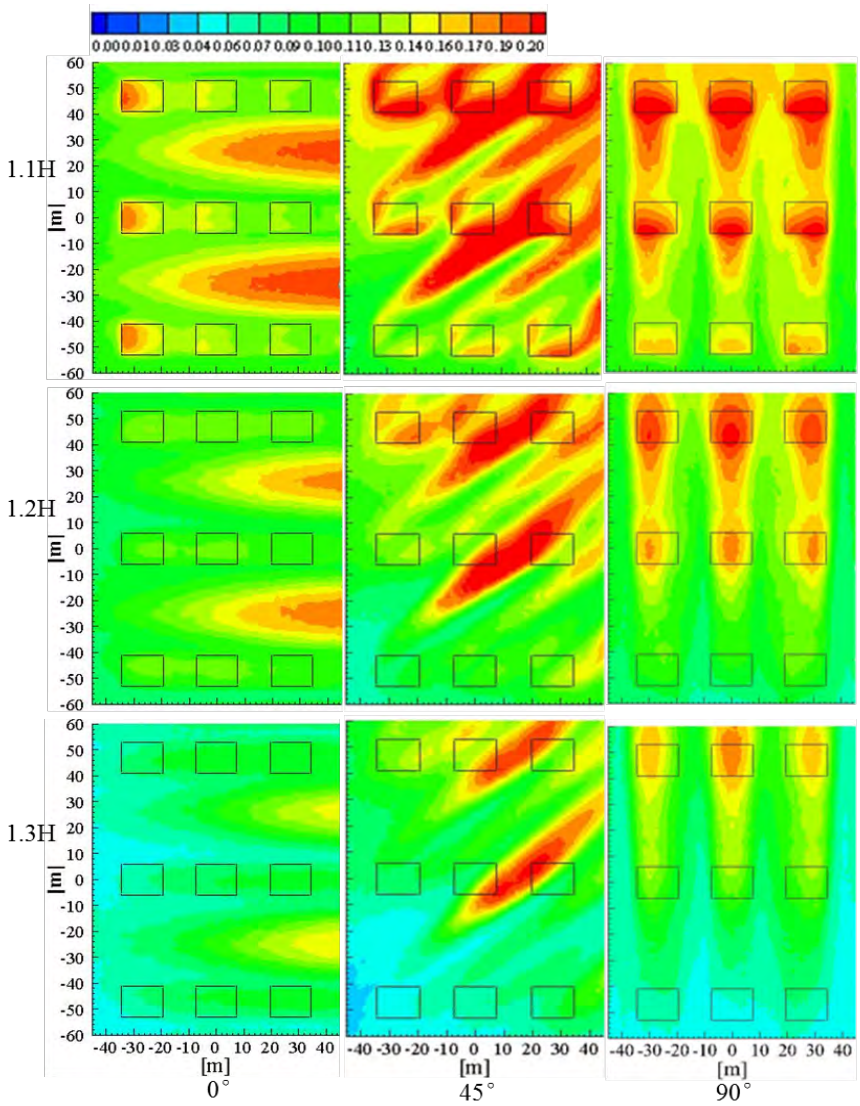

Fig. 2 Turbulence intensity above the roof level for λ_p=26% building array

For building cluster with λ_p=26% (Fig. 2), a wind turbine is not suitable to install below the height of 1.1H; When the height is higher than 1.2H, all the positions of the first flat roof of the building group may consider the installation of wind turbines on the roof. When the installation height is above 1.4H, it can be installed in any position in all buildings.

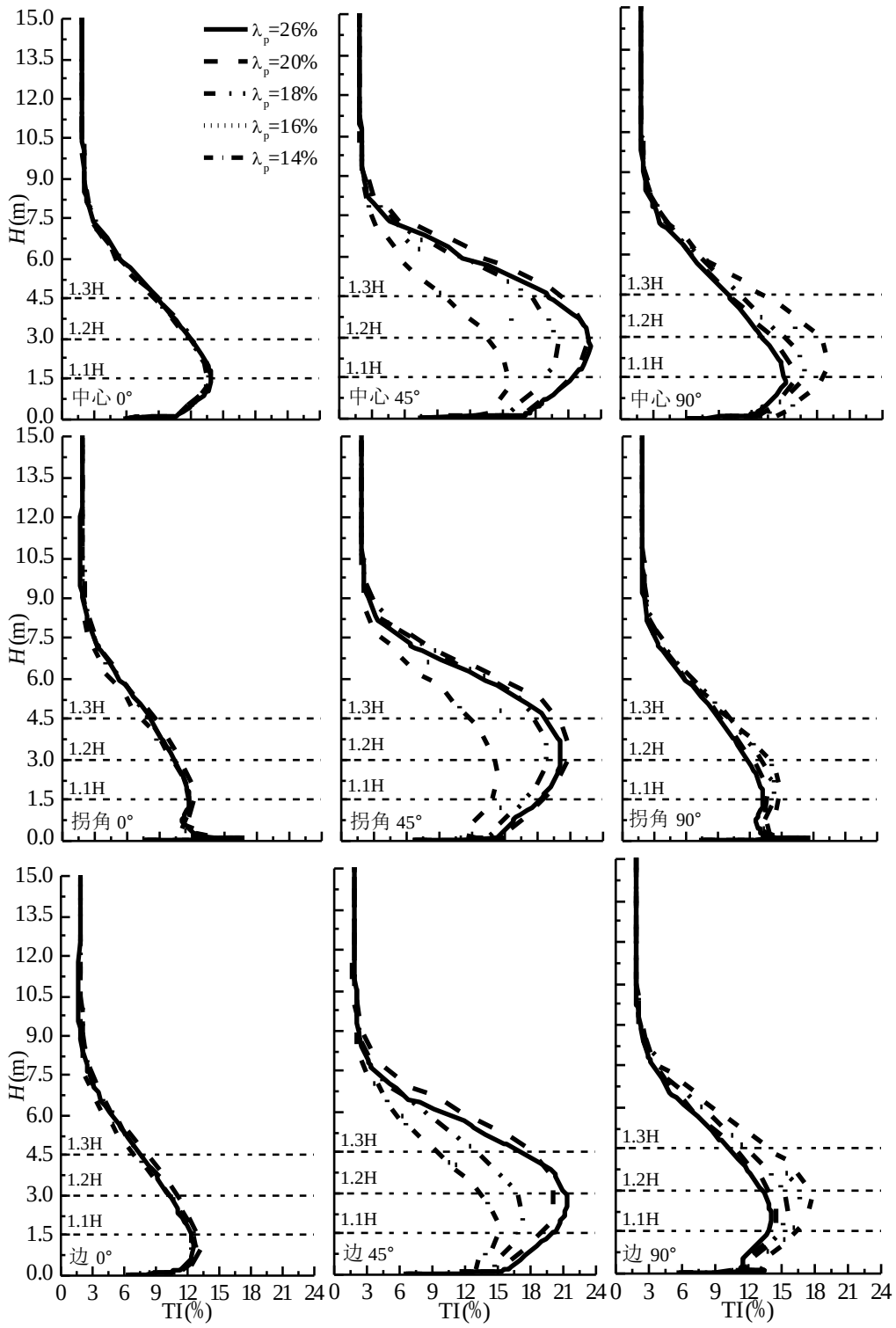

Fig. 3 Turbulence intensity at the center, corner and edge of the building

For building cluster with λ_p=26%,λ_p=20%,λ_p=18%,λ_p=16%,λ_p=14%, respectively, a wind turbine is not suitable to install below the height of 1.1H;And the height of roof wind turbine must be higher than 1.2H in order to avoid the strong turbulence intensity above the top of the building

group. When the height is higher than 1.4H, influence of the plan densities on turbulence intensity is neglected. At the same time, roof wind turbine can be installed in any position in all buildings.

For the first flat roof of the building group, influence of the plan densities on turbulence intensity is neglected when the height is higher than 1.2H, and roof wind turbine can be installed in any position of the first flat roof of the building group.

1.4.5.11.2 Velocity field analysis

Contours of C_v above the roof level for λ_p=26% and λ_p=14% building array are listed. The value of C_v is wind acceleration factor.

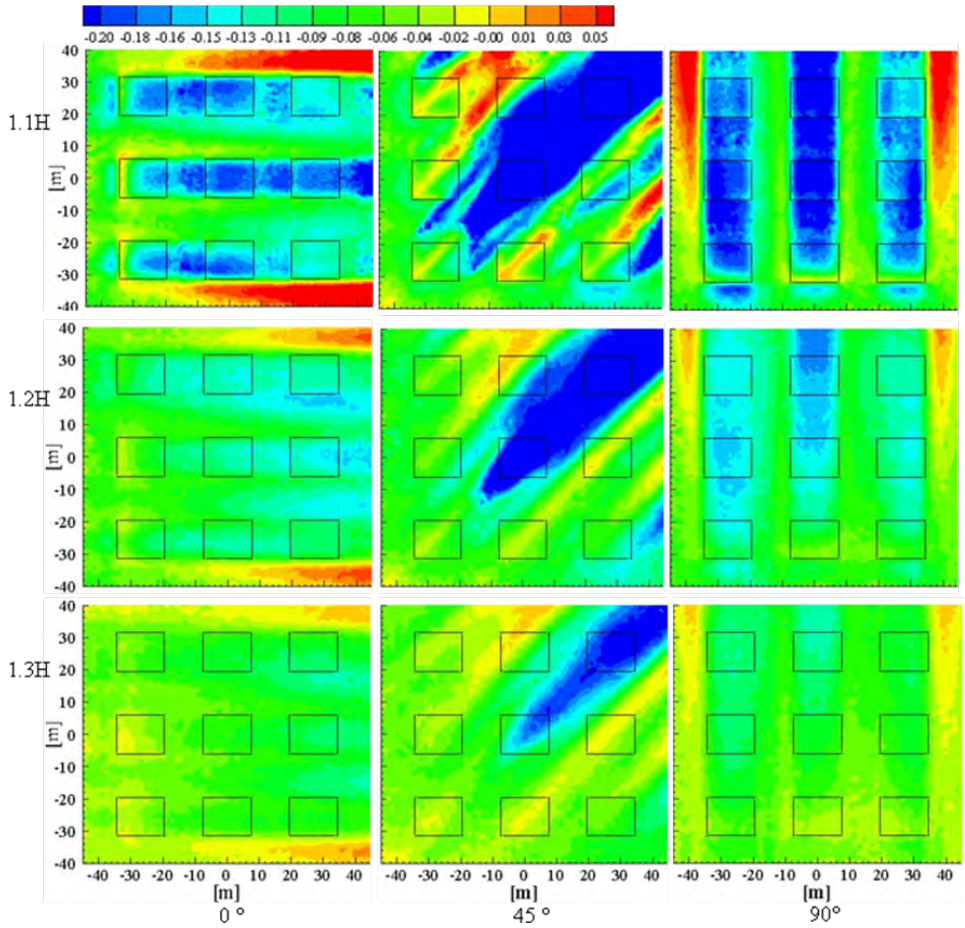

Fig. 4 Contour *of* C_v above the roof level for λ_p=26% flat roof array

For building cluster with λ_p=26% (Fig. 4), there is no obvious acceleration effect on the top of the building, and the wind speed is gradually recover to the arrival of wind speed with the height. When the height is higher than 1.3H, wind speed of all the positions of buildings in the group, expect B(2-2) and B(3-3), return to the arrival of wind speed; When the height is higher than 1.5H, wind speed of all the positions of buildings in the group recover the arrival of wind speed.

For building cluster with λ_p=14% (Fig. 5), there is no obvious acceleration effect on the top of the building. When the height is higher than 1.2H, wind speed of the first flat roof of the building group return to the arrival of wind speed; When the height is higher than 1.5H, wind speeds of all the positions of buildings in the group recover the arrival of wind speed.

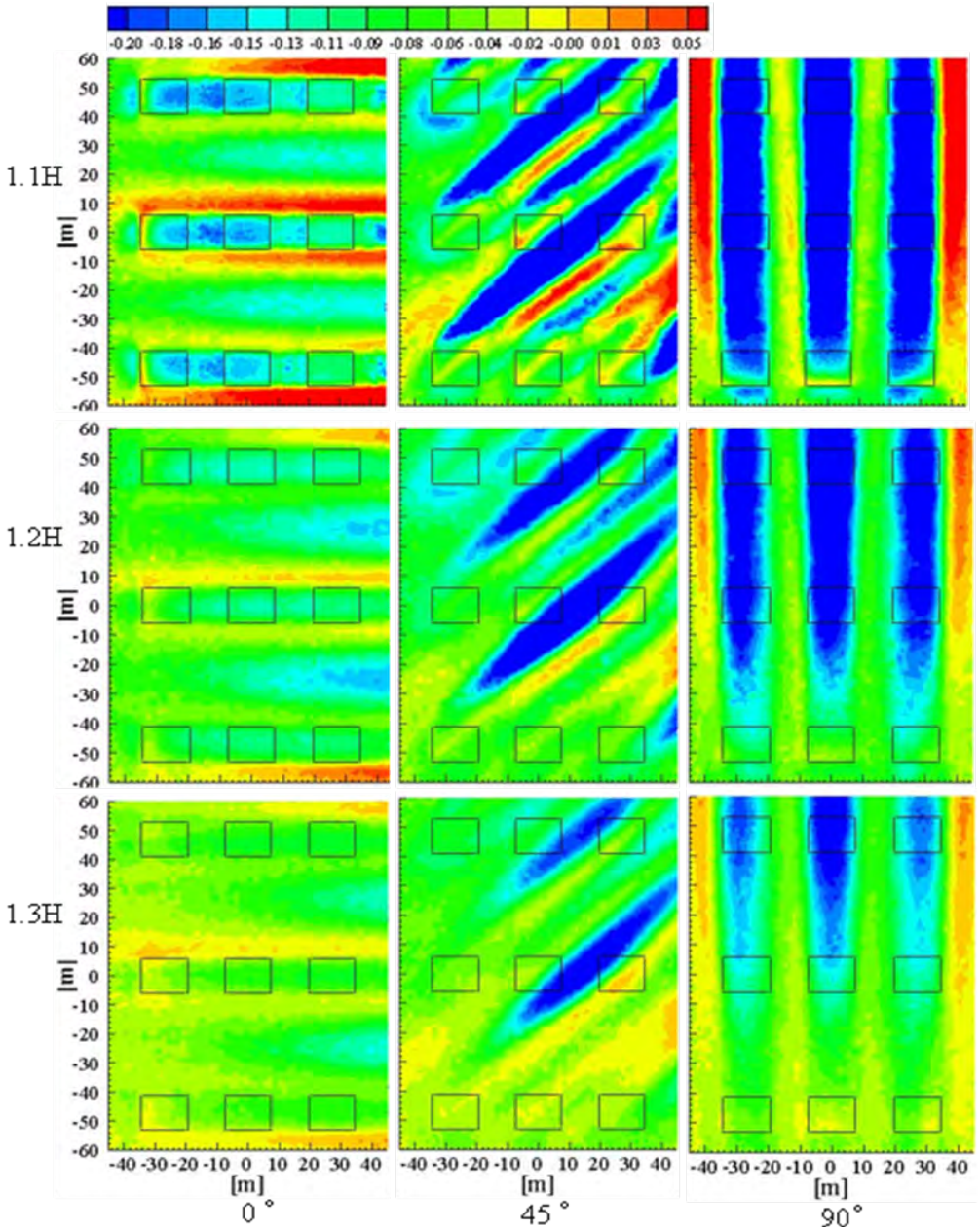

Fig. 5 Contour *of* C_v above the roof level for λ_p=14% flat roof array

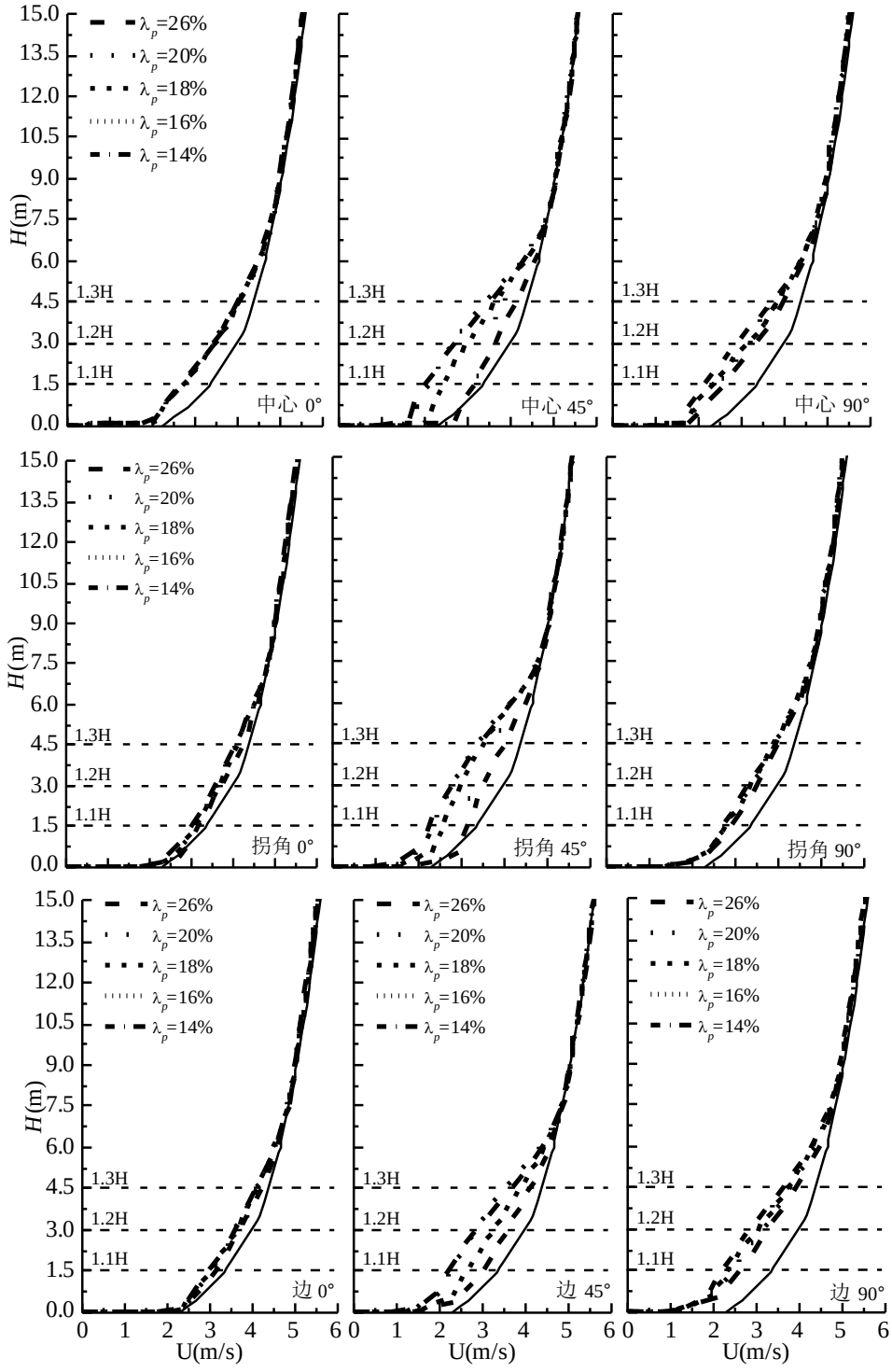

Fig. 6 Vertical profiles of mean wind speed above the roof level for different λ_p building array

Fig. 6 shows that: influence of the plan densities on the wind speed above the top of building array is small, and when the plan densities is larger, wind speed recovers more slowly. When the height is higher than 1.5H, influence of the plan densities on wind speed is neglected, at the same time, wind speed above the top of building array returns to the arrival of wind speed.

1.4.5.11.3 Findings

When the plan densities of the building cluster is bigger, areas with I>16% above the top of the building cluster are larger, and the turbulence intensity above the top of the building cluster recovers more slowly;

When the plan densities of the building cluster is bigger, wind speed above the top of the building cluster recovers more slowly, and the areas for installing wind turbine are smaller.

When the height is higher than 1.4H, influence of the plan densities on turbulence intensity above the top of the building cluster is neglected; When the height is higher than 1.5H, influence of the plan densities on wind speed above the top of the building cluster is neglected;

For the first flat roof of the building group (B1 column), influence of the plan densities on installation position and height of roof wind turbine is neglected. And the height of roof wind turbine must be higher than 1.3H.

1.5 DENMARK (active 2009 – 2016)

1.5.1 Fence experiment test and measurements

We present shelter measurements of a fence from a field experiment in Denmark. The measurements were performed with the WindScanner lidar-based system, scanning on a vertical plane downwind of the fence.

1.5.1.1 SWT site characterization

The “fence experiment” took place at Risø’s test site (DTU Wind Energy), which is approximately 7 km north from Roskilde and approximately 35 km west from Copenhagen, Denmark. Figure x shows the macro and micro-locations of the Danish fence experiment.

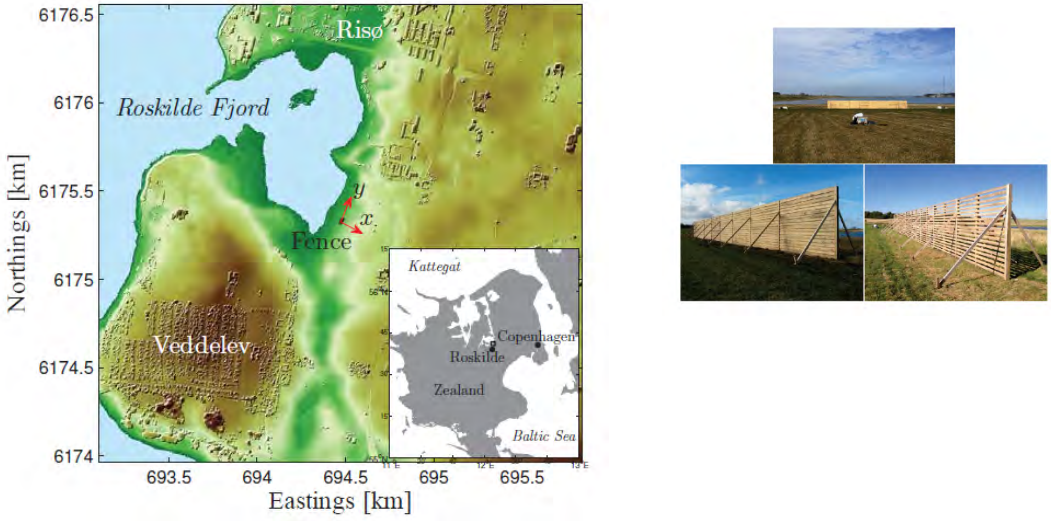

Fig. x Photos of Danish fence experiment test site

1.5.1.2 Diagram and describe the surrounding obstacles with distances noted

The fence is oriented approx. 42° from the true north (winds from the direction 312°, approaching from the fjord, are normal to the fence).The fence is 3 m high, 30 m wide, and 0.04 m thick. The terrain at the site is slightly hilly and the surface is characterized as a mix between cropland, grassland, artificial land, and coast.

1.5.1.3 Off-site/reference wind measurement description

The inflow conditions are based on sonic anemometer observations of a nearby mast at 6 and 12m above the ground. The mast recorded time series of the three wind-speed components and temperature at 20 Hz.

1.5.1.4 Data acquisition approach

The three velocity components on the vertical plane behind the fence are measured using three short-range LiDARs that are synchronized both in time and space. The LiDARs are set to scan from a position 1m downwind the fence up to a distance of 10 h and at seven different levels following the terrain elevation. The LiDARs were continuously acquiring line-of-sight velocity spectra at 49 Hz.

The spectra are gridded in 1m cells and spatially averaged in each cell leading to 31 space- and time-averaged spectra per line. The final scanning grid has thus 31x7 points in the x–z plane, which is denoted as a “full-scan”.

Besides the 10 min mean and turbulence sonic anemometer statistics, we derive another set of statistics based on the time period that the LiDAR system takes to complete each full-scan (around 21 s for most days of the campaign).

1.5.1.5 Measurement location

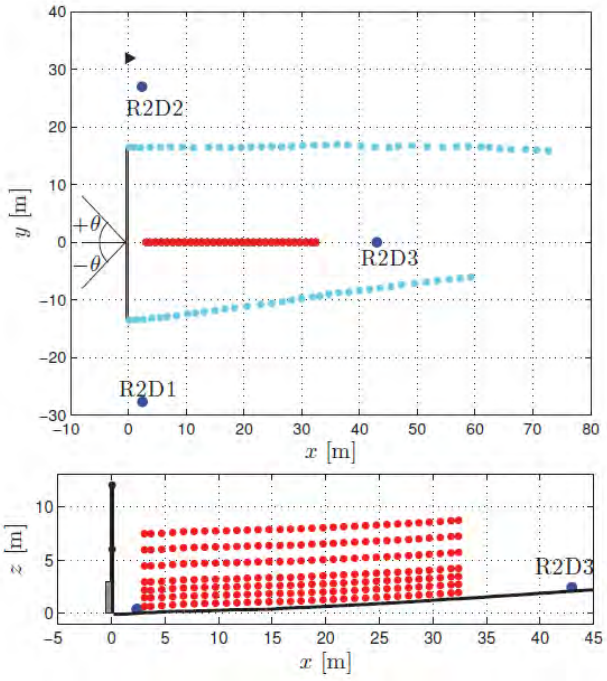

Figure 7: Fence experiment in the reference coordinate system. The positions of the fence (gray rectangle), the lidars (blue circles), the mast (black triangle and black thick line), scanning grid (red circles). The GPS measurement of the terrain (cyan circles) and the terrain elevation is also shown.

1.5.1.6 Duration and results of data collection efforts - highlight any maintenance or downtime issues

The measurement campaign was conducted during two periods: from 10 March to 1 April the fence was solid and from 29 September to 2 October 2015 the fence was made porous.
The LiDAR system was mostly operated when the sonic anemometer measurements indicated westerlies and during periods without rain.

1.5.1.7 Data processing strategy, quality assurance methods

We classify the data from the LiDAR system's full-scans into the cases in Table 1. The horizontal velocities from the LiDARs are then ensemble-averaged within each case. The wind-speed ratio is estimated by normalizing these averages by the case-correspondent "mean" inflow profile from sonic anemometer measurements.

Case	Porosity	θ [deg.]	$\langle z_o \rangle$ [m]	$u_{*\mathrm{est}}$ [m s^{-1}]	$\langle z/L \rangle$	No. of full-scans
I	solid	0 ± 15	0.0016	0.36	0.021	159
II	solid	0 ± 30	0.0019	0.36	0.015	304
III	solid	-30 ± 15	0.0037	0.34	0.023	604
IV	solid	-60 ± 15	0.0131	0.39	0.045	583
V	solid	30 ± 15	0.0016	0.35	0.007	62
VI	solid	0 ± 30	0.0019	0.28, 0.27	0.044	92
VII	porous	-30 ± 15	0.0016	0.25	−0.068	128

Table 1: Seven cases are defined based on the relative wind direction to the fence, the fence porosity, and the inflow conditions.

1.5.1.8 Conclusion of results

Plots

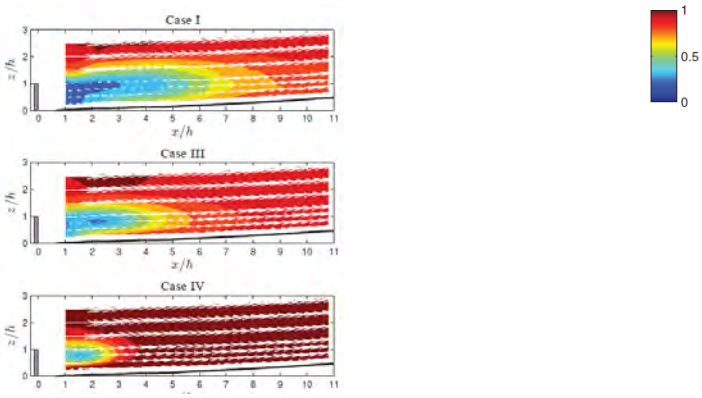

Figure 8: Average wind-speed ratio (colourbar) behind the fence for a number of cases. Vectors indicates the magnitude and sign of the average u-component

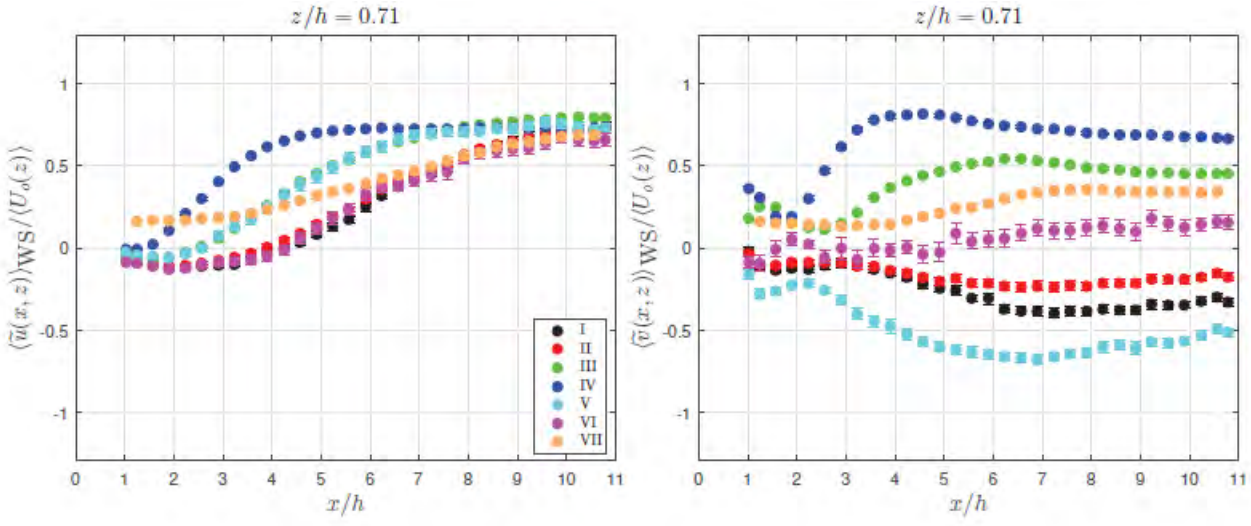

Figure 9: Averaged wind-speed ratio (separated into u and v components) on one of the vertical level behind the fence for a number of study cases

1.5.1.9 Summary of your findings and conclusions

The wind-speed ratio follows the expected behaviour; for increasing relative directions and in the far wake, the flow is less disturbed by the fence and within the near-wake region, the porous fence has a lower effect on the flow than the solid fence.

The larger the relative wind direction, the lower the effect of the shelter. A stronger shelter effect is noticed when comparing a near-neutral to a stable case. The porous fence has a lower impact on the flow close the fence compared to the solid fence.

The shelter is highest below 1.46 fence heights and can sometimes be observed at all downwind positions (up to 11 fence heights downwind).

For model evaluation, the relative direction distribution needs to be taken into account, as its effects are obvious.

We observe a deeper effect of the fence on the flow in the stable compared to the near-neutral case with the same relative-direction interval; model comparison is encouraged to distinguish if this is a result of stability or of the relative direction distribution.

1.5.1.10 References

[1] PeñaA. et al. (2016). "The fence experiment -- full-scale lidar-based shelter observations". In: Wind Energy Science 1.2, pp. 101-114. URL: http://www.wind-energ-sci.net/1/101/2016/
[2] Measurements are made available at http://www.fence.vindenergi.dtu.dk/

1.6 IRELAND (active 2009 – 2018)

1.6.1 Case Study 1 – Post installation operation assessment of 6 small wind turbines at consumer sites in Ireland

1.6.1.1 1.0 Introduction

This case study is based on field measurements from six operating small wind turbines, carried out over an 18 month period from January 2011 to June 2012 at different consumer site locations in Ireland. The six small wind turbines consist of 3 pairs of similar turbine products. Measured wind and power data are analysed to assess the wind conditions at each site and the corresponding power and energy performance the turbines. An overview of the physical features about each turbine location is given i.e. local obstacles such as building and trees and regional topography. The observed impacts on the directional electrical energy output performance of the wind turbines are outline in each case. Key observations and lessons learned are highlighted from a consumer's point of view are also given.

The case study begins by summarising the small wind turbine products and data monitoring equipment used. This is followed by a short description of the raw data acquired and quality checks carried out so that valid data is used in the assessments.

The 3 turbines pairs are then assessed in turn. In each case descriptions of the site location is given. Post quality checked data for each turbine the pair is analysed to obtain the site wind speed distribution along with raw and binned turbulence intensity curves and power curves. The power curves are also compared to the published accredited power curves.

The binned turbulence intensity values and standard deviations are also tabulated to show the more frequent turbulence intensity values that the turbine experiences in each of the measured wind speed bins.

To gain insights into how local obstacles impact the power and energy output of the turbine binned directional power, turbulence intensity curves for in 8 sectors are given. As consumers are most interested in the energy (kWh) their turbine will give them a 72 sector (5° width) directional energy output rose or an electrical energy rose [1] is plotted and overlaid on a local plan view of the site to give.

A summary of key findings are collated and conclusions are listed below.

1.6.1.2 Wind turbine systems and monitoring equipment

Table 2.1 - 6 turbine systems in 3 pairs

Wind turbine pair	**Turbine Product***	**Rating** (kW)**	**Hub height**	**Site type**
1	Proven 6	5.2	15	Rural
	Proven 6	5.2	15	Peri-urban
2	Evance R9000	4.7	12	Rural
	Evance R9000	4.7	15	Rural
3	Skystream 2.4	2.1	10	Rural
	Skystream 2.4	2.4	10	Rural

1.6.1.3 Monitoring equipment and data parameter measurements

In all cases the same sensors and logging equipment were used at each site. This equipment is outlined in Table 2.2

Table 2.2 - Monitoring equipment

Wind Speed	2D-Cup, A100LM
Wind Vane	NRG 200P
Ambient temperature & Relative humidity	RS Hygroclip

Barometric pressure	SETRA (CS100)
Power (Energy) meter	ISKRA EC1-80 (Wh pulse meter, 1 pulse/Wh)
Data Logger	Second Wind Nomad 2
Data sample rate	1 second sample rate logged in 1 minute averages

The measured data parameters and their corresponding sample rates and logged averages are given in Table 2.3

Table 2.3 - Measured parameters used

Measured Raw Data	**Unit**	**Logged averages**	**Sample rate**
Wind speed	m/s	1 minute	1 second
Wind speed standard deviation	m/s		
Wind direction	degree	1 minute	1 second
Wind direction standard deviation	degree		
Power	W	1 minute	1 pulse/Wh

The met mast setup and wind turbine monitoring equipment was guided, as much as possible, by the procedures of the IEC 61400-12 standard available at the time.

1.6.1.4 Data quality checks

A number of factors can impact the quality and quantity of measured data available. These include turbine maintenance down times, turbine operational faults, grid outages, spurious data from sensor faults or sensor unavailability and data gaps due to faults in the data logging system. Data values based on the definition of an operational time fraction in the IEC 61400-12 wind turbine power performance standard.

3.0 – 5.0 Analysis and Results

Please see separate documents for each of the turbine pairs.

1.6.1.5 Conclusions

Small wind turbines power curves:

- Are site and system specific

- Can widely vary from accredited power curves (especially at more complex sites)
- Variation increases uncertainly in site specific annual energy prediction (AEP)

Influencing factors:

- Site: local obstacles, terrain, (turbulence)
- System: turbine design, hub height, control (inverters) and turbine size
- Installer: site selection, system setup

Technical challenges and opportunities

- Better understanding of wind resource and the behaviour of turbines in complex areas
- Smarter/intelligent turbine control systems that are adaptive to specific site conditions
- More than one accredited power curve based on turbulence
- Training programmes in site assessment /selection and system setup for installers
- Manufactures should analyse all raw data measured at accredited test sites to give a more complete picture on how their turbines may perform in the field. This can help distributors better inform consumers and anticipate problems.

Consumers

- Need to be more aware of what to expect from a small turbine in relation to the general wind conditions at their specific site location

1.6.1.6 Some considerations when deciding to install a small wind turbine

- Allow a 2 year timeframe to decide upon and implement a small wind turbine (especially if you are making a significant investment)
- Become familiar/gain local knowledge of the wind resource at your site such as prevailing wind direction(s), diurnal and seasonal variations through your own observations and weather information and wind maps
- Consider regional topography within a 20km radius of your location
- Consider local obstacles within a 500m (1km) radius of your site
- Refer to online free/low cost tools (e.g. Google earth)
- Use as high a tower as possible i.e. that gives best project/energy economics even if planning/building code compliance demands greater effort
- Broad obstacles with a height of 20% of turbine tower height or greater up to 500m (1 km) away in prevailing wind direction(s) can have an negative impact on energy performance
- If obstacles greater than 20% of proposed tower height occupy more than 30% of the field of view in prevailing wind direction then increase tower height or reconsider the project

Note: the above are based on observations from a small sample of sites from the field.

Ref:
[1]: Byrne, R., Hewitt, N. J., Griffiths, P. & MacArtain, P., 2018. Observed site obstacle impacts on the energy performance of a large scale urban wind turbine using an electrical energy rose. Energy for Sustainable Development, Vol 43, pp. 23 - 37.

1.6.1.7 Comparison of two Proven 6 wind turbines at different sites

Fig 3.1.1: Turbine locations

1.6.1.8 Site A – Location

This turbine is located in the west of Ireland ~ 13km from the coast of the Atlantic Ocean.

Table 3.1.1: Site location

Location Co-ordinates	52° 55’17.5’’N - 9°14’05.8’’ E
Elevation (a.s.l) (m)	68

Fig 3.1.2: - Wind turbine at Site A

1.6.1.9 System description

Table 3.1.2: System description

Wind turbine	Proven 6
Rated Power*	5.2 kW @ 11 m/s
Tower height (monopole)	15 m (monopole)
Inverter	SMA 5000
Application	Grid connected, residential house

3.1.3 Site A – Site description

Fig 3.1.3: Plan view of site (● mast, ● wind turbine)

This site is in a rural setting with open view in the general prevailing wind direction.to the west. There are some trees in the north and northwest sectors. To the northeast is a house and trees. The local topography is more rugged with some sparse trees in the southerly and south easterly sectors.

Looking W

Looking N

Looking S	Looking SE

Fig 3.1.4: On site views from turbine location

1.6.1.10 Site A - Performance

Table 3.1.3 summarises mean wind speed energy and turbulence indicators during the test.

Time under test (hrs)	8038
Mean wind speed (m/s)	6.1
Metered Energy (kWh)	13703
TI (%) + 1std dev (%) [15m/s bin]	11.7 + 2.8
TI (%) + 1std dev (%) [5m/s bin]	12.7 + 4.6

1.6.1.10.1 Site A – Wind Analysis and Power curve performance

The mean wind speed of 6.1 m/s over the test period with a corresponding wind speed distribution is shown in figure 3.1.4. The wind rose shows the dominant wind directions are from WSW to WNW along with a smaller contribution from the SE. Winds from the other directions are much reduced.

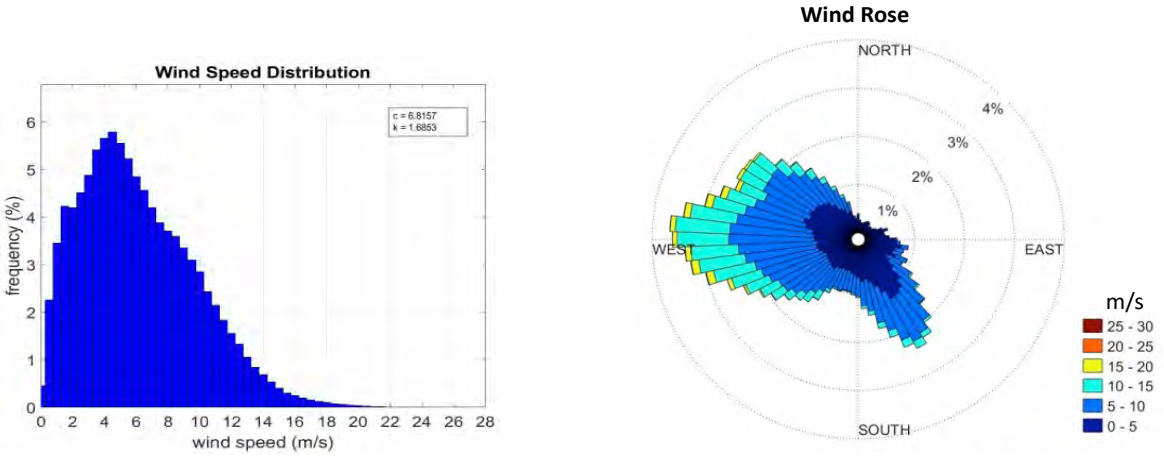

Fig 3.1.5: Wind speed distribution and wind rose

Scatter and binned plots of the measured power curve and turbulence intensity are show in figure 3.1.6.

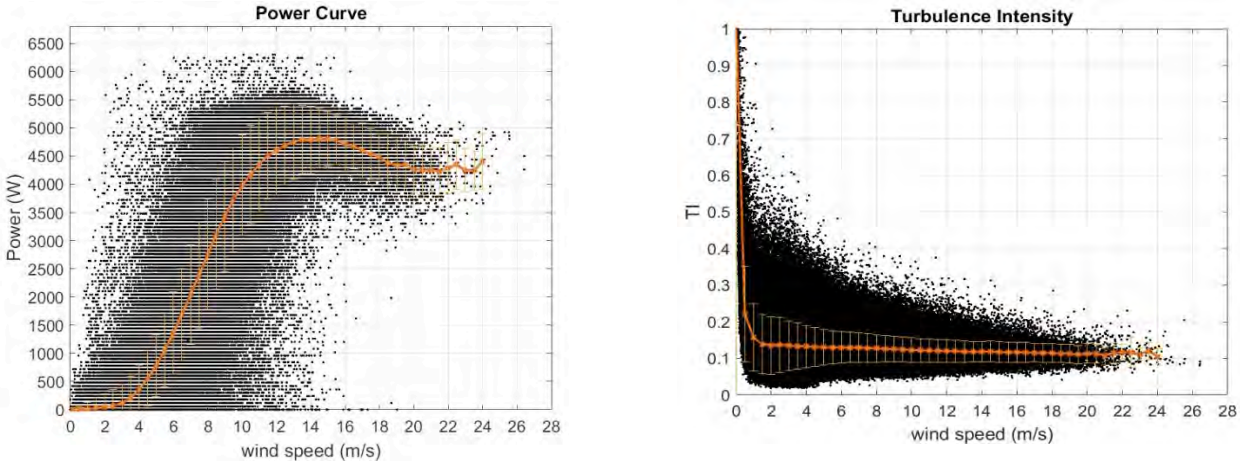

Fig 3.1.6: Power curve and turbulence intensity curve

The plots of measured data and error bars of the binned power curve and turbulence data demonstrate the site specific of scatter of these parameter. The degree of scatted can be influenced by a number of factors such as:

- Wind turbulence due to site specific influences
- Met mast and turbine not at exact same location i.e. no site calibration (as is done at accredited test sites)
- Behavioural response of the total wind turbine system to wind conditions

The turbulence intensity value at 15m/s falls below the range of the current value of 0.18 used in the IEC 61400-2-ed3 small wind tubines standard.

1.6.1.10.2 Site A – Directional power and turbulence curves and analysis

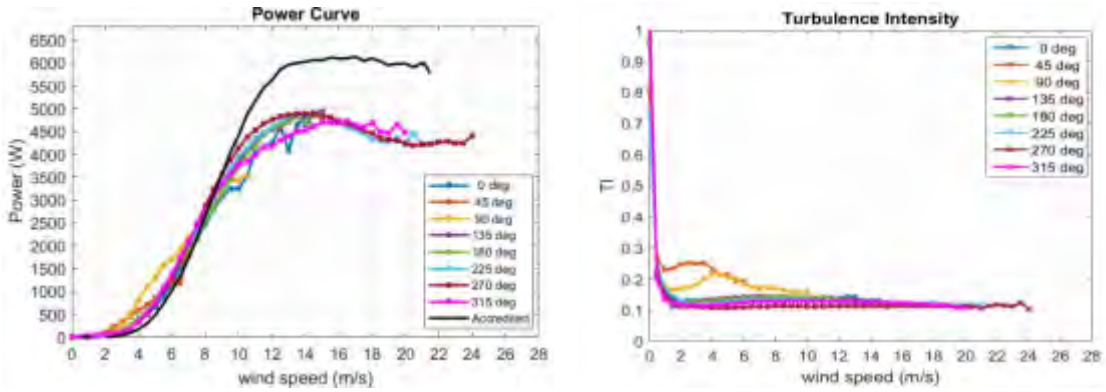

Fig 3.1.7: Directional power curves and turbulence intensity curves

The turbulence intensity curves and power curves vary with direction as shown in figure 3.1.7 respectively. As the mast is located to the southwest of the turbine it is in the wake of turbine when winds come from the northeast. The effect of the turbine wake on the mast can be seen for the east and northeast directions. The lowest turbulence intensity occurs when winds are from the west. This best curve above wind speeds of approximately 8 m/s also occurs when wind come from the west. Interestingly at lower wind speeds below 8 m/s the power output is better in higher turbulence directions. When compared to the accredited power curve from the summary test report, shown in black, many of the directional power curves exceeds the accredited power curve at these lower wind speeds but then deviate significantly below the accredited power curve and wind speeds above 10 m/s. One of the reasons for the deviation of the power curves at higher wind speed is that it is limited by the operating power limits of the single 5kW rated inverter. A different inverter was used in the accredited testing [x]. This highlights the need for consistency in what systems are is being certified and what consumers are getting.

1.6.1.10.3 Site A – Directional Energy and Obstacles

Electrical energy (kWh) is of most relevance to consumers. An electrical energy rose shows the kWh output with direction [x]. This is plotted in figure 3.1.8. The shape of the electrical energy rose shows that the majority of useful electrical energy generated by the turbine is generated in the westerly sectors with a small proportion from the SE. There appears to be very little electrical energy output from the NNW to SE with distinct influences to S to SW sectors and the NW sectors.

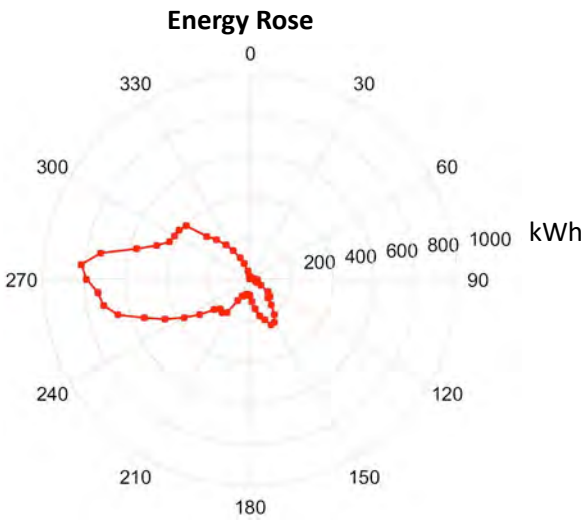

Fig 3.1.8: Electrical Energy Rose

An overlay of the output energy rose on a local plan view is shown in figure 3.1.9. Local obstacles are numbered and described in table 3.1.4

Fig 3.1.9: Electrical Energy Rose overlaid on plan view with number obstacles

Table 3.1.4: Local obstacle descriptions (values are rough approximates)

Site	distance	Height	Width WT View	Comments
1	30m	4	50	House/trees
2	150m	10	150	Trees
3	260m	10	20	House
4	420m	10	70	Farm Sheds
5	475m	4	50	House
6	120m	4	40	Small farm shed/complex local topography

The house/trees (Obstacle 1) to the NE combined with this direction not being the prevailing wind direction means that very little energy is comes from that sector. The cluster of trees (Obstacle 2) in the northwest sector appears to have an energy reducing impact as does the rugged topography

around the small shed (Obstacle 6) to the SW. It is not clear that local obstacles alone influence the south and southeast sectors.
The electrical energy rose overlaid on a regional plan view in figure 3.1.10 shows hills 5km to 15km (Feature D) with a valley to the east of these hills that may be channelling, at the mesoscale, some of the southerly winds into the southeast sector at the turbine site. This combined with local Obstacle 6 to the south shape the energy rose in south and south east sectors.

Fig 3.1.10: Electrical Energy Rose overlaid on regional plan and labelled topographical features

Table 3.1.5: Regional topographical description (values are rough approximates)

Feature	Distance	Elevation	Comments
A	10-20km	100m-270m	Gently rising topography
B	25-40km	20-200m	Hills/some forested areas
C	30-50km	35-400m	Hills/some forested areas
D	5-15km	60-380m	Hills/some forested areas
E	1-5km	60-100m	Small sparse forested areas

Despite local obstacle and regional influences this turbine performed to high satisfaction of the turbine owner. Views from the turbine location, Figure 3.1.4, shows a good wind fetch in the in the prevailing wind direction where there are the fewest local obstacles. This highlights the importance of an obstacle free prevailing wind direction. The shape of the electrical energy rose show that the width of obstacles must be considered and well as the height.

1.6.1.11 Site B – Location

This turbine is located in an urbanised area the west end of Dublin city near the east coast of Ireland.

Table 3.2.1: Site location

Location Co-ordinates	53º 17’ 28.88’’ N - 6º 21’’ 55.68’’ E
Elevation (a.s.l) (m)	97

Fig 3.2.2: - Wind turbine at Site B

1.6.1.12 System description

Table 3.2.2: System description

Wind turbine	Proven 6
Rated Power*	5.2 kW @ 11 m/s
Peak Power*	6.1 kW @ 17 m/s
Inverter	Two SMA 2500 inverters
Application	Grid connected on college campus

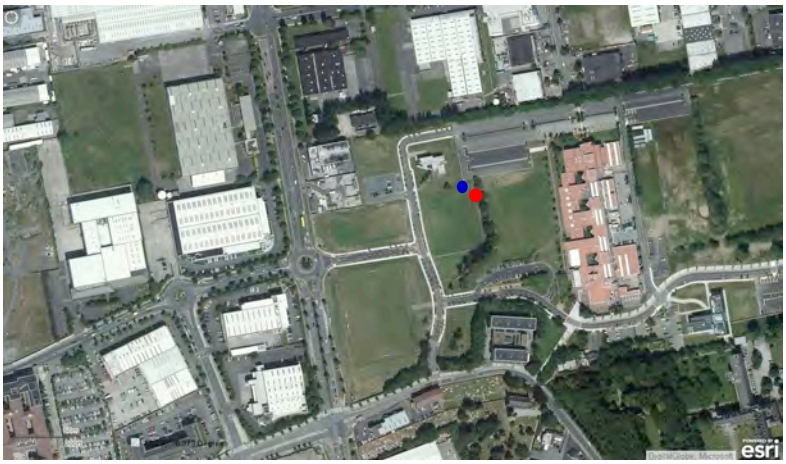

Fig 3.2.3: Plan view of site (● mast, ● wind turbine)

The turbine location is surrounded in all directions by building obstacles and some trees. The buildings are low rise building with heights from 4m to 12m i.e. lower than the turbine hub height of 15m.

Looking Easterly	Looking Northerly
Looking Southerly	Looking Westerly

Fig 3.2.4: On site views from turbine location

1.6.1.12.1 Site B - Performance

Table 3.2.3 summarises mean wind speed energy and turbulence indicators during the test

Time under test (hrs)	6,370
Mean wind speed (m/s)	4.5
Metered Energy (kWh)	4,181
TI (%) + 1 std dev (%) [15m/s bin]	18.1 + 3.6
TI (%) + 1 std dev (%) [5m/s bin]	19.6 + 5.8

1.6.1.12.2 Site B – Wind Analysis and Power curve performance

With a mean wind speed of 4.5 m/s over the test period, the dominant wind direction is from the westerly sectors, with little or no wind from NW in a clockwise direction SW.

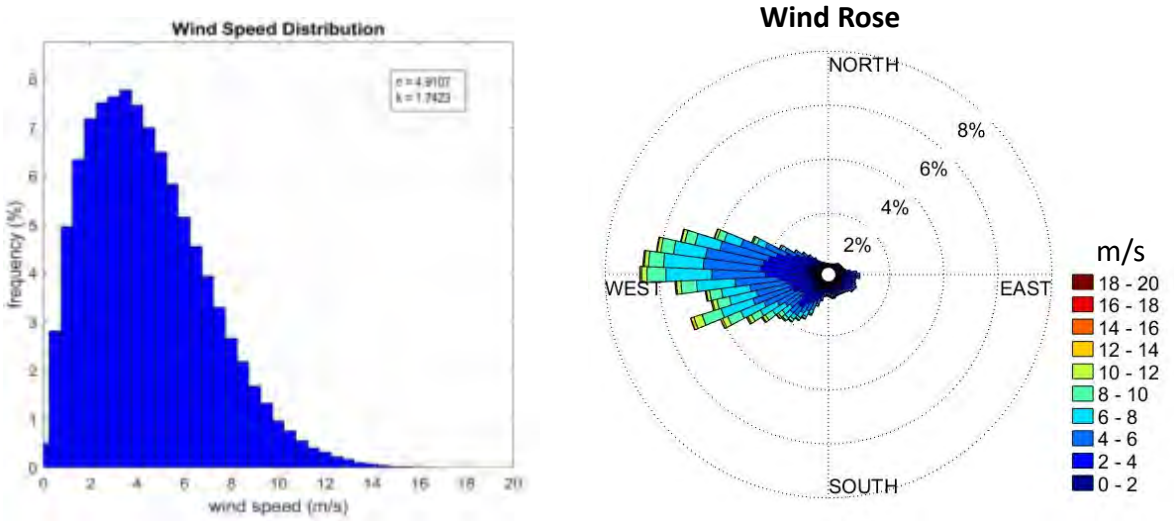

Fig 3.2.5: Wind speed distribution and wind rose

Scatter and binned plots of the measured power curve and turbulence intensity are show in figure 3.2.6.

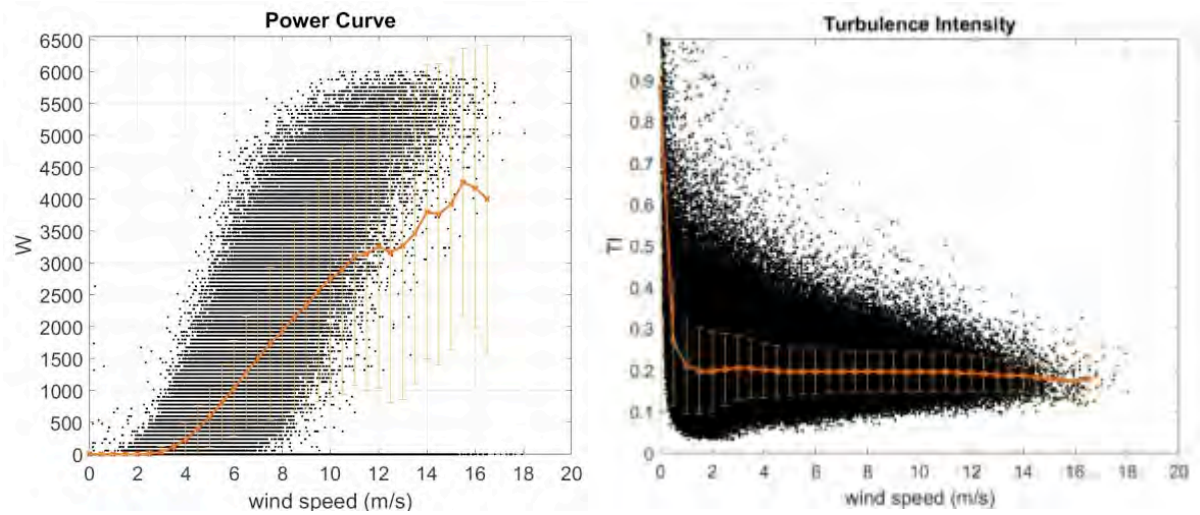

Fig 3.2.6: Power curve and turbulence intensity curve

There is more scatter in the power and turbulence intensity curves compared to site A. The turbulence intensity is higher compared to site A, and power performance is poorer particularly at higher wind speeds. The power level is zero in many instances when the wind speed is high. The inverter system in this case consists of two 2500W rated inverters. A slow activation response time of the second inverter to the highly variable power output of the wind turbine generator may explain the poorer power curve at higher wind speeds. The inverter configuration is also different to that use in the accredited testing [x]

The mean turbulence intensity value at 15m/s just exceeds 0.18 used in the IEC 61400-2-ed3 small wind turbines standard and has a high likelihood of up to ~ 0.22.

1.6.1.12.3 Site B – Directional power and turbulence curves and analysis

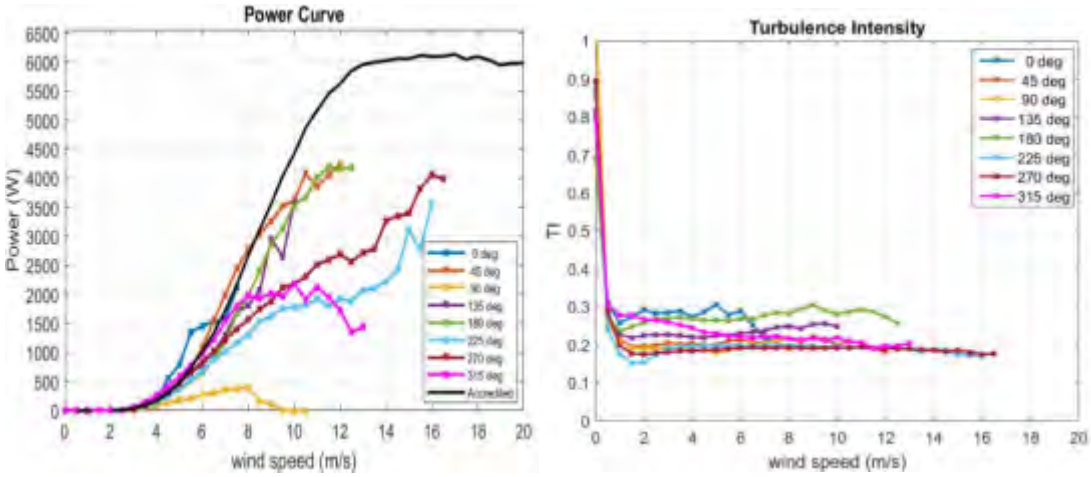

Fig 3.2.7: Directional power curves and turbulence intensity curves

The turbulence intensity and power curves vary with direction. As the predominant wind direction is from the west there are statistically fewer data points from the remaining direction that will influence the variability of the turbulence intensity and power curves from these other directions. The dominant westerly (270deg) power curve is closest to the overall power curve shown in figure 3.2.6 but deviates significantly from the accredited power curve above 6 m/s. The higher turbulence at the site combined with overall system response in the site wind conditions may explain the difference.

1.6.1.12.4 Site B – Directional Energy and Obstacles

An electrical energy rose shows the kWh output with direction [x]. This is plotted in figure 3.2.8. Like the wind rose is has a distinct shape showing that the majority of useful electrical energy generated by the turbine is generated in the westerly sectors with little or no electrical energy output from other directions.

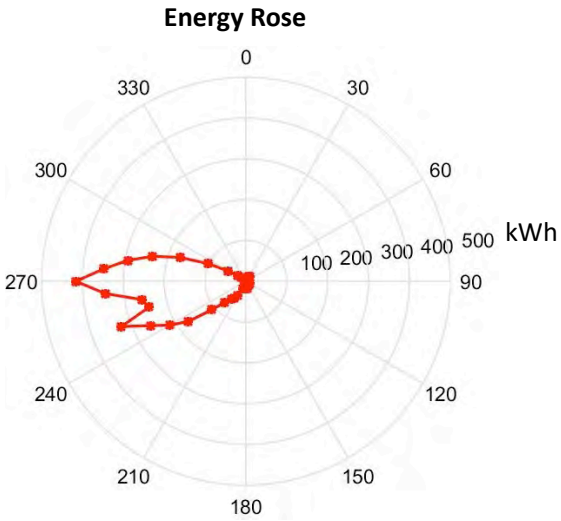

Fig 3.2.8: Electrical Energy Rose

An overlay of the output energy rose on a local plan view is shown in figure 3.2.9. Local obstacles are numbered and described in table 3.2.4.

Fig 3.2.9: Electrical Energy Rose overlaid on plan view with number obstacles

As the measured prevailing wind is to the west the electrical energy come from between buildings 2 and 3 and buildings 3 and 4. Building 4 is lower than building 3 so that build 3 has more of a blocking impact in the prevailing wind direction. The local building and city in all other directions combined with these not being in the prevailing wind direction appear to reduce the electrical energy output from these directions.

Table 3.2.4: Local obstacle descriptions (values are rough approximates)

Obstacle	Shortest distance to turbine	Dimensions NS x EW	Width WT View	Height
1	275m	52m x 55m	78	12m
2	242m	37m x 68m	70 (90)	12m
3	233m	60m x 90m	75(85)	12m
4	265m	100m x 62m	121	9m
5	184m	43m x 46m	84	4m
6	130m	10m x 25m	25(50)	4m
7	107m	90m x 70m	60	4m
8	94m	175m x 62m	145	12m
9	75m	Trees (50m)	45	10m
10	138m	Trees/building (65m-60m)	80	12m

11	220m	Trees/buildings (50m x 80m	64	10m/4m
12	77m	Long row of trees	345	10m

A regional plan view shows that the main city is to the east of the site and that there are hills 5km to 15km (Feature A) to the south which may also have a blocking impact from the southerly direction. These may also explain why winds and energy output observed at site are from the westerly sectors only.

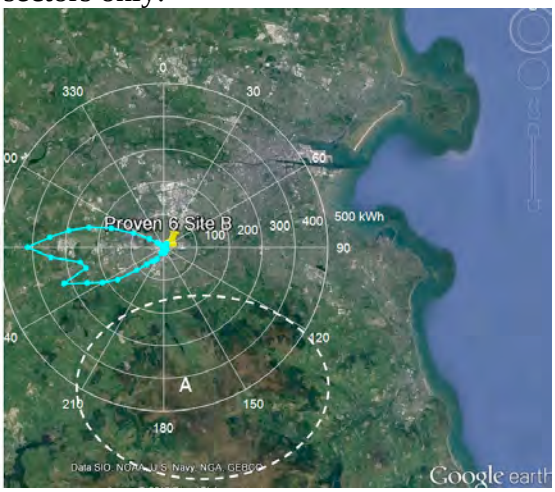

Fig 3.1.10: Electrical Energy Rose overlaid on regional plan and labelled topographical features

Table 3.1.5: Regional topographical description

Feature	distance	Elevation	Comments
A	5-15km	90m-750m	hills

This site shows that in more dense urban areas roads and streets the run along the direction of the prevailing wind can channel wind flow between buildings into a location and lower buildings between higher buildings can also allow wind flow onto a site.

Comparisons of the power curves of site A and B with the accredited power curve are shown in figure 3.2.11. They demonstrate that site power curves are site specific and can vary from their published accredited power curves.

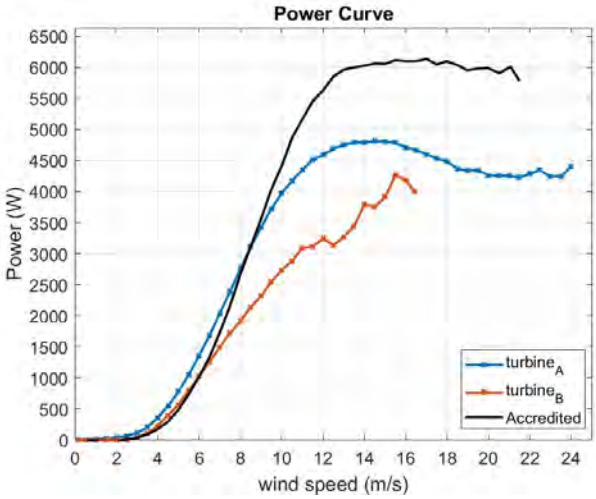

Fig 3.2.11: Site power curve comparison with accredited power curve

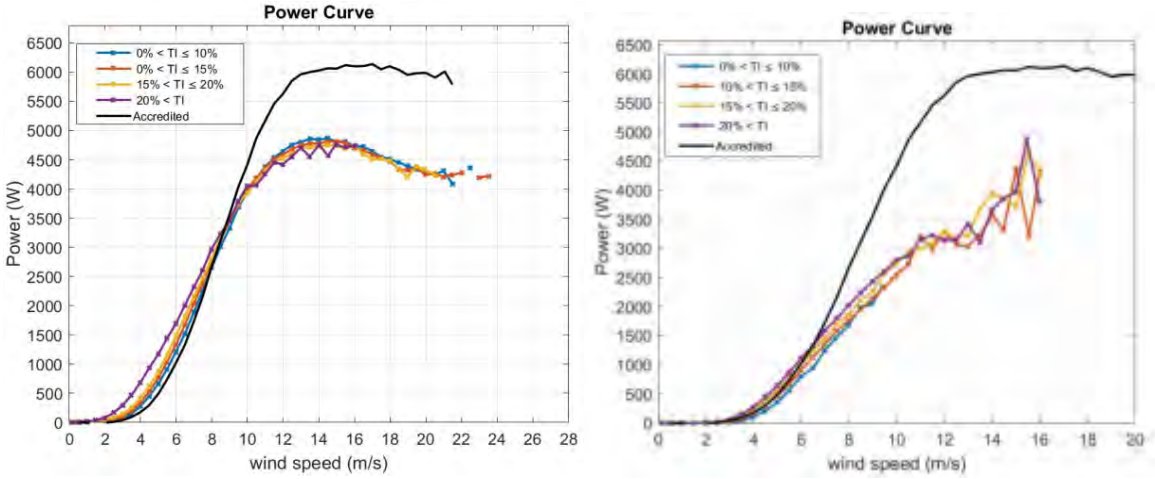

Fig 3.2.12: Site power curve comparison with accredited power curve for different turbulence ranges

1.6.1.13 Comparison of two Evance R9000 wind turbines at different sites

Fig 4.1.1: Turbine locations

1.6.1.13.1 Site A – Location

The site is located in the northern part of Ireland in a rural location. The turbine is elevated above its local surroundings on a small hill.

Table 4.1.1: Site location

Location Co-ordinates	52º 55’17.5’’N - 9º14’05.8’’ E
Elevation (a.s.l) (m)	77

Fig 4.1.2: - Wind turbine at Site A

1.6.1.13.2 System description

Table 4.1.2: System description

Wind turbine	Iskra Evance R9000
Rated Power*	4.7 kW @ 11 m/s
Tower height (type)	12 m (monopole)
Inverter	Two SMA 2500 inverters
Application	Grid connected to a house

1.6.1.13.3 Site A – Site description

Fig 4.1.3: Plan view of site (● mast, ● wind turbine)

This site is in a rural setting with open view in the general prevailing wind direction.to the west. There is a small village to the west and northwest. Sparse obstacles such as houses and farm building can be found in the other directions. There is a small lake to the east. The location is also at the edge of a drumlin belt, a region of very small hills, characteristic of this part of Ireland. These hills have a similar elevation to the turbine location. These can be seen from the W clockwise to the NE.

Looking NW	Looking E
Looking NE	Looking SW

Fig 4.1.4: On site views from turbine location

1.6.1.13.4 Site A - Performance

Table 4.1.3 summarises mean wind speed energy and turbulence indicators during the test.

Table 4.1.3: Summary results

Time under test (hrs)	8732
Mean wind speed (m/s)	5.1
Metered Energy (kWh)	8963
Capacity factor	
TI (%) + 1 std dev (%) [15m/s bin]	13.4 + 3.1
TI (%) + 1 std dev (%) [5m/s bin]	12.7 + 4.1

1.6.1.13.5 Site A – Wind Analysis and Power curve performance

The site has a mean hub height wind speed of 5.1 m/s over the test period, which is just over 1 year. This wind speed distribution and wind rose are shown in figure 4.1.5. The dominant wind directions are from southwest.

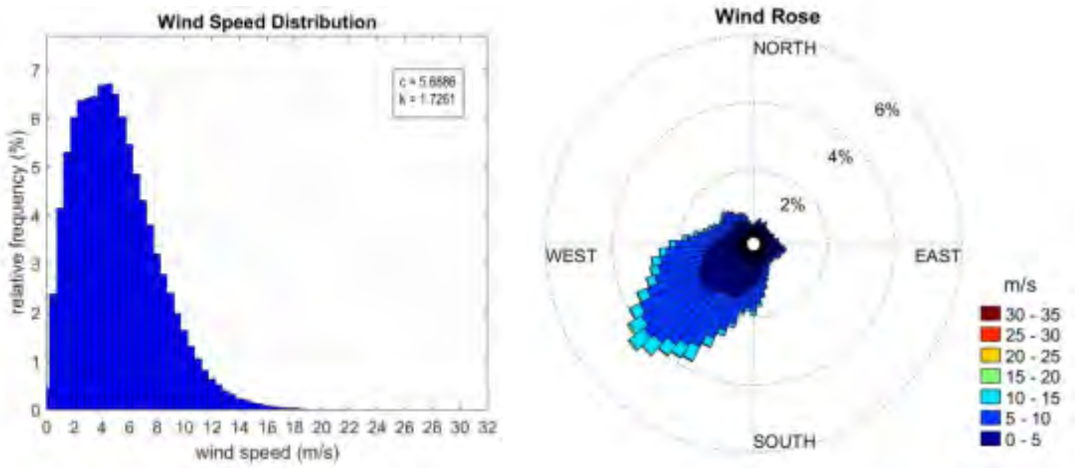

Fig 4.1.5: Wind speed distribution and wind rose

Scatter and binned plots of the measured power curve and turbulence intensity are show in figure 4.1.6.

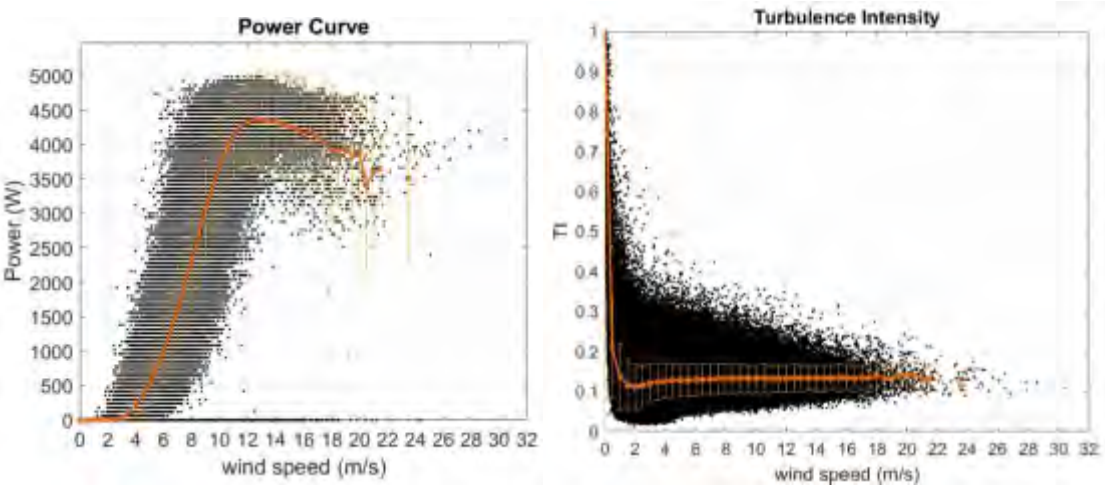

Fig 4.1.6: Power curve and turbulence intensity curve

The plots of measured data and error bars of the binned power curve and turbulence data demonstrate the site specific of scatter of these parameter. The mean turbulence intensity value at 15m/s is 0.13 with a high probability of reaching 0.17 falls under 0.18 used in the IEC 61400-2-ed3 small wind standard.

1.6.1.13.6 Site A – Directional power and turbulence curves and analysis

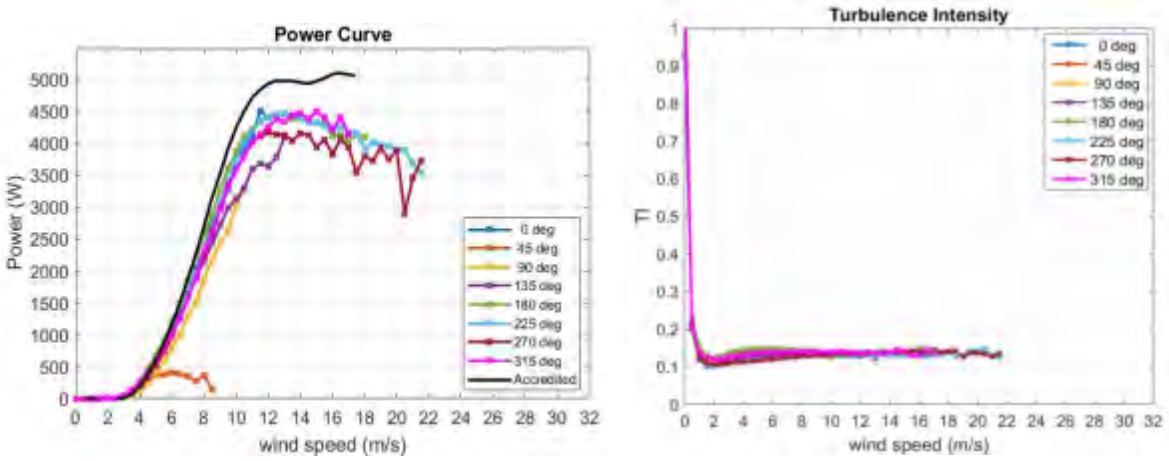

Fig 4.1.7: Directional power curves and turbulence intensity curves

The turbulence intensity and power curves vary with direction. As the predominant wind direction is from the south west there are statistically fewer data points from the remaining direction that will influence the variability of the turbulence intensity and power curves from these other directions. The dominant south westerly (225deg) power curve is closest to the overall power curve shown in figure 4.1.7 but deviates significantly from the accredited power curve above 5 m/s. The poorest power curve in the easterly direction aligns with the lake to the east and cooler it more stable atmospheric conditions.

1.6.1.13.7 Site A – Directional Energy and Obstacles

An electrical energy rose shows the kWh output with direction [x]. This is plotted in figure 4.1.8. Like the wind rose is has a distinct shape showing that the majority of useful electrical energy generated by the turbine is generated in the south west sectors with little or no electrical energy output from other directions.

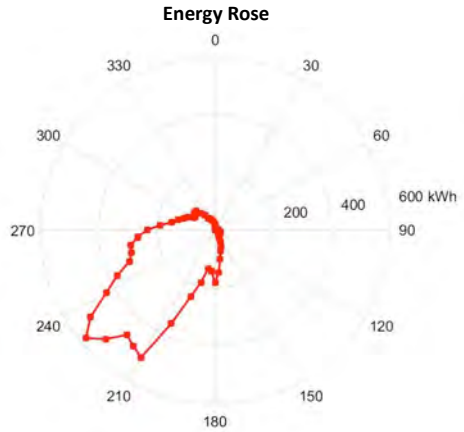

Fig 4.1.8: Electrical Energy Rose

An overlay of the output energy rose on a local plan view is shown in figure 4.1.9. Local obstacles are numbered and described in table 4.1.4.

Fig 4.1.9: Electrical Energy Rose overlaid on plan view with number obstacles

Table 4.1.4: Local obstacle descriptions (values are rough approximates)

Obstacle	Distance (m)	Height (m)	Width WT view	Comments
1	210-570	9	150	Village houses
2	320-700	9	80	Village houses
3	240-560	9	200	Houses
4	90-100	9	35	House
5	300-380	12	135	Farm sheds
6	312-430	3	65	Bushes
7	720-1420	0	980	Lake (N-S length 1.3km)
8	355-430	12	70	Farm sheds
9	230-350	3	40	Commercial
10	560-1000	12	260 (half way)	Farm sheds

There is an open fetch to the south west which is the direction of prevailing wind and the direction where most of the electrical energy comes from. The village (Obstacles 1 and 2) appear to have an energy reducing impact from the west while the houses to the north and northeast (Obstacles 3,4)combines with these not being prevailing wind direction has result in little or no energy output from these directions. The local topography from NW to east beyond obstacle 5 (i.e. ~ 500m east of turbine location) comprise of small hills of the drumlin belt, some of which are at a slightly higher elevation than the site. They may be another cause of reduced energy output from this direction.

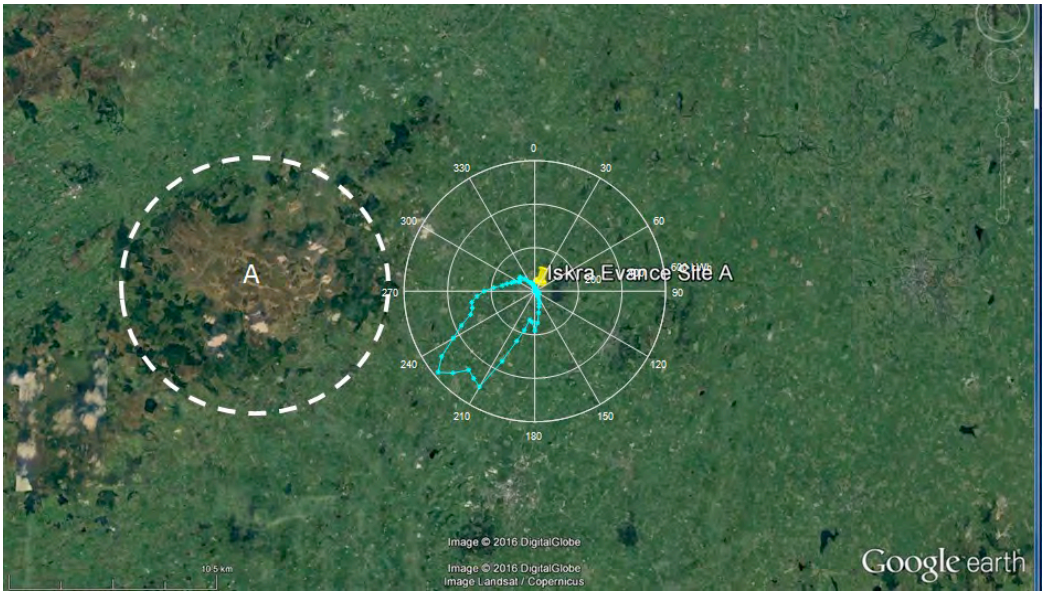

Fig 4.1.10: Electrical Energy Rose overlaid on regional plan and labelled topographical features

Table 4.1.5: Regional topographical description (values are rough approximates)

Feature	distance	Elevation	Comments
A	8-16km	80m-346m	hills

In the case of the broader regional topography there are hills 8km to 16km away to the west. The may have a mesoscale effect in on reducing wind from the west or steering winds on the site for the south west direction.

1.6.1.13.8 Site B – Location

The turbine located in a rural location in the southern part of the Irish midlands. The site has a number of obstacles such houses to the west and trees in the south west directions.

Table 4.2.1: Site location

Location Co-ordinates	52°30'44.25"N, 7°48'43.54"W
Elevation (a.s.l) (m)	150

Fig 4.2.2: - Wind turbine at Site B

1.6.1.13.9 System description

Table 4.2.2: System description

Wind turbine	Iskra Evance R9000
Rated Power*	4.7 kW @ 11 m/s
Tower height (type)	15 m (monopole)
Inverter	Two SMA 2500 inverters
Application	Grid connected to a house

Fig 4.2.3: Plan view of site (● mast, ● wind turbine)

There are dense clusters of trees to the SW, buildings to the NW and sparse trees to the N.

Looking NW

Looking N

Looking E

Looking S

Fig 4.2.4: On site views from turbine location

1.6.1.13.10 Site B - Performance

Table 4.2.3 summarises mean wind speed energy and turbulence indicators during the test.

Table 4.2.3: Summary results

Time under test (hrs)	9385
Mean wind speed (m/s)	4.2
Metered Energy (kWh)	7908
Capacity factor	
TI (%) + 1 std dev (%) [15m/s bin]	15.9 + 3.7

TI (%) + 1 std dev (%) [5m/s bin]	17.9 + 5.3

1.6.1.13.11 Site B – Wind Analysis and Power curve performance

The site has a mean hub height wind speed of 4.2 m/s over the test period with a speed distribution shown in figure 4.2.5. As shown by the wind rose the dominant wind directions are from SSW and WNW with a notable reduction in wind speed in the southwest sector.

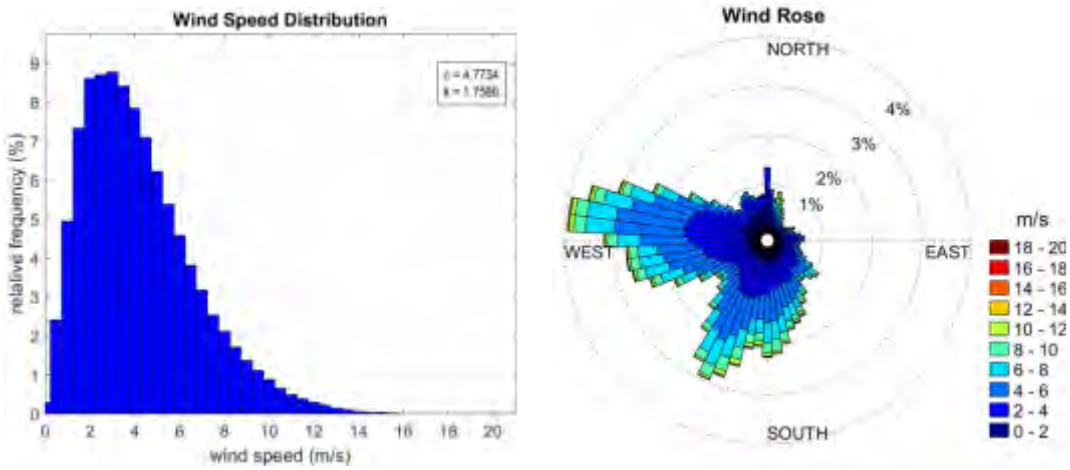

Fig 4.2.5: Wind speed distribution and wind rose

Scatter and binned plots of the measured power curve and turbulence intensity are shown in figure 4.2.5.

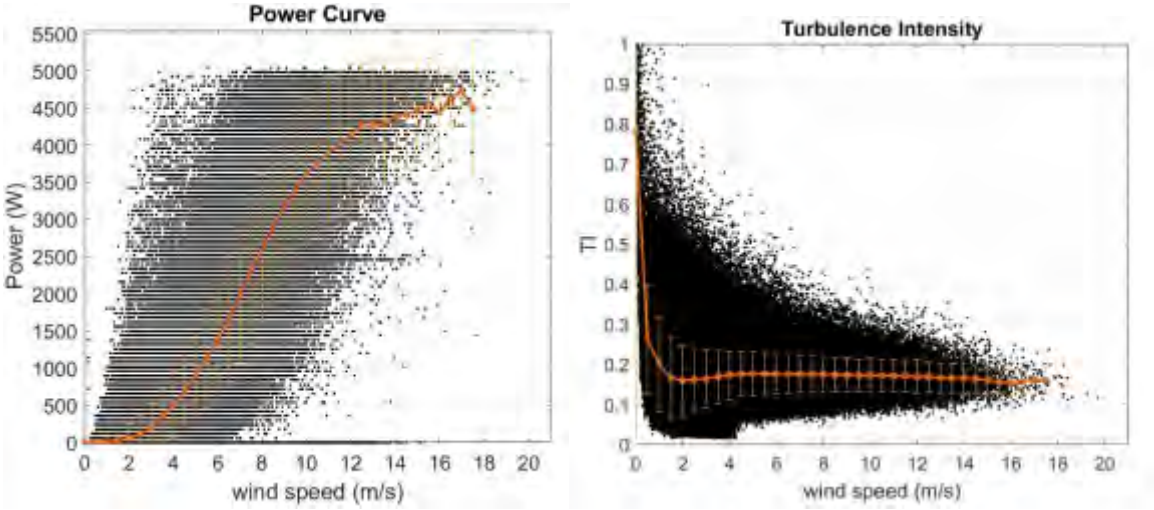

Fig 4.2.6: Power curve and turbulence intensity curve

There is more scatter in the power and turbulence intensity curves compared to site A. The met mast because of its location is under the influence of the wake of the turbine from the and nearby trees. As the inverter system in this case consists of 2 stacked or cascaded 2500W rated inverters, a slow activation response time of the second inverter to the highly variable power output of the

wind turbine generator may explain the poorer power curve at higher wind speeds. The inverter configuration is also different to that use in the accredited testing [x].
The mean turbulence intensity value at 15m/s is 0.16 i.e. lower than 0.18 used in the IEC 61400-2-ed3 small wind standard but has a high probability of exceeding 0.19 i.e. 1 standard deviation above the mean turbulence intensity value at 15m/s.

1.6.1.13.12 Site B – Directional power and turbulence curves and analysis

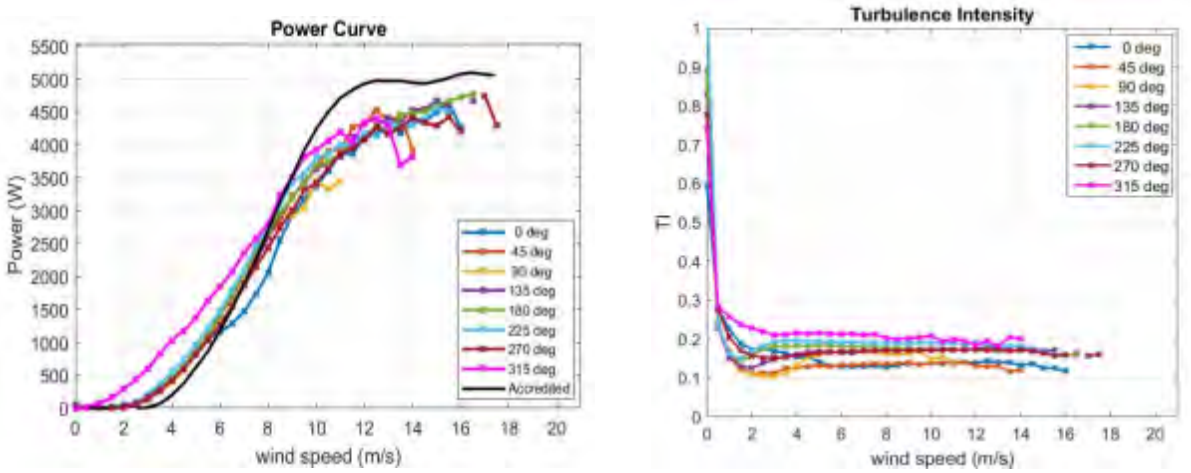

Fig 4.2.7: Directional power curves and turbulence intensity curves

The turbulence intensity and power curves vary with direction. Because the met mast is located to the southeast of the turbine the power curve for the northwest sector (315 deg) is overestimated due to the met mast being in the wake of the turbine i.e. it is not representative of the site power curve for this direction. Ignoring the 315 deg direction the turbulence intensity curves the highest values in the south west direction.

1.6.1.13.13 Site B – Directional Energy and Obstacles

An electrical energy rose shows the kWh output with direction [x]. This is plotted in figure 4.2.8. Like the wind rose is has a distinct shape showing that the majority of useful electrical energy generated by the turbine is generated in the south SW and WNW sectors with little or no electrical energy output from other directions.

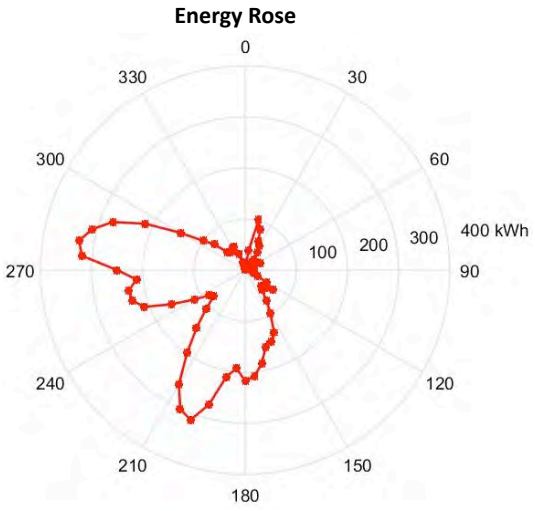

Fig 4.2.8: Electrical Energy Rose

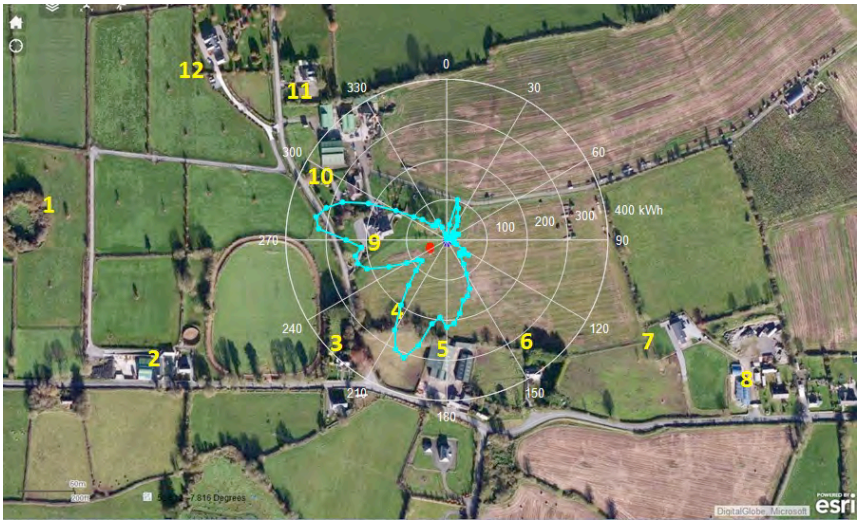

Fig 4.2.9: Electrical Energy Rose overlaid on plan view with number obstacles

An overlay of the output energy rose on a local plan view is shown in figure 4.2.9. Local obstacles are numbered and described in table 4.2.4.

Table 4.2.4: Local obstacle descriptions (values are rough approximates)

Site	Distance (m)	Height (m)	Width WT view	Comments
1	405-470	10	70	Low dense trees
2	260-460	9	50(77)	House trees
3	100-170	12	85	Dense trees/house
4	80-107	15	70	Less trees
5	94-175	12	53	Sheds
6	145-215	9	50	Trees/house

7/8	265-480	9/12	75 (at 355)	House/sheds
9	42-75	9	55	Owners house
10	130-195	12	63	Farm sheds
11	220-260	9	40	House
12	335-435	12	120	Farm shed

The SW which is the general direction of the prevailing wind does not have an open fetch. Obstacles 3, 4, 5, 9 and 10 appear to have an energy reducing impact from the SW.

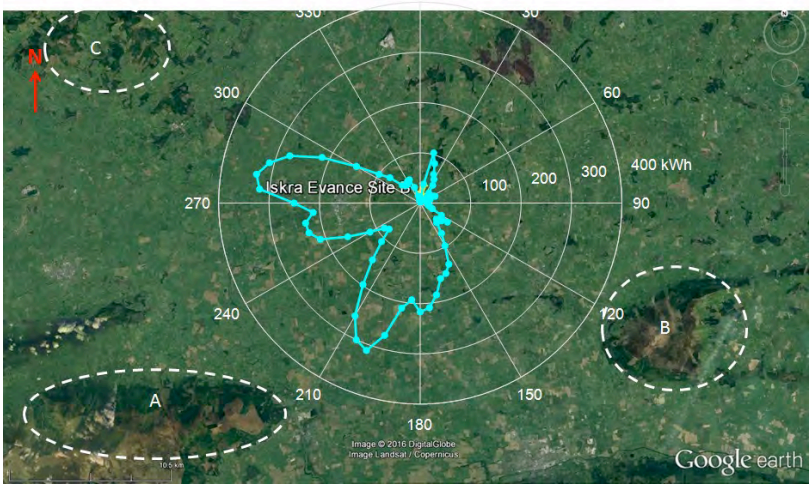

Fig 4.2.10: Electrical Energy Rose overlaid on regional plan and labelled topographical features

Table 4.2.5: Regional topographical description (values are rough approximates)

Feature	Distance (m)	Elevation (m)	Comments
A	22-33	746	hills
B	16-19	544	hills
C	22.5	421	hills

In the case of the broader regional topography all hills are greater that 16km away and don't appear to have a significant impact on the shape of the energy rose implying that local obstacles are the dominating influence.

Comparisons of the power curves of site A and B with the accredited power curve are shown in figure 4.2.11. They demonstrate that site power curves are site specific and can vary from their published accredited power curves.

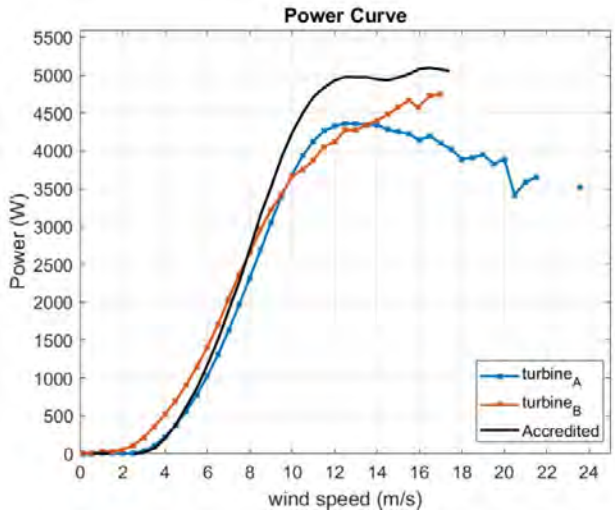

Fig 4.2.11: Site power curve comparison with accredited power curve

Inter- comparison of the power between site A and B demonstrate that site power curves are specific and can vary from their published accredited power curves.

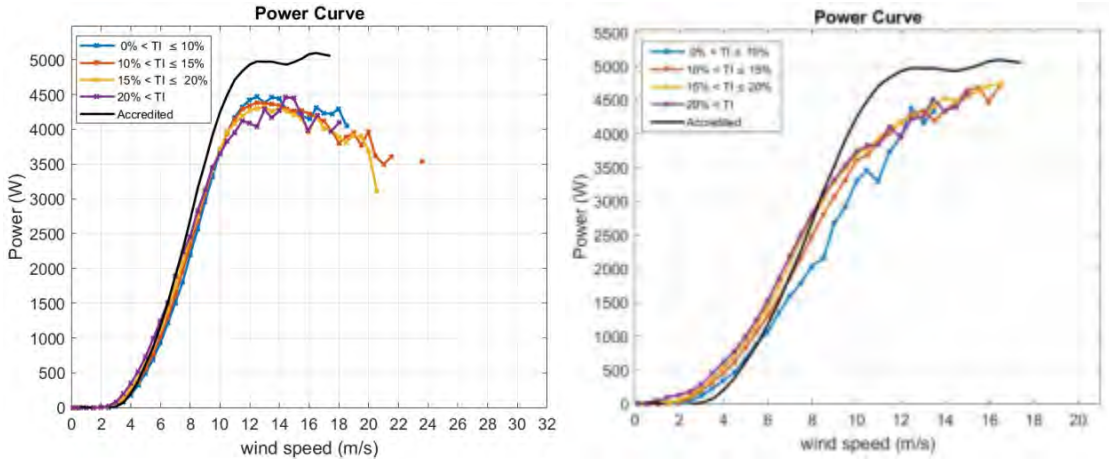

Fig 4.2.12: Site power curve comparison with accredited power curve for different turbulence ranges

1.6.1.14 Comparison of two Skystream wind turbines at different sites

1.6.1.14.1 5.1.1 Site A – Location

This turbine is located in the southeast of Ireland ~ 2.5km from the coast. The turbine is elevated above its local surroundings on a small hill.

Table 5.1.1: Site location

Location Co-ordinates	52°11'35.02"N, 7°15'43.98"W
Elevation (a.s.l) (m)	70

Fig 5.1.2: - Wind turbine at Site A

1.6.1.14.2 System description

Table 5.1.2: System description

Wind turbine	Skystream 3.7
Rated Power*	2.1 kW @ 11 m/s
Tower height (type)	10 m (monopole)
Inverter	Internal to system
Application	Grid connected to a house

1.6.1.14.3 Site A – Site description

Fig 5.1.3: Plan view of site (● mast, ● wind turbine)

The site is turbine is located on a small hill that is elevated above its surroundings. There are houses located in direction from E clockwise to NW. Some short trees exist to the W of the site. The view to the NE is relatively open with few obstacles.

Looking W

Looking N

Looking S

Looking E

Fig 5.1.4: On site views from turbine location

1.6.1.14.4 Site A - Performance

Table 5.1.3 summarises mean wind speed energy and turbulence indicators during the test.

Table 5.1.3: Summary results

Time under test (hrs)	9015
Mean wind speed (m/s)	4.7
Metered Energy (kWh)	3927
Capacity factor	
TI (%) + 1 std dev (%) [15m/s bin]	19.1 + 4.0
TI (%) + 1 std dev (%) [5m/s bin]	19.7 + 5.4

1.6.1.14.5 Site A – Wind Analysis and Power curve performance

This site has mean wind speed of 4.7 m/s over the test period and corresponding wind speed distribution shown if figure 5.1.5. The dominant wind direction is from the southwest. The westerly and southerly sectors show distinct reductions in wind speed.

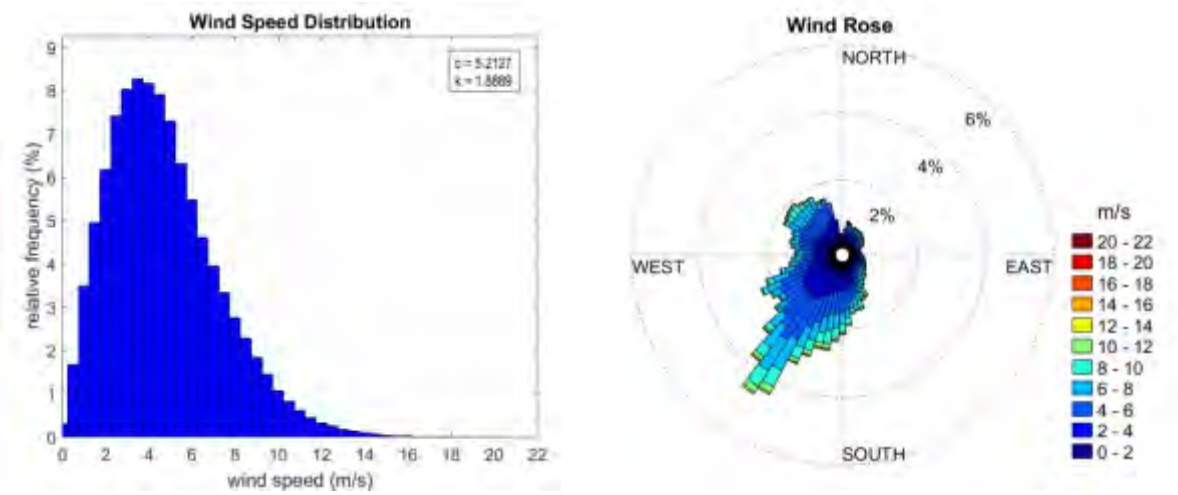

Fig 5.1.5: Wind speed distribution and wind rose

Scatter and binned plots of the measured power curve and turbulence intensity are show in figure 5.1.6.

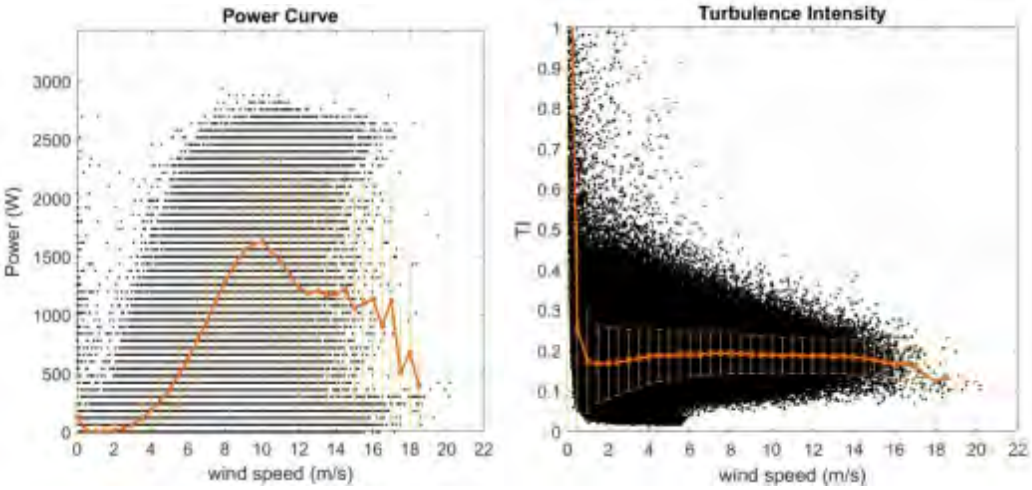

Fig 5.1.6: Power curve and turbulence intensity curve

A high degree of scatter in the power curve data is observed. The mean turbulence intensity value of 0.19 at 15m/s exceeds 0.18 prescribed in the IEC 61400-2-ed3 small wind standard but has a high probability of reaching 0.23 i.e. 1 standard deviation above the mean turbulence intensity value.

1.6.1.14.6 Site A – Directional power and turbulence curves and analysis

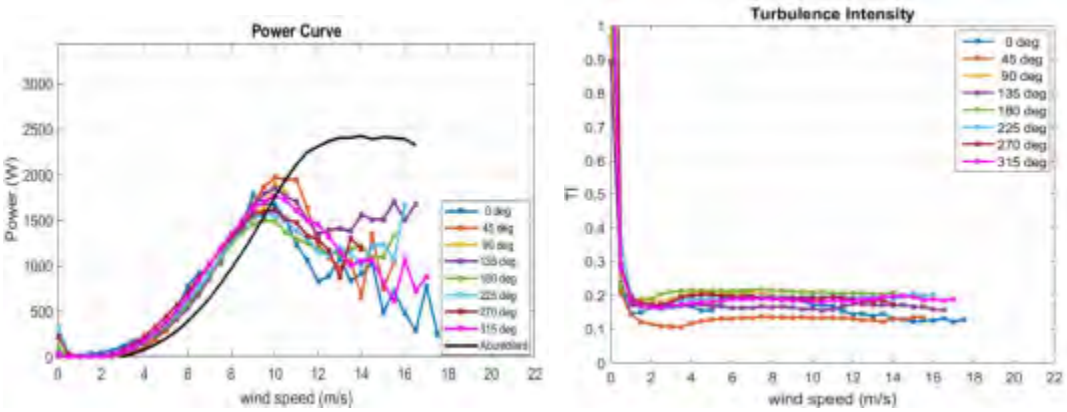

Fig 5.1.7: Directional power curves and turbulence intensity curves

The turbulence intensity and power curves vary with direction. The power curve exceeds the accredited power curve up to ~ 9m/s and rapidly deviates bellow the accredited power curve above this wind speed. All directional sectors have high turbulence with the exception of the north east (45 deg) which has an unobstructed fetch. The power curve in this direction reaches the highest values at 10m/s but it lower than the other directional power curves below 8m/s which indicate that this turbine performs better in higher turbulence at lower wind speed.

1.6.1.14.7 Site A – Directional Energy and Obstacles

An electrical energy rose shows the kWh output with direction [x]. This is plotted in figure 5.1.8. Like the wind rose is has a distinct shape showing that the majority of useful electrical energy generated by the turbine is generated from the SSW sectors some contributions from NSW and NW.

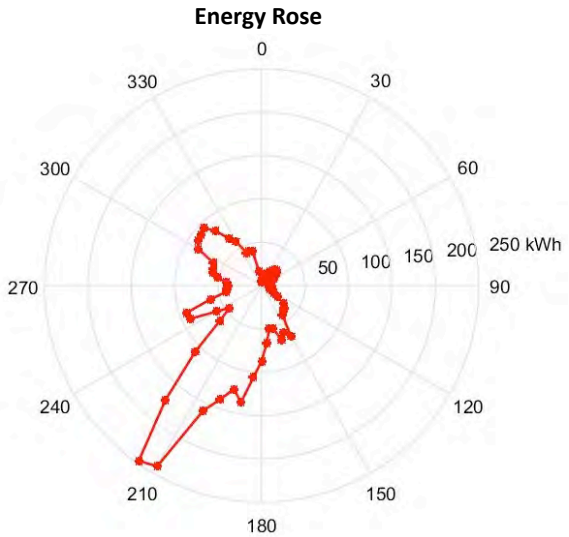

Fig 5.1.8: Electrical Energy Rose

An overlay of the output energy rose on a local plan view is shown in figure 5.1.9. Local obstacles are numbered and described in table 5.1.4

Fig 5.1.9: Electrical Energy Rose overlaid on plan view with number obstacles

The energy rose appears to be shaped by a number of obstacles in the west and south west directions with most of the energy coming from between obstacles 5 and 6. The influence of Obstacles 1 and 5 have an influence with energy coming from between them. Obstacles 2, 3, and 8 to the SE combine with this direction not being a prevailing wind direction result in little energy from the SE. The NE is not the prevailing wind direction with little or no energy despite being relatively obstacle free.

Table 5.1.4: Local obstacle descriptions (values are rough approximates)

Obstacle	Distance (m)	Height (m)	Width WT view	Comments
1	120-345	9	125	houses
2	26-45	9	16	Owner's house
3	80-106	9	28	House
4	142-160	9	20	House
5	100-122	9	30	House
6	90-114	12	50	trees
7	184-302	9	40(70)	Houses (trees)
8	126-136	9	15	house
9	250-260	9(12)	20 (70)	Houses (trees)
10	305-417	9(12)	30(66)	House/Dense trees
11	135-170			Bushes/scrub
12	150-270	9 (12)	70 (102) (134)	Houses (trees)
13	450	86 (elevation)	130	Small hill

Fig 5.1.10: Electrical Energy Rose overlaid on regional plan and labelled topographical features

In the case of the broader regional topography all hills are greater than 22 km (Feature A) away and don't appear to have a significant impact on the shape of the energy rose implying that local obstacles are the dominating influence.

Table 5.1.5: Regional topographical description

Site	Distance (km)	Elevation (m)	Comments
A	22.5	705	hills
Coast	2.5	0	Ocean

1.6.1.14.8 Site B – Location

The turbine located in a rural location in the southeast of Ireland.

Table 5.2.1: Site location

Location Co-ordinates	52°19'23.69"N, 6°52'41.34"W
Elevation (a.s.l) (m)	51

Fig 5.2.2: - Wind turbine at Site B

5.2.2 System description

Table 5.2.2: System description

Wind turbine	Skystream 3.7
Rated Power*	2.1 kW @ 11 m/s
Tower height (type)	10 m (monopole)
Inverter	Internal to system
Application	Grid connected to a house

Fig 5.2.3: Plan view of site (● mast, ● wind turbine)

The site has a number of obstacles such as houses and to north, forest to the south and east and more sparse obstacles to the west.

Looking N

Looking E

Looking S

Looking WSW

Fig 5.2.4: On site views from turbine location

1.6.1.14.9 Site B - Performance

Table 5.2.3 summarises mean wind speed energy and turbulence indicators during the test.

Table 5.2.3: Summary results

Time under test (hrs)	9317
Mean wind speed (m/s)	3.3
Metered Energy (kWh)	2041
Capacity factor	

TI (%) + 1 std dev (%) [15m/s bin]	19.8 + 4.3
TI (%) + 1 std dev (%) [5m/s bin]	22.4 + 5.8

1.6.1.14.10 Site B – Wind Analysis and Power curve performance

The site has a mean hub height wind speed of 3.3 m/s over the test period with a speed distribution shown in figure 5.2.5. The dominant wind directions are from the SW with contributions from W and NW as shown by the wind rose.

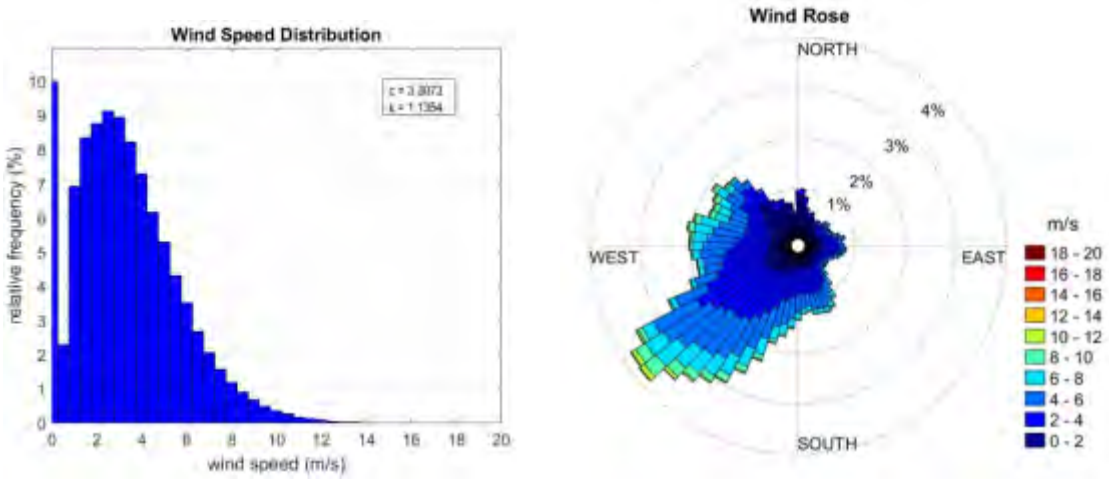

Fig 5.2.5: Wind speed distribution and wind rose

Scatter and binned plots of the measured power curve and turbulence intensity are show in figure 5.2.6.

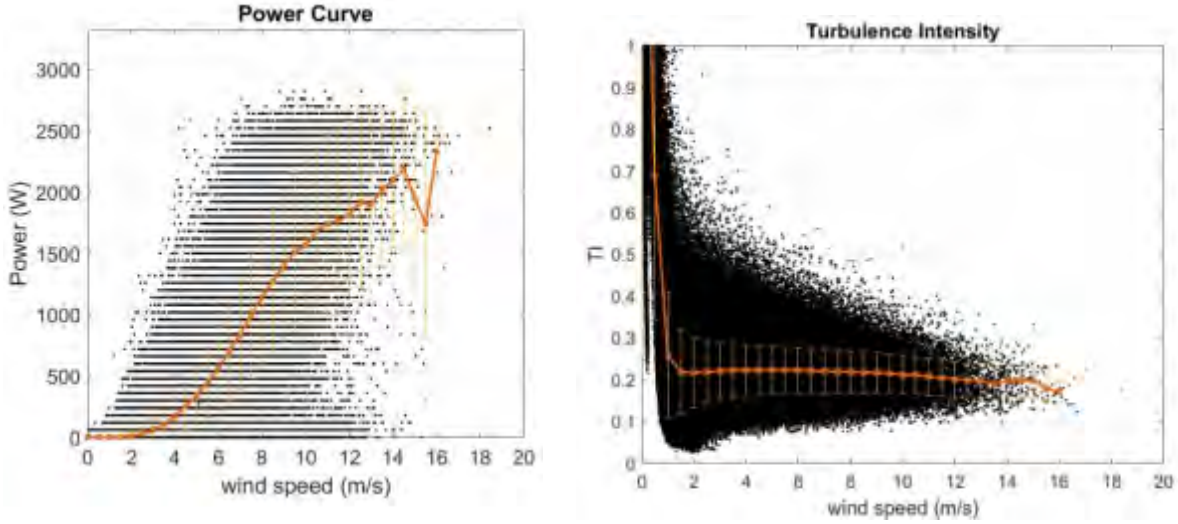

Fig 5.2.6: Power curve and turbulence intensity curve

There is also a high degree of scatter in the power and turbulence intensity curves compared to site A. The integrated controller is programmed differently compared to the previous system that contributes a different power curve. The mean turbulence intensity value at 15m/s exceeds 0.18

prescribed in the IEC 61400-2-ed3 small wind standard but has a high probability of reaching 0.24 i.e. 1 standard deviation above the mean turbulence intensity value of ~ 0.12 at 15m/s.

1.6.1.14.11 Site B – Directional power and turbulence curves and analysis

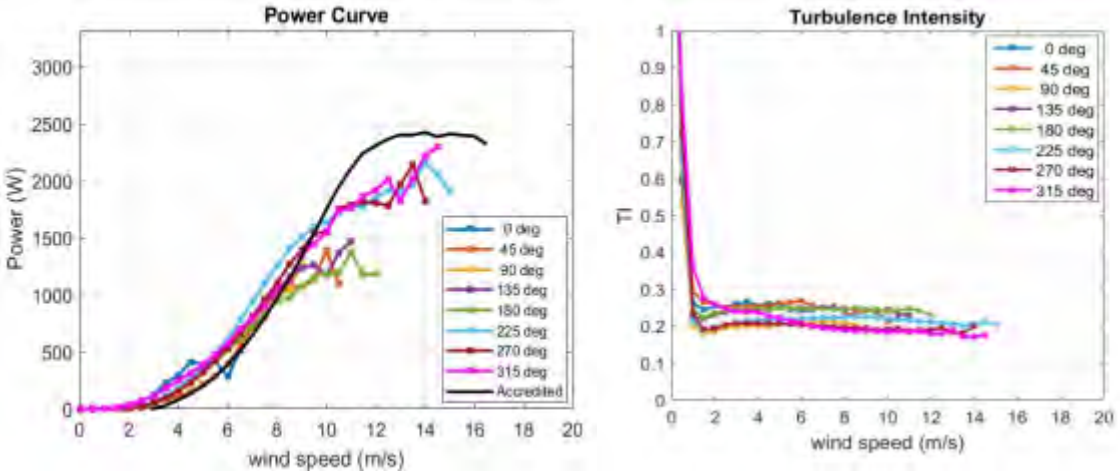

Fig 5.2.7: Directional power curves and turbulence intensity curves

The turbulence intensity and power curves vary with direction. The power curves exceed the accredited power curve up to ~ 8m/s and rapidly deviates bellow the accredited power curve above this wind speed. All directional sectors have high turbulence. The north west (315 deg) has lowest turbulence above 5 m/s and maintains the highest output power at higher wind speeds. All power curves below 8m/s have higher values than the accredited power curve which indicate that this turbine performs better in higher turbulence at lower wind speed.

1.6.1.14.12 Site B – Directional Energy and Obstacles

An electrical energy rose shows the kWh output with direction [x]. This is plotted in figure 5.2.8. This is highly directional with the majority of the energy from SW and some contribution for the NW.

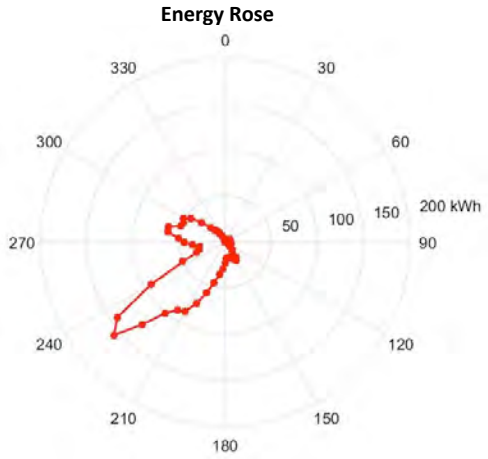

Fig 5.2.8: Electrical Energy Rose

An over lay of the energy rose on a site plan shows a forest (4, 5 and 6) to the south and hedge row (7) south of the turbine running east-west which a have a significant energy reducing impact. Most of the energy comes between obstacles 7 and 1 where there is a narrow opening where utility lines enter the site and create a long wind channel from the south west. Some contribution from the northwest between obstacles 1 and 9 where there are some small openings is seen e.g. a gap north of obstacle 1 and a more porous hedgerow. Trees and houses to the north and northeast combined with non-prevailing winds reduce energy output from these directions to almost nothing.

Fig 5.2.9: Electrical Energy Rose overlaid on plan view with number obstacles

Table 5.2.4: Local obstacle descriptions (values are rough approximates)

Obstacle	Distance (m)	Height (m)	Width WT View	Comments
1	260-330	12	112	Farm sheds

2	24-60	24	50	trees
3	64-180	9	30	houses
4	210		312 across Forest	Forest corner E
5	260		130 (4 to 5)	Forest corner middle
6	212		200 (5 to 6)	Forest corner SE
7	160-260	10	40	Hedge
8	485-680	12	110	Farm sheds
9	355-396	9	40	House

Fig 5.2.10: Electrical Energy Rose overlaid on regional plan and labelled topographical features

Table 5.2.5: Regional topographical description (values are rough approximates)

Site	Distance (km)	Elevation (m)	Comments
E coast	30	0	Ocean
S Coast	17	0	Ocean

In the case of the broader regional topography there are no significant hills to have any impact on the shape of the energy rose implying that local obstacles are the dominating influence.

Comparisons of the power curves of site A and B with the accredited power curve are shown in figure 5.2.11. They demonstrate that site power curves are site specific and can vary from their published accredited power curves.

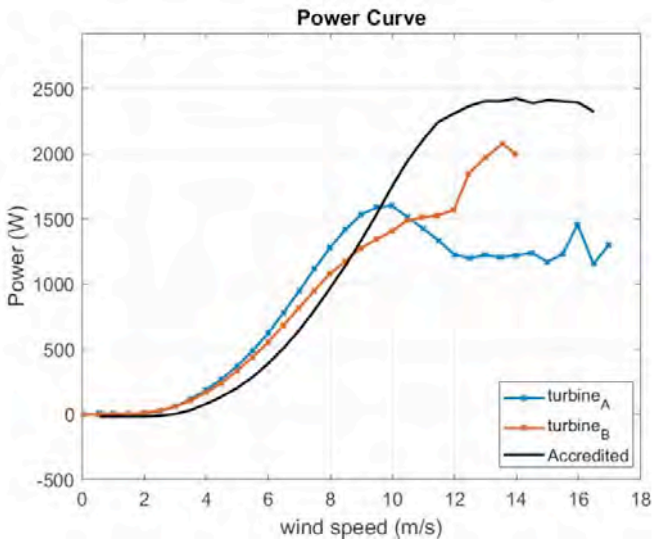

Fig 5.2.11: Site power curve comparison with accredited power curve

Inter- comparison of the power between site A and B demonstrate that site power curves are specific and can vary from their published accredited power curves.

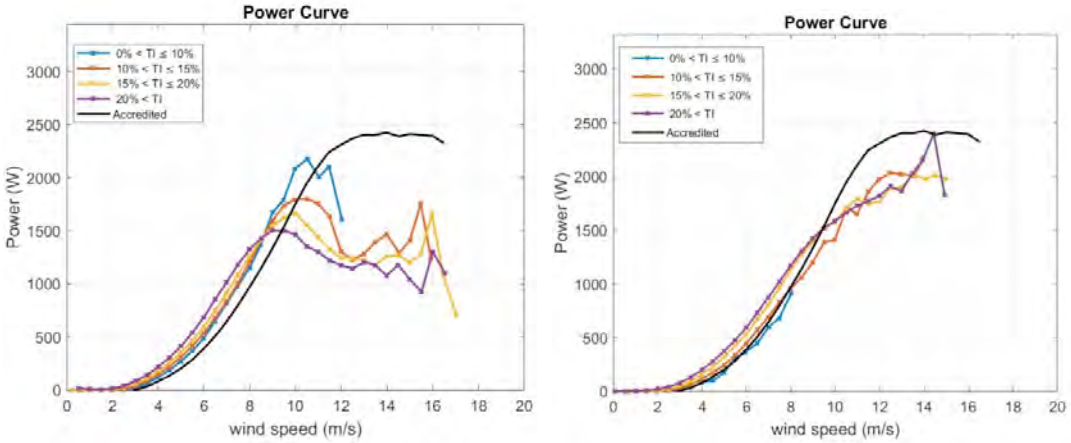

Fig 5.2.12: Site power curve comparison with accredited power curve for different turbulence ranges

1.6.2 DKiT WW Comparison V52 measurements and energy production

1.6.2.1 Introduction

This case studies consists of multiple wind resource measurements at 4 different locations in Ireland ranging from rural to peri-urban so as to assess the characteristics of the wind resource in terms of speed, direction and turbulence intensity. It aims to draw conclusions on site specific factors that have the most significant impacts when considering the installation a wind autoproducer. The measurement time periods range from months, carried out within the timeframe

of the project, to longer multi-annual data measuring periods from prior measurement campaigns. The data consists of 2D measurement from traditional cup anemometers and wind vanes, and multi-annual SCADA data from an operating large scale wind auto producer. Three case studies are presented that explore the mesoscale and microscale factors that need to be considered when siting a wind auto producer.

1.6.2.2 Measurement Sites

1) Rural elevated

Two met masts installed 6.8km apart in a hilly upland region of Co. Wicklow. Both sites are relatively free of local obstacles and the focus of this case study is on mesoscale impacts of regional topography on the measured wind characteristics. Measurements were at taken 13m at one site and at 40m at the other. These height were chosen to represent tower heights that an individual farm might use for a single small to medium scale turbine in an on-farm auto production application.

2) Peri-Urban Area

Wind and energy performance measurements of a large scale wind auto producer with 60m hub height, wind measurements from 10m mast. This case study represents industrial and small business users who wish to deploy wind auto production.

1.6.2.3 Data quality checks

A number of factors can impact the quality and quantity of measured data available. These include spurious data from sensor faults or sensor unavailability and data gaps due to faults in the data logging system. In the case of the wind turbine data assessment, maintenance down times, turbine operational faults and grid outages.

1.6.2.4 Case Studies

1.6.2.4.1 Case study 1 – Two mast comparison at elevated rural sites 6.8km apart

Figure 1 show the location of two met masts M1 and M2 in a rural upland hilly area. Both sites are approximately 20km from east coast. The masts are 6.8km apart (as the crow flies). M1 is a 13m mast located on top of a hill with an elevation of 258m above sea level. M2 is a 60m mast located on top of another hill elevated at 410m and has multiple measurement heights. A 40m measurement height at M2 was used in this study.

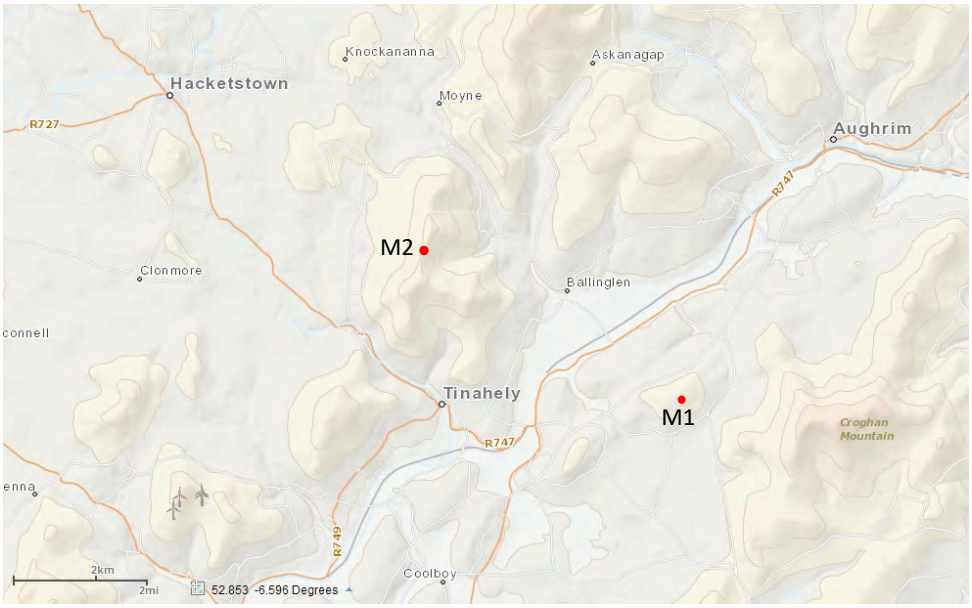

Figure 4.1

Table 4.1 Measuring equipment

Parameter	M1	M2
Wind Speed	2D cup anemometer: NRG 40C	2D cup anemometer: NRG 40C
Wind Direction	Wind vane: NRG 200P	Wind vane: NRG 200P
Data logger	Second Wind Nomad	Second Wind Nomad
Sampling rate	1 s	1 s
Logging interval	1 minute	10 minute

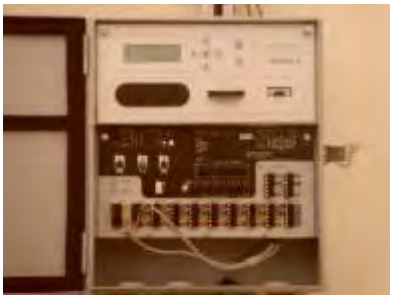

Figure 4.2: Data logger

Site M1

Figure 4.3

Site M1 is a relatively has a relatively low surface roughness with no significant local obstacles.

Results of data analysis for M1

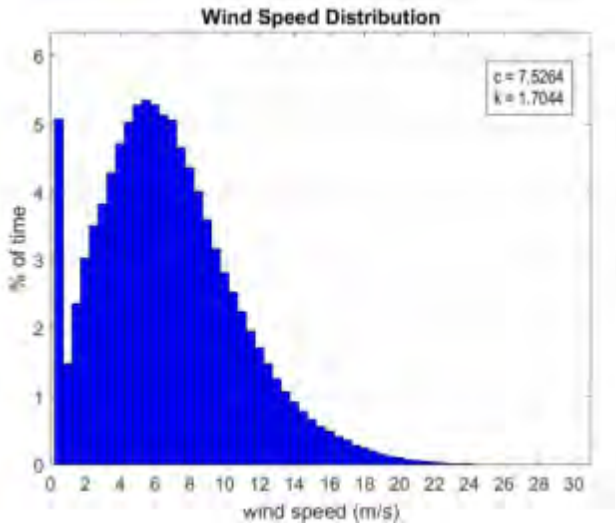

Figure 4.4

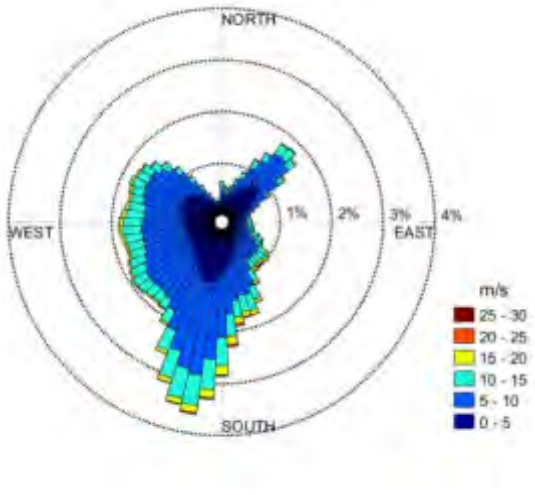

Figure 4.5

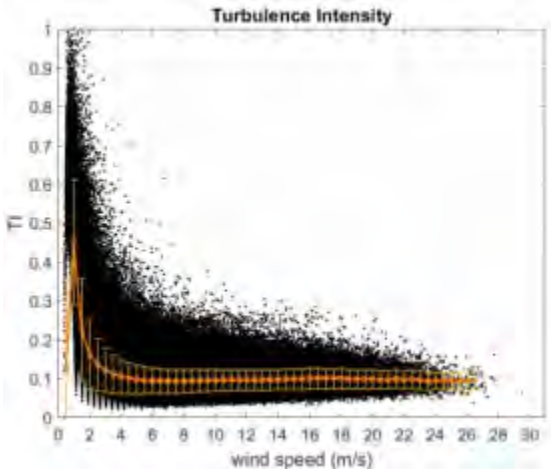

Figure 4.6

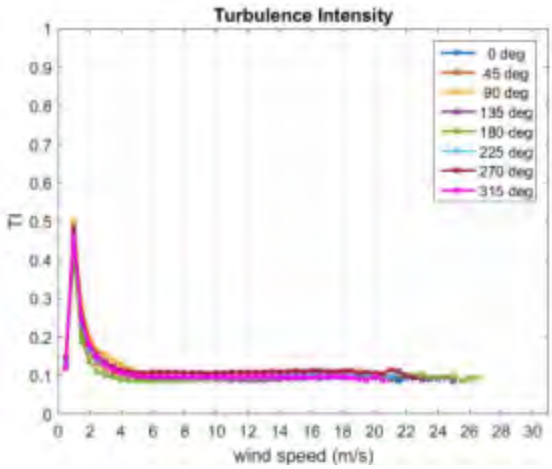

Figure 4.7

Table 4.2

Measurement height (m) a.g.l	Mean wind speed (m/s)	1-second max Wind speed (m/s)	Turbulence Intensity @ 15 m/s
13	6.7	34.5	0.1

Table 4.2 show that this site is a good wind site with a high mean wind speed and low turbulence intensity (@ 15m/s) for the given measurement height of 13m. There are no specific increases in turbulence intensity with direction which can be an expected result as the site is relatively free of local obstacles. The distinctive features of the results appear in the wind rose shown in figure 4.5 where winds appear to come from distinct directions. Specifically the best winds come from the south southwest direction, with a distinct lack of wind from the north and easterly sectors. When regional topography (mesoscale) features are examined in figure 4.1 it can be seen that there are distinct features in excess of a 10km radius around the mast location. Figures 4.8 and 4.9 shows the north westerly views from M1 where the elevated regional topography can be seen.

Figure 4.8

Figure 4.9

Figure 4.10

Figure 4.11

Figure 4.10 shows the M1 mast location from north west of the site looking towards the east. The ~600m high mountain in the background which is ~ 3km east of M1 mast is responsible for the significant lack of winds in the easterly sector. Figure 4.11 show the best wind sector as displayed on the wind rose i.e. south southwest direction looking from M1 mast which shows ~ 35km to 40km fetch in this direction

1.6.2.5 Site M2

Site M2 at an elevation of 410m has a relatively low surface roughness to the west with some low forestry trees to the east and north resulting in the surface roughness being higher than at M1. Measurements at mast M2 here are taken at a height of 40m above ground level.

Figure 4.12

1.6.2.5.1 Results of data analysis for M1

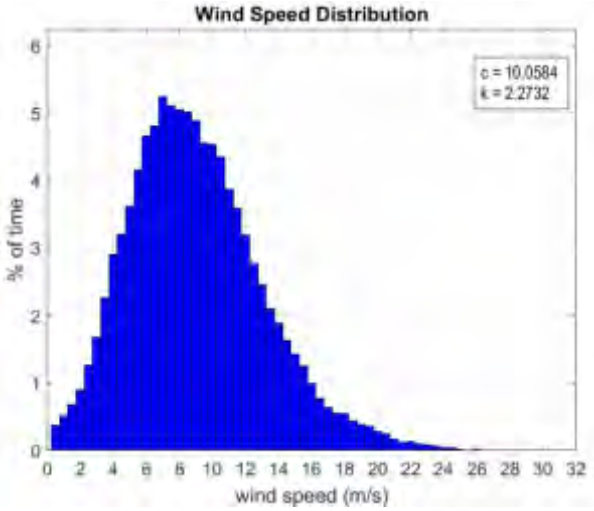

Figure 4.13

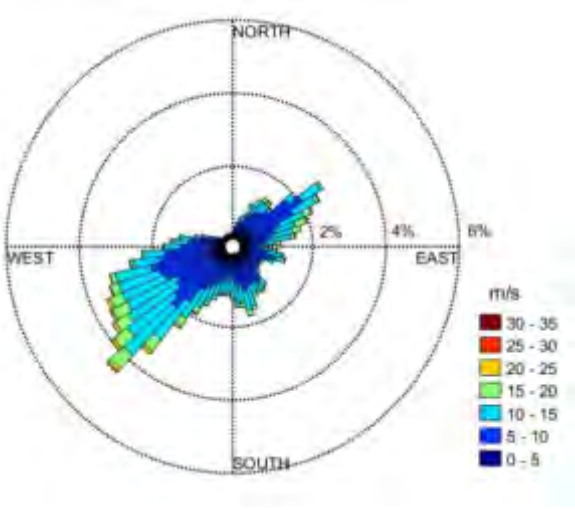

Figure 4.14

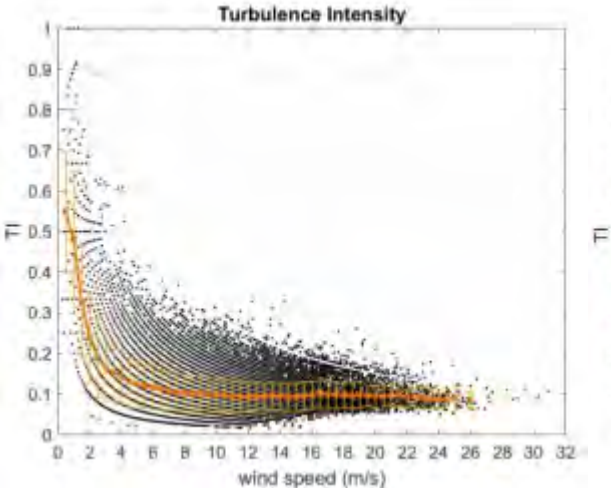

Figure 4.15

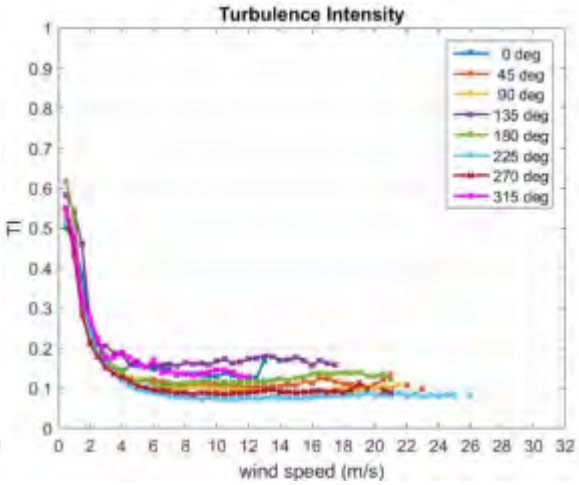

Figure 4.16

Table 4.3

Measurement height (m) a.g.l	Mean wind speed (m/s)	1-second max Wind speed (m/s)	Turbulence Intensity @ 15 m/s
40	9	38.3	0.1

Table 4.3 shows that this site is a very good wind site with a high mean wind speed and low turbulence intensity (@ 15m/s) for the given measurement height of 40m. Differences in turbulence intensity with direction can be seen in figure 16 with higher turbulence in the north to east to south sectors which is a reflection of the forested areas in these directions. However turbulence intensity remains below 20% @ 15m/s in all cases. The wind rose also shows distinct south west and north east dominant wind directions. These are not exactly the same as for M1 despite it being only 6.9km away. This show that regional (mesoscale) topography many km from a given mast location can have influence over short distances (few km) from the mast.

Figure 4.17

Figure 4.18

Figure 4.19

Figure 4.17 show the south westerly views from M2 which has a fetch in the region of 40km. The northwest to northerly view in Figure 4.18 is looking into a higher elevated topography (covered in cloud) resulting in reduced winds from that direction. Figure 4.18 show the south easterly sector which has also reduced winds. This appears to due to the mesoscale blocking effect of the same 600m high mountain that reduced winds in the easterly sector for mast M1. (It is ~ 10km from M2).

A comparison of the wind roses M1 and M2 of overlaid on a topographic is show in figure 4.20. Here the mesoscale directional influences are more evident. Both locations are affected from the north and east. The hills to the west of M1 have result in the more southerly prevailing wind at M1. Because both location are ~ 20km from east coast both have north easterly components likely from easterly onshore wind steered through the gaps/valleys to the north east of both mast locations.

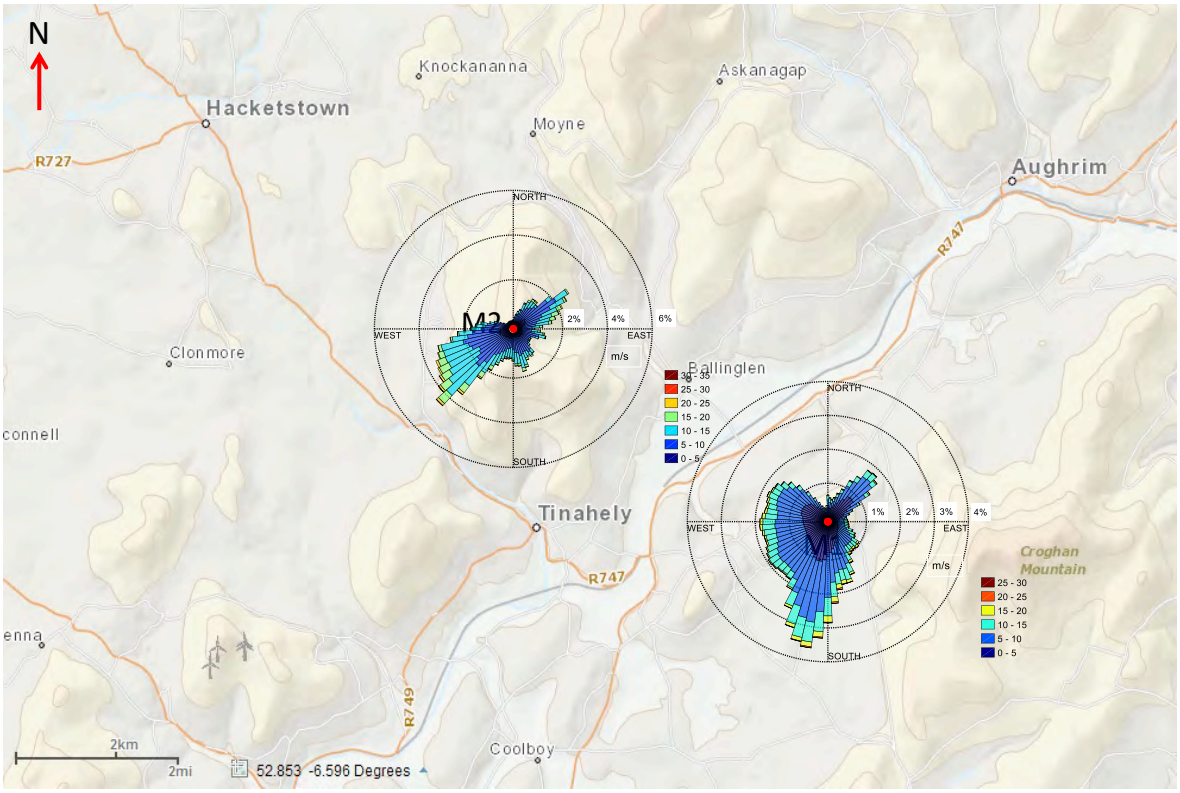

Figure 4.20

1.6.2.6 Key learning from case study 1

- When siting a wind turbine in any location the potential of mesoscale influences within a 20km radius of the site should be taken into account. This is particularly important when there is higher elevated topography within 20km, in what would be considered the general prevailing wind direction, that could result in blocking or direction steering of wind. Similarly a site within 20km of the coast may have extra energy to be gained from onshore winds due to land/sea influences and topography between the site and coast should be considered.

1.6.3 Case Study 2-Rural at low elevation

Figure 4.21 show the location a 13m met mast at the Louth Co. Co dog pound located a at low elevation of 10m in a rural location ~ 5km from the east coast. The mast is surrounded by nearby obstacles such as the building itself and neighbouring houses and motor way service stations. Figures 4.22 and 4.23 shows a plan view of the site at defend scales showing the mast location and Table 4.4 gives approximate distances and heights of local obstacles from the mast location

Figure 4.21

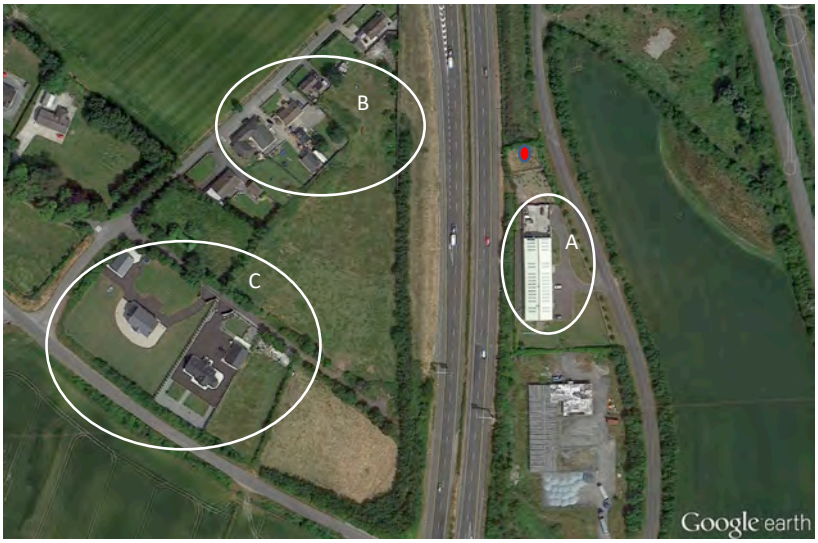

Figure 4.22 : mast location

Figure 4.23 : mast location

Table 4.4

Obstacle	Distance Range(m)	Mean height(m)
A	50-185	5
B	270-400	4
C	75-240	4
D	420-510	9
E	500-600	9
F	415-720	5
G	360-570	5

The local obstacles consist of the building itself to the south of mast location along with nearby single houses and clusters of houses to the westerly and easterly sides. Further south and northwest there are motor way service stations (D and E). There are also dispersed trees/hedge rows around the site and a motorway flyover bridge exist in the south south-westerly direction (i.e. between A and D)

1.6.3.1.1 Results of data analysis

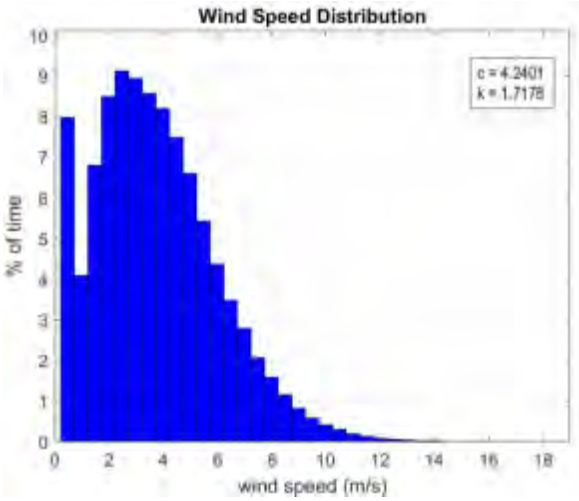

Figure 4.24

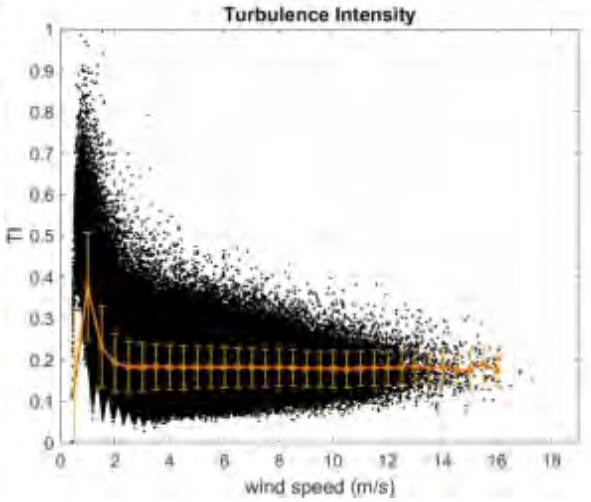

Figure 4.25

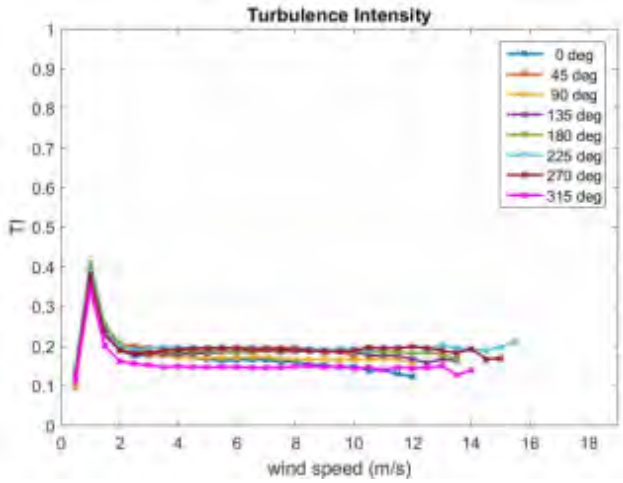

Figure 4.26

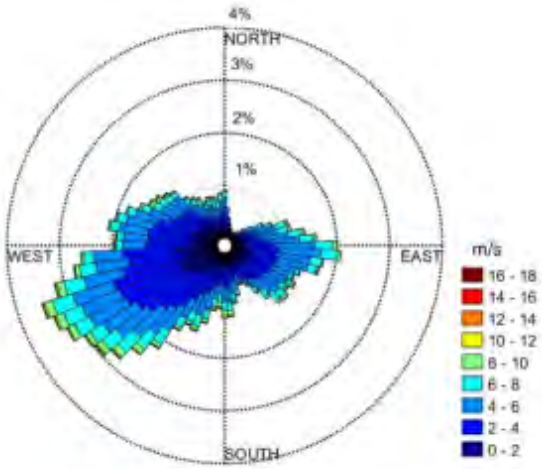

Figure 4.27

Table 4.5

Measurement height (m) a.g.l	Mean wind speed (m/s)	1-second max Wind speed (m/s)	Turbulence Intensity @ 15 m/s
13	3.8	25.0	0.17

Table 4.5 show the site has relatively low mean wind speed and increased turbulence intensity (@ 15m/s) for the given measurement height of 13m. Differences in turbulence intensity with direction can be seen in figure 4.26 with higher turbulence in the south to west sectors which is a reflection of the manmade obstacles (buildings) in these sectors. It is also noted that turbulence intensity exceeds 0.2 @ 15m/s in the south west sector. This is above the design turbulence intensity of 0.18 @15m/s in the current IEC 61400-2 Ed 3 small wind standard. The wind rose also shows distinct features with reduced wind to the north and northwest sectors and also the southerly sector. The

building (A) at the site itself which is 50m from the mast combined with building (D) and a motorway flyover (~ 250m away) bridge further significantly reduce the southerly wind as seen by the mast. In the southwest sector the peak of the wind rose occurs between obsticals in B and C. There is a higher density of houses in B which appear to have more significant influnce on wind flow that the sparcer obsticles in C. Significant easterly winds are also observed due to proximity of site to east coast. An overlay of the wind rose on the site plan in figure 4.28 shows how the wind rose is shaped by local obstacles. Referring to the distances show in Table 4.5 it is evident that obstacle less at significant distances may have influence on the wind flow at the mast itself. E.g. a broad clusters of houses in regions F and G which are ~ half the mast height and a least 360m away (~ 30 mast heights) appear to shape easterly wind flow.

Figure 4.28

1.6.3.2 Key learning from case study 2

- The energy output from small wind turbine sited at low elevations can be greatly impacted upon by local obstacles at significant distances from the site location (~ 30 hub heights by obstacles ~ half of the height). Clusters of low obstacles have bigger reduction impact than sparse single obstacles. Turbulence intensity can exceed that used in current small wind design standards (i.e.0.18 @ 15m/s). This may be significant for the operating life of a turbine if the high turbulence sector is also the prevailing wind direction.

1.6.4 Case study 3 - DkIT Site – Peri-urban area

In this study a multi annual analysis of SCADA data recorded at 60m in 10 minute averages from an existing 850kW wind auto producer was carried out. 2D measurements of wind speed and direction were also taken at 10m on the same site to assess conditions for small wind.

Figure 4.29

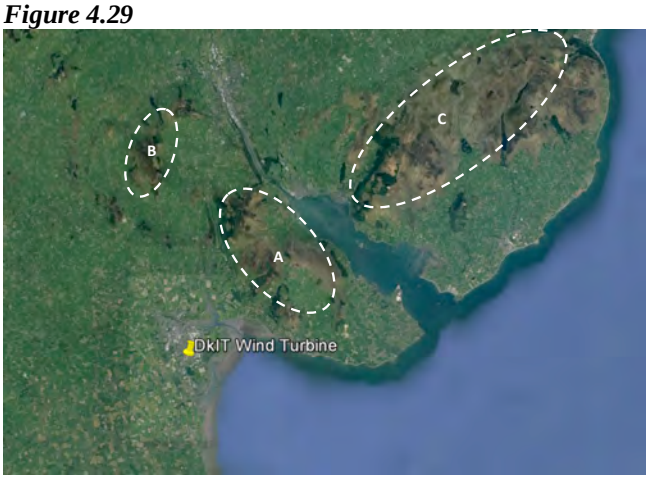

Figure 4.30

The turbine is located on the east coast of Ireland at 9 m above sea level. 7 km to the northeast of the site there are hills that rise to elevations from 300 m to 600 mas shown in figure 30. The terrain to the south and west is low lying. The regional (mesoscale features) are outlined in Table 4.6

Table 4.6

Regional site features

Site	Distance [km]	Elevation [m]
A	7.5-15	75-563
B	13-18	10-540
C	17-40	0-663

A range of local obstacles (building) exit around the turbine location. There are shown in Figure 4.31 and a description of these is given Table 4.7.

Figure 4.32 (X = turbine location)

Table 4.7

Local site features	
Obstacles	Distances, heights and description
1	Industrial buildings 150 m to 1.2 km away from turbine. Majority are 11 m high with one small block 25 m high. The total building cluster width is 670 m as seen from the turbine. The area also included a row of houses to the west that are ~ 7 m high.
2	Hotel and office blocks 350 m to 650 m away from turbine. The hotel 47 m high and 33 m wide. The office blocks are 12 m height and 220 m wide as seen from turbine
3	Sports field to north east with town to north (not shown)

1.6.4.1 Results from Turbine data analysis

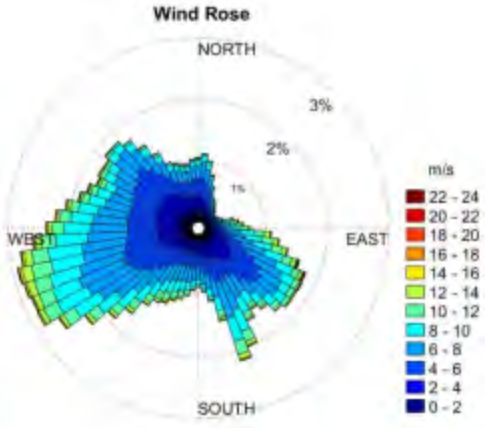

Figure 4.33

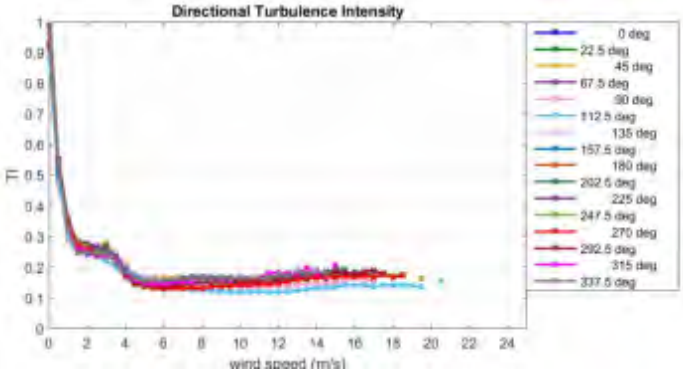

Figure 4.34

The wind rose show distinctive features with notable reduction wind as seen by the turbine at 60m in the south to south west directions and north east directions. The directional turbulence intensity also shows variation with lowest turbulence towards east south east (112.5 degrees) and the higher values in southwest and northwest directions. The turbine energy output with direction (energy rose) was further investigated as shown in figure 4.35. This reveals a very distinct shape particularly in the north east southeast and south west sectors.

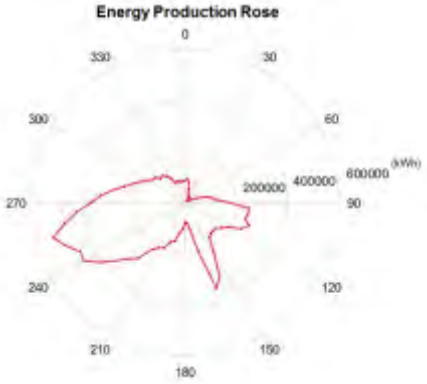

Figure 4.35

Overlays of the energy rose on the plan view of both local and regional maps are show in figures 4.35 and 4.36.

Figure 4.35

Figure 4.36

Referring to the local and regional site features given in Tables the follow is observed
Low broad buildings, ~ 1/5 of hub height within 20 hub heights of the turbine, in the south southwest sector appear to have a large energy reducing impact (similar observations in Case study 2). The view as seen the turbine a hub height in this directional sector is shown in figure 4.37. Taller narrow buildings appear to have less an impact i.e. building width is important. Hills to the northeast 7 km away at a higher elevation have a significant energy blocking effect (mesoscale impacts and was observed in Case study 1)

Figure 4.37

Ten year annual energy production totals are shown in Figure 4.38. Internal variation in energy output can occur depending on each wind year. In this case the mean annual energy production 1,507,200 kWh, standard deviation 173,880 kWh i.e. (+/- 11%). An exceptionally low wind year (e.g. 2010) can have big bearing on longer term annual energy output totals assessments. The power curve for the turbine is shown in Fig 4.39. All measured wind turbine power curves show some degree of scatter and are site and technology specific i.e. can deviate from manufactures published power curves. This is an ongoing area of research.

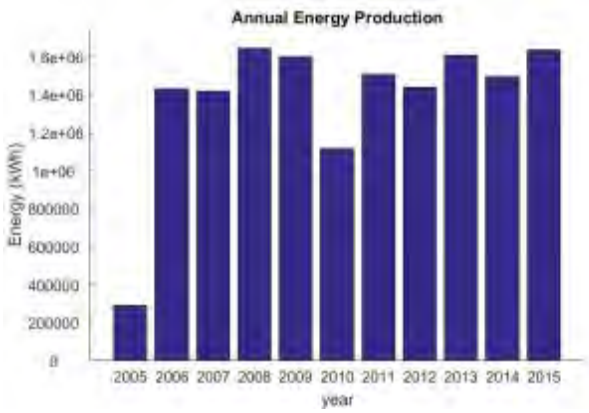

Figure 4.38

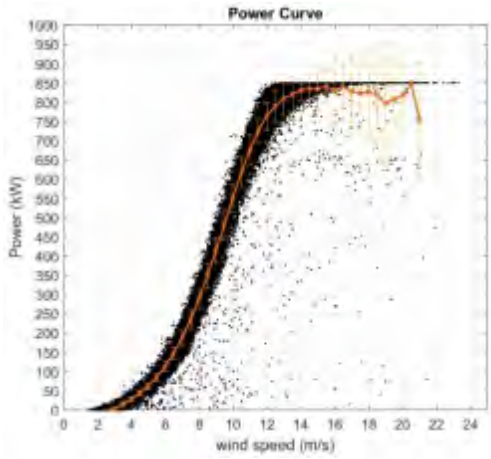

Figure 4.39

1.6.4.2 DkIT 10m mast measurements

In addition to data from the turbine measurements were also made at 10m at the DkIT site at ~ 80m to the east of turbine. The location is show in figure 4.40

Figure 4.40

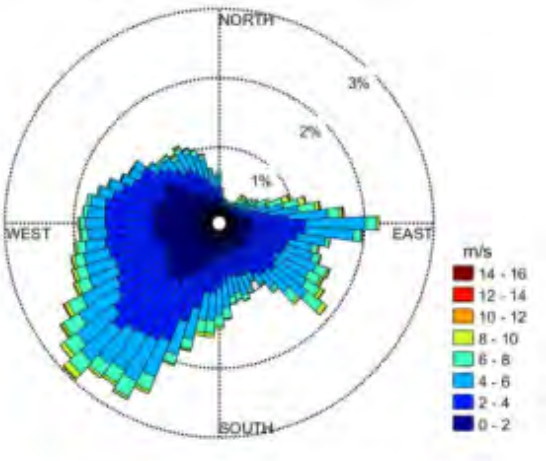

Figure 4.41

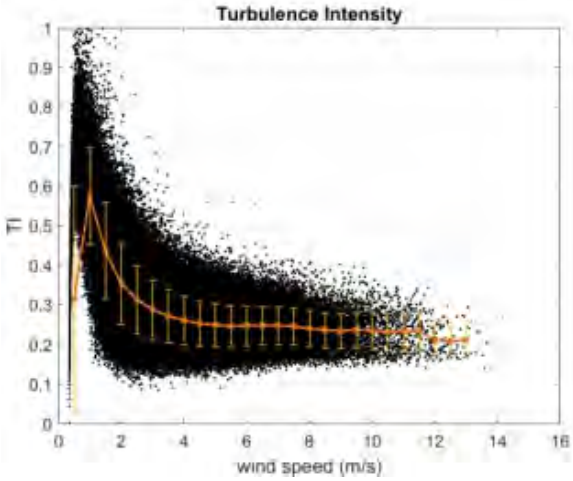

Figure 4.42

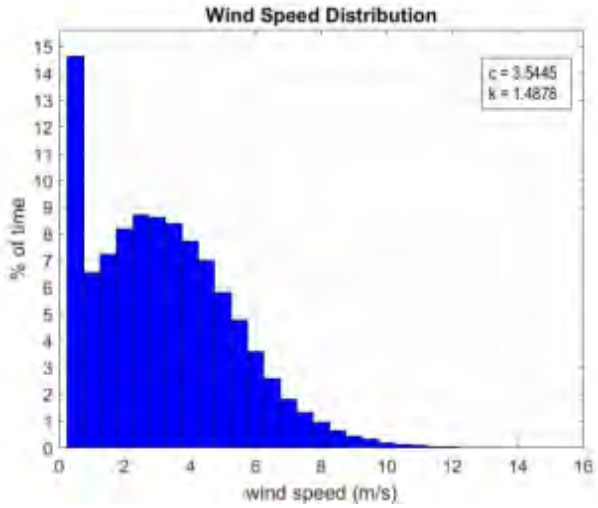

Figure 4.43

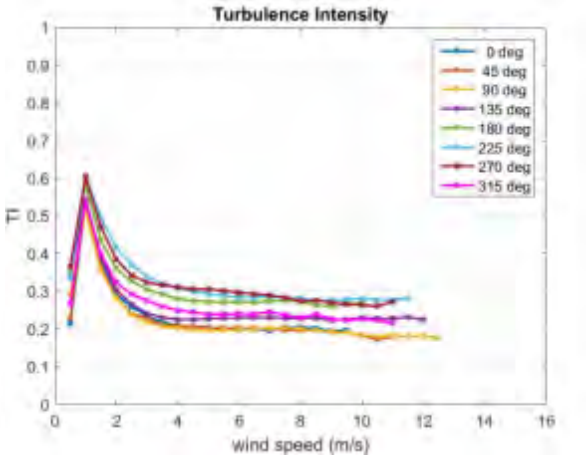

Figure 4.44

Table 4.7 (*estimated TI @15m/s as measurements did not contain sufficient number of data points in this bin)

Measurement height (m) a.g.l	Mean wind speed (m/s)	1-second max Wind speed (m/s)	Turbulence Intensity @ 15 m/s
10	3.2	28.2	0.20*

Table 4.7 show the site has low mean wind speed and high turbulence intensity (@ 15m/s) for the given measurement height of 10m. Differences in turbulence intensity with direction can be seen in Figure 4.44 with higher turbulence in the south to west sectors which is a reflection of the manmade obstacles (buildings) in these sectors with the lowest in the easterly sector which look across flat sports fields to the coast It is also estimated that turbulence intensity is close to 0.3 @ 15m/s in the south west sector. This is well above the design turbulence intensity of 0.18 @15m/s in the current IEC 61400-2 Ed 3 small wind standard. It suggest that 10m hub heights are suitable heights in this environment.

1.6.4.3 Key learnings from case study 3

- Low broad buildings, ~ 1/5 of hub height within 20 hub heights of the turbine, in the south southwest sector appear to have a large energy reducing impact.
- Taller narrow buildings appear to have less an impact i.e. building width is important.
- Hills at higher elevations than the site location 7 km away at a higher elevation have a significant energy blocking effect
- Standard deviation in annual energy output for a single large scale wind autoproducer at DkIT 11% based on 10 years of data
- To see mean wind speeds of at least 5m/s for small wind turbine in areas of low elevation, tower heights of a least 30m are required.
- Short towers (e.g. 10m) are not likely to be energy viable options for small wind turbines in areas of low elevation.
- Low broad buildings, ~ 1/5 of hub height within 20 hub heights of the turbine, in the scan have a large energy reducing impact on a large scale wind autoproducer
- Taller narrow buildings appear to have less an impact i.e. building width is important.
- Hills at higher elevations than the site location 7 km away at a higher elevation have a significant energy blocking effect on a large scale wind autoproducer
- Standard deviation in annual energy output for a single large scale wind autoproducer at DkIT 11% based on 10 years of data
- Short towers (e.g. 10m) are not likely to be energy viable options for small wind turbines in areas of low elevation.

1.6.4.4 Summary conclusions

- When siting a wind turbine in any location the potential of mesoscale influences within a 20km radius of the site should be taken into account. This is particularly important when there is higher elevated topography within 20km, in what would be considered the general prevailing wind direction, that could result in blocking or direction steering of wind. Similarly a site within 20km of the coast may have extra energy to be gained from onshore winds due to land/sea influences and topography between the site and coast should be considered.
- The energy output from small wind turbine sited at low elevations can be greatly impacted upon by local obstacles at significant distances from the site location (~ 30 hub heights by obstacles ~ half of the height). Clusters of low obstacles have bigger reduction impact than sparse single obstacles. Turbulence intensity can exceed that used in current small wind design standards (i.e.0.18 @ 15m/s). This may be significant for the operating life of a turbine if the high turbulence sector is also the prevailing wind direction.

1.7 JAPAN (active 2009 – 2018)

1.7.1 CFD findings – rectangular building

Software used:

FrontFlow/red (Japanese open-source software) [1]

Flow type:

Incompressible flow in neutral atmospheric conditions

Governing Equations:

Filtered continuity equation

Filtered Navier-Stokes equations

Turbulence model:

Standard Smagorinsky model

Discretization:

Finite volume method on a collocated grid system

Advection term → 2nd order central difference (90%)

+ 1st order upwind difference (10%)

Other term → 2nd order central difference

Velocity pressure coupling: SMAC method

Time integration: Implicit Euler method

Computational grid:

Type→ An O-type structured grid around the building, an unstructured outside the O-type structured grid, and a Cartesian grid outside the unstructured grid

Spacing→ 0.01*b* at the corners of the building, 0.0025*b* at the first layer of the grid points next to the walls. Here, *b* is the building breadth.

Number of grid points→ 1.2 million

Table Boundary Conditions for velocity and pressure

Boundary	Velocity	Pressure
Inlet	Time-dependent inflow	Zero-gradient
Outlet	Neumann	Zero-gradient
Lateral	Free-slip	Zero-gradient
Upper	Free-slip	Zero-gradient
Bottom	Law of the wall	Zero-gradient
Building wall	Law of the wall	Zero-gradient

Time dependent turbulent inflow data assumptions:

The data was generated by using Kataoka's rescaling approach[2], in which the height of the turbulent boundary layer assumed to be the same in a short distance in the streamwise direction.

Reynolds number, time step and statistics:

Reynolds number→ Approximately 23,000 based on *b* and on the streamwise wind velocity at the building height, *h*, at the inlet boundary (3.25*h* upwind of the building center.)

Time step→ 0.0002 s

Statistics→ 1.2 million

Inflow boundary condition assumptions:

Neutral turbulent atmospheric boundary layer over terrain classified as Terrain Category IV, which is defined in wind loading standards and design criteria of Architectural Institute of Japan[3].

Conclusions*:*

Incoming mean wind flow separates at the overall leading edge of the building and a low wind speed region is formed near the roof surface.

At all heights, the wind power density (WPD) above the vicinity of the windward corners of the building is larger than the WPD of the upwind region where the effect of the building (WPD_{inlet}) is negligible. In addition, WPD above the vicinity of the building's leading edge becomes larger than WPD_{inlet} from a relatively small distance from the roof surface.

The magnitude of the mean horizontal wind velocity $\overline{U}$ over the roof significantly depends on the length of the windward edge of the roof. The variation in $\overline{U}$ over the roof tends to become smaller with a decrease in the horizontal aspect ratio (HAR) of the building. This tendency is more prominent as the wind direction α increases. Here, α is defined as the angle between the vector of the stream-wise wind direction and the normal vector of the building's leeward face with longer roof edge.

At the windward corners of the roof, wind conditions are generally favorable at relatively low heights. However, when HAR ≤ 0.5 and α = 22.5º, the bottom of the height range of favorable wind conditions at the windward corner between the roof's shorter windward edge and its longer leeward edge is relatively high. In addition, when α = 45º or when HAR ≤ 0.5 and α = 67.5º, $\overline{U}$ at the windward corner between the two windward edges is low.

In many cases with HAR and α, wind conditions at the midpoint of the roof's windward edge are not favorable at relatively low heights. When α = 0º or 90º, wind conditions at this location are not favorable at relatively low heights. In addition, when α = 22.5º or HAR = 0.25 and 45º, the wind conditions at the midpoint of the roof's windward longer edge are not favorable at relatively low

heights.

At the leeward locations of the roof, the bottoms of the height range of favorable wind conditions are generally higher than those at the windward locations, but the favorable wind conditions are much better than those at the windward locations. When α = 0º or 90º, the order of the bottoms of the height range of favorable wind conditions at the leeward roof locations does not change with HAR; the bottom of the height range at the midpoints of the roof's edges parallel to the wind direction is lowest among the leeward representative locations. In addition, when α = 45º, the bottom of the height range at the center of the roof is lowest among the leeward representative locations.

Under the condition where there is no prevailing wind direction, the center of the roof is the most optimal location for installing SWTs. In addition, compared with the midpoints of the roof's long edges, the midpoints of the roof's short edges are more favorable for installing SWTs. Moreover, it is less favorable to install SWTs at the corners of the roof than at the center and midpoints of the roof's short edges. However, although the turbulence intensity is significantly larger than that of undisturbed wind, at relatively low heights at the corners, the turbulence intensity and wind velocity are significantly smaller and larger, respectively, than those at other representative locations.

***Reference**:*

[1] Unemura, T., Zhang, H. and Taniguchi, N., Development of the Fluid Dynamics Simulation Software "FrontFlow/Red," Seisan Kenkyu, 2004, 56, 40–43.

[2] H. Kataoka, Numerical simulations of a wind-induced vibrating square cylinder within turbulent boundary layer, Journal of Wind Engineering and Industrial Aerodynamics, 96 (2008) 1985–1997.

[3] Y. Tamura, T. Ohkuma, H. Okada, J. Kanda, Wind loading standards and design criteria in Japan, Journal of Wind Engineering and Industrial Aerodynamics, 83 (1999) 555–566.

1.7.2 Nasu Denki Tekko Rooftop Test Site

1.7.2.1 Measurement strategy:

Measurement data is collected from an anemometer and wind vane, set up at about 9.5 m agl on the roof of the two-story building in Tokyo, surrounded by structures of different types. The height of the building is 8 m. A small wind turbine of 135 W rated power and 1 m rotor diameter, from Nasu Denki Tekko, is located 3.4 m from the sensors.

Table 1: Sensors used

	Anemometer	**Wind vane**
Type:	3-cup type	
Range:	0.5 m/s to 40 m/s	0° to 540° (180° overlap)
Accuracy:	2 % (full range)	±3°

Dynamic response:	3.5 m	2.5 m

1.7.2.2 1.1.3.2 Site photographs and layout drawings

Fig. 1: Site location (Source; Google Maps)

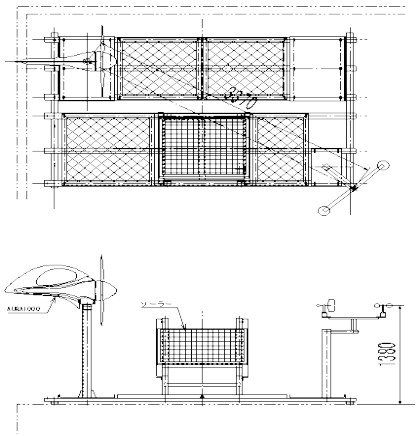

Fig 2: Sensor setting

Fig 3: Objective buildings

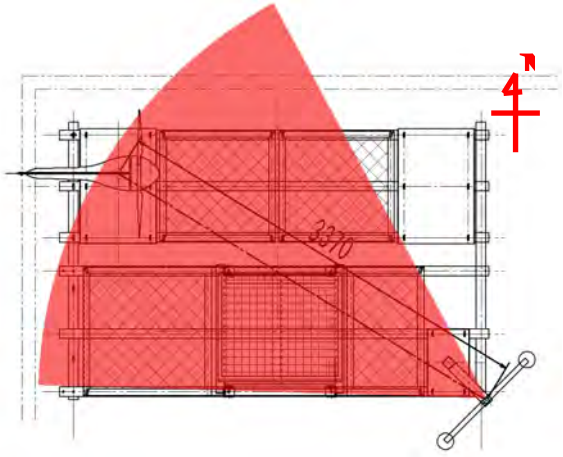

Fig 4: Sector of exclude

Data is removed in the range where the turbine's wake influences the sensors. The excluded sector is 60° wide (273° to 333°) <N=0° , E=90° , S=180° , W=270° >

Table-2 site location (each direction)

North side	East side
South side	West side

1.7.2.3 Wind conditions:

Wind rose

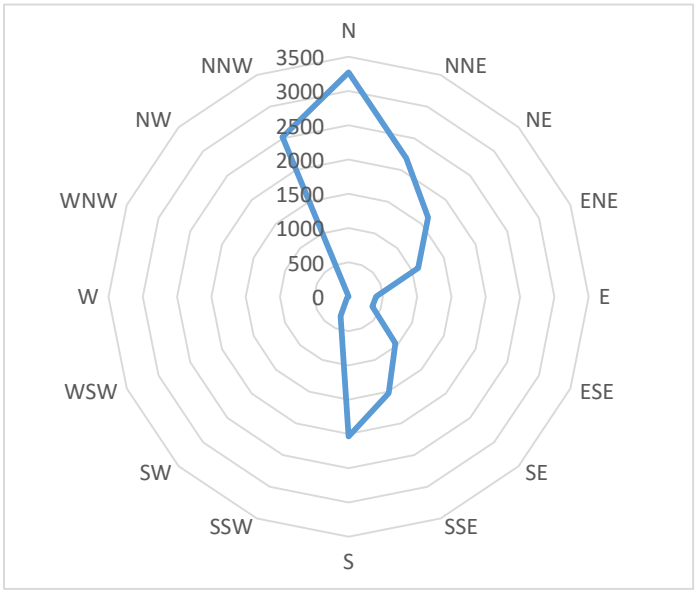

Fig 5: Wind rose 10min average data (exclude from W to NW)

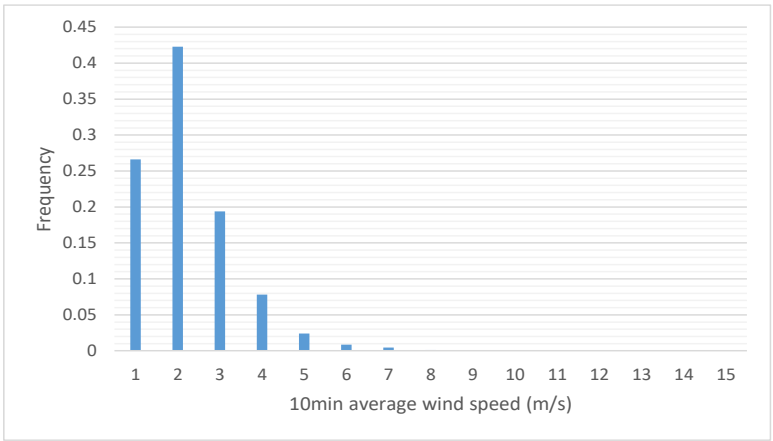

Fig 6: Wind speed frequency 10min average data (exclude from W to NW)

1.7.2.4 Summary Turbulence Intensity Test Results Compared to NTM

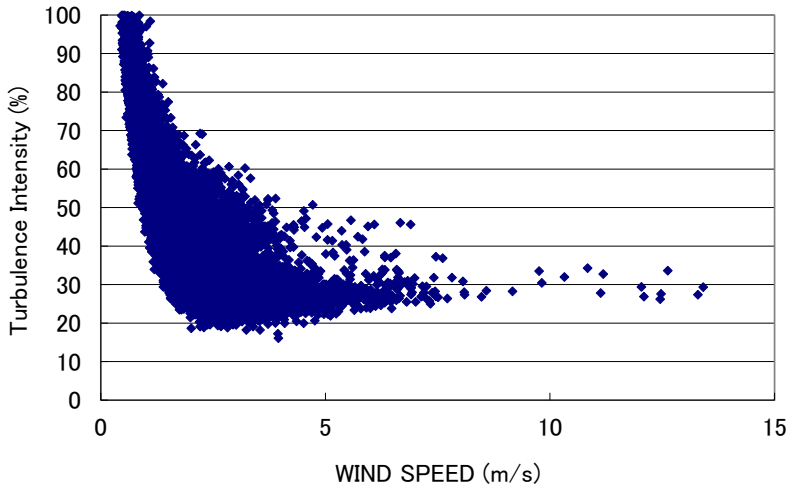

Fig 7: Wind speed vs Turbulence intensity (10min average data)

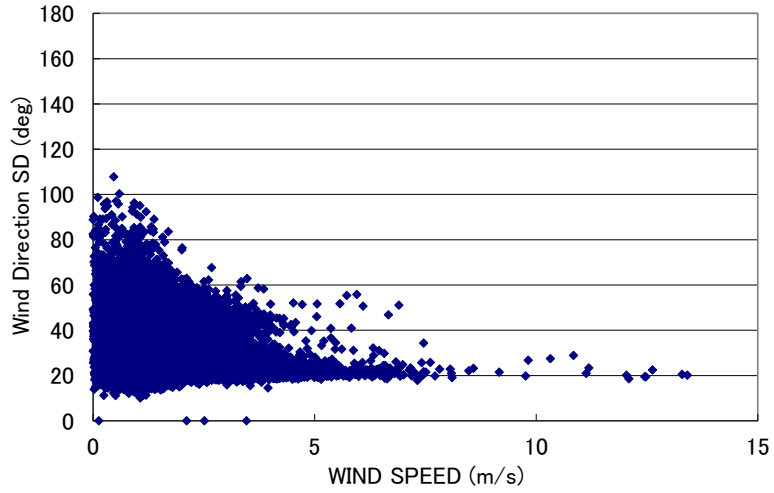

Fig 8: Wind speed vs Standard deviation of wind direction (10min average data)

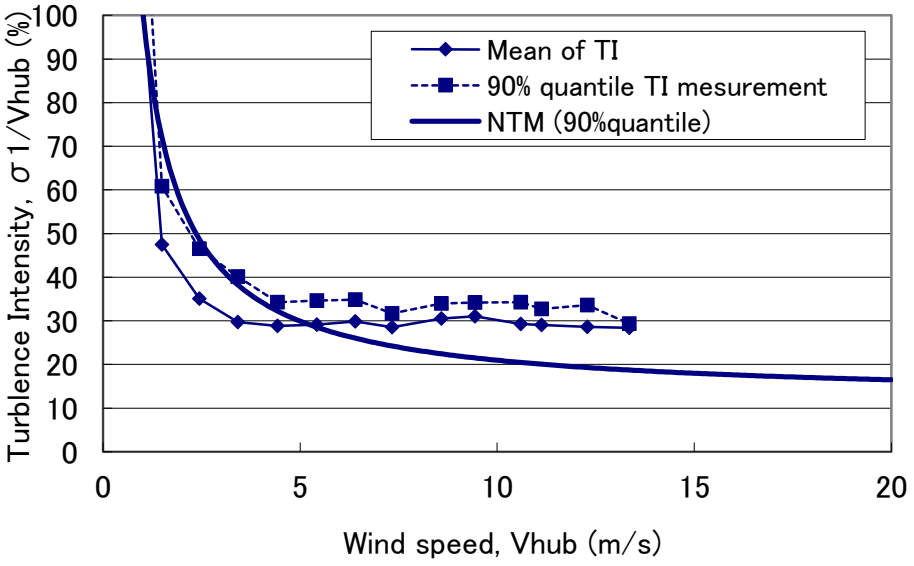

Fig 9: Wind speed vs Turbulence intensity (Compared with IEC model)

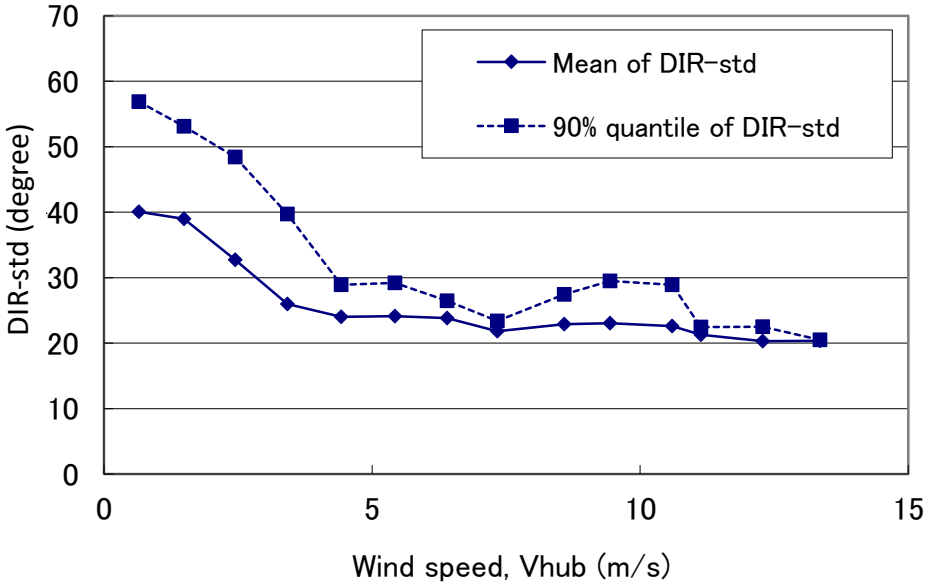

Fig 10: Wind speed vs Standard deviation of wind direction (Wind speed bin data)

1.7.2.5 EDC Results

Procedure of EDC analysis

① The measured wind direction is calculated as an angular velocity per unit time.

② As “The duration of the wind direction change transient = 6sec”, the wind direction change magnitude is calculated to a 6sec simple moving average for the wind direction angular velocity.

③ The objective wind speed is calculated to the 6sec simple moving average.

④ This calculation of the relation between the wind speed and the wind direction change magnitude is done for all measured data.

⑤ Because a moving wind direction change magnitude (6sec) for all measured data is calculated from this analysis, representative values of the average wind speed(Vhub),the wind direction change magnitude(D_{MAG}), and the moving average wind speed(V_{AVE6}) are determined in each data set.

⑥ In each representative value, the relation between the wind speed and the extreme wind direction change magnitude is evaluated in the 1m/s wind speed BIN based on Vhub.

※In the 1m/s wind speed BIN, 90 percentile is the concluding representative extreme wind direction change.

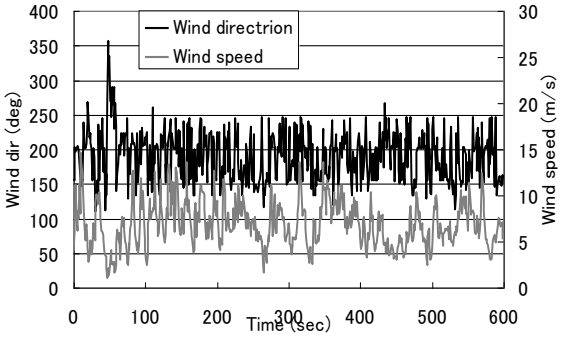

Fig 11: Raw data

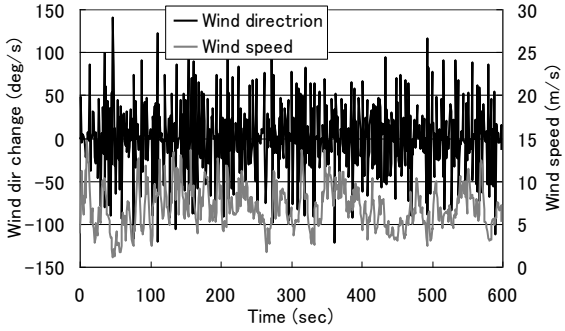

Fig 12: Calculation of angular velocity (methd①)

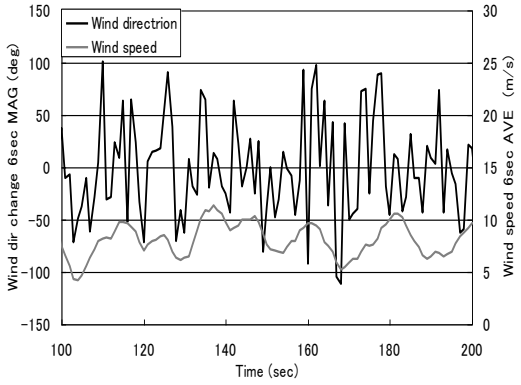

Fig 13: Wind DIR change magnitude - 6 sec

(method②③④)

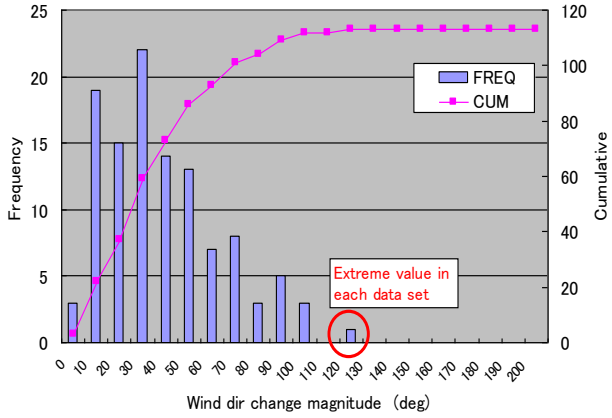

Fig 14: Selection of EDC in each data set

(method⑤)

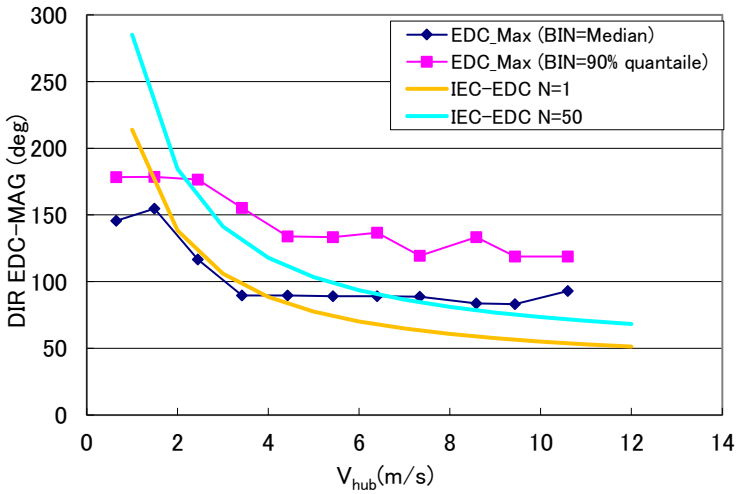

Fig 15: Wind speed(Vhub) vs EDC-magnitude

The main findings regarding the turbulence intensity and EDC are summarized as follows.

- Representative Turbulence Intensity is 0.3. (Estimated I_{15} is also 0.3.)
- EDC can be 120° even wind speed of more than 10m/s

1.7.2.6 Wind conditions (Compared with ultrasonic and 3-cup)

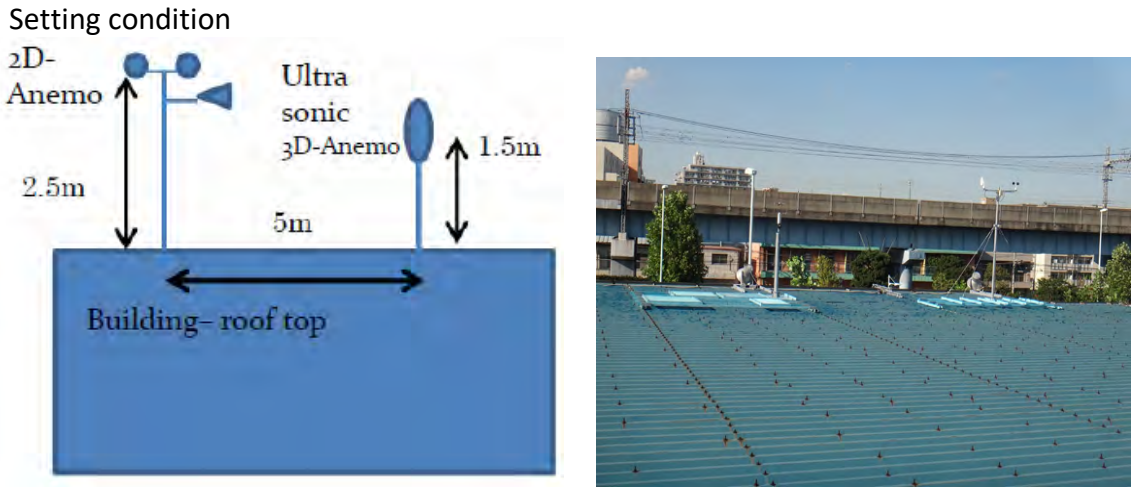

Fig 16: Anemometer setting condition (Replace previous measurement systems)

3D- Anemometer : Ultra sonic (measurement items= u, v, w and temp. 20Hz)
2D- Anemometer : 3cup and vane type (measurement items= u, v. 1Hz)
Compare with 2 types anemometer about turbulence characteristics

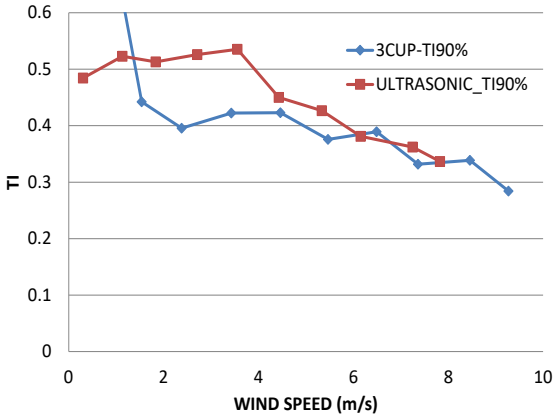

Fig 17: Wind speed vs Turbulence Intensity

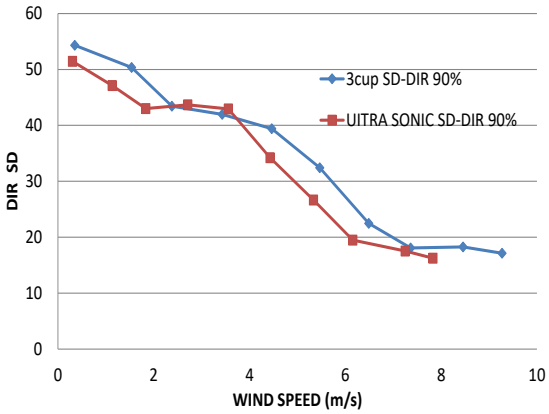

Fig 18: Wind speed vs Standard Deviation of Wind direction

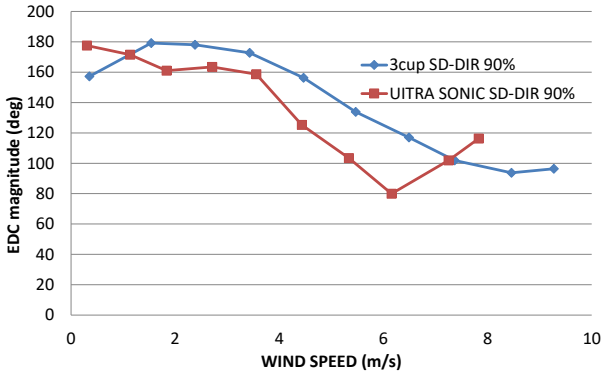

Fig 19: Wind speed (Vhub) vs EDC-magnitude

Turbulence characteristics (turbulence intensity, standard deviation of wind direction and magnitude of extreme direction change) were indicated similar tendency in spite of deference anemometer type.

1.7.2.7 Characterize turbine and its power production

Objective wind turbine

Objective wind turbine is “AURA1000” made in NASU DENKI－TEKKO CO., LTD.

This wind turbine has 1m in diameter, 5 blades, and rated power 135W (wind speed 10m/s).

This wind turbine is shown in Figure-1, and basic specifications are shown in Table-3.

Table -3 Specification of AURA1000

Rated output	135W(10m/s)
Rated Revolution	550rpm(10m/s)
Cut-in	2m/s
Cut-out	13m/s (Battery 12V)
	16m/s (Battery 24V)
Maximum output	280W(Battery 12V)
	500W(Battery 24V)
Survival wind speed	60m/s

1.7.2.8 Field test site

This site is same the evaluation of "Wind Resource Measurement". Details of this site information are referenced by section 1.1.3. This test term is three months in total between March and May, 2007. Measuring points are the wind speed, the wind direction, the generation voltage (DC-V), and the generation current (DC-A). The connected state to the load is the same as the wind-tunnel test, and the wind turbine is connected to the battery through the control circuit.

Field data measured in the sampling frequency is 0.5Hz, and it is automatically saved to the PC through the data logger. Furthermore, the installing position of the anemometer and the anemoscope from the wind turbine mast is 3.3m (3.3D) and 3.5m (3.5D).

1.7.2.9 Results

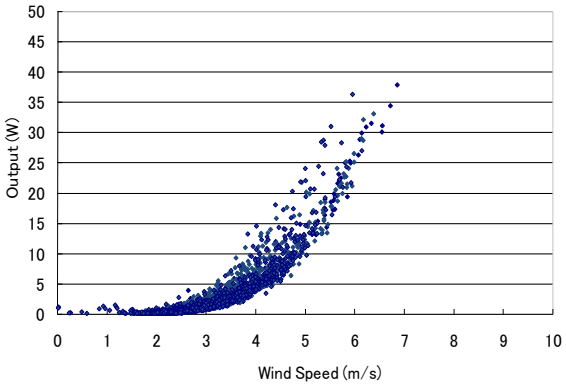

Fig 20: Wind speed vs Power output

10 min average data

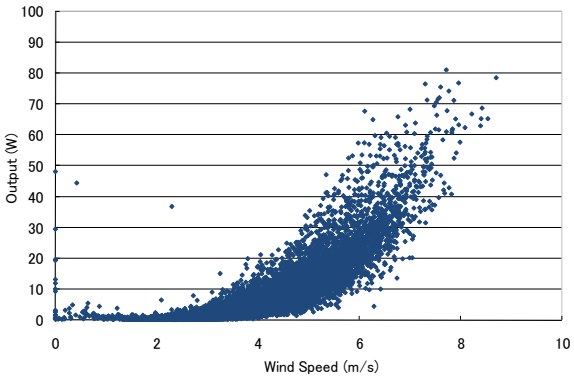

Fig 21: Wind speed vs Power output

10 min average data

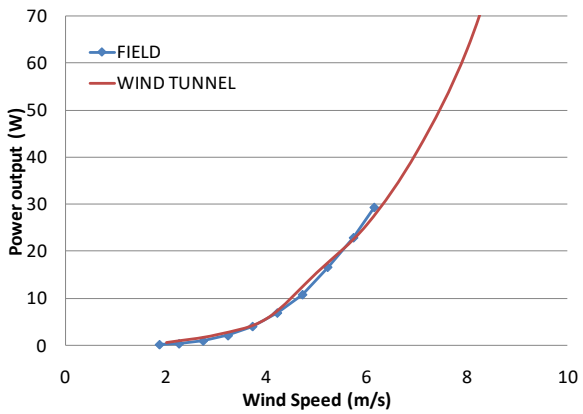

Fig 22: Wind speed vs Power output

10 min average (wind speed bin)

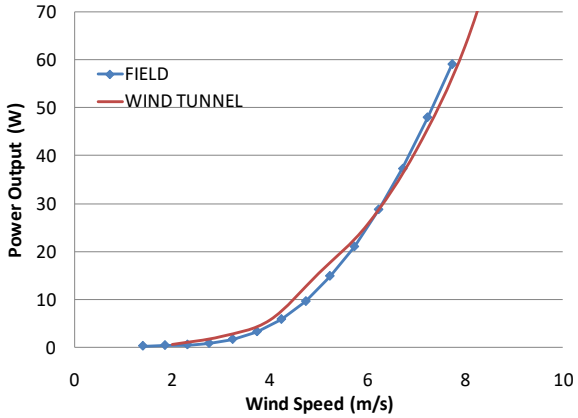

Fig 23: Wind speed vs Power output

1 min average data (wind speed bin)

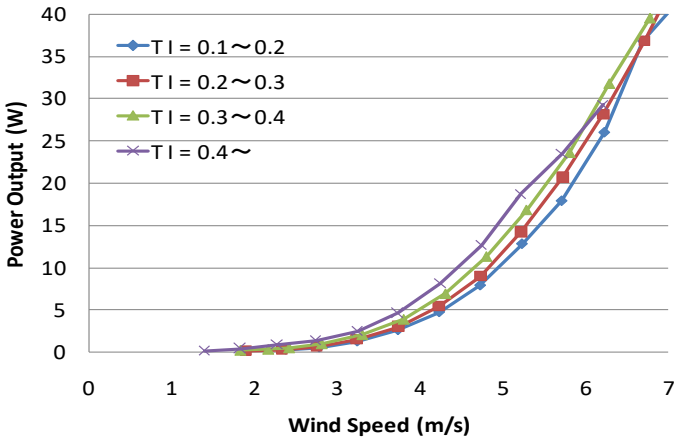

Fig 24: Wind speed vs Power output (1 min average wind speed bin)

for each turbulence intensity

In the case of 1 minute data set, the power curve that was adjusted by the bin method also fitted data from the wind-tunnel test with high precision. Furthermore, 1 minute data set could be evaluated the power curve in the wide wind range by comparison with 10 minutes data set. This result is only for the specific wind turbine (AURA1000). Therefore, it cannot be applied for all wind turbines. Especially, the chasing characteristic in the change of the wind direction and responsiveness in the change of the wind speed are different at each wind turbine. Their characteristics have the influence to power performance from natural wind.

In this result, when the wind turbine was superior to the chasing characteristic and responsiveness of the wind direction, it was clear that the power curve from the field test fitted the wind-tunnel test by the bin method even the urban site that was large turbulence of the wind speed and the wind direction.

1.7.3 Ashikaga Institute of Technology Rooftop Test Site

1.7.3.1 Wind Resource Measurement Results

1.7.3.1.1 SWT Site Characterization

SWT site is located next to the building of the wind turbine museum at Ashikaga Institute of Technology. Due to the issue of permission, the turbine and measurement instruments are all mounted on a building scaffold.

1.7.3.1.2 Diagram and describe surrounding obstacles with distances noted

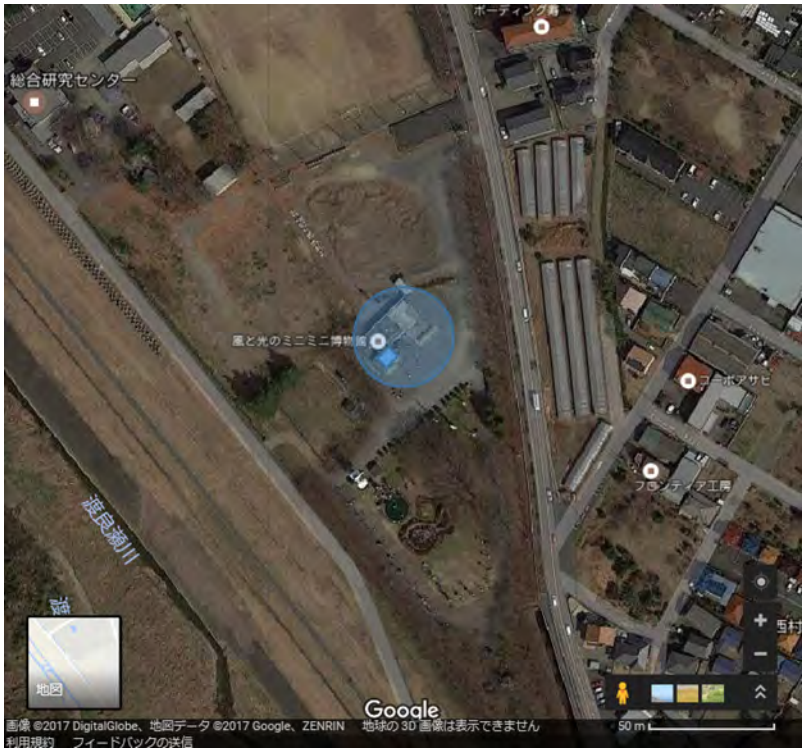

Figure 10 Satellite view of the test site (blue circle is the circular area with the radius of 20D blue block is the second floor of a building assumed as a significant obstacle)

Significant obstacles for the anemometer and the wind vane are listed below with their direction to the anemometer.

The tested turbine(Figure 16, direction is north east (45° from north).)
A utility Pole(Figure 11, direction is North west(315° from north).)
Hand rails of the building (Figure 11, Figure 12, all around the building about 0.8m height)
The Second floor of the building(Figure 12, direction is south west (210° from north))

Other than above obstacles there is no significant thing within the radius of 20D (=20m) as shown in Figure 10.

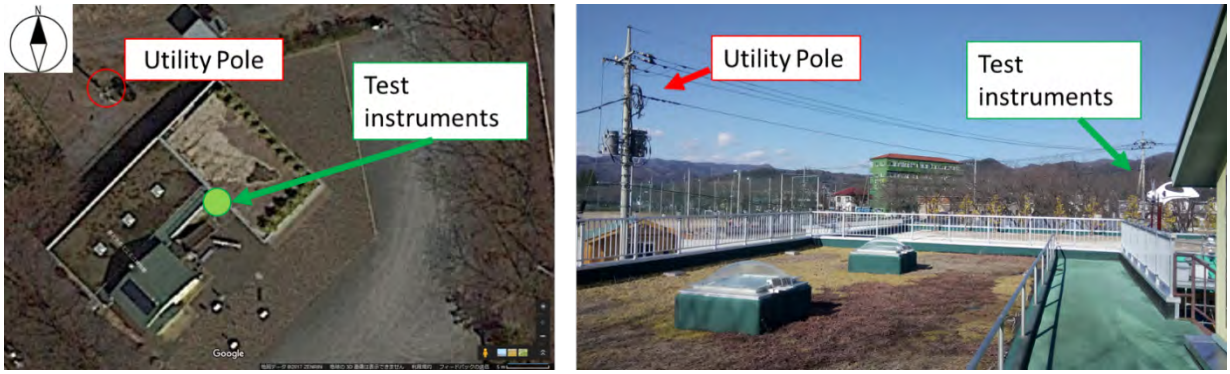

Figure 11 geometric layout of the utility pole (Hand rails are also shown in the right figure)

Figure 12 geometric layout of the second floor of the building (Hand rails are also shown in the right figure)

The tested wind turbine is only assumed as a significant obstacle for determination of exclusion sector. Because the dominant direction of this test site includes the direction of the obstacle and the obstacle is reasonably far from the measurement instruments and can be assumed as the inflow condition to the tested wind turbine. Consequently, the exclusion sector is 45° ±45.6° which is calculated based on Annex. A of IEC 61400-12-1 Ed.1.

For the site characterization, sector exclusion is not considered. Site characterization should be basically done without the tested wind turbine and should include all the wind directions. In this study, accepting some error due to the tested wind turbine is ignored to include data of all the wind direction. However as presented in Table 2, 90% of the data are included out of excluded sector. For the performance measurement, the exclusion sector above is applied. Because the performance measurement is not necessary need all the data.

1.7.3.1.3 Wind rose

Wind rose from during measurement for the site characterization is presented in Figure 13.

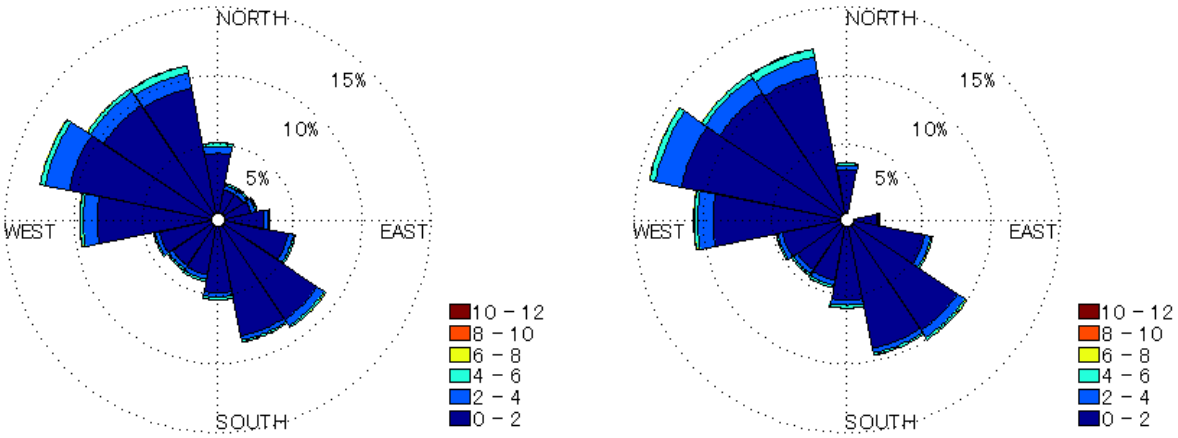

Figure 13 Wind rose (2014 Feb. to 2015 Jan. , left: all direction right: sector excluded)

1.7.3.1.3.1 Energy rose

1.7.3.1.3.2 Average TI, TKE

10 min. average turbulence intensity is presented in Figure 14.

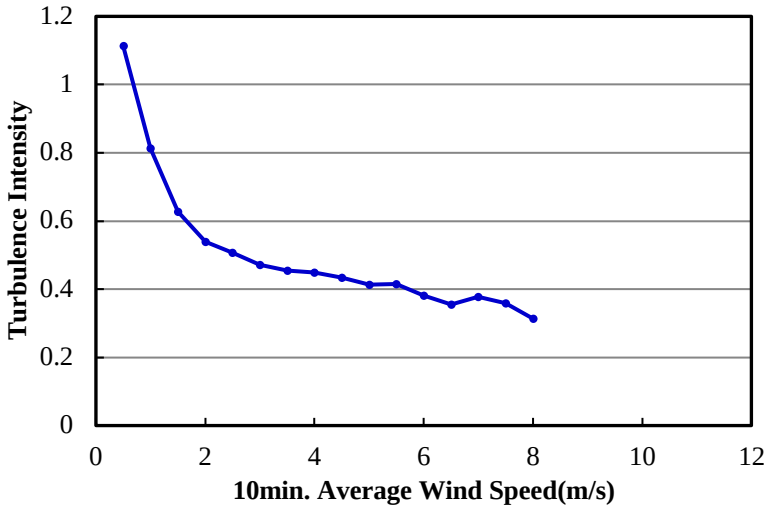

Figure 14 90% quantile turbulence intensity (2014 Feb. to 2015 Jan.)

1.7.3.1.3.3 Wind speed frequency distribution

Wind speed frequency distribution is presented in Figure 15.

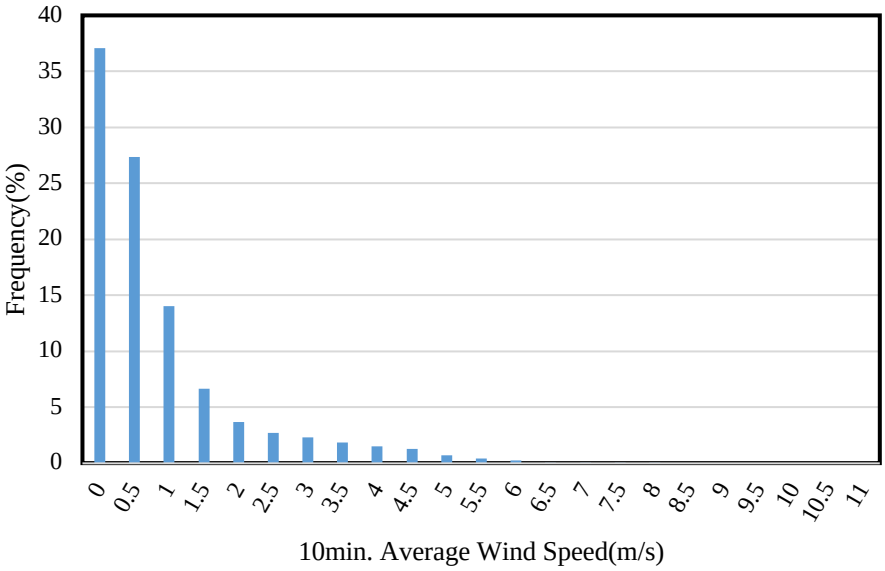

Figure 15 Wind speed frequency distribution (2014 Feb. to 2015 Jan.)

1.7.3.1.3.4 Off-site/reference wind measurement description

In this site, there is no off-site or reference wind measurement representing free stream wind speed.

1.7.3.1.4 Data Acquisition Approach

List of measurement instruments are presented in Table 1. Sampling rate is 10 Hz for all the measurement items.

Table 1 List of measurement instruments

Measured Value	Instruments	Type and manufacturer
1.5m height wind speed	Cup anemometer	Climatec.inc CYG-3002
1.5m height wind direction	Wind vane	
5m height wind speed	Cup anemometer	Climatec.inc CYG-3002
5m height wind direction	Wind vane	
Temperature	Temperature sensor	R. M. Young company 41342
Humidity	Humidity sensor	
Atmospheric pressure	Pressure sensor	
Current to the battery (I1)	Current transducer	URD HCS-20-10-AP
Current to the dummy load (I2)	Current transducer	URD HCS-20-10-AP
Load Voltage	Data Logger (including AD converter)	YOKOGAWA Datum-Y XL100

*Height is defined from rooftop (4m above ground level)

1.7.3.1.5 Measurement location

The anemometer and the wind vane is mounted on the same support structure equipped on the turbine supporting scaffolds. The distance between the anemometer and the tested wind turbine is 1.7m. Other measurement instruments are also mounted on the same scaffolds

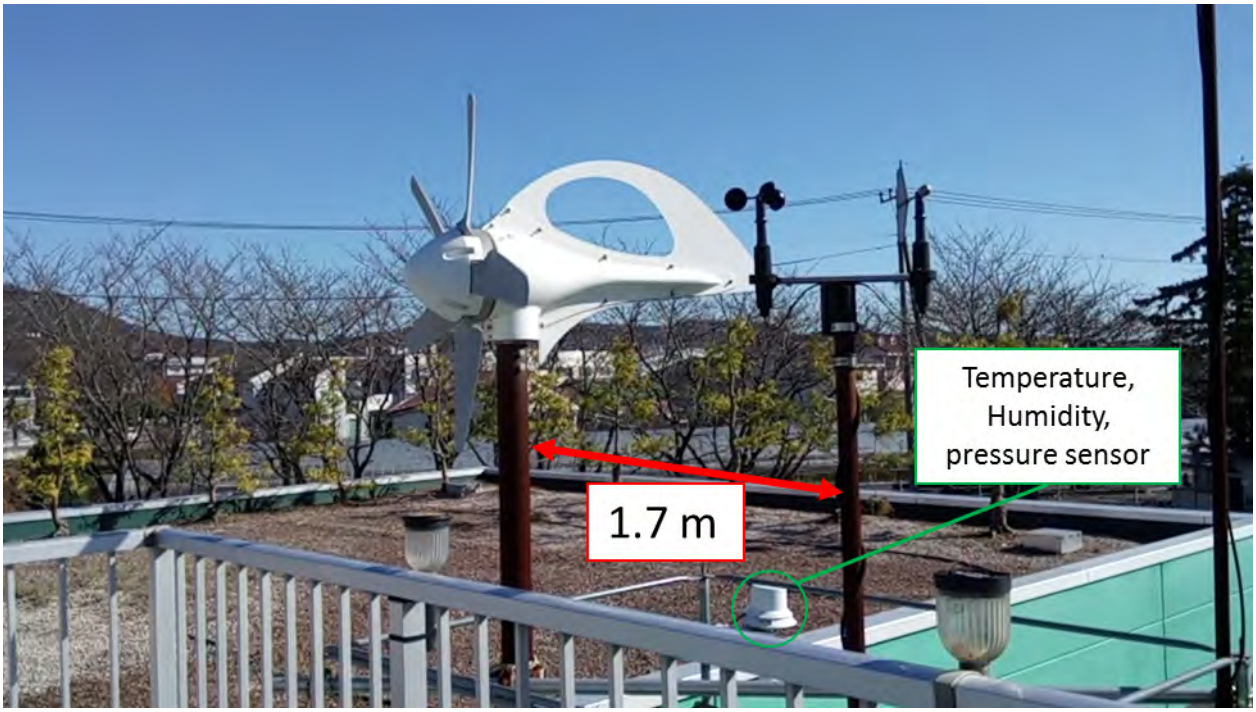

Figure 16 position of anemometer, vane and other environmental measurement instruments

1.7.3.1.5.1 Duration and results of data collection efforts - highlight any maintenance or downtime issues

Data before 2016/11/04 were not used for the turbine performance measurement. Before that date, the battery is used for power source of some sensors and consequently over discharged in 2 weeks. After 2016/11/04, 23V DC power source connected to the grid is equipped in parallel to the battery. Despite the failure of the wind turbine, measurement of the environmental parameters are done from 2014/02/07 to 2014/01/19. Data on the day of data collection was excluded because Data Collection need to stop the tested turbine. Because the tested turbine do not send any signals related to operating state (i.e. cut-out, stand-by), data exclusion from the operating state is not done.

1.7.3.1.6 Data processing strategy, quality assurance methods

Visual inspection using time-series plot was done and no significant error was found. Wind speed was corrected based on air density defined in IEC 61400-12-1. Averaging time is 1 minute and 10 minutes. In the latter of the report, both of the results are presented. Number of available data for each wind speed is shown in Table 3, 2. Wind speed bin with less than 30 datasets are highlighted as insufficient bins. Even though there are some insufficient bins, all the bin including insufficient bin is presented other than the discussion in Characterize turbine and its power production section.

Table 2 Number of 10min. data sets for wind resource measurement (2014 Feb. to 2015 Jan.)

Vave	Number of Data (All data sets)	Number of Data (sector excluded)
0	17551	16171
0.5	12961	11549
1	6655	5987
1.5	3145	2810
2	1760	1574
2.5	1288	1112
3	1087	913
3.5	888	722
4	724	595
4.5	604	487
5	353	291
5.5	215	177
6	110	95
6.5	23	18
7	6	6
7.5	1	1
8	1	1
8.5	0	0

Table 3 Number of 1min. data sets for turbine performance measurement (2016 Nov. to 2017 Feb.)

Vave	Number of Data (All data sets)	Number of Data (Sector excluded)
0	35664	32208
0.5	19343	17963
1	19019	17948
1.5	13818	13218
2	8872	8640
2.5	7016	6874
3	6625	6512
3.5	6247	6127
4	5277	5177
4.5	4268	4183
5	3140	3076
5.5	2279	2229
6	1487	1460
6.5	965	944
7	579	567
7.5	364	358
8	196	190
8.5	104	104

9	46	46
9.5	29	29
10	15	15
10.5	2	2
11	3	3
11.5	2	2
12	0	0

Table 4 Number of 10min. data sets for turbine performance measurement (2016 Nov. to 2017 Feb.)

Vave	Number of Data	Number of Data (Sector excluded)
0	2515	2285
0.5	3011	2771
1	2071	1952
1.5	1255	1197
2	759	715
2.5	619	570
3	656	609
3.5	705	631
4	637	574
4.5	534	476
5	321	277
5.5	206	182
6	127	113
6.5	65	58
7	23	23
7.5	23	21
8	8	8
8.5	0	0
9	1	1
9.5	0	0

1.7.3.1.7 Conclusion of results

This chapter shows the result of wind resource measurement based on the datasets showed in Table 2

1.7.3.1.8 Plots of TI, TKE

Average TI at each wind speed bin is presented in Figure 17.
TI vs direction is also presented in Figure 18.

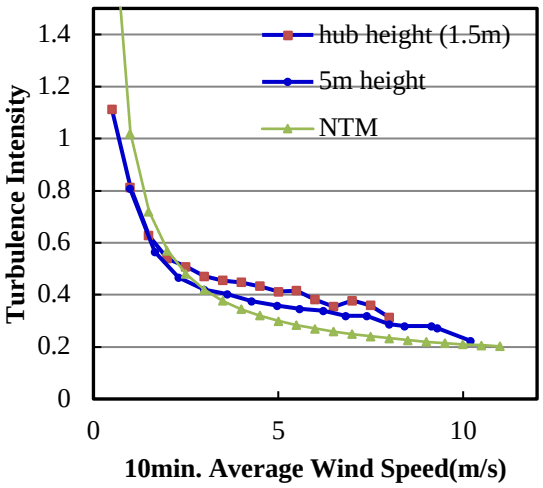

Figure 17 Turbulence intensity at 5m and hub height(1.5m)

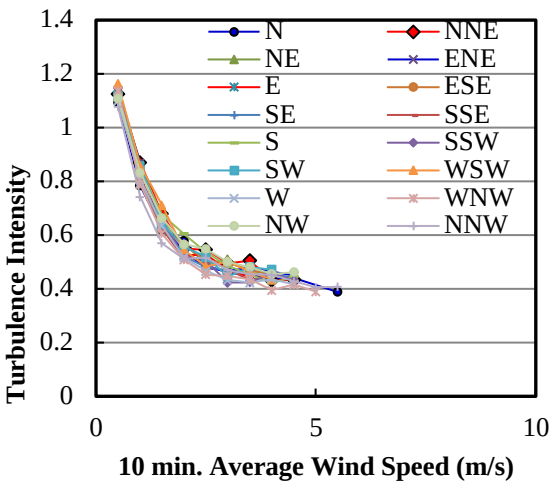

Figure 18 Turbulence intensity for each wind direction

1.7.3.1.9 Wind resource characterization, annual wind speed (at specific height), monthly wind speed, wind speed frequency distribution, maximum 3 second gust, etc.

Monthly average wind speed is presented in Figure 19. Annual average wind speed is 0.89m/s at hub height and 1.45m/s at 5m height.

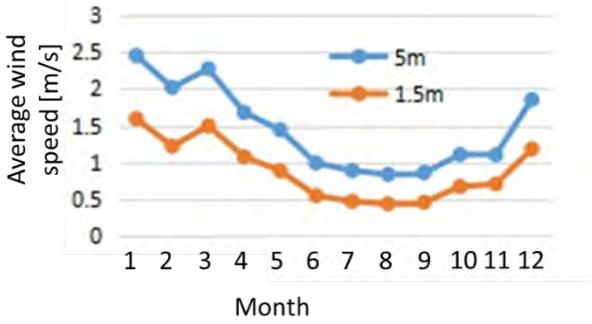

Figure 19 Monthly average wind speed

1.7.3.1.10 Summary of your findings

This test site has heavily season dependent wind environment. In winter the wind speed almost doubled compared to summer. The dominant direction of winter and it of summer is also different. These results are because of a seasonal wind blowing from north mountain area in winter. But even in winter the average wind speed at the hub height (1.5m height from the building) is very low. As for turbulence intensity, TI at hub height (1.5m height) is larger than that of 5m height. This tendency is usually shown due to atmospheric boundary layer. For the most of the wind speed range, turbulence intensity at both hub height and 5m height is larger than that defined in IEC 61400-2 Ed.3. Also for all the wind direction, turbulence intensity is larger than that defined in IEC 61400-2 Ed.3.

1.7.3.1.11 Conclusions

As a conclusion, the wind speed at the test site is very low on average. However there is some days when the wind speed is more than 7 or 8 m/s at 10 min. average. And the turbulence intensity of this site is larger than that defined in IEC standard. Therefore, it could be said the turbine performance could be possible at this site even though this site is not suitable for power generation or getting large generated electricity.

1.7.3.2 Characterize turbine and its power production

10 min. averaging and 1 min. averaging are both done for the performance measurement of the tested turbine.

1.7.3.2.1 Turbine type & model number

A horizontal axis wind turbine AURA 1000 135W from Nasu-denki-tekko Ltd. is tested.

Figure 20 AURA 1000

Table 5 Specification of AURA 1000

Rated Power [W]	135
Rated Wind Speed [m/s]	10
Cut-in Wind Speed [m/s]	2
Cut-out Wind Speed [m/s]	16
Design Rotational Speed ω_{design} [RPM]	1170
Rotor Diameter [mm]	1000
Number of Blades	5
Yaw Control	Free Yaw (with Fixed Rudder)
Rotational Speed Control	Variable Speed

1.7.3.2.2 Tower height and type

Tower is made by Building scaffolding. Tower is 4m at its top base. Hub height is 1.5m from the top of the tower (5.5m from the ground).

Figure 21 Mounting tower of the tested SWT

1.7.3.2.3 SWT Site Characterization

1.7.3.2.3.1 Photo (360)

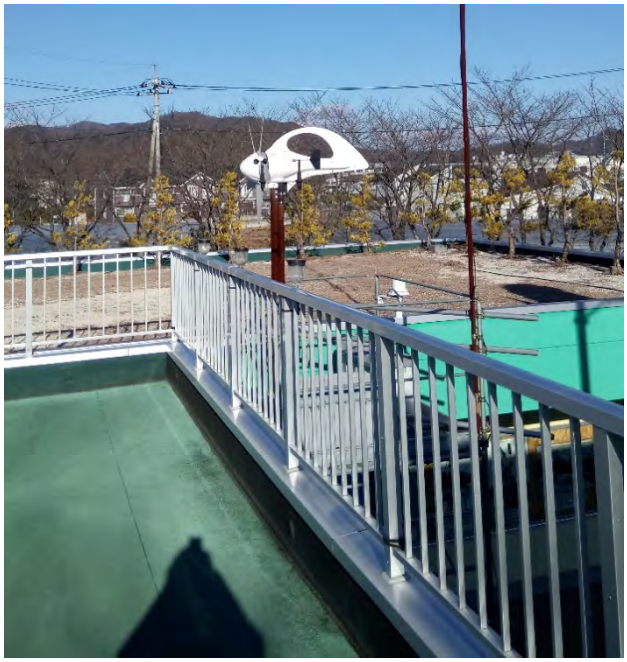

Figure 22 View from south west

Figure 23 View from north west

Figure 24 View from north east

Figure 25 View from south east

1.7.3.2.4 Diagram and describe surrounding obstacles with distances noted

Surrounding obstacles are noted in the section of SWT Site Characterization. The tested turbine is connected to the controller including AC-DC converter and variable speed controller circuit. Battery is charged from the grid via AC-DC converter with a backflow prevention diode. Dummy load is turned when the battery voltage exceeds 25V. Connection diagram is presented in Figure 26

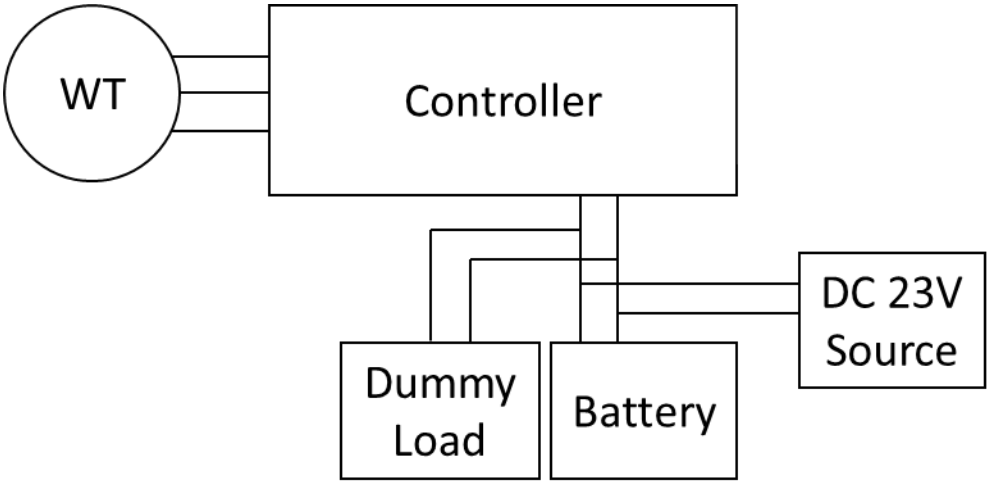

Figure 26 Connection diagram

1.7.3.2.4.1 Wind rose

Wind roses are shown in Figure 27 and Figure 28. Dominant wind direction is WNW because of seasonal wind from mountain area in winter season.

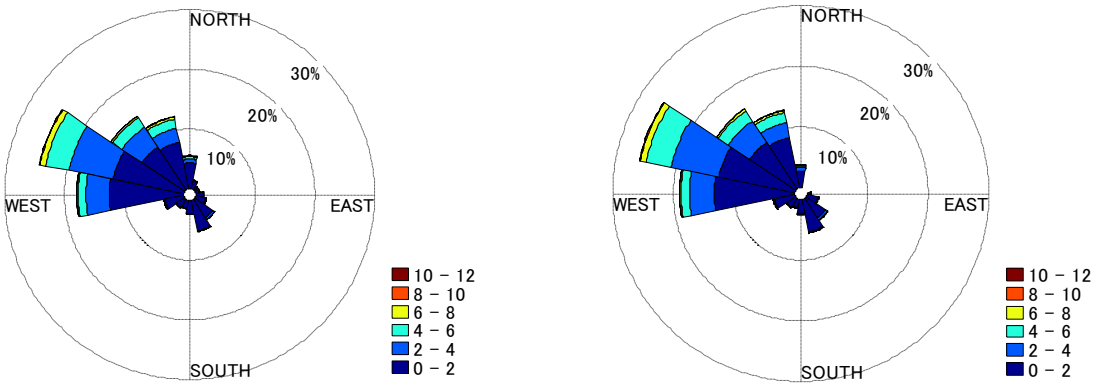

Figure 27 Wind rose during the turbine performance test (1 min. average, left: without sector exclusion right: with sector exclusion)

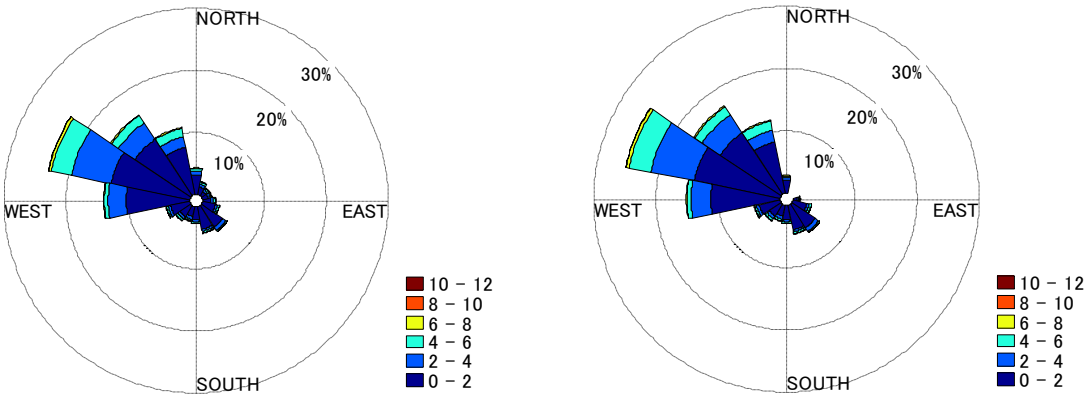

Figure 28 Wind rose during the turbine performance test (10 min. average, left: without sector exclusion right: with sector exclusion))

1.7.3.2.5 TI

Turbulence intensity at hub height is presented in Figure 29 to Figure 32. Turbulence intensity at 5m height is also presented as a reference for raw data.

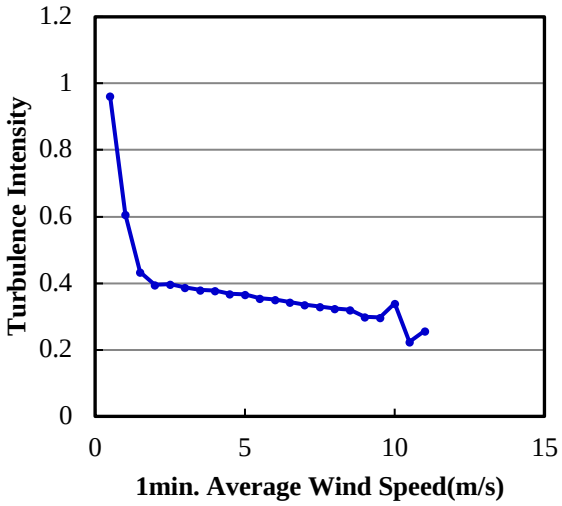

Figure 29 1 min. bin turbulence intensity at hub height (90% quantile)

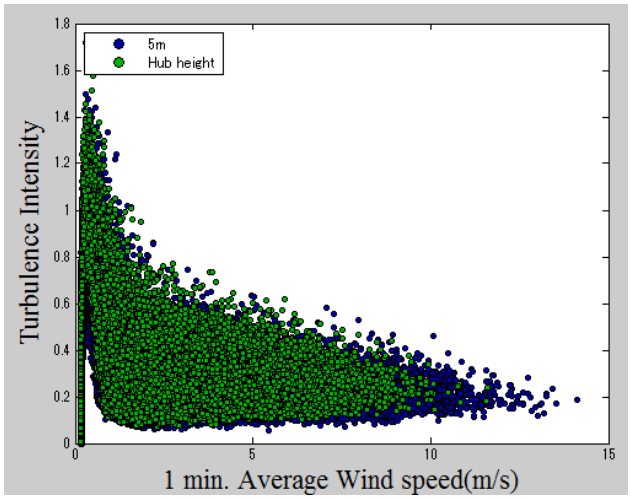

Figure 30 1 min. raw turbulence intensity

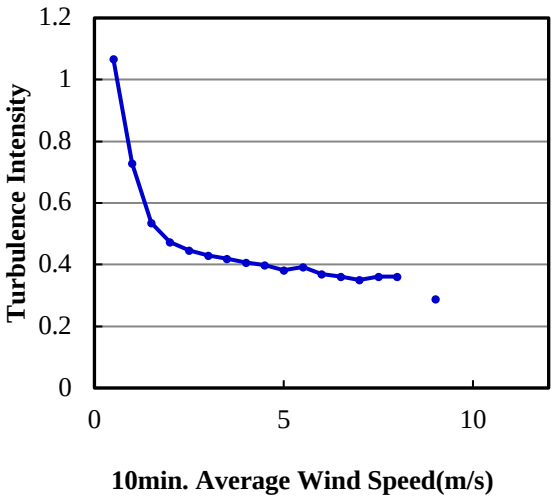

Figure 31 10 min. bin turbulence intensity at hub height (90% quantile)

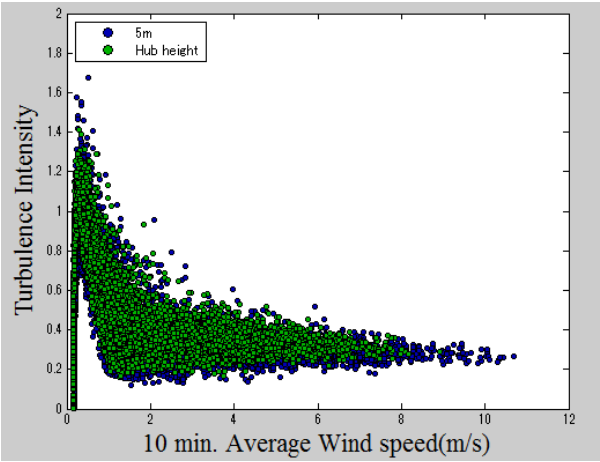

Figure 32 10 min. raw turbulence intensity

1.7.3.2.6 Wind speed frequency distribution

Wind speed frequency distribution during the performance test is presented in Figure 33 and Figure 34.

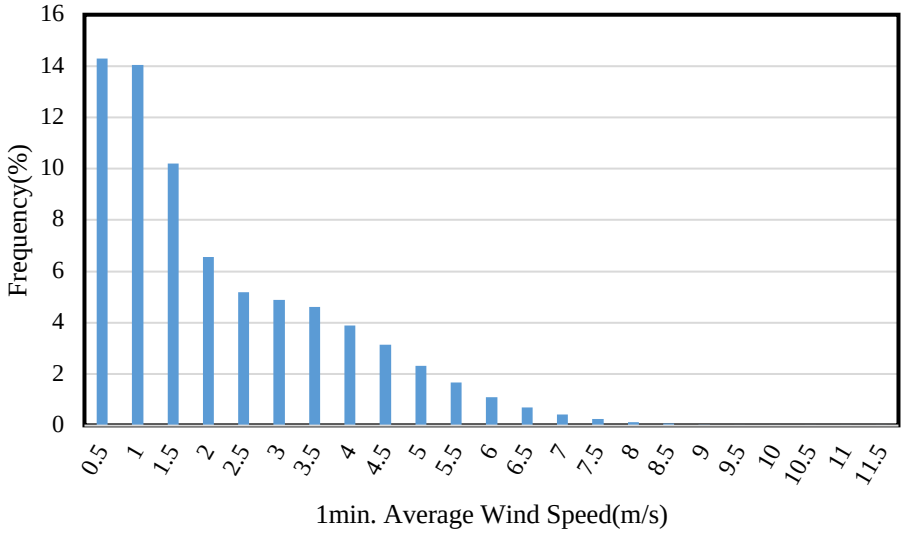

Figure 33 1min. average wind speed frequency distribution

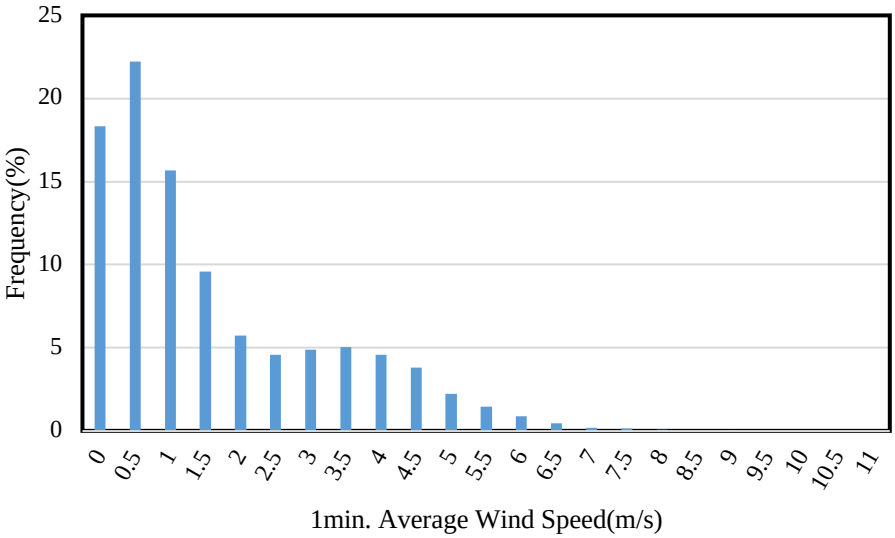

Figure 34 10min. average wind speed frequency distribution

1.7.3.2.7 Off-site/reference wind measurement description

There is no off-site or reference wind measurement representing free-stream wind speed. All the performance test are based on hub height wind speed.

1.7.3.2.8 Power curve comparison with accredited power curve for good and bad sites

Measured power curve for 10 min. and 1 min. is presented in Figure 35. Power curve shows similar values regardless of averaging time. Both results shows higher output power for low wind speed region and lower output power at high wind speed region (above 9m/s). The higher output performance is possibly because of increased inflow energy due to high turbulence intensity. The lower output performance is possibly because of cut-out because of instantaneous gust occurring in highly fluctuating wind speed.

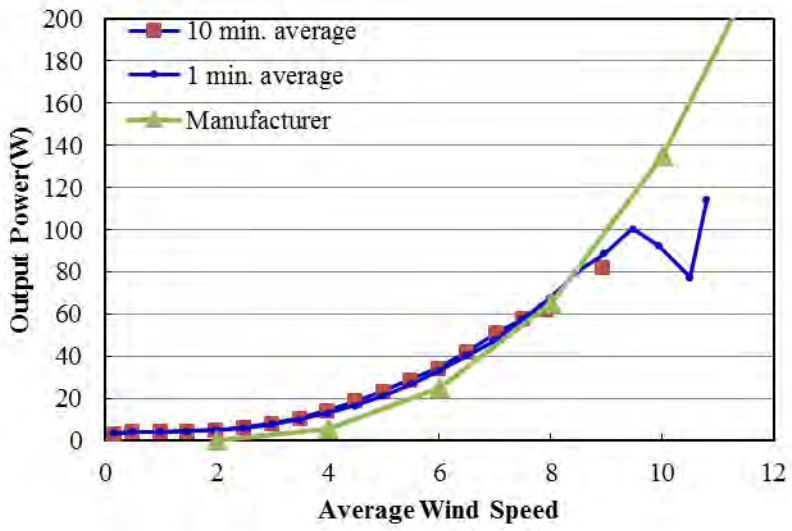

Figure 35 Measured power curve (10 min. average)

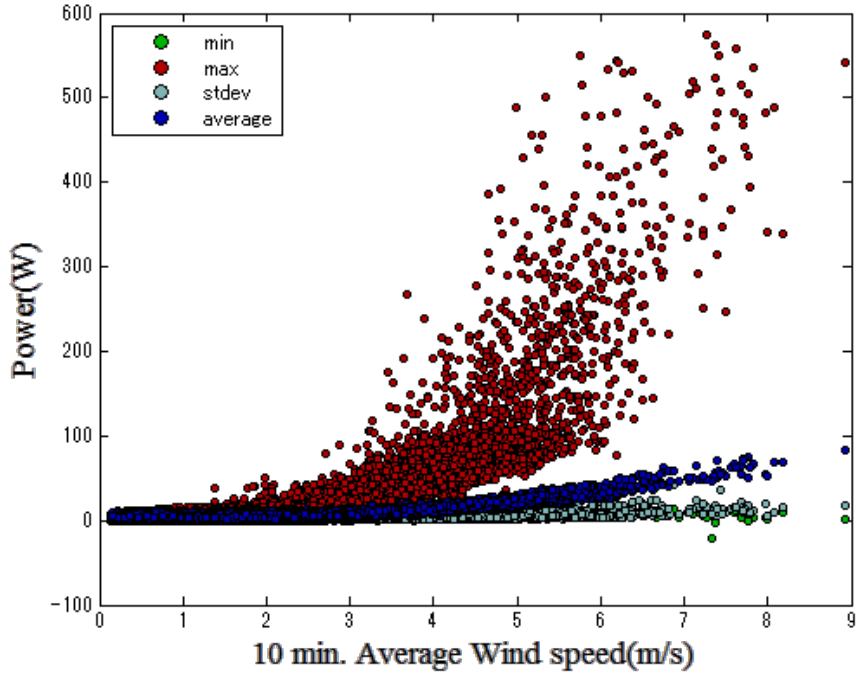

Figure 36 10 min. average raw measured power

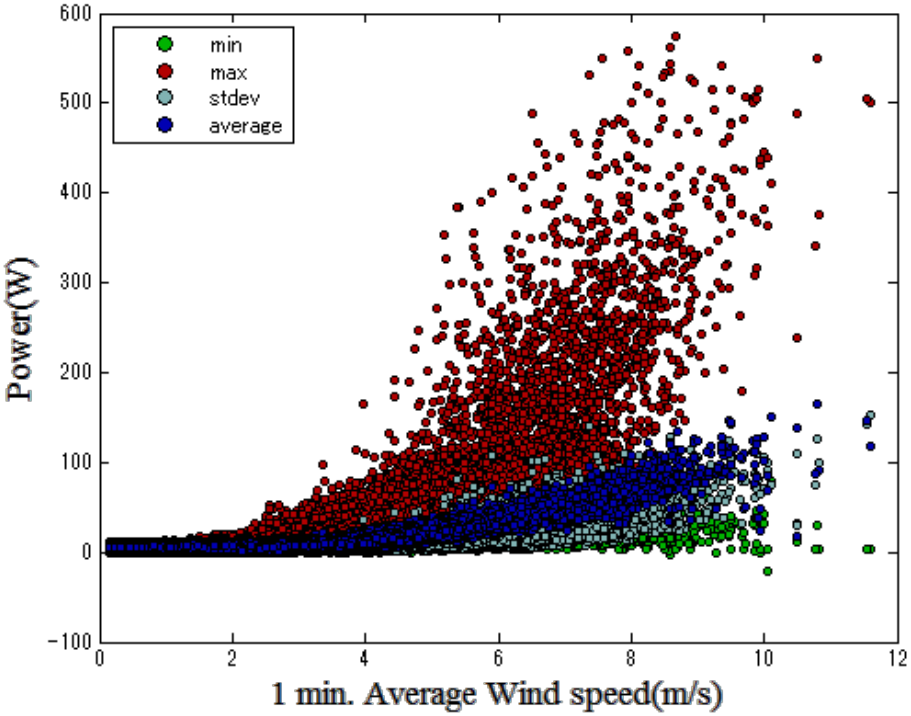

Figure 37 1 min. average raw measured power

1.7.3.2.9 Turbine owners opinion of SWT success

The tested turbine is used for only academic purpose. As described in the site characterization, this test site has very low wind speed and therefore is not suitable for SWT power generation. However the performance of the wind turbine shows very good agreement with the manufacturer provided power curve. So, it could be said the turbine capable of generation at this highly turbulent near building site.

Additional Analysis on the effect of buildings・power curve for each sector (16 direction)
This section focuses on the effect of surrounding structures on the performance of the tested wind turbine. As shown in previous sections, surrounding structures are non-uniform to the wind direction. Therefore, this section discusses the performance per each wind direction.
First, Figure 38 shows power curves per each 16 wind direction bins. The curve only shows bins with more than 30 data sets. From the figure, higher output power is observed in N NW, NNW than in W and WNW.

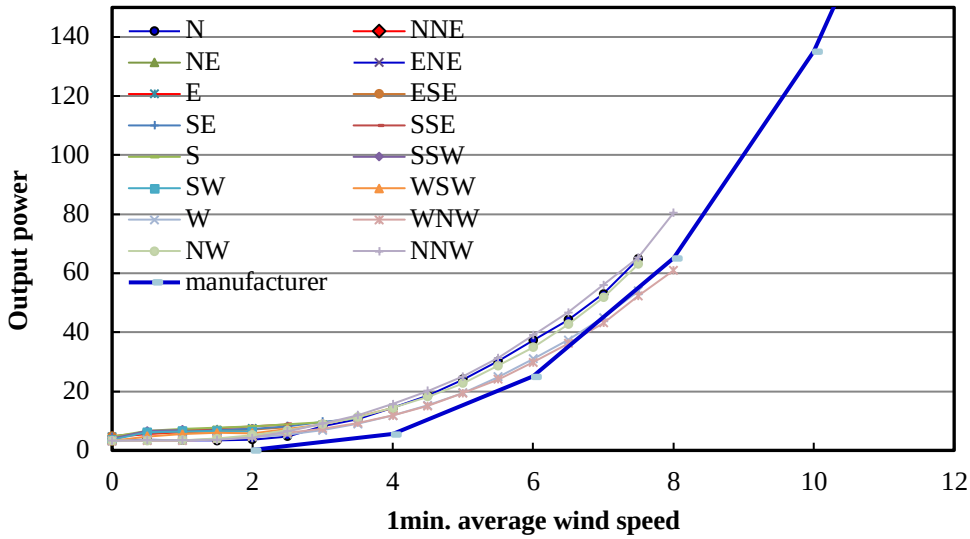

Figure 38 1 min. average power curve per wind direction bin

Before analyzing the reasons of difference of power curve between wind directions, Power curve sorted by 1 min. average turbulence intensity is presented in Figure 39 in order to confirm that turbulence intensity is one of the main factors of characterizing the power curve of the tested turbine. For the latter figures, all the bins are presented including bins with less than 30 data sets. From the figure, it is clear that the output power increases as turbulence intensity increase in low speed region under 8 or 8.5 m/s and the output power reduces as turbulence intensity increase above 8.5m/s. The dominant reason for the first trend is possibly the increased energy of wind due to increased turbulence intensity. The second trend above 8.5 m/s might be mainly due to existence of frequent cut-out due to instantaneous gust under high turbulence intensity. So, increase of turbulence intensity increases power output and reduces virtual cut-out wind speed. From this result a general effect of turbulence intensity regardless of wind direction is revealed.

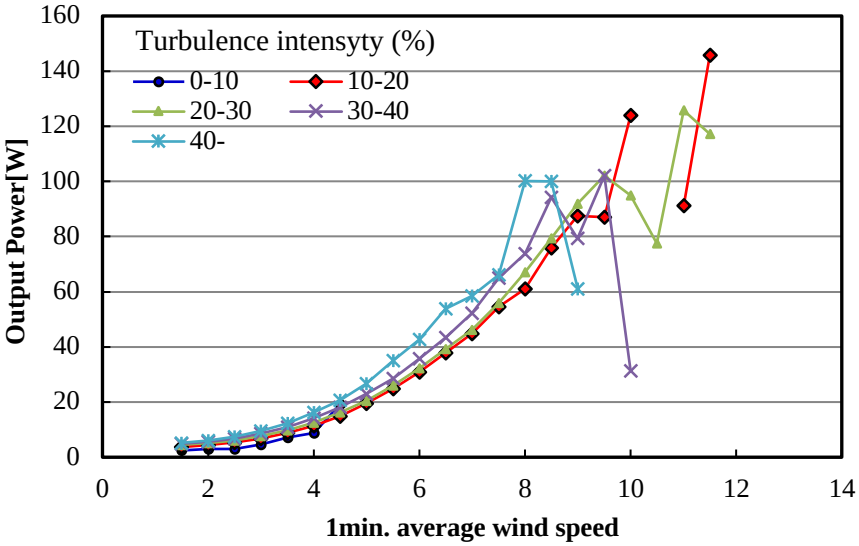

Figure 39 Power curve sorted by turbulence intensity (1 min. average)

Next, Figure 40 shows 1 min. turbulence intensity per wind direction bin. Turbulence intensities of NW and NNW are higher than those of W and WNW. This can reasonably explain the power of NW and NNW are higher than those of W and WNW. However, turbulence intensity of north is lowest even though the power output of north is higher than those of W and WNW.

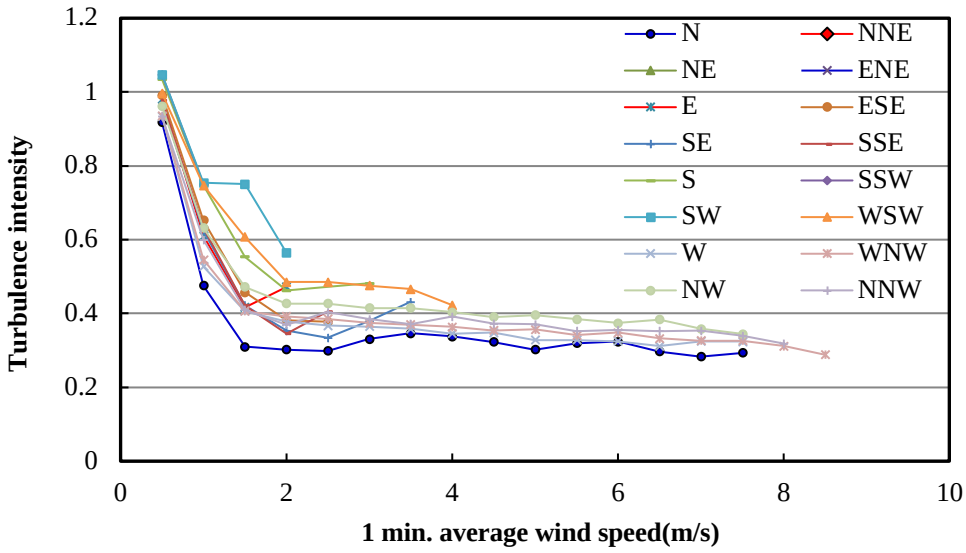

Figure 40 1 min. turbulence intensity per wind direction bin

The effect of turbulence intensity to the output performance is reasonably explained by Figure 39. However the reason that the power at north is high level even though TI is low is not clearly explained from Figure 39 and Figure 40. To get further insight to the directional change of the power performance, power curve for the same TI bins are presented in Figure 41 to Figure 45.

From the figures, output powers in N, NW and NNW are higher than those of WNW and W even with the same level of TI. One possible reason is special difference of TI between the point of the

anemometer and the point of the tested wind turbine. As Figure 43 and Figure 44 shows similar trends to Figure 39, the actual TI is possibly higher in N and NNW than in NW, WNW and W. However this effect of special difference might be averaged in the analysis including all wind directions likewise Figure 39. Therefore in order to discuss further on the directional effect, more careful measurement design should be necessary.

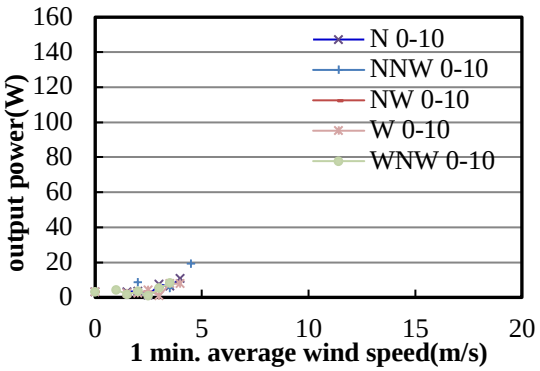

Figure 41 Power curve per wind direction (TI =0 to 10%)

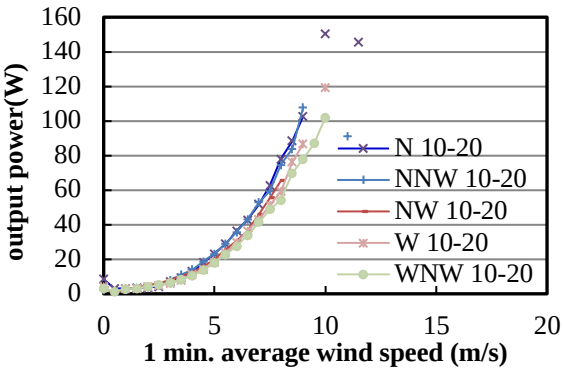

Figure 42 Power curve per wind direction (TI =10 to 20%)

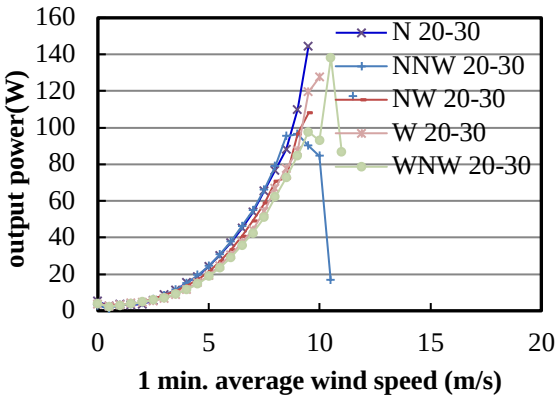

Figure 43 Power curve per wind direction (TI =20 to 30%)

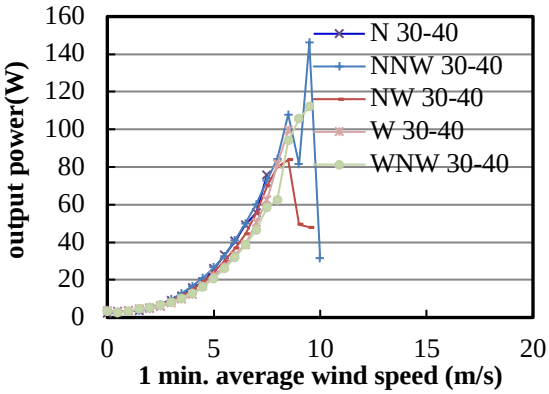

Figure 44 Power curve per wind direction (TI = 30 to 40%)

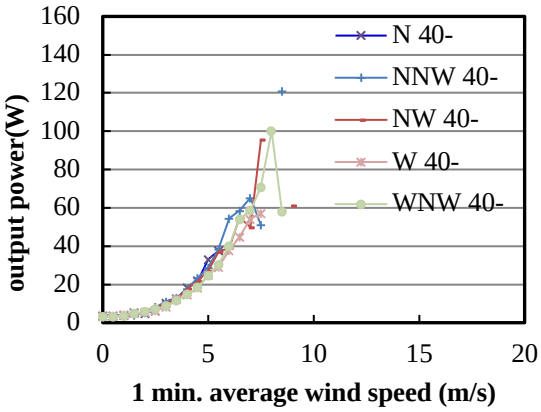

Figure 45 Power curve per wind direction (TI = 40% or more)

1.7.3.2.10 Conclusions

In this experiment, a micro wind turbine is installed near the building and the performance and wind resource are measured. Despite the turbulent wind near the building, the wind turbine

performance itself showed a difference of about 10% of the power curve given by the manufacturer. It can be said that the power generation performance of the tested wind turbine under high TI was good. From the measurement result, a power curve to the turbulence intensity was subtracted, and a certain reasonable result was obtained, that the increased energy from high TI and consequent increase of the output power.
However the performance varies depending on the wind direction even for the same turbulence intensity bin. It was indicated that this may be due to the difference between the inflow wind into the anemometer and the inflow wind into the wind turbine. In future turbulence analysis related to wind direction, measurement must be redesigned such as increasing the number of measurement points. CFD flow field analysis might be also useful.
In addition, consideration of another viewpoints such as analysis of yaw error, intensity of the change of wind direction, quantification of frequency of cut-out are also a subject in the future.

1.7.4 CFD model of V52 on campus of Dundalk Institute of Technology

1.7.4.1 Introduction

Figure 1.6.4.1 shows the Energy rose of the wind turbine in the campus of Dundalk Institute of Technology. In the case of the wind direction where a tall, skinny building is upwind, the amount of the generated power is large. On the other hand, in the case of the wind direction where widely distributed low-rise buildings are upwind, the amount of the generated power is small. Therefore, there is a possibility that a tall, skinny building might have a lower impact on the wind resource compared to widely distributed low buildings.

In this study, we conducted CFD analysis to clarify how much the buildings around the wind turbine affect the wind speed at the rotor center of the wind turbine.

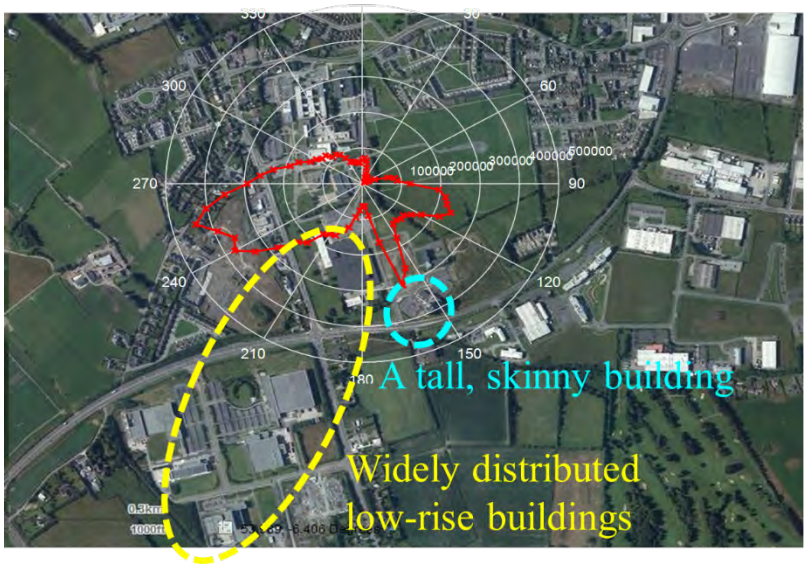

Figure 1.6.4.1 Energy rose of the wind turbine in the campus of Dundalk Institute of Technology

1.7.4.2 Computational Approach

1.7.4.2.1 Simulation cases

Figure 6.4.2.1 shows the horizontal computational domains. We conducted CFD simulations with 4 different wind directions. In the case of 50 degrees, there is no buildings upwind of the wind turbine and the occurrence frequency of high wind speed is low. In the case of 150 degrees, there is a 40-meter tall building upwind of the wind turbine and the occurrence frequency of high wind speed is low. In the case of 190 degrees, there are widely distributed low-rise buildings upwind of the wind turbine and the occurrence frequency of high wind speed is low. In the case of 250 degrees, there are a few low-rise buildings upwind of the wind turbine and the occurrence frequency of high wind speed is high. In addition to these 4 cases with different wind directions, we conducted a CFD simulation for the case with no building. The size of the computational domain for the case of no building is the same as other cases.

The computational domain is a one five hundredth scale model of an equivalent length of 3.5 km, width of 2.75 km and height of 0.45 km.

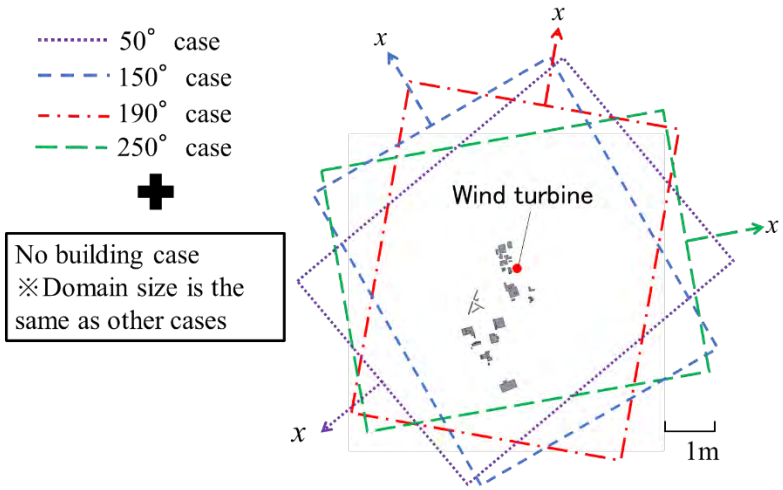

Figure 1.6.4.2 Horizontal computational domains

1.7.4.2.2 Computational conditions

We used a CFD software ANSYS 17.2. The flow field was considered as two-dimensional, unsteady, viscous and incompressible. The governing equations were the Reynolds-averaged continuity equation and the Reynolds-averaged Navier-Stokes (RANS) equations. The Reynolds stresses were computed using the standard k-ε turbulence model. The advection term was discretized by Quadratic Upstream Interpolation for Convective Kinematics (QUICK) scheme. Other spatial derivatives were discretized by the second-order central difference scheme. The Semi-Implicit Method for Pressure-Linked Equations (SIMPLE) algorithm was used for velocity-pressure coupling.

Total numbers of computational cells for cases with buildings and without buildings were approximately 6.2 millions and 3.2 millions, respectively. Unstructured meshes were used around the buildings. On the surface of the buildings and ground, boundary layer mesh is used.

As the inlet boundary conditions for the streamwise velocity and turbulent kinetic energy, we set the profile of Meng and Hibi's wind tunnel experiment.

1.7.4.3 Results and Discussions

Figure 1.6.4.3 shows the simulation results of streamwise velocity and turbulent kinetic energy for the case of 50°. Purple line indicates the results for the case with 50 degrees and black line indicate the results for no building case. At the hub height of wind turbine, the discrepancy of streamwise velocity between 50°case and no building case is very small. So, it can be considered that at the hub height, the effects of the buildings around the wind turbine is very small.

In Figure 1.6.4.3, blue line indicates the results for the case of 150°. There is a 40-m-tall-skinny building upwind of the wind turbine. The height of the 40-m building is indicated by dotted line. At the hub height of wind turbine z/H_{wt} = 1.0, the streamwise wind velocity is 6 % lower than no building case. In addition, below the hub height, the streamwise velocity of 150 °case is significantly lower than no building case. The cause of this phenomenon can be that the increase in turbulence due to the 40-m building promoted the transport of momentum toward the ground.

In Figure 1.6.4.4, the red line indicates the 200° case and the green line indicate the 250° case. The dotted lines indicate the heights of buildings upwind of the wind turbine. At hub height, the discrepancies of the streamwise velocity among three cases are very small. So, it can be considered that at the hub height of the wind turbine, the effects of buildings upwind of the wind turbine on the streamwise velocity are small.

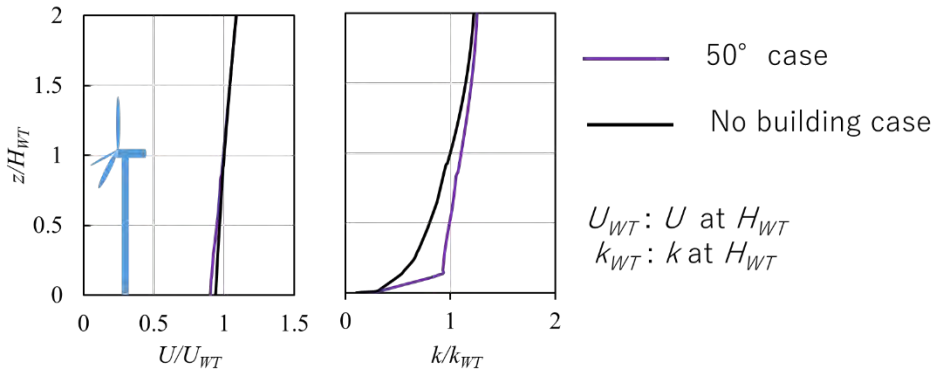

Figure 1.6.4.3 Vertical profiles of the streamwise velocity and turbulent kinetic energy for the case of 50°

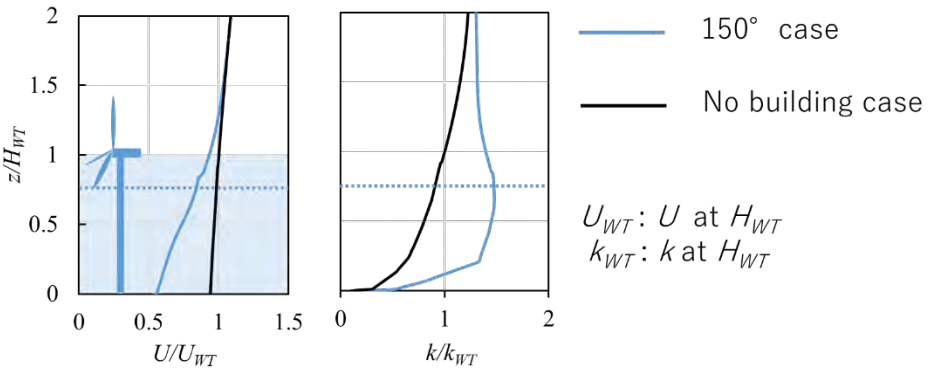

Figure 1.6.4.4 Vertical profiles of the streamwise velocity and turbulent kinetic energy for the case of 150°

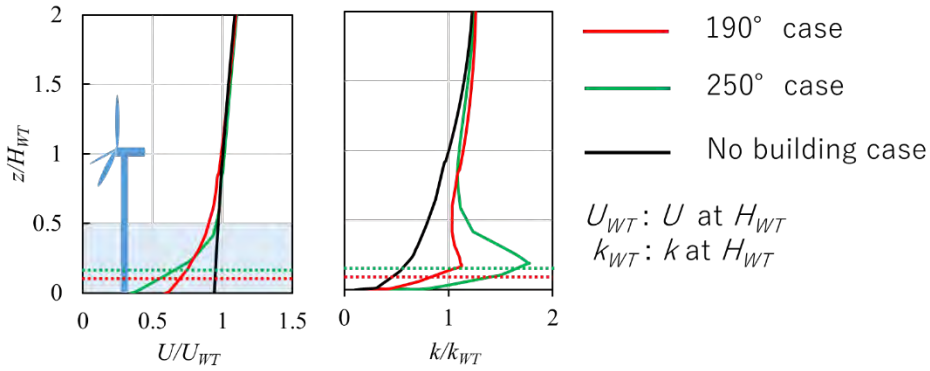

Figure 1.6.4.5 Vertical profiles of the streamwise velocity and turbulent kinetic energy for the cases of 190° and 250°

1.7.4.4 Summary

The findings of this study are summarized as follows.

1. Skinny 40-meter tall building upwind of the wind turbine reduces the streamwise wind velocity at the rotor center by 6 %.

2. Low-rise buildings widely distributed upwind of the wind turbine has little effects on the streamwise wind velocity at the rotor center.

1.7.5 Simplified Load Methodology for VAWTs

Simplified load methodology for vertical-axis wind turbine (VAWT) was developed by the experts in Mie Univ. and JSWTA (Japan Small Wind Turbines Association) under the NEDO R&D Program (FY 2008~2012). This R&D activity intended to form the regal background for Japanese Feed-in Tariff system starting in 2012 for witch several commercial small VAWTs would be able to apply.

This simplified load methodology was developed along the same logics as the simplified load methodology for horizontal-axis wind turbine (HAWT) described in IEC61400-2. Most simplified load equations were lead based on conventional mechanical engineering and fluid dynamics supported by wind tunnel testing.

In 2013, the R&D result was added into JSWTA0001 standard (Small Wind Turbine Performance and Safety Standard), which is a national industrial standard almost equivalent with IEC61400-2. This simplified load methodology is written in Annex C (formative) of JSWTA0001 entitled “Development of the simple design equations for a vertical-axis wind turbine (VAWT)”

As JSWTA0001 standard is written in Japanese, a draft translation was presented at TASK 27 meeting held in China in 2014 in order to start international discussions.

1.7.5.1 Main Features

Some main features of Annex C will be introduced below:

Note: For the understanding of technical concepts, detailed definitions of parameters or equations are not shown.

1.7.5.1.1 Scope is defined as follows in C.1 Scope

— This annex applies to a vertical-axis rotor symmetry with respect to its equatorial plane.

— This annex applies to a rotor with a number of blade(s) within 5.

— A design with this simplified equations is valid when the deflection of the rotor shaft is not larger than 0.3 % at its center under the load case H and thereby such a cantilever structure system that the rotor shaft is supported at its first bearing may be taken dynamically stable.

— No wind shear is considered.

The reason that the maximum number of blades is 5 is the wind tunnel experiments were undertaken up to five blades. The limit of deflection of the rotor shaft was delivered from MATLAB Simulink Simulation. Wind shear effect on fatigue needs not to be considered, because the cyclic variation of blade angle of attack due to its rotation is much larger than that due to wind shear.

1.7.5.1.2 Load case A: Normal operation

(1) Loads on blade

For design rotor speed, the difference between the maximum force and the minimum force on a blade during one cycle (= maximum amplitude) is given by Equation (C.4) based on experimental result of flap-wise force under various tip speed ratio:

$$\Delta F_{\mathrm{xB}} = \frac{1}{2}\rho A_{\mathrm{proj,B}}(1.5V_{\mathrm{design}})^2 \cdot \left(8.5\lambda_{\mathrm{design}} - 3.2\right) \cdots\cdots\cdots\cdots\cdots\cdots (\mathrm{C}.4)$$

ΔF_{xB} is the amplitude of the force acting on a blade in X_B direction (flap-wise direction and in the radial direction of the rotor)

$A_{\mathrm{proj,B}}$ is maximum projection area of a blade (area in plain view)

The numerical values in Eq. (C.4) were determined from the highest value calculated for 7 airfoil sections NACA0008、0012、0016、0020、0024、0028、0032.

The thrust on the rotor shaft in operation is given as:

$$F_{\mathrm{T}} = C_{\mathrm{T}}\frac{1}{2}\rho(1.5V_{\mathrm{design}})^2 A \cdots\cdots\cdots\cdots\cdots\cdots\cdots\cdots\cdots\cdots (\mathrm{C.8})$$

Thrust coefficient C_T = 1.2 was determined by wind tunnel tests for 2, 3, 4 and 5- bladed VAWT. (Fig.5.6.4.1)

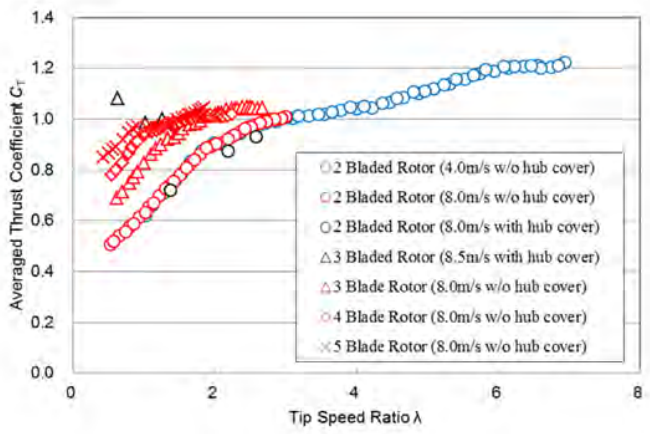

Fig.5.6.4.1 Wind tunnel test data:

Averaged Thrust Coefficient vs. Tip Speed Ratio for 2, 3, 4 and 5- bladed VAWT

1.7.5.1.3 Load case H: Survival wind, Loads on Rotor shaft

The drag acting on the blades of a parked rotor generates wind force on the rotor shaft:

$$F_{\text{shaft}} = C_{\text{Fshaft}} \frac{1}{2} \rho A_{\text{proj,B}} V_{\text{e50}}{}^2 \quad \text{.....(C.23)}$$

The values of thrust coefficient C_{Fshaft} are given in Table C.1 depending on the number of blades.

Table C.1—Thrust coefficient C_{Fshaft} acting on a parked rotor

B	1	2	3	4	5
C_{Fshaft}	1.1	2.0	2.0	2.9	3.2

The values of thrust coefficient C_{Fshaft} was determined by wind tunnel tests for 2, 3, 4 and 5-bladed VAWT.

1.8 POLAND

Piotr Domagalski[1], Maciej Karczewski[1], Lars Morten Bardal[2] , Lars Sætran[2]
[1]Institute of Turbomachinery, Lodz University of Technology, Lodz, Poland
[2]Department of Energy and Process Engineering, Norwegian University of Science and Technology, Trondheim, Norway
piotr.domagalski@p.lodz.pl, maciej.karczewski@p.lodz.pl , lars.satran@ntnu.no

Country: Norway

Location: Skipheia, Frøya (Trøndelag), 63.6666 N 8.3416 E.

Campagin timeline: 2009-2015;

Hardware summary: 6 pairs of 2D sonic anemometers at 10, 16, 25, 40, 70, 100 m above the ground, independent temperature measurements at the same heights; pressure and relative humidity from local meteostation (20 km away).
Database summary: approx. 180 000 of 10 min data samples of full data recovery.

SWT Site Characterization

Wind data have been collected from a Skipheia meteorological station on the island of Frøya on the western coast of Norway, Trondelag. The site shown in Figure 1 (together with reference meteostation) represents an exposed coastal wind climate with open sea, land and mixed fetch from various directions.

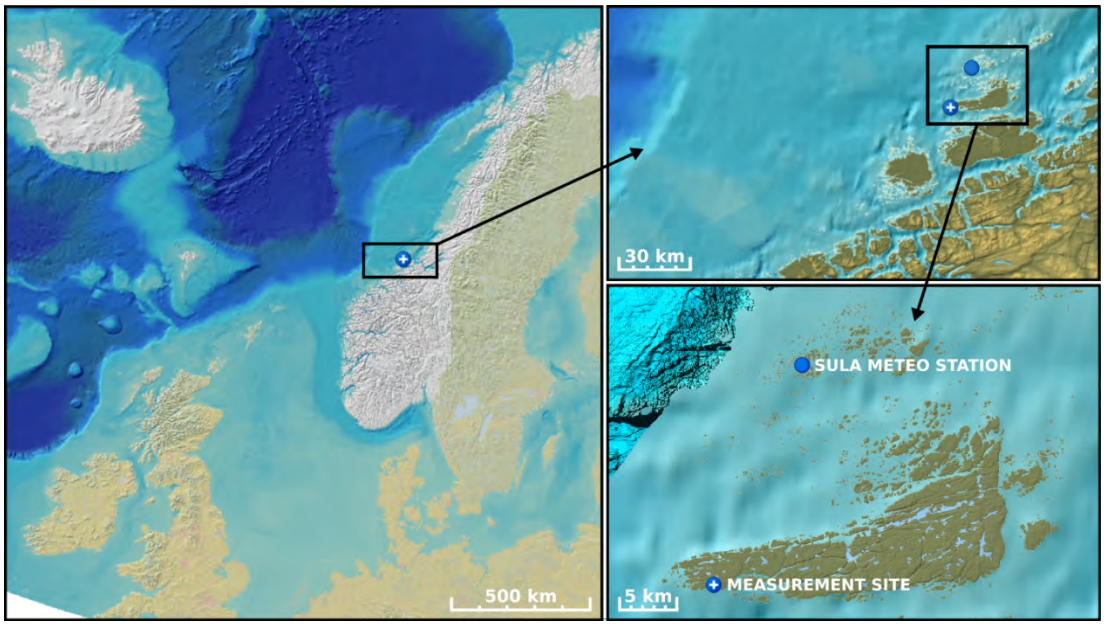

Figure 1. Localization of the met mast in Norway

The terrain surrounding the site, presented in Figure 2 and Figure 3 consists of a combination of bare rock, wetlands, low vegetation like heaths, heather, moss and low shrubs as well as complex sealine.

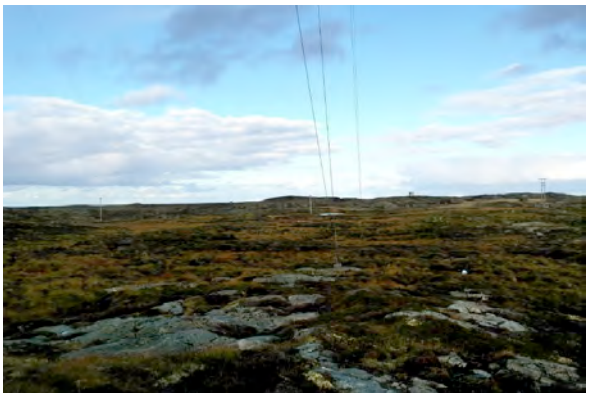

North view

East view

South view

West view

Figure 2. Site surroundings in different directions (source: Ingunn Sletvold Øistad, Projectwork EPT-P-2014-117, Department of Energy and Process Engineering, NTNU, 2014)

Figure 3. Panoramic view from the top of the met mast

As visible on the topographic map of the surroundings (Figure 4), the landscape is relatively flat, although some wind channeling due to coastline characteristics is visible and will be shown later on wind roses. There are also no nearby obstacles which could influence the wind measurements significantly. The local topography is characterized by small hills with few meters in height. Interactive maps can be found via Norwegian Mapping Authority resources norgeskaart.no, or directly at

https://www.norgeskart.no/#!?project=seeiendom&layers=1002,1015&zoom=12&lat=7076573.06&lon=169752.46&sok=63.6666%20%20N%20%208.3416%20%20E .

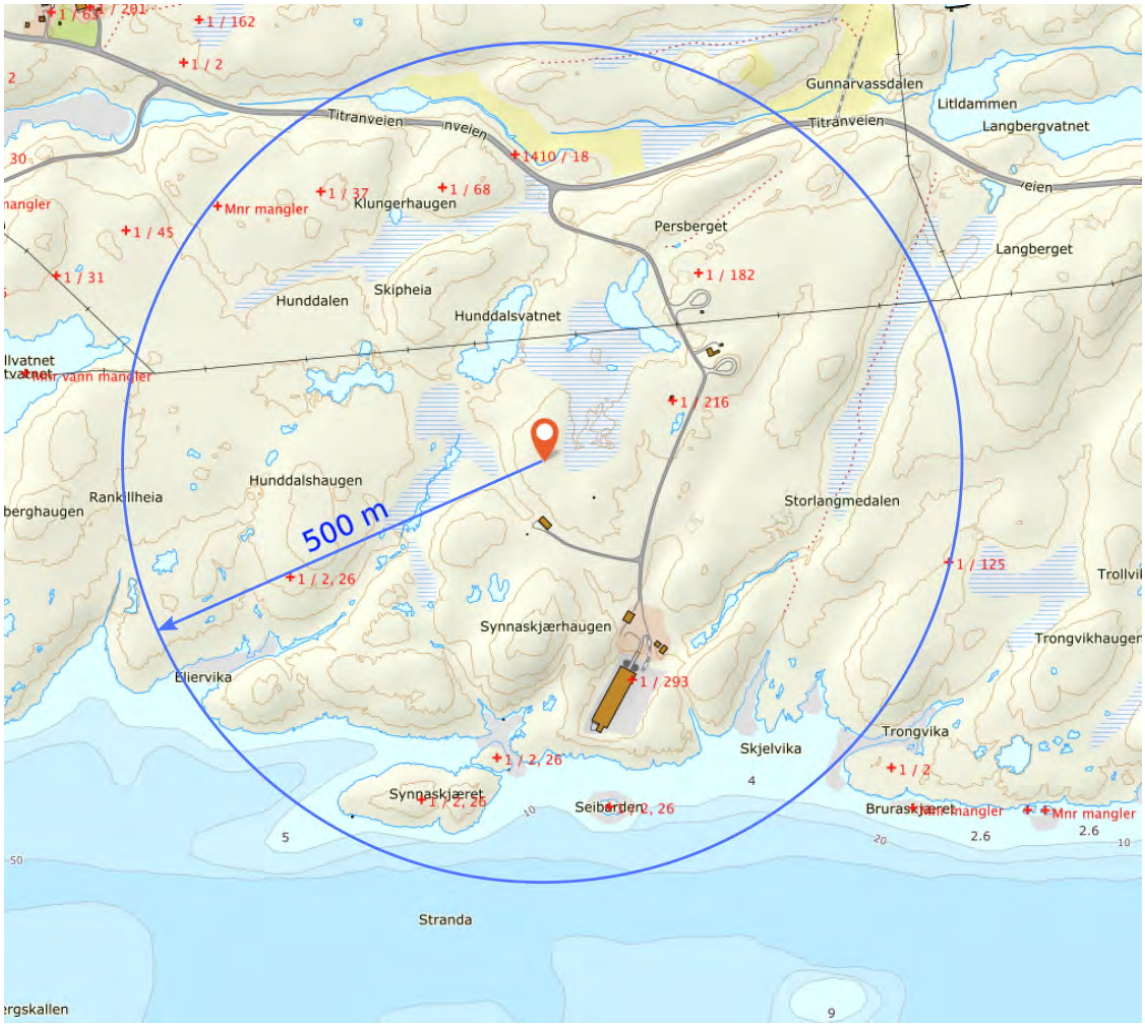

Figure 4. Map of site surroundings. 500 m distance from the measurement tower is marked.

Although no obstacles are present while the vegetation and surface conditions can be considered constant with regards to the direction, due to the coastal character of the site the distance to a sea line is an important factor influencing the wind flow pattern. The sudden sea-land surface roughness transition leads to generation of an internal boundary layer.

Depending on the direction, the distance from the measurement location to the shoreline varies, although is typically in the range of few km (4-4,5 km, West and North), few hundred meters (South) to approx. 30 kilometers in East and North-East directions. The distance to the shoreline as a direction function is presented in Figure 5, also showing the vertical ground profiles (scales are not the same).

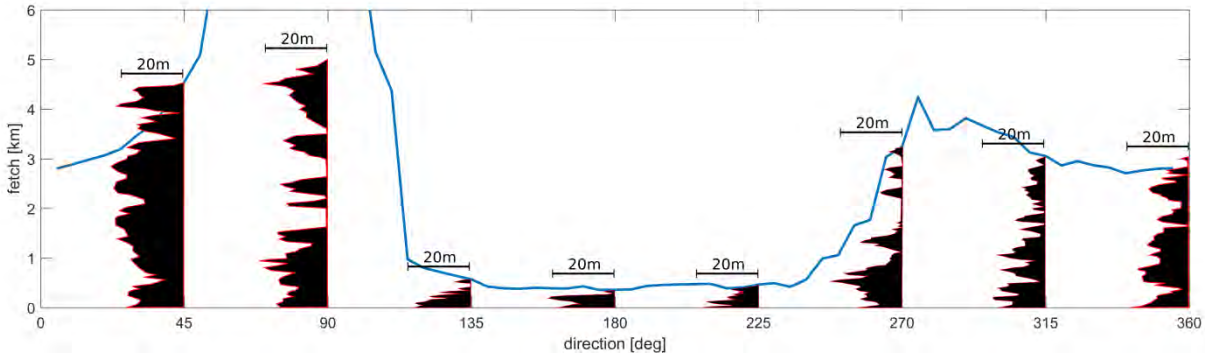

Figure 5. The distance to the shoreline (blue) as the direction function and corresponding vertical terrain profiles (scales of fetch distance and height scale differ).

SWT site general wind climate characterization

The wind climate characteristics of the site can be described as typical oceanic and coastal, with average roughness length of z_0=0.0086 m and a power law exponent of α=0.107 (least square fit based on approximately 10000 neutrally stratified 10-minute periods containing data for all altitudes). The mean wind speed at z=100 m was measured as u_{100}=8.31 m/s and the Weibull distribution parameters for the wind velocity at z=10 m were calculated as k=1.83 and c=7.23 m/s.

Figure 6 presents mean monthly wind velocities at measured heights that were 10, 16, 25, 40 and 70 m above the ground level.

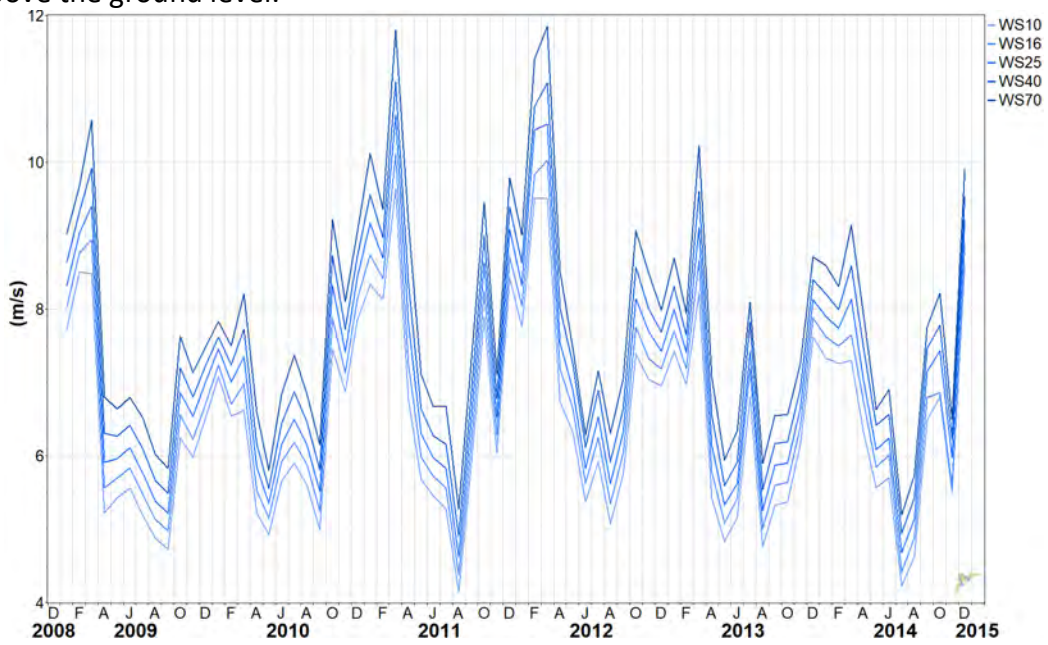

Figure 6. Mean monthly wind velocities at measured heights (gaps filled with interpolated data).

Wind and Energy rose together with the wind speed frequency distribution for 10 m and 70 m altitudes are presented in Figures 7-14.

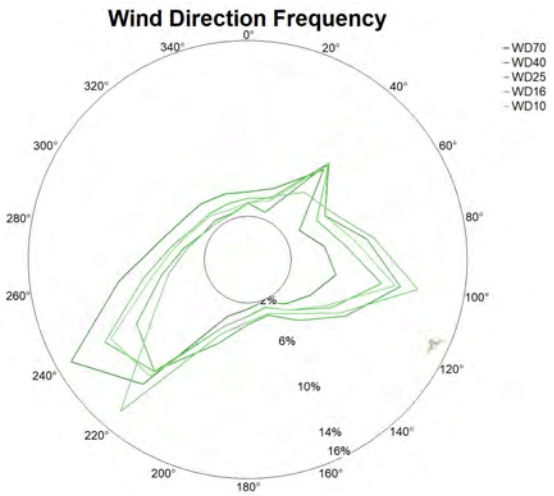

Figure 7. Wind rose at the height of measurements (WD - Wind Direction at 10, 16, 25, 40 and 70 m)

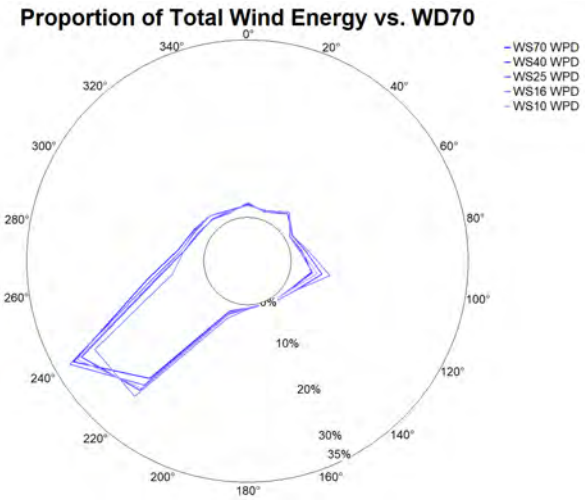

Figure 8. Energy rose at the height of measurements (WD - Wind Direction at 10, 16, 25, 40 and 70 m)

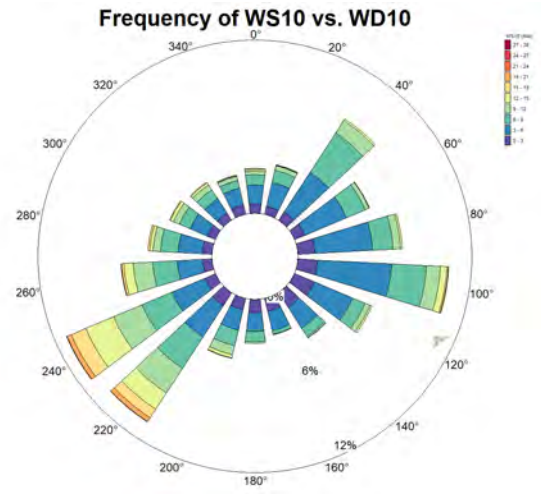

Figure 9. Wind speed frequency distribution at 70m (with respect to the wind direction)

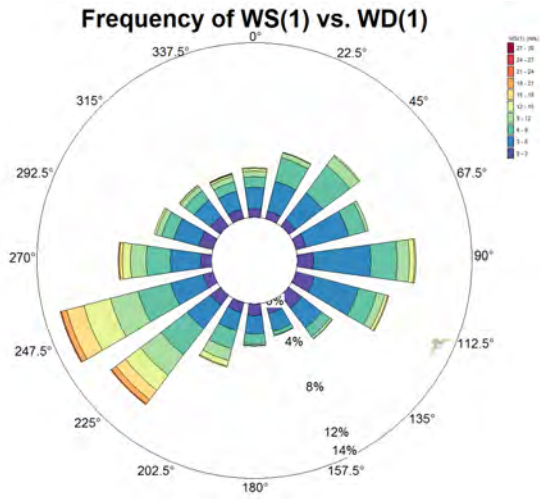

Figure 10. Wind speed frequency distribution at 10m (with respect to the wind direction)

Wind and power roses show the SW and WSW (247.5&225^0) as a prevailing wind direction. Comparison of the wind rose at 10m to the wind rose at 70 m shows no wind skewness. A distinguishable wind inflow, visible for the sector of 90-100^0, is believed to be an effect of wind channeling by a sea passage between the Frøya island and main continental part of Norway. The energy rose (Fig. 8) shows evidently that the main part of kinetic energy carried by wind comes from SW and WSW (247.5&225^0)). The S, SW, N&NE directions show distinct reduction in the wind speed. Such direction pattern is connected with large scale patterns of wind climate and the shape & topography of the Scandinavian Peninsula: long, near coastal mountain chains and SW-NE oriented shoreline. Distributions of wind velocity at 10 m and 70 m are presented in figures 11 and 12. They present Weibull distribution with 5 and 6 m/s as the most frequent wind speeds. The wind shear is presented in figure 13 showing the velocity change with height (using mean of monthly means). Fitting log and power law to all the data (not only to samples of neutral atmospheric stability) shows vertical distribution parameters of α=0.098 and z_0=0.00098m (power law exponent and surface roughness). The turbulence intensity lowers from 20% near the ground level to approx. 10% at 70 m. The TI distribution as a function of altitude can be fitted with a power law equation with the exponent of α_{TI}=-0.21.

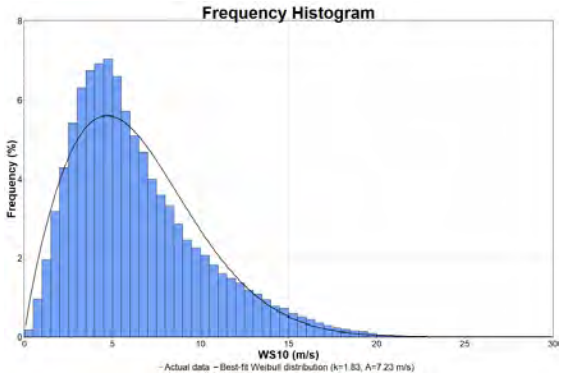

Figure 11. Wind speed frequency distribution at 10 m.

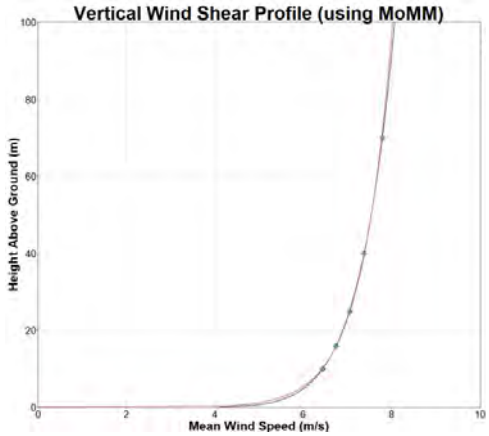

Figure 13. Average vertical wind profile

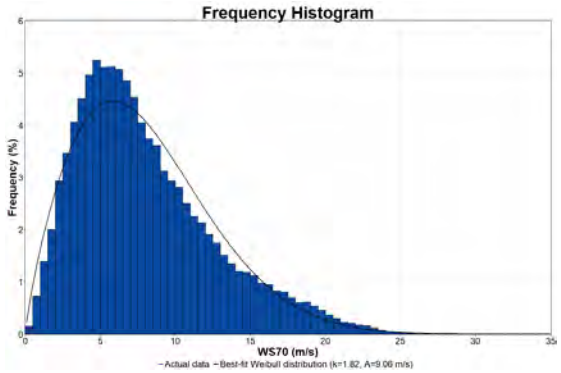

Figure 12. Wind speed frequency distribution at 70 m

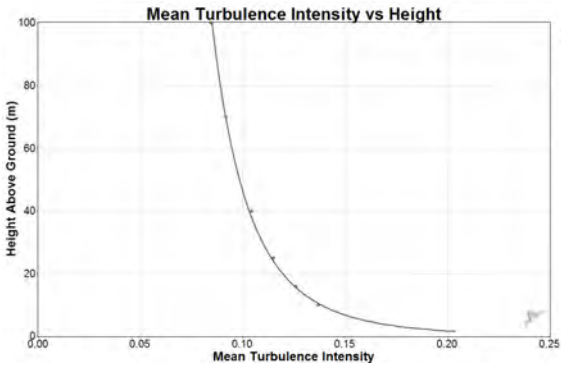

Figure 14. Average turbulence intensity profile

SWT reference wind measurements and quality assurance

The wind data from the nearby Sula meteorological station was used as the reference wind measurement. The location of this national meteorological station is approximately 20 km from the Froya measurement site. For this purpose the measure-correlate-predict method (MCP) was used to compare the time extrapolated wind series.

Due to the lack of relative humidity and pressure measurements at the featured measurement site (Skipheia, Frøya), these data, needed for a virtual potential temperature calculations, were taken from the Sula meteorological station.

The Skipheia measurement site described here was evaluated in 2014 according to MEASNET Guidelines 'Evaluation of Site Specific Wind Conditions'. The detailed report containing additional analyses is presented in the attachment (Ingunn Sletvold Øistad, Projectwork EPT-P-2014-117, Department of Energy and Process Engineering, NTNU, 2014).

Data Acquisition Approach

The Skipheia wind measurement station was raised in 1980. Currently two climbable lattice towers of 100 m high and approx. 1 m^2 cross section are being used. The measurement equipment is installed and managed by qualified staff from NTNU (Norwegian University of Science and Technology, NTNU Trondheim) and TUL (Technical University of Lodz, Lodz, Poland). Location coordinates of mast 2, used for data collection for current analysis is 63.6666 N 8.3416 E. The mast is located approx. 20 m above the sea level.

During the measurement campaign six pairs of Gill WindObserver 2D ultrasonic anemometers were installed on one of the masts at heights of 10, 16, 25, 40, 70 and 100 meters. All the anemometers were working with 1Hz sampling rate, presented analysis are based on 10-minute averages. Independent temperature measurement at the same heights was realized with Campbell Scientific 109 temperature probes. Data acquisition and conditioning was done by Campbell Scientific CR3000 micrologger.

In the current work we analyze the data gathered in the time period between November 2009 and December 2014. The data set covers approximately 160 000 data points for each height (10-minute averages). Gaps in the data time series, caused mainly by equipment failures related to severe atmospheric conditions, did not result in any time dependent trend on any of the plots characterizing the wind conditions at this site.

The time series of wind velocity are presented in Figure 15 showing the downtimes caused by power losses and equipment failures. Corresponding gaps in data recovery rates are visible in Figure 16.

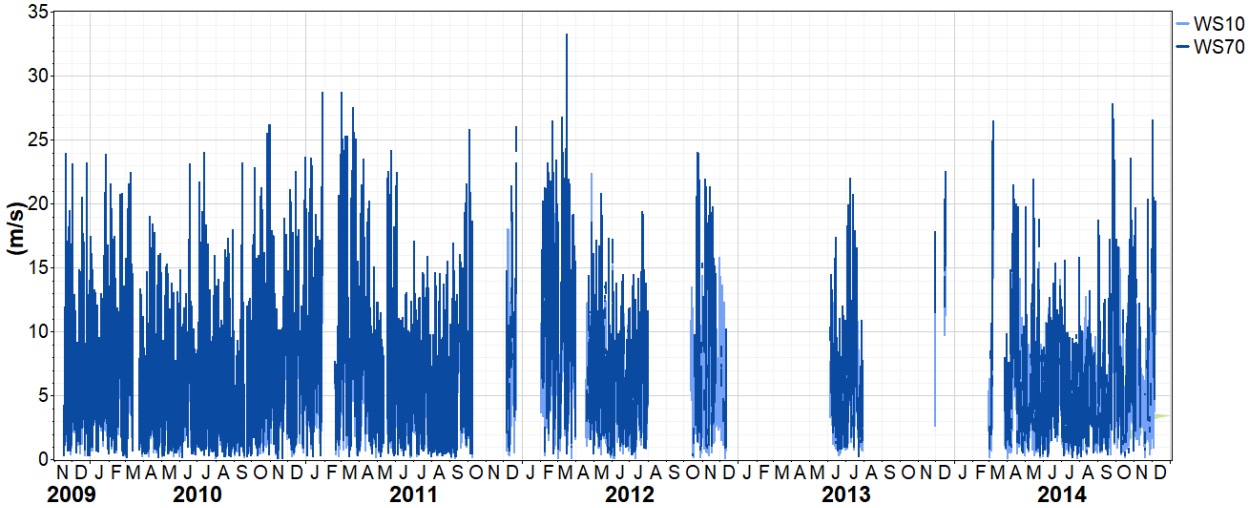

Figure 15. Time series of wind speed (WS) measurement at 10 and 70 m.

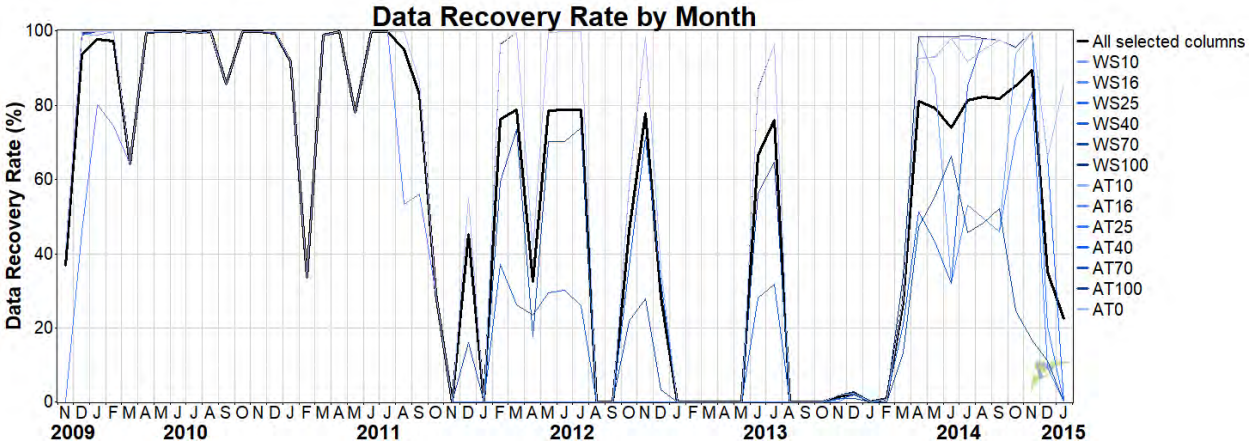

Figure 16. Time series of the data recovery rate for WS and atmospheric temperature (AT)

Data processing strategy, quality assurance methods

Data were processed in Matlab (MathWorks USA) based on 10-minute averages and in Windographer software (AWS Truepower, LLC, USA).

In a pre-processing stage the tower aerodynamic shading was filtered out: only the upwind anemometer was taken into account and all the nonphysical recordings were removed (eg. temperatures over 50 ^{0}C). Finally only the time stamps with data for all sensors were used.

For the atmospheric stability calculations we used the bulk Richardson number defined as:

$$Ri = \frac{g}{\overline{\theta_v}} \frac{\Delta\overline{\theta_v} z_m}{(\Delta u)^2}$$

where g is the gravitational acceleration, z_m is the altitude difference between respective measurement heights, u is a velocity and θ_v is virtual potential temperature.

The virtual potential temperature was calculated according to equation:

$$\theta_v = T\left[1 + 0.61\left(0.622\,\frac{e}{p - 0.378e}\right)\right]\left(\frac{100000}{p}\right)^{2/7}$$

where T is an ambient temperature, p is atmospheric pressure and e water vapour pressure (at given p and T is calculated from relative humidity).
The barometric pressure (which was available at the sea level from the Sula meteorological station) was adjusted for altitude and temperature according to ISO guidelines5.
The friction velocity u_*, roughness length z_0, and power law exponent α were fitted by linear least square method from mean vertical wind profiles over the entire measurement period. In order to present their diurnal profiles a 1h averages were used.

Results

Due to the coastal character of the measurement site and resulting mixed sea/land fetch we decided to divide the analysis according to direction sectors. The proposed division visible in Figure 17 consists of land fetch (sector II) in direction 40-100°, open sea offshore fetch (sector IV) in direction 190-260° and two intermediate cases, where the offshore wind is disturbed by 2-5 km of land (sector I) – direction 260-40° and oppositely the wind from inlands travels through over 10 km of undisturbed sea before the measurement (sector III).

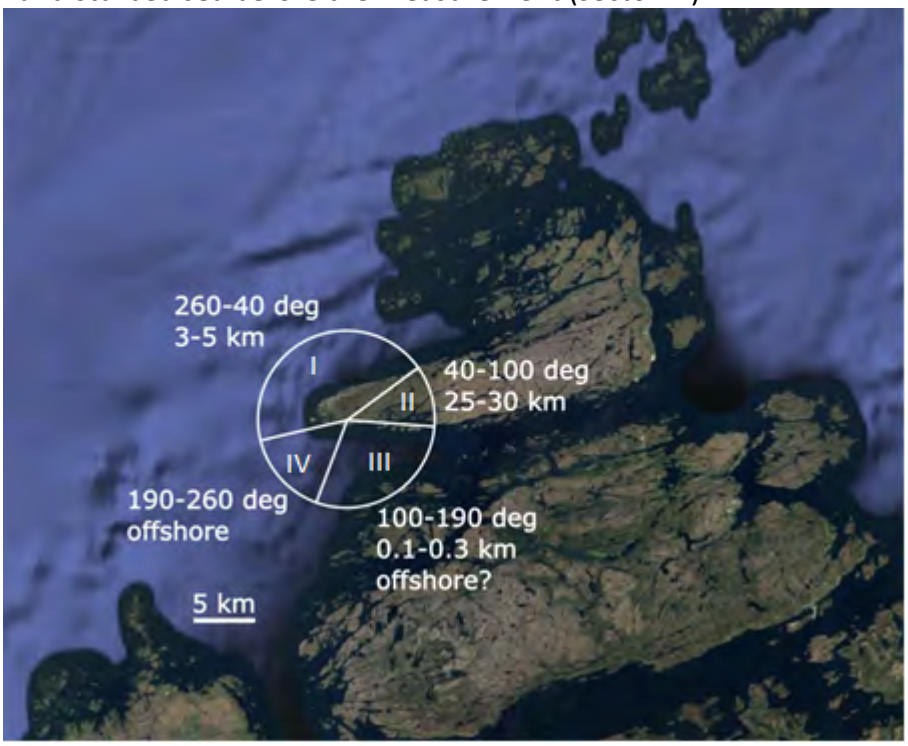

Figure 17. Division of direction sectors according to fetch characteristics.

Characteristics of atmospheric stability and wind turbulence in form of vertical wind profile parameters (all stabilities included), friction velocity, sample count, Richardson number distribution and turbulence intensity plots are presented below in Fig. 18.

[5] Atmosphere, S. (1975). International organization for standardization. ISO, 2533, 1975

Sector I, 260-40 deg , 2-5 km distance to a shore line.	Sector II, 40-100 deg typical land fetch	Sector III, 100-190 deg	Sector IV, 190-260 deg offshore, undisturbed wind
$\alpha = 0.11$; $z_0 = 0.015$ m	$\alpha = 0.10$; $z_0 = 0.017$ m	$\alpha = 0.079$; $z_0 = 0.00035$ m	$\alpha = 0.10$; $z_0 = 0.00075$ m
$u_* = 0.34\ m/s$	$u_* = 0.30\ m/s$	$u_* = 0.18\ m/s$	$u_* = 0.36\ m/s$
$n = 22405$	$n = 17540$	$n = 17365$	$n = 27398$

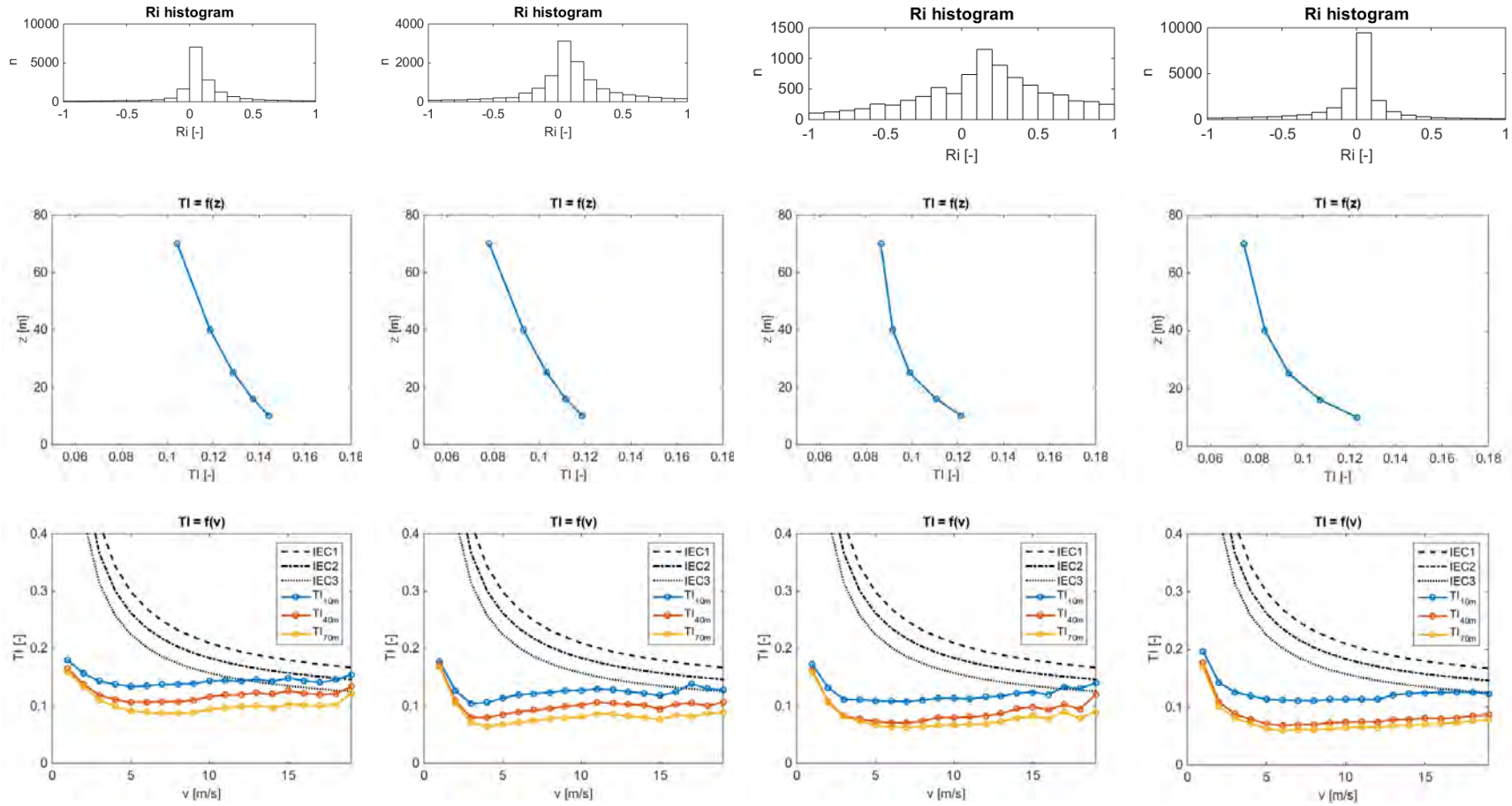

Figure 18. Site characteristics by sector: TI, α, z_0 & u_* without division into atmospheric stability.

Figure 18 shows that offshore direction sectors are characterized by very low surface roughness, order of magnitude lower than land sectors. That character is also visible comparing the power law exponent, however the difference is not so striking. Extremely small values of surface roughness, below 1 mm, calculated by fitting the velocity profile shall be treated as an approximation only due to the high sensitivity of fitting parameter (surface roughness) to small changes in profile in such a low range.

Richardson number histograms show non-stable atmospheric conditions as the prevailing state. More precise description of the stability distribution with regards to velocity is shown in Fig. 21, where the stability classification is based on Obukhov length calculated from Richardson number as $\mathrm{L} = \frac{\mathrm{z_m}}{\mathrm{Ri}}$ for non-stable conditions and $\mathrm{L} = \frac{\mathrm{z_m}}{\mathrm{Ri}}(1 - 5\mathrm{Ri})$ for $0 \leq \mathrm{Ri} \leq 0$.

Bins of Obukhov length ware set as $(-500 \leq \mathrm{L} < -200)$ for unstable, $(-200 \leq \mathrm{L} \leq 0)$ for very unstable, $(|\mathrm{L}| > 500)$ for neutral, $(200 \geq \mathrm{L} > 0)$ for very stable, and $(500 \geq \mathrm{L} > 200)$ for stable stratification. Velocity is presented on the horizontal axis, fraction of the observation samples is presented on the left vertical axis and the number of samples for the observation study is on the right vertical axis.

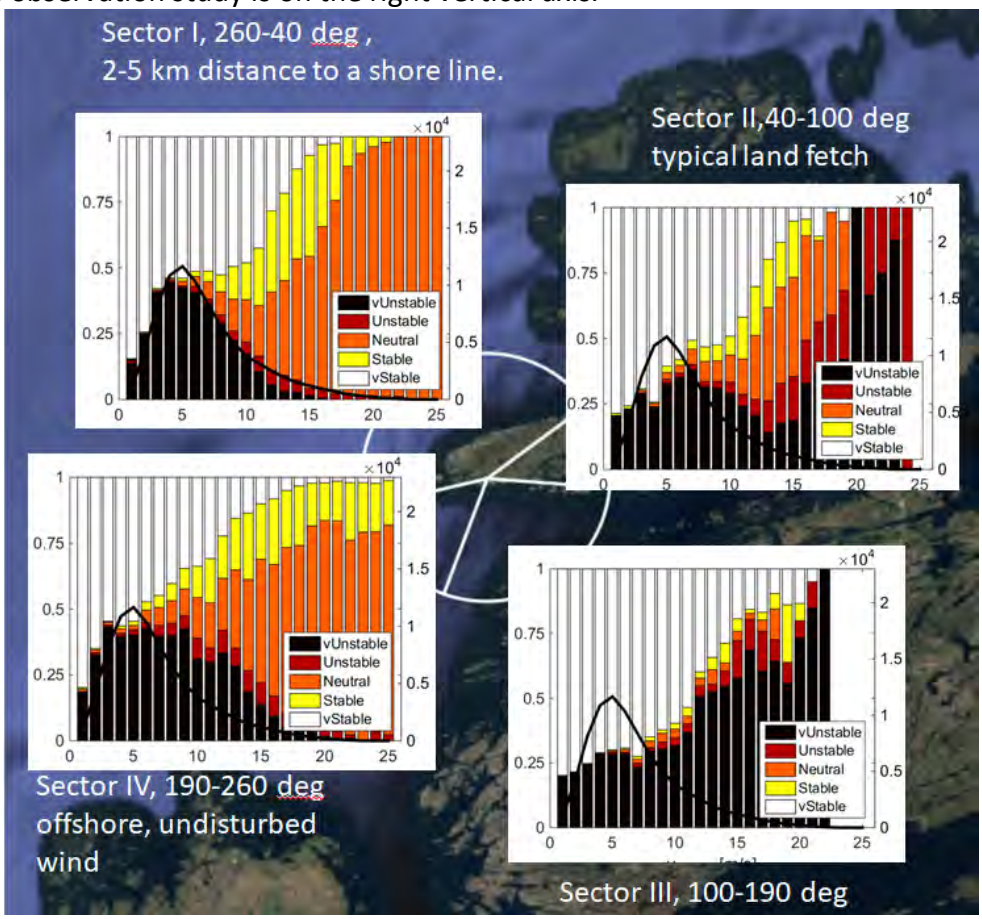

Figure 21. Stability histograms for all sectors (as based on Obukhov length).

Stability histograms presented in Fig. 21 are showing that at low to moderate wind speeds very unstable stratification is also very common. Neutral stratification is not occurring except for higher velocities, and its frequency is dependent on the direction sector.
The seasonal evolution of wind shear in form of power law exponent and its diurnal cycles divided to different months are shown in Fig. 22 and Fig. 23.

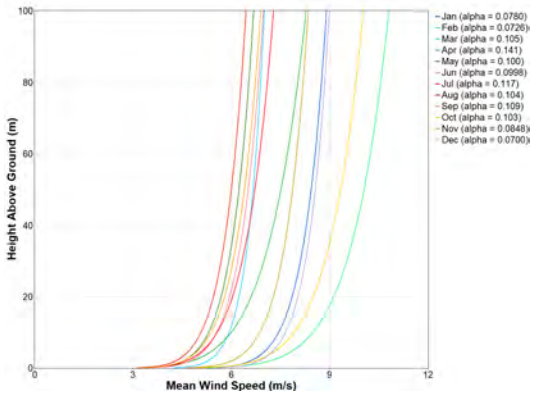

Figure 22. Monthly changes in the wind shear.

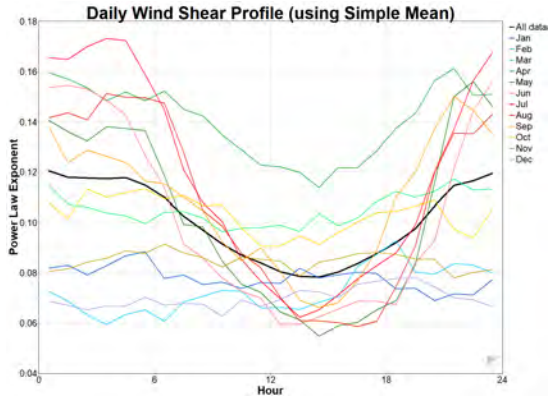

Figure 23. Diurnal&monthly shear changes.

Analysis of shear data presented in Fig. 22 and Fig. 23 shows that the wind shear is highly dependent on the time of the year and its monthly changes are significant, from power law exponent $\alpha = 0.12 - 0.1$ during summer time to $\alpha = 0.14$ during April. Analysis of α diurnal profile shows drastic diurnal changes during summertime and stable values during winter months indicating its dependence on the sun radiation and atmospheric stability changes.
Such highly dynamic behavior is also confirmed by data in Fig. 24 presenting diurnal changes of wind velocity and turbulence intensity at 10 m and 70 m altitude divided into separate months of the year. It is again visible, that during late spring to mid summer time, from May to August, the wind speed diurnal profile exhibits high peaks in the afternoon hours, much more intensive near ground level. That indicates that diurnal profile is related to atmospheric stability as lower, near ground levels are directly affected by heat radiation from the ground. The mid day peaks are also visible on turbulence intensity diurnal profiles in non winter months. The turbulence intensity diurnal changes, not as much as in case of the wind speed, are only slightly affected by the altitude change; its diurnal profiles are fairly similar at both altitudes.

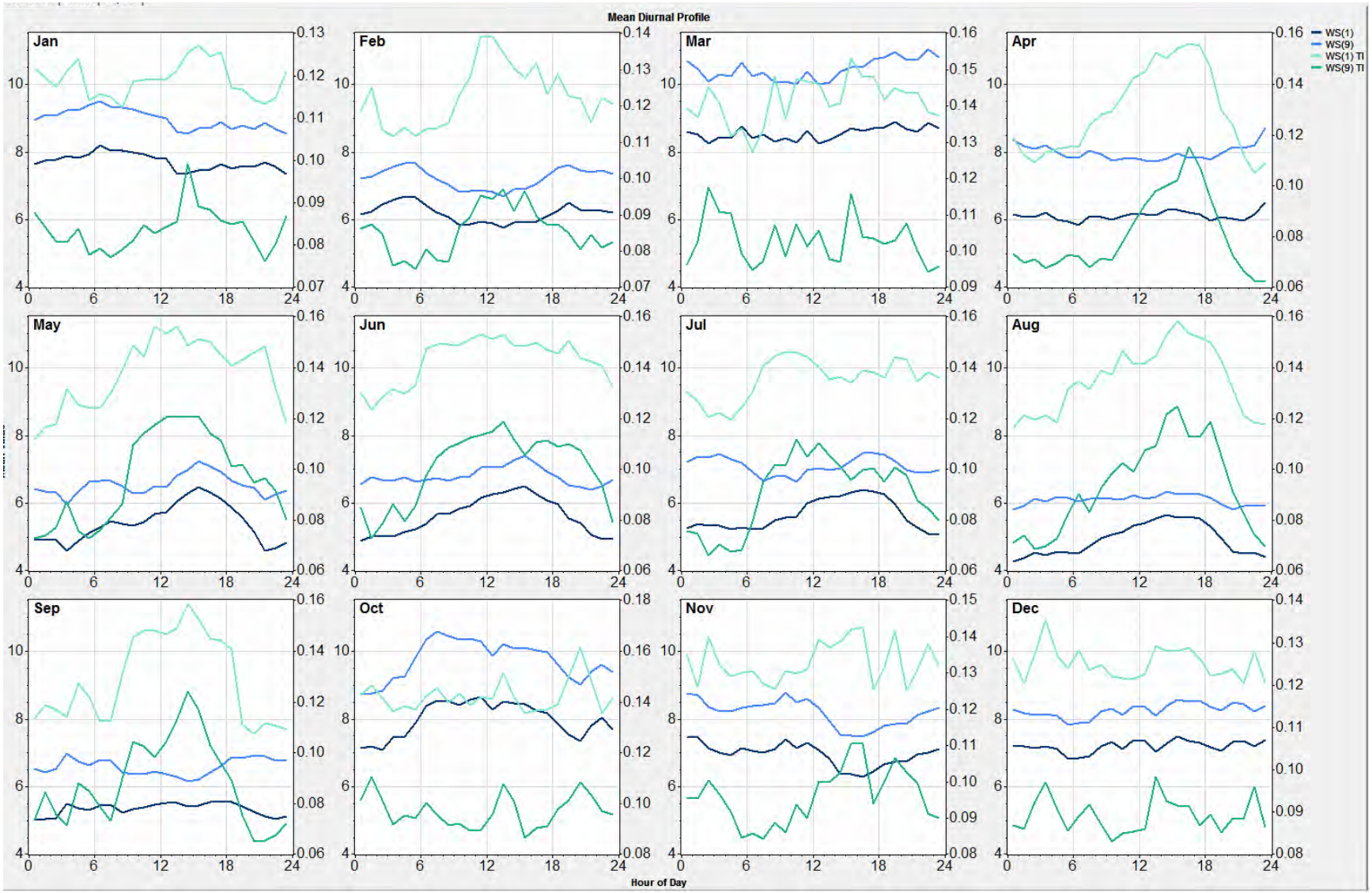

Figure 24. Diurnal and monthly wind speed (WS, blue lines) and turbulence intensity (WS TI, green lines) profiles at 10 m and 70 m height.

Figure 25 presents diurnal profiles of shear (power law exponent) and friction velocity for different sectors. On the diurnal profiles the hourly means are marked with circles and the line is added for visualization purposes, created by a moving average filter data.

Analysis of Fig. 25 confirms that there are differences between offshore and land fetch sectors. While there is a visible change in shear and friction velocity during the day-night cycle in sector I and sector II, sector IV (offshore) presents no such changes. Analysis of data for sector III, in which the offshore wind is obstructed by few hundred meters of inclined land, shows that although the vertical wind profile parameters suggest the offshore wind characteristics, even few hundred meters of land fetch could be responsible for changing the wind profile in the lower part near the ground. Therefore wind parameters, established from such a profile, shall be treated with caution.

From physical point of view such a behavior could be explained by a tendency of stable air to adhere to the surface as opposed to unstable which breaks into convective eddies, increasing the shear near the ground. However this would not be visible in stability independent, time averaged statistics (Neil Kelley, personal communication). More detailed investigation is necessary to address this issue.

Sector I, 260-40 deg , 2-5 km distance to a shore line.

$\alpha = 0.11$; $z_0 = 0.015$ m

$u_* = 0.34\ m/s$

$n = 22405$

Sector II, 40-100 deg typical land fetch

$\alpha = 0.10$; $z_0 = 0.017$ m

$u_* = 0.30\ m/s$

$n = 17540$

Sector III, 100-190 deg

$\alpha = 0.079$; $z_0 = 0.00035$ m

$u_* = 0.18\ m/s$

$n = 17365$

Sector IV, 190-260 deg offshore, undisturbed wind

$\alpha = 0.10$; $z_0 = 0.00075$ m

$u_* = 0.36\ m/s$

$n = 27398$

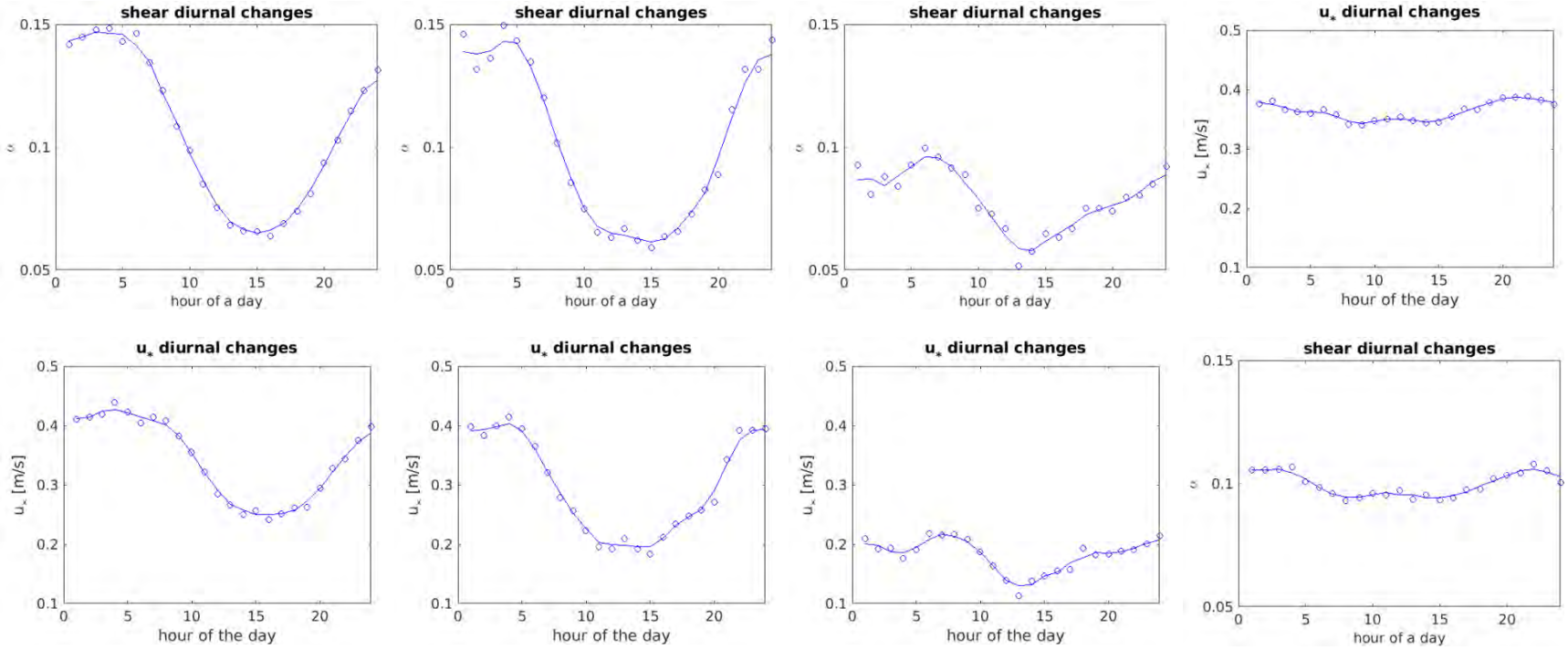

Figure 25. Diurnal changes of shear and friction velocity by sector

Conclusions

The analysis of 5 year wind data from Skipheia, Frøya, mid Norway, measured by 6 pairs of 2D sonic anemometers at 10, 16, 25, 40, 70, 100 m above the ground accompanied by temperature measurements allows to draw conclusions summarized below:

- Measurement site exposed to coastal wind climate with open sea, land and mixed fetch from various directions delivered significant amount of data for off-shore, on-shore wind and mixed coastal wind.
- Offshore & onshore wind climate division is clearly visible analyzing wind shear in form of surface length & power law exponent.
- Analysis of turbulence intensity vertical profile shows that in case of offshore directions the turbulence intensity decreases quickly with the height compared to onshore directions. Also the TI vertical profile is highly non-linear in case of offshore directions while it is almost linear for onshore or long land fetches.
- Stability analysis showed that stratification at this site is predominantly stable. A major quantity of timesteps, approx.. 50%, are characterized as stable & very stable. In low to moderate velocities range, including the most frequent velocities the stability is either very stable or very unstable. Other stabilities, including neutral stratification are present only during stronger, over 10 m/s, winds. Extrapolation of velocities to desired hub-height, for example with logarithmic law, shall include stability corrections like the one suggested by DNV CR-205. This shall be done with caution as described in DNV stability correction functions as prediction capabilities deteriorate in stable and very stable atmosphere.
- At this stage we cannot make a clear statement about correlation between Ri number and TI. Further computations are necessary to analyze the relations between stability and turbulence intensity.
- Analysis of friction velocity suggests that high values of friction velocities can be connected with wide Richardson number distribution meaning wide range of stabilities – see sector III (100-190 °) of Figure 18. Although the physical mechanism behind this observation shall be investigated.
- All the wind climate characteristics, mean velocity, shear, turbulence intensity, friction velocity show high dependence on time of a day, especially during non-winter seasons showing strong relation with atmospheric stability.
- Although the diurnal distribution of power law exponent α does not present peak values at dusk and dawn, its abrupt changes during these periods could be responsible for increased loads on turbines. These time characteristics correspond to results of other researchers showing this is the time of the day, where probability of the occurrence of high blade loads is the biggest.
- The above observation connected with the fact that the diurnal profiles of turbulence intensity show distinct peak values in the middle of a day – afternoon of warm and hot

seasons may suggest that probability of small wind turbine failure is more related to abrupt changes of wind shear during the diurnal cycle than to turbulence intensity.

Additional data&analisys of the described site (&nearby sites) wind characteristics can be found at:

Andersen, O. J., & Løvseth, J. (2010). Stability modifications of the Frøya wind spectrum. Journal of Wind Engineering and Industrial Aerodynamics, 98(4-5), 236-242.
Andersen, O. J., & Løvseth, J. (2006). The Frøya database and maritime boundary layer wind description, Marine Structures, 19(2-3), 173-192.
Bardal, L. M., & Sætran, L. R. (2016). Wind gust factors in a coastal wind climate. Energy Procedia, 94, 417-424.
Bardal, L. M., & Sætran, L. R. (2016, September). Spatial correlation of atmospheric wind at scales relevant for large scale wind turbines. In Journal of Physics: Conference Series (Vol. 753, No. 3, p. 032033). IOP Publishing.
Bardal, L. M., & Sætran, L. R. (2017). Influence of turbulence intensity on wind turbine power curves. Energy Procedia, 137, 553-558.
Bardal, L. M., Sætran, L. R., & Wangsness, E. (2015). Performance test of a 3MW wind turbine–effects of shear and turbulence. Energy Procedia, 80, 83-91.
Bardal, L. M., Onstad, A. E., Sætran, L. R., & Lund, J. A. (2018). Evaluation of methods for estimating atmospheric stability at two coastal sites. Wind Engineering, 0309524X18780378.
Domagalski P., Bardal, L. M., & Sætran, L. R. , Vertical Wind Profiles in Non-neutral Conditions - Comparison of Models and Measurements from Frøya, Journal of Offshore Mechanics and Arctic Engineering, under review.

The authors would like to acknowledge the support of European Commission in form of MaRINET2 project funded under FP7-INFRASTRUCTURES Programme in accessing the research infrastructure & data.

1.9 REPUBLIC OF KOREA (active 2009 – 2018)

1.9.1 Wind Profile Measurements on KIER Rooftop

1.9.1.1 Introduction

Rooftop is an attractive location for small wind turbine installation because higher hub height is easily obtained with less installation cost. Mean wind speed is improved as hub height increases but wind profiles are disturbed by rooftop shapes which may reduce wind turbine performance and lifetime structural safety.

The effects of rooftop shapes on wind profiles are qualitatively analyzed by wind speed measurements using 3-D ultra-sonic anemometer and the results shows that rooftop increases turbulence intensity and averaging time period is critical parameter to evaluate how much wind flow is influenced by rooftop.

1.9.1.2 Measurement Site Characteristics

The site is located in Jeju Island in Korea and surrounded by flat terrain and ocean as shown in Fig. 1. The location coordinates are 33º33’48”N and 126º 46’ 56”E and it elevation is 18m a.s.l. The only obstacles at the site is 1.5MW wind turbine just beside the building, in which the ultra-sonic anemometer is installed. The prevailing wind directions are 290º and the secondary is 90º.

Fig. 1 Measurements Site View

1.9.1.3 Measurement Setup

Fig. 2 shows the rooftop shape and the location of ultra-sonic anemometer. The distance between the rooftop and the anemometer is 2.4m. The reference met-mast is installed to measure undisturbed wind profiles at 360º and 25m away from the building. Undisturbed wind profiles are measured using an ultra-sonic anemometer. Both of the anemometers are the same model from Thies. The measurements period is from March 2015 to February 2016.

Measured wind velocities from rooftop and met mast are averaged in 1 minute and 5 minutes, respectively to clarify whether averaging time period effects on disturbed wind profiles in terms of magnitude. Based on the measured velocities, turbulence intensities (TI) and turbulent kinetic energy (TKE) are calculated and compared.

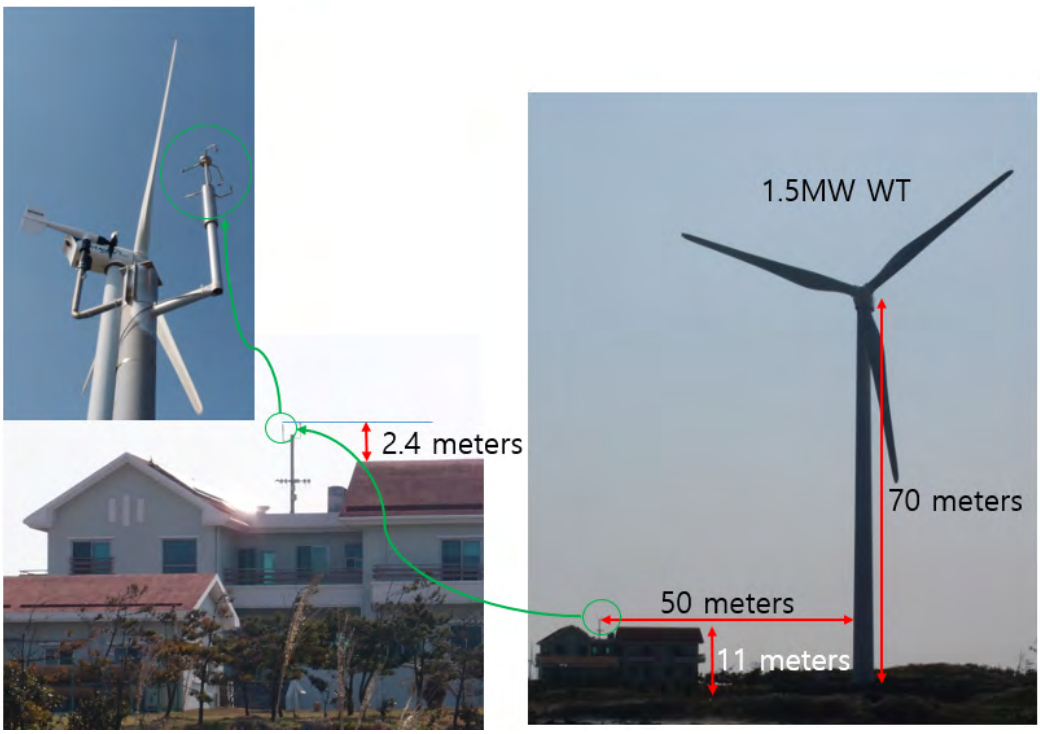

Fig. 2 Rooftop Shape and Measurement Arrangement

Fig. 3 Reference Met Mast (the same height of 13.4m as of the rooftop's one)

1.9.1.4 Measurement Results

1.9.1.4.1 Wind Direction

Fig. 4 shows prevailing wind directions measured by rooftop and met mast, respectively. Prevailing wind direction at the site depends on season. 290º is prevailing wind direction during summer but 90º is the one during winter season.

The prevailing wind directions from the rooftop is slightly different from the met mast because incoming wind is faced with the roof and then changes its direction but the magnitude is negligible.

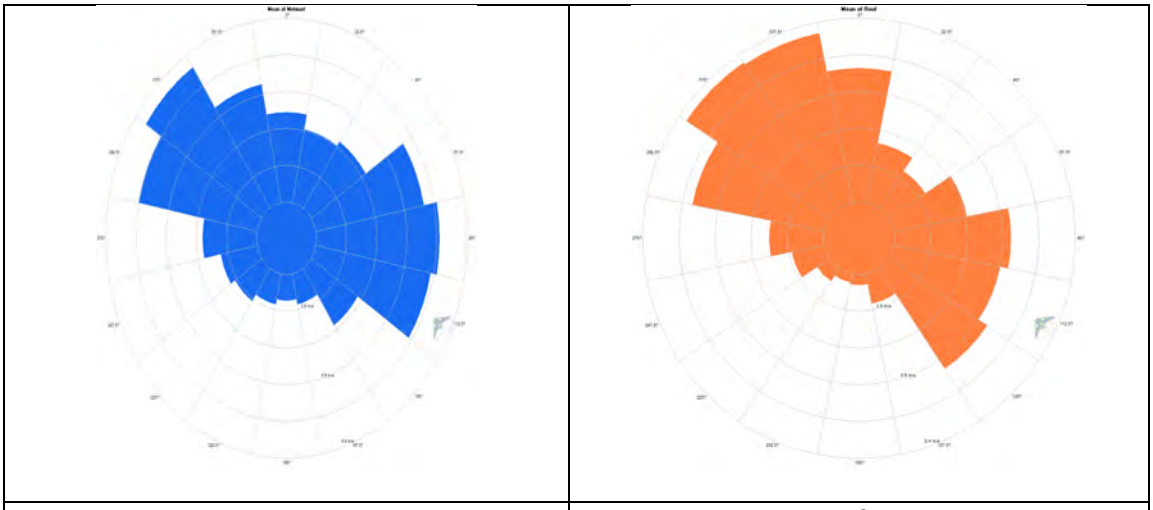

(a) met mast | (b) rooftop

Fig. 4 Comparison of Wind Directions

1.9.1.4.2 Wind Velocity Distributions

Measured wind velocities are averaged in 1 minute and 5 minutes and compared for both met mast and rooftop. X-coordinate is horizontal direction to the ground and Y-coordinate is lateral. Z is vertical to the ground.

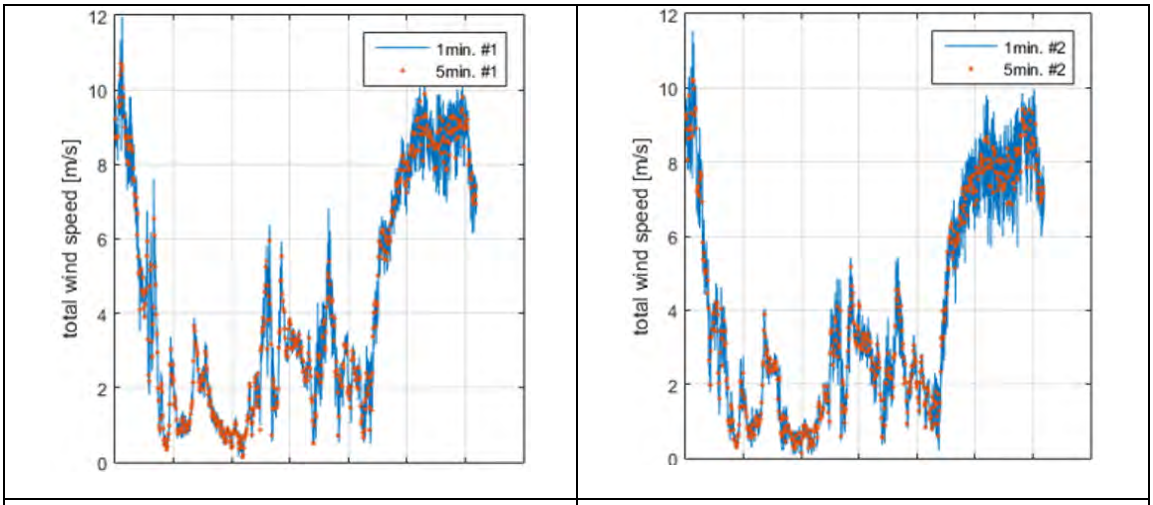

(a) met mast | (b) rooftop

Fig. 5 Total Velocity Distributions

Total velocity distributions of met mast and rooftop has similar profiles without any significant differences for the same sample measurement period of September 2015.

Velocity components of met mast and rooftop in X and Y-directions (U and V, respectively) also show the same profiles but the profiles in Z-direction(W) shows significant change in terms of averaging time and velocity distributions.

One minute averaged profiles has wider range of variations compared to 5 minute averaged. That is, longer averaging time period tends to underestimates wind speed variations which shall be

considered for micrositing of small wind turbines. For the magnitude of vertical wind speed components, rooftop measured values have higher positive values than met mast measured values because the rooftop shape induces upward flow.

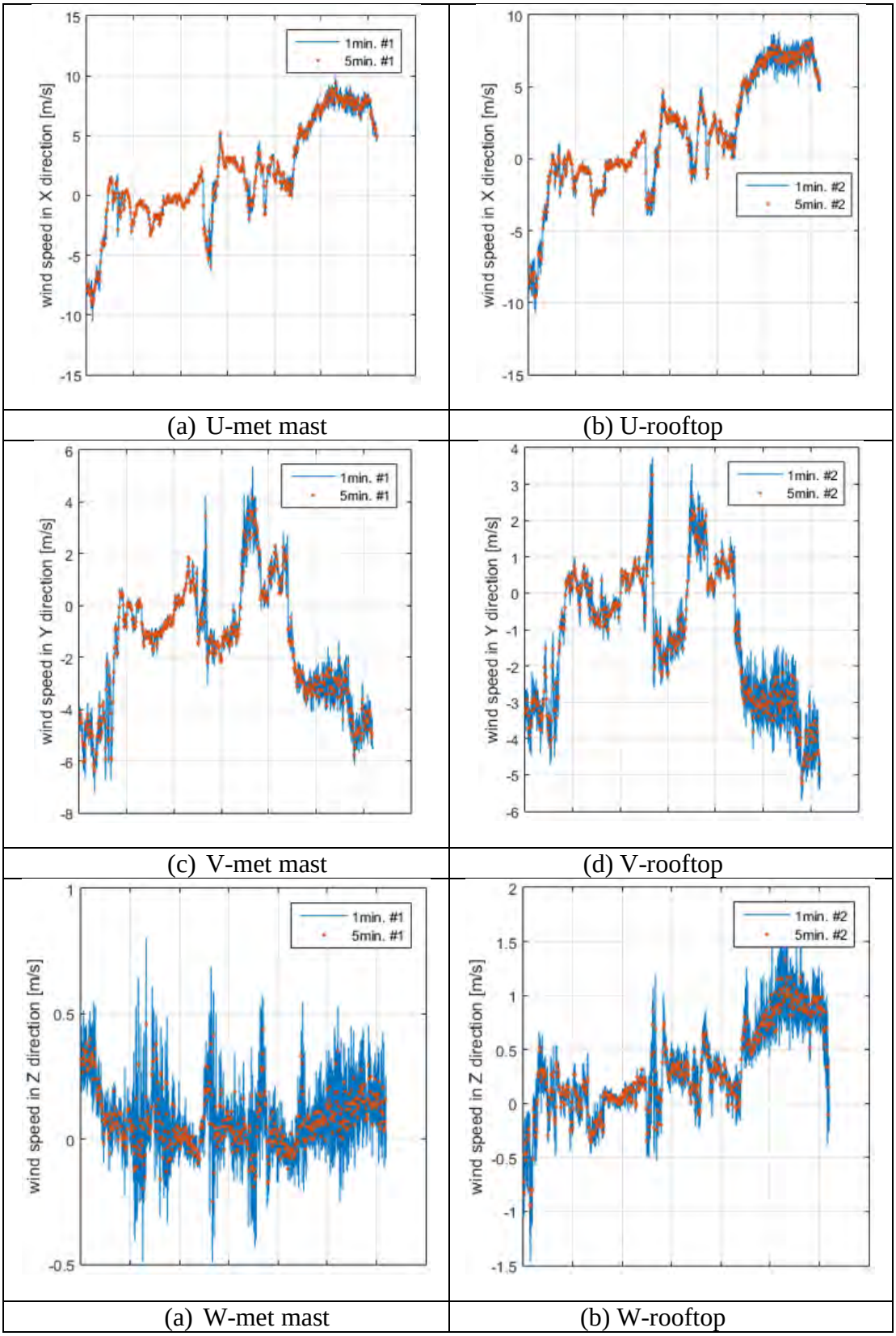

(a) U-met mast (b) U-rooftop

(c) V-met mast (d) V-rooftop

(a) W-met mast (b) W-rooftop

Fig. 6 Variation Profiles of Velocity Components in terms of Magnitude and Averaging Time Period

1.9.1.4.3 Turbulent Kinetic Energy (TKE)

TKE measured for one (1) month in September 2015 at met mast and rooftop show expected profiles. The rooftop anemometer is surrounded by the roofs as shown in Fig. 1 and Fig. 2 so that TKE values at rooftop are almost doubled over the azimuth compared to met mast profiles.

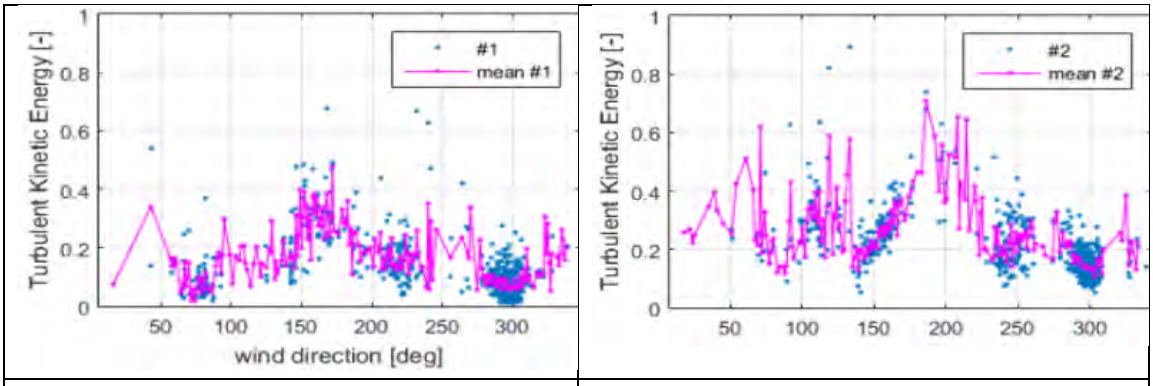

(a) TKE-met mast (b) TKE-rooftop

Fig. 7 TKE Comparison between Rooftop and Met mast

1.9.1.4.4 Conclusions

Ten minute averaged wind profiles are usually utilized for micro siting but the results shows longer averaging time tends to underestimates wind fluctuations induced by rooftop. In urban environment, it is hard to avoid disturbed wind by various artificial structures and disturbed wind influences performance and life time structural safety of small wind turbines.

Therefore, shorter averaging time of mean wind speed profiles are recommended for small wind turbine micro siting in urban environments.

1.10 SPAIN (active 2009 – present)

1.10.1 CFD model on Windflow results

1.10.1.1 Software used

OpenFOAM

1.10.1.2 Flow type

Neutral stratified atmosphere is assumed because strong windy conditions are considered. The steady-state simpleFoam solver for incompressible turbulent flow is used to solve the partial differential equations.

1.10.1.3 Governing Equations

Mass conservation:

$$\frac{\partial \bar{u}_i}{\partial x_i} = 0$$

Momentum:

$$\frac{\partial(\bar{u}_i \bar{u}_j)}{\partial x_j} = -\frac{1}{\rho}\frac{\partial \bar{p}}{\partial x_i} + \frac{\partial}{\partial x_j}\left(\nu \frac{\partial \bar{u}_i}{\partial x_j} - \overline{u_i' u_j'}\right)$$

1.10.1.4 Turbulence models

Extensive comparison among RANS turbulence models: SKE, RNG, MMK, Durbin, and nonlinear Shih.[6]

1.10.1.5 Spatial discretization of differential operators

The Gaussian integration was used with different interpolation schemes. The 2nd order linear interpolation was applied for Gradient terms, the 2nd order upwind interpolation for Divergence terms, while for the Laplacian terms the 2nd order linear interpolation was used with explicit non-orthogonal correction.

1.10.1.6 Linear system solvers

Generalized geometric-algebraic multi-grid solver (GAMG) with DIC smoother is used for the pressure, and preconditioned bi-conjugate gradient solver for asymmetric matrices (PBiCG) with diagonal incomplete (DILU) preconditioner is used for the rest of variables. Second order accurate numerical schemes (both central differencing and upwind) must be used at least in order to avoid problems with false diffusion.

1.10.1.7 Computational grid

The external domain (i.e. inlet, outlet, ground, sky and sides) is implemented using the conventional blockMesh application of OpenFOAM with a grading of 4 in vertical direction. The buildings geometry, previously designed with a CAD tool and saved in STL format, is embedded into the external mesh using the snappyHexMesh application. The snappyHexMesh application is an adaptative refinement meshing utility of OpenFOAM very appropriate to mesh complex geometries, such as buildings with different shapes from stereo-lithography (STL) CAD files.
Depending on the case complexity, total number of cells was in the range 3-9M cells, having an averaged value of the non-dimensional wall distance of around y^+=300-400.

1.10.1.8 Boundary conditions

Boundary conditions imposed at each boundary of the domain. Nomenclature: C = calculated; fV = fixed value; iP = inlet profile; sl = slip; sP = symmetry plane; wF = wall function; zG = zero gradient.

	U	k	ε	ν_t	p
Inlet	iP	iP	iP	C	zG
Outlet	zG	zG	zG	C	fV zero
Ground	fV zero	kqRwF	epsilon wF	nutkrough wF	zG
Building	fV zero	kqR wF	epsilon wF	nutk wF	zG
Sky	sl	sl	sl	C	zG
Sides	sP	sP	sP	sP	sP

1.10.1.9 Time dependent turbulent inflow data assumptions

Steady-state is assumed.

[6] F. Toja-Silva et al. Roof region dependent wind potential assessment with different RANS turbulence models. Journal of Wind Engineering and Industrial Aerodynamics 142, 2015: 258-271.

1.10.1.10 Reynolds number

Reynolds number is in the order of $5 \cdot 10^4$ for the reduced-scale (wind tunnel) CFD simulations and 10^7 for full-scale building simulations. Scaling issues were found and analyzed in the investigations[7].

1.10.1.11 Conclusions

A value of turbulence intensity (TI) of 0.15 is used as a maximum admissible for the horizontal axis wind turbines (HAWT). On conventional buildings (prismatic shape), the most appropriate areas to install HAWT are above z/H=0.19 from the roof surface upstream and above z/H=0.31 downstream. Note that z and H corresponds to the height and the building height, respectively. It is recommended to incline the horizontal axis of the HAWT 5° downwards at the upstream region below z/H=0.31. Below these heights, the installation of a vertical axis wind turbine (VAWT) is more appropriate since it is not affected by the wind direction fluctuations and it resists better the velocity fluctuations of the wind. Additionally, the VAWT can be installed in horizontal position at the central-upstream region close to the roof surface, in order to take the most of the recirculation of the flow. After different incident wind analysis, we conclude that, in general, an HAWT can be placed above z/H=0.31 anywhere at the roof, regardless of the incident wind direction.[8]

The results of the building edge roof shape analysis show a similar behavior of the flow over a simple edge and a cantilever edge. With a railing edge, a massive recirculation of the flow that exceeding the roof length is observed, and the height of the TI threshold of TI=0.15 increases. On the curved edge, there is a very small recirculation of the flow on the roof, a speed-up is observed around the upstream edge, and the TI threshold height substantially decreases.[9]

An optimum building-roof shape for the wind energy exploitation necessarily passes by the use of curved shapes. Specifically, the curved roof shape that shows the best performance is the spherical roof shape, leading to velocity (U) speed-up and TI decrease. The transition between walls and roof has a strong influence on the behavior of the flow. The optimum building roof shape obtained is a spherical roof coupled with a cylindrical wall. Both U and turbulent kinetic energy (k) are strongly affected by the presence of surrounding buildings. The TI threshold for HAWT is reached close to the roof surface in all cases with surrounding buildings. Therefore, VAWT may be considered close to the roof surface although HAWT can be installed at a higher height (z/h=1.05-1.15). Slender shapes (low aspect ratio, AR) are confirmed as the most interesting building shapes for the wind energy exploitation, leading to a higher speed-up and to a lower TI. Since the wind power is proportional to the cube of the wind speed, the available wind power increase due to the optimum building-roof shape reach maximum values close to 3 (the available wind power is multiplied by 3 compared with the open field) for the isolated building. The available wind power increase is higher for the slender shapes (AR = 1:1:4), and it is positive (concentration effect of the wind) for $h/H < 0.8$. Note that h and H correspond to the height of the target building and to the height of the surrounding buildings, respectively. As an example,

[7] F. Toja-Silva et al. Effect of roof-mounted solar panels on the wind energy exploitation on high-rise buildings. Journal of Wind Engineering and Industrial Aerodynamics 145, 2015: 123-138.

[8] F. Toja-Silva et al. Roof region dependent wind potential assessment with different RANS turbulence models. Journal of Wind Engineering and Industrial Aerodynamics 142, 2015: 258-271.

[9] F. Toja-Silva et al. On roof geometry for urban wind energy exploitation in high-rise buildings. Computation 3, 2015: 299-325.

the instantaneous power generation on the roof was evaluated for U_{ref} = 8.8 ms^{-1}, yielding 8 kW and 9.3 kW for VAWT and HAWT, respectively.[10]

1.10.2 CEDER rooftop test site wind measurement and analysis results

Test site and layouts

CEDER-CIEMAT rooftop test facility is located is an area that can be considered semi-urban. Next picture shows a description of the test site and its more important obstacles.

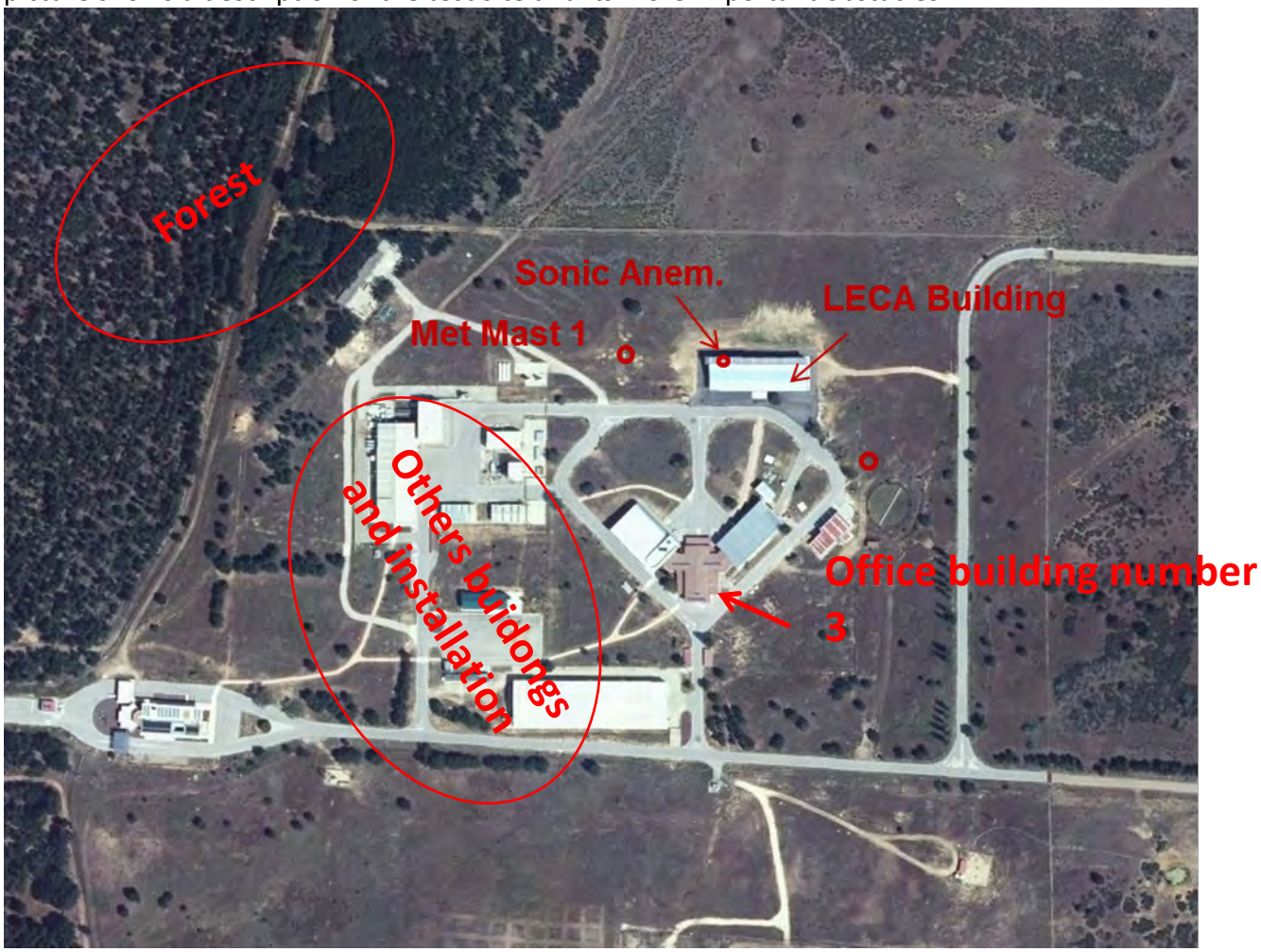

Figure XX CEDER Rooftop test site description.

The measurement in the rooftops has been carried out in two different building:

- LECA building

  The rooftop of this building has got an aerodynamic shape with a horizontal terrace in the north side of the building with the purpose of installing there several small wind turbines.

[10] F. Toja-Silva et al. An empirical-heuristic optimization of the building-roof geometry for urban wind energy exploitation on high-rise buildings. Applied Energy 164, 2016: 769-794.

The maximum height of this building is 11.40. The other dimensions are 20m (width) and 60 m (length). Over the rooftop a portable 4.8 m. met mast has been installed with a sonic anemometer in the top.

The met mast consists of 4 concrete pieces in the base, and three steel bars to joint them, forming an H-shaped structure. The mast is a tube with 4 wires to keep the mast safer and more static.

- Office building number 3

  The rooftop of this building is a gabled roof with lined tiles. The height of the highest point of it, where the met mast was installed, is 9 meters. There are also several PV modules installed on it in the south and west directions, that can be considered and an obstacle in several months.

The met mast is a 4.8 m height with a sonic anemometer in the top and a cross bar where two cup anemometers were installed. The purpose of these anemometers was to evaluate if it's possible to measure the vertical component of the wind without the use of sonic anemometers which commission is more expensive and difficult.

Besides these buildings met masts, a higher met mast has been installed in the west direction of the LECA building 55 m away from the anemometer in the building. The election of this distance is because there is a tree in this direction and it was need to have a non-perturbed wind in this tower.
The tower height is 23.5 m and several devices have been installed in it.

DAS commissioning.
The equipment used is:

- 3 sonic anemometers Model GILL Wind Master. This 3-axis wind anemometer monitors wind speeds up to 50 m/s with a sample rate up to 32 Hz.

The height of each sonic anemometer is:

	LECA building	Office building number 3	23.5m Met mast
Height (m)	17.20	14.60	11.60

The 3-axis wind speed (U, V and W) were also obtained. The data were sent to a computer where specific software developed by the Gill Company was installed. Communication RS422 was used because of the distances. A RS422/RS485 from ABB was also used.

The installation of each anemometer was not carried out in the same moment. So the first installation was the sonic anemometer in LECA building that was installed in March of 2014.

The sonic anemometer in the 23.5 m met mast was installed in March of 2015. And the anemometer in office building number 3 was installed in July of 2017

The sampled rate of each one has been:

	LECA building	Office building number 3	23.5m Met mast
Sample rate (Hz)	20 (in the beginning) 1	10	20 (in the beginning) 1

- Cup anemometers

There are 2 cup anemometers in the 23.5 met mast. Next figure shows the heights of each one. Wind speed has been monitored with a National Instruments Compact Field Point devices and has saved in a computer thanks a software developed in Labview by CEDER researchers.

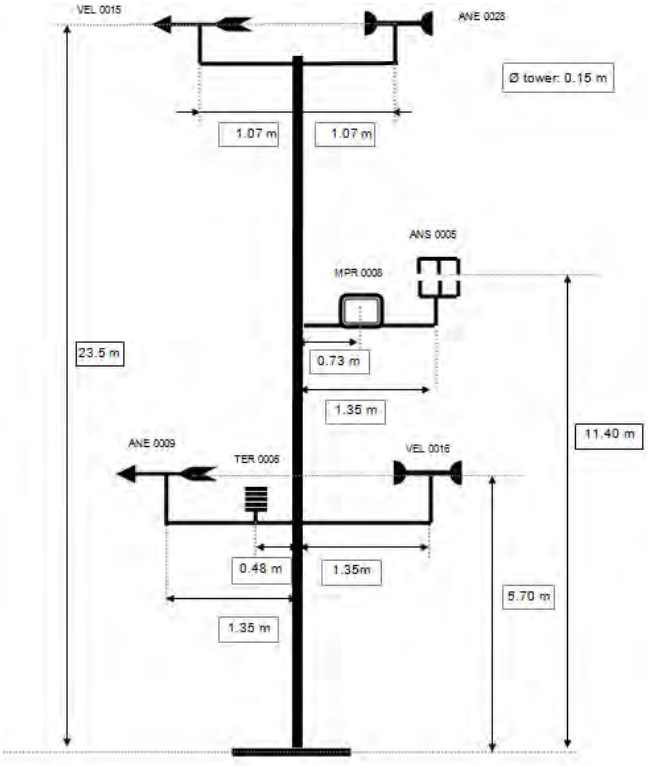

The manufacturer of these anemometers is SEAC a Spanish company and the model are SV5. Data was sampled at 1 Hz.

There also were 2 cup anemometers in the Office building number 3, in a cross bar at 0.6 m. below the sonic anemometer. Next pictures show that one of the anemometers is a horizontal position. This is because it's expected to measure the vertical component of wind speed making some study between vertical and horizontal plane instead of a sonic anemometer.

- Other sensors.

  Measurements of temperature, humidity and atmospheric pressure have been also monitored. They are located in the 23.5 met mast and the heights of each one are in a figure above. The sample rate of these measurements is 1 Hz.

Data analysis. TI and vertical component.

The first analysis CIEMAT researchers committed was an study of wind shear exponent α as a function of wind direction taking into account the values of 3 heights in 23.5 met mast. It was noticed that the variable is impotent just because another value in higher height should be used.

Obstacles	Section (º)		V_{ave} top (m/s)	V_{ave} under (m/s)	Wind shear exponent α
_	0	9	3.64	2.09	0.39
Tree	9	27	4.19	2.22	0.45
_	27	86	3.44	2.07	0.36
LECA Building	86	107	3.13	1.34	0.60
Buildings	107	257	3.23	1.75	0.43
Propane tanks	257	275	3.78	2.35	0.34
_	275	360	3.24	2.12	0.30

Later a comparison among the components u, v and w in the wind speed vector was carried out taking into account the 90º north, and west

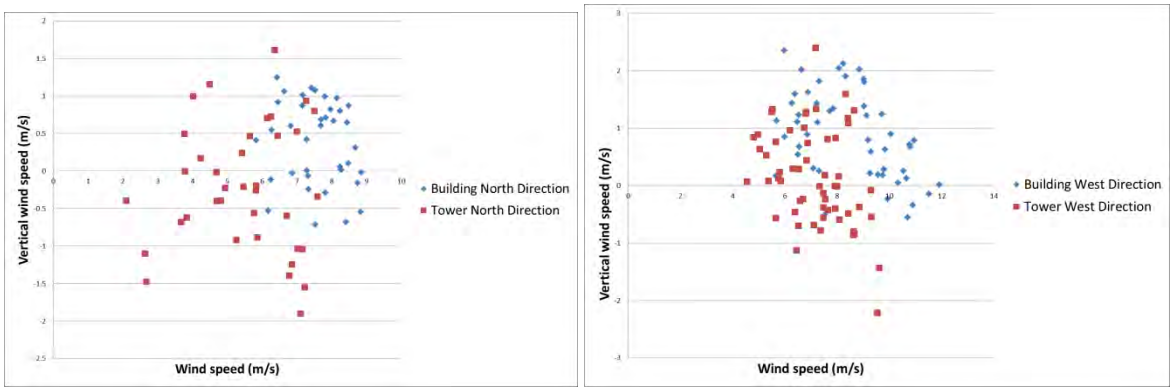

Figure XX Vertical wind speed in the building and the met mast tower in the north and west directions

The study of the correlation among then in the north direction and in the west direction was also carried out. It can be noticed than there is a significant variation in u and v. This is because of the tree that intercepts the north wind before the measurement in the tower.

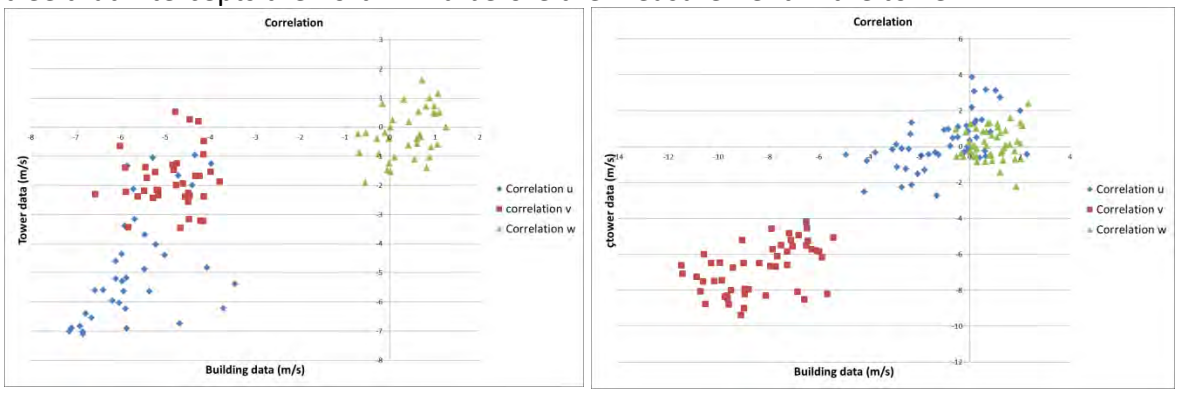

Figure XX Wind speed correlation between the building and the met mast tower in the north and west directions

A correlation between the vertical TI in the building and the tower was also committed.

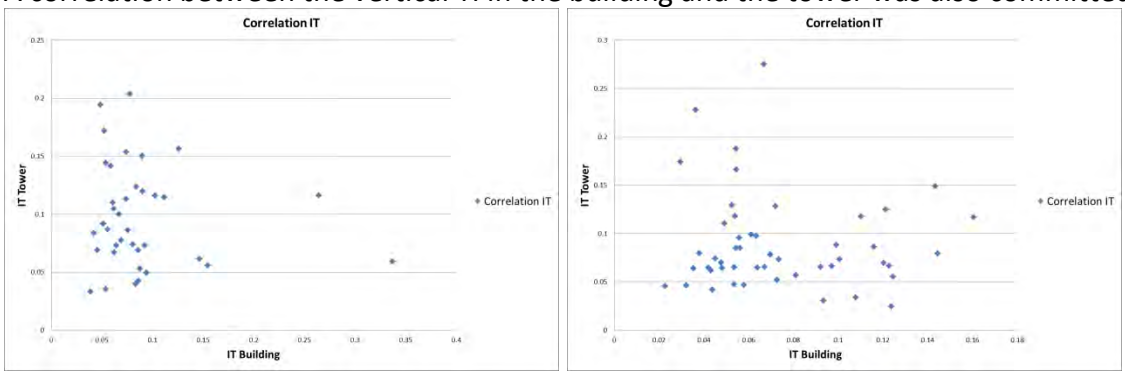

Figure XX Vertical TI comparison between the building and the met mast tower in the north and west directions

The easements carried out in the office number 3 were also split by direction. And the TI in each wind direction and component of wind speed are shown in the next graphs.

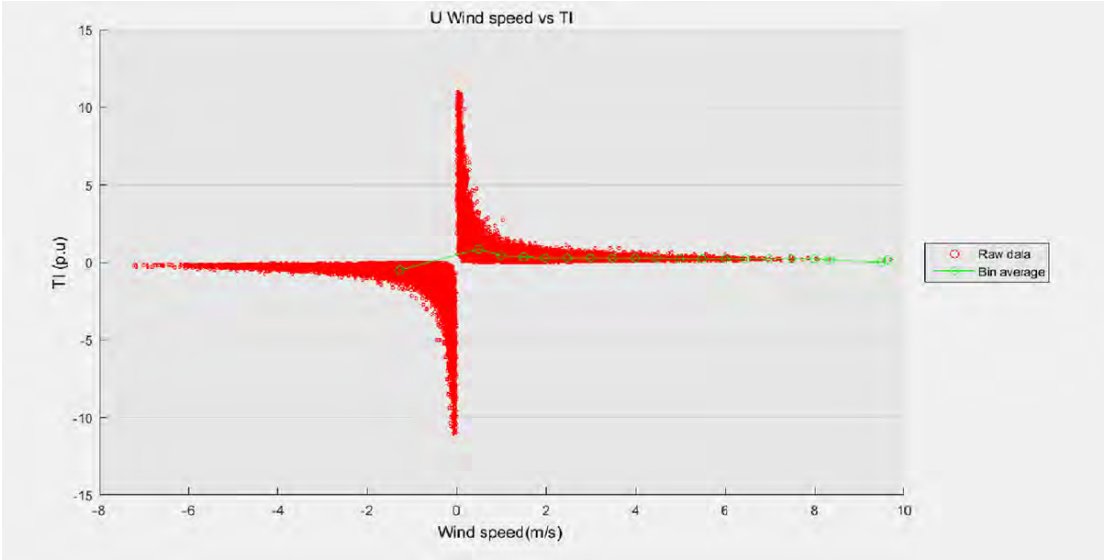

Figure XX TI vs U wind speed in the north -south directions

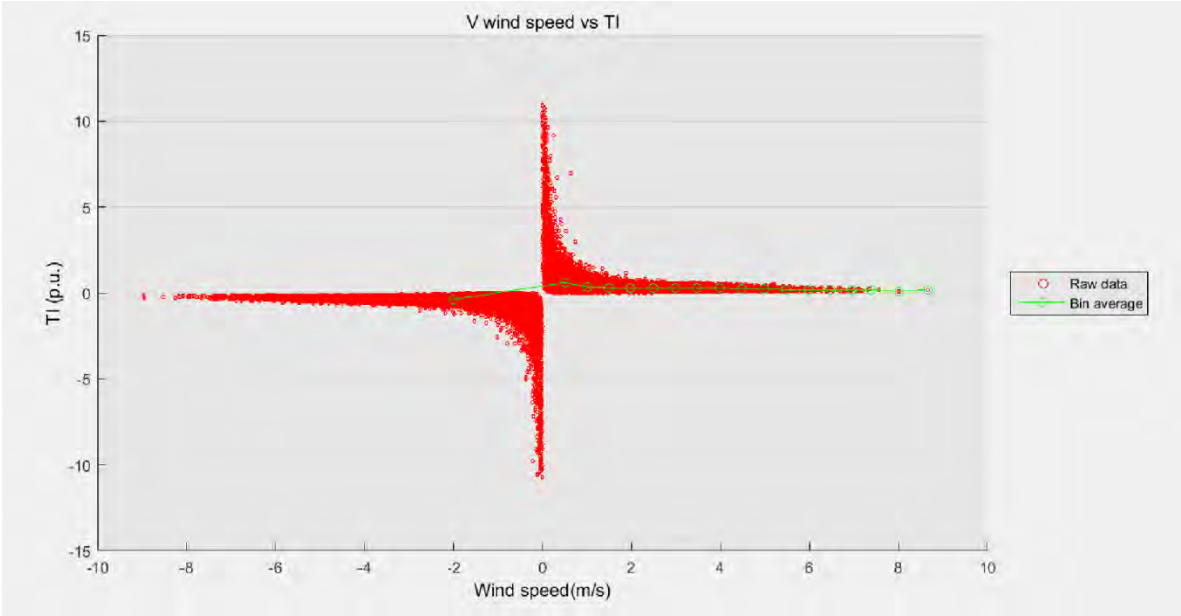

Figure XX TI vs V wind speed in the west-east directions

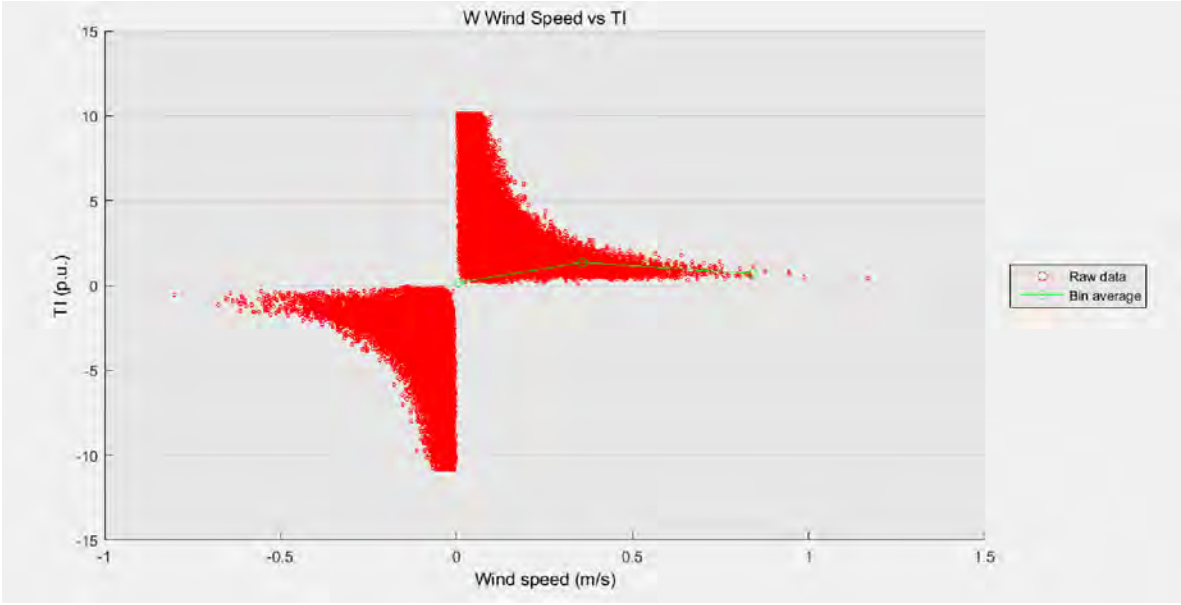

Figure XX TI vs W wind speed in the vertical direction

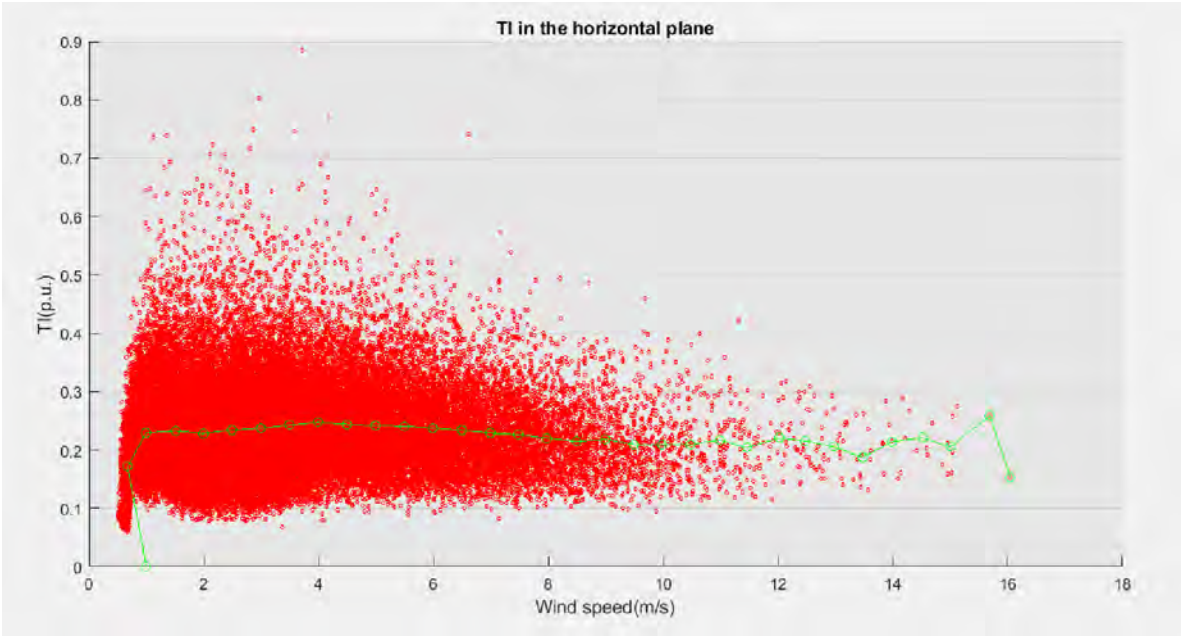

Figure XX TI vs horizontal wind speed

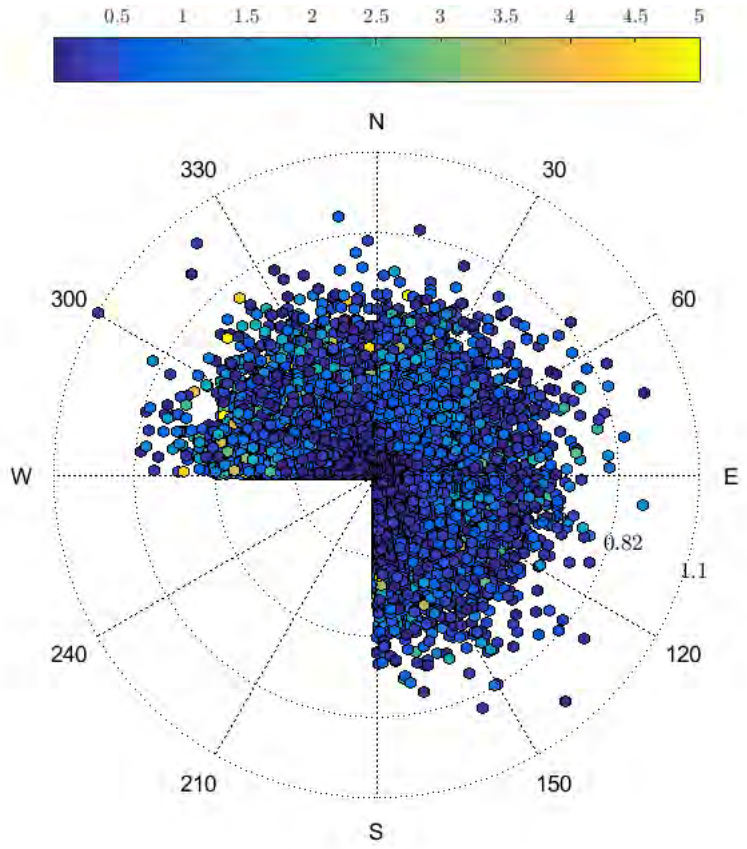

Figure XX TKE vs rose direction

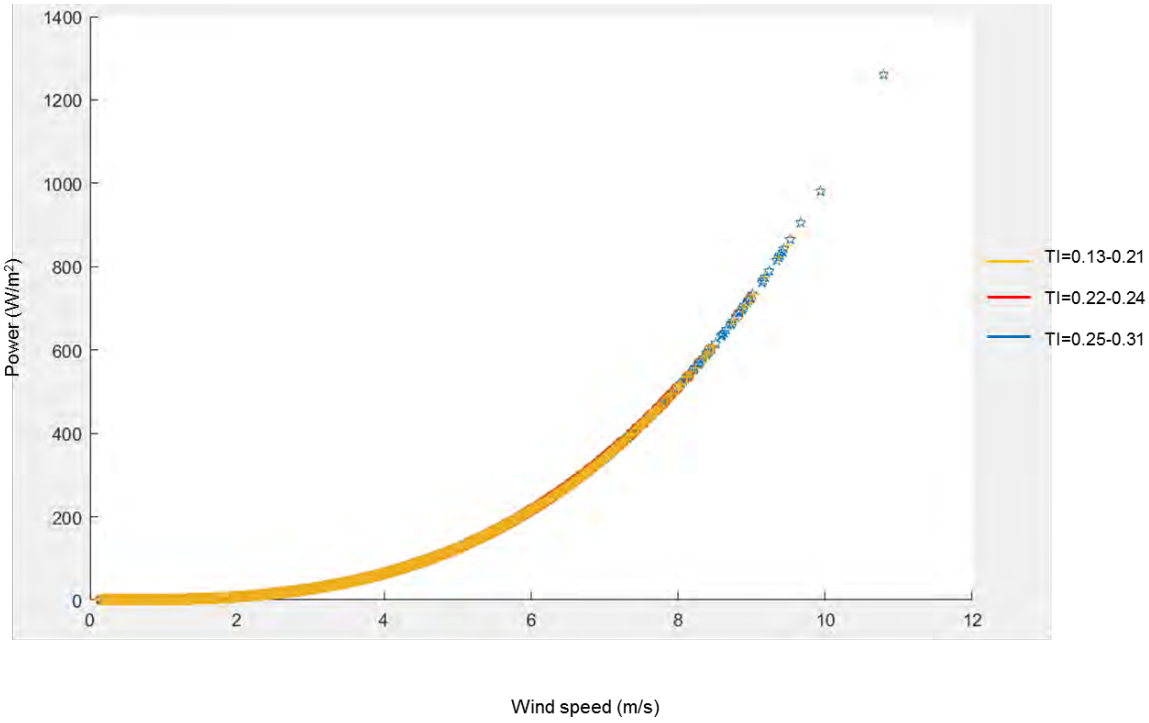

Figure XX Power vs horizontal wind speed

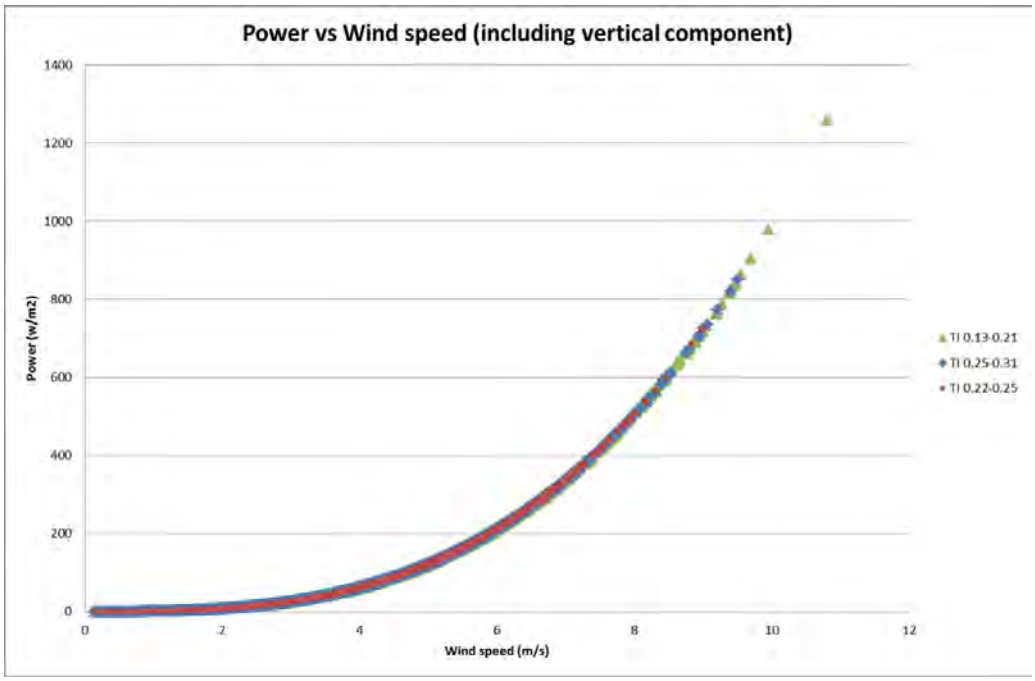

Figure XX Power vs wind speed (including vertical component)

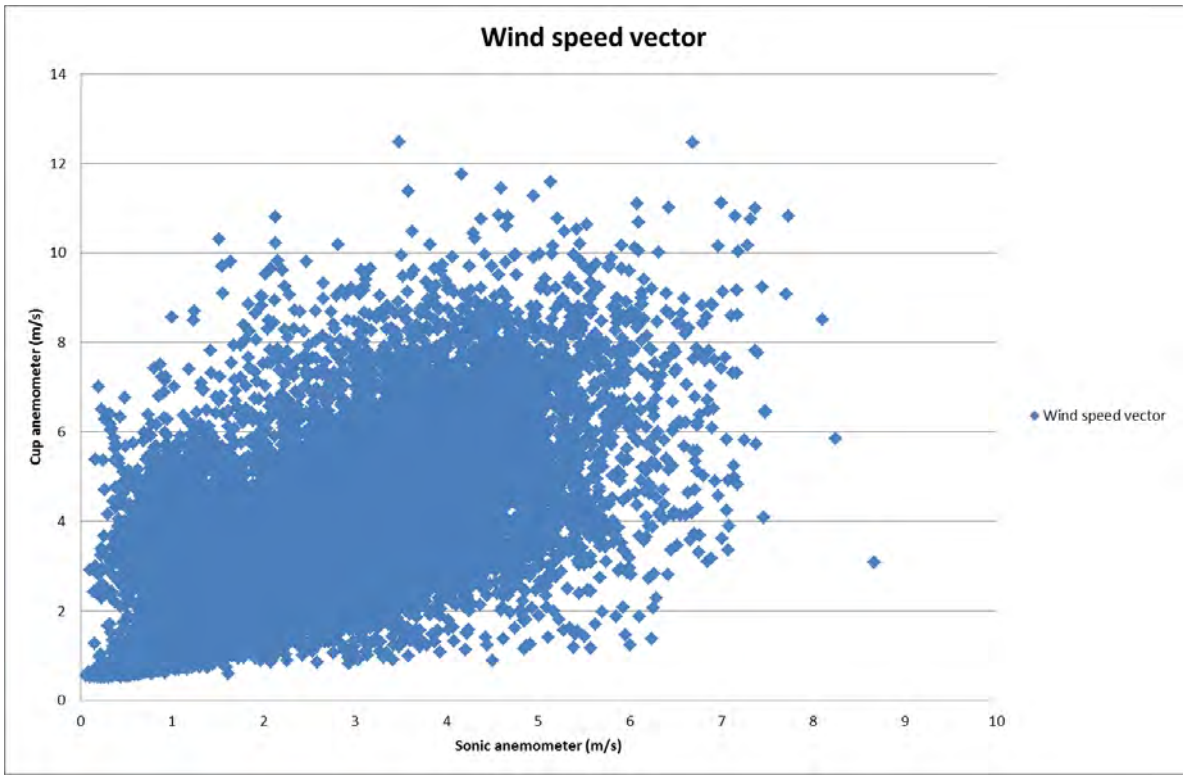

Figure XX Wind speed vector measure wit cup anemometer vs sonic anemometer

1.11 SWEDEN (active 2009-2011)

1.11.1 Forest data

Over a forest at 5m above treeline the I_5 is estimated to be 58%, which is higher than 5 m above a building. A ballpark figure places I_{15} in the range 25-30% for these kinds of non-open sites

These data are from a forest in Norunda Research Station (North of Uppsala) with a 102m met mast.

- Wind data from 33 m -complex air flow
- Wind data from 97 m –more uniform air flow
- Approximate mean tree top height = 28 m
- Ultrasonic measurements at 10Hz

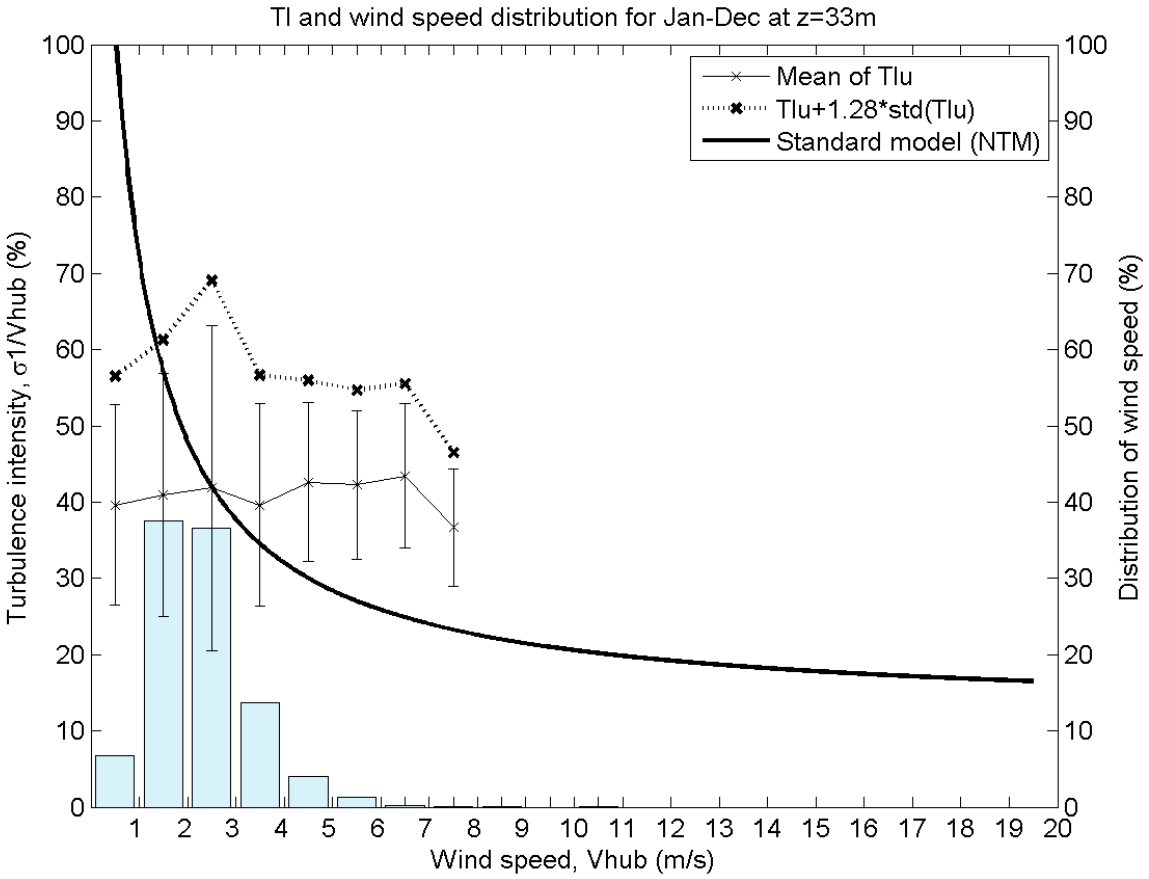

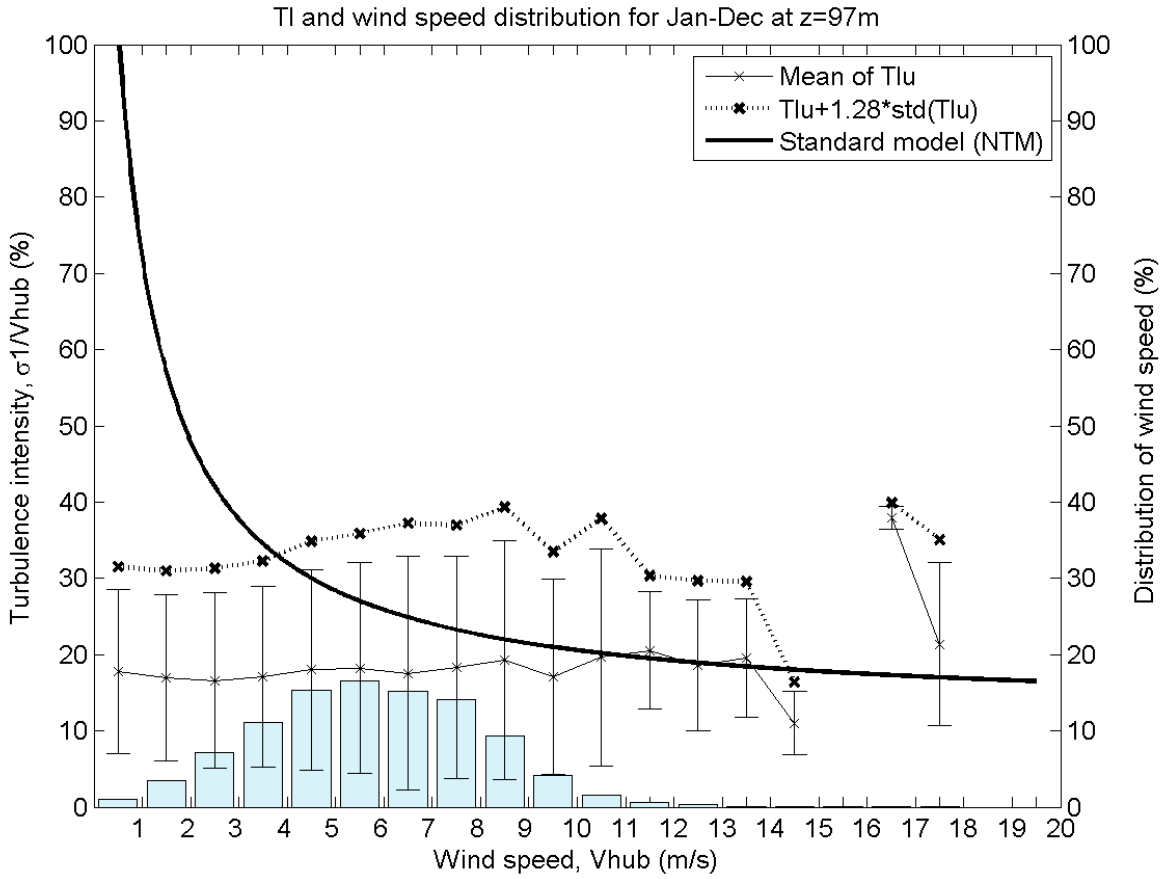

1.12 UNITED STATES (active 2009 – 2018)

1.12.1 Wind Resource Measurement Results – NASA Building 12

1.12.1.1 Overview

NASA has undertaken an improvement project for Building 12 at the Johnson Space Center, which includes technology pilot projects for green roof technology as well as building mounted wind turbine technology. These projects are meant to push understanding of building sustainability and provide education for the scientific community. The Building 12 wind turbines represent an opportunity for advancement of scientific knowledge in the area of urban wind energy. The Building 12 project was a collaboration between NASA, DOE, and the US National Renewable Energy Laboratory (NREL). The project focus is on a wind turbine performance assessment that runs from pre-construction through to operational turbine assessment as part of the building 12 improvement project.

The NASA building 12 project created a living laboratory for distributed wind technology (DWT) as part of the planned building 12 improvement project. NREL along with NASA created an experimental setup, which would mimic and test the standard industry wind project development process. This will help researchers to understand how to site wind turbines effectively in the urban environment as well as assess their performance and safety. Below is an outline of the project work packages:

1.12.1.2 Project Work Packages:

- Data Collection:
  - Phase I: Pre-construction Data Collection for Wind Resource Characterization and Assessment (March 2014 to November 2014)
    - Wind resource measurements
  - Phase II: Post-construction data collection
    - Turbine Performance (power & availability) assessment with wind measurements in parallel (December 2014 to present)
- Data analysis
  - Wind resource characterization (statistical summaries)
  - Power and availability characterization (statistical summaries)
- Reporting
  - Built Environment Lessons learned document
    - NASA Building 12
    - Additional case studies
- Project closeout and next steps
  - Data archival and dissemination

This report is limited to coverage of the Phase I data collection and data analysis.

1.12.1.3 SWT Site Characterization

NASA Building 12 is located in the middle of Johnson Space Center in Clear Lake, TX. It is located just to the southwest of Building 30 also known as mission control. The building is approximately 2 stories tall and is surrounded by taller buildings in most directions. The instrumentation is located on top of the building on the green roof. The building is located at: 29.557188°N, 95.088429°W.

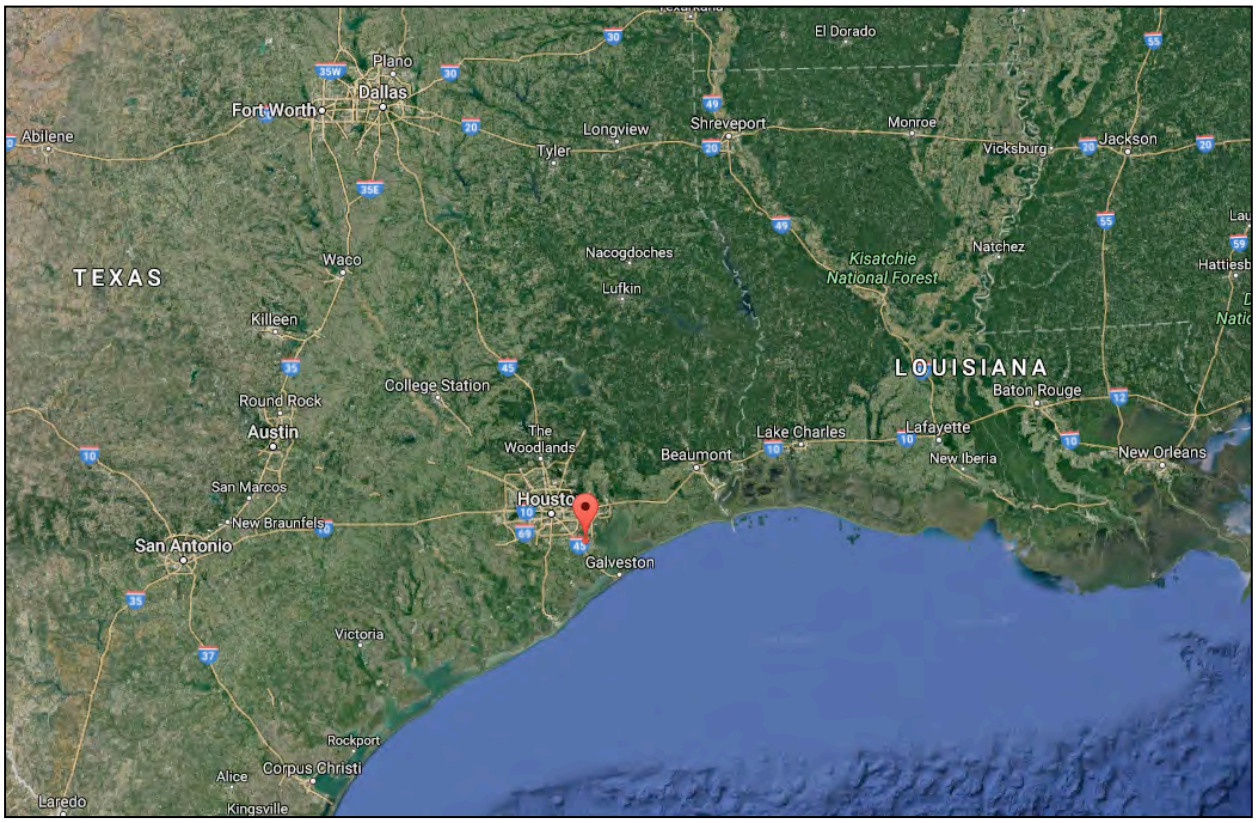

Figure 46: Regional Overview of Site (site shown by red balloon)

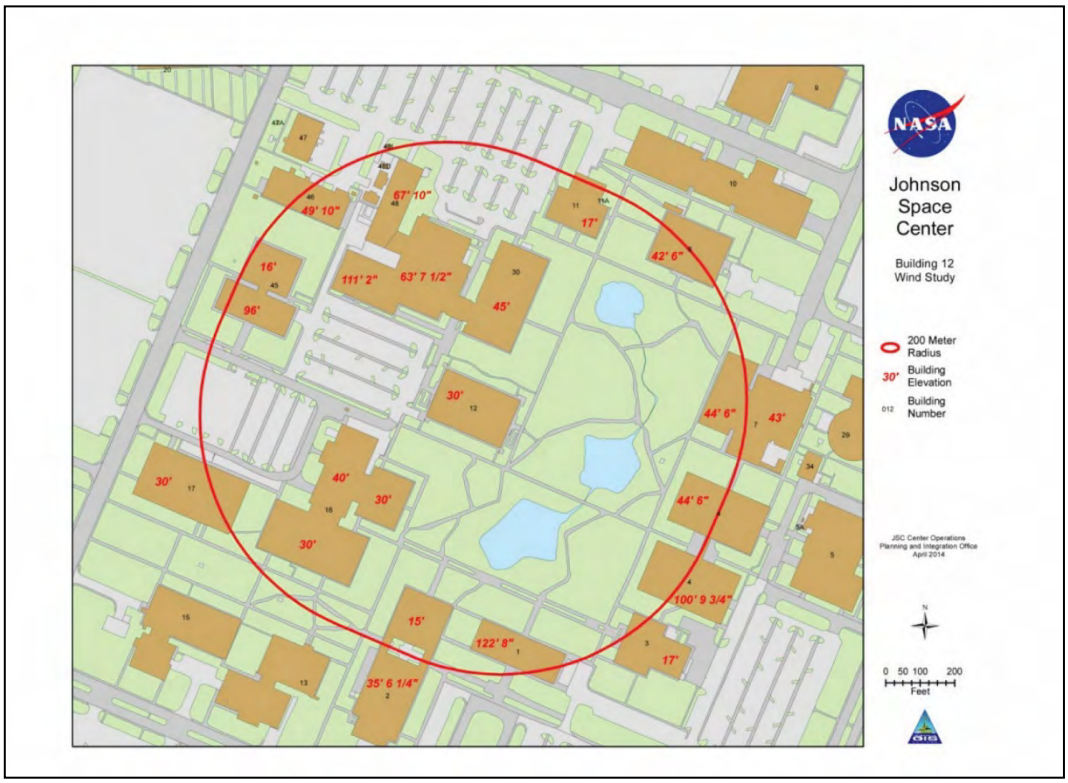

Figure 47: Aerial depiction of Building 12 and surroundings.

Figure 48: Trees surrounding Building 12.

Figure 14. Aerial satellite photo showing the layout of the NASA Building 12 project

1.12.1.4 Photos (360)

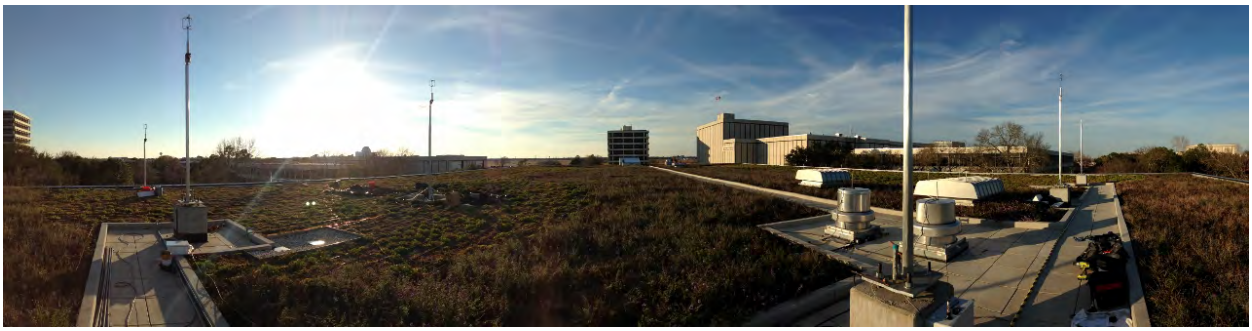

Figure 49: Wind Speeds 1-7 (Roof Panorama)

Figure 50: Wind Speeds 1-6 (Tower Panorama)

1.12.1.5 Wind Roses

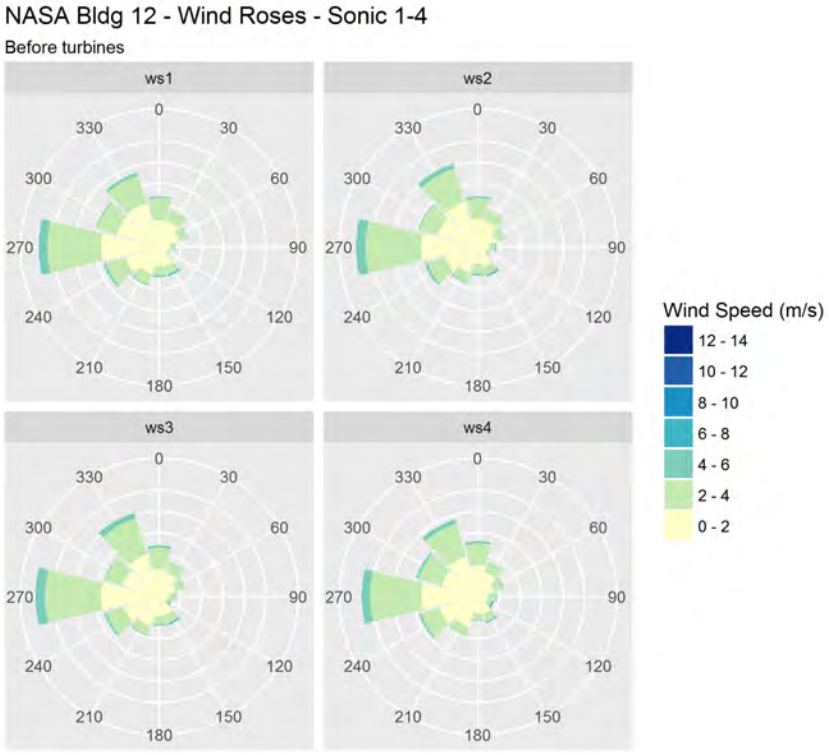

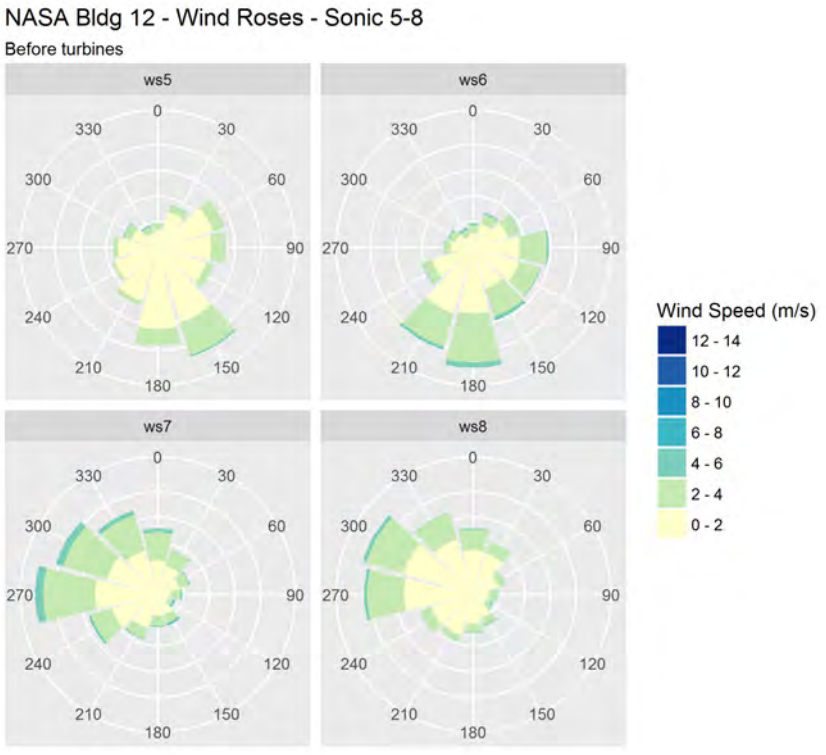

1.12.1.6 Energy Roses

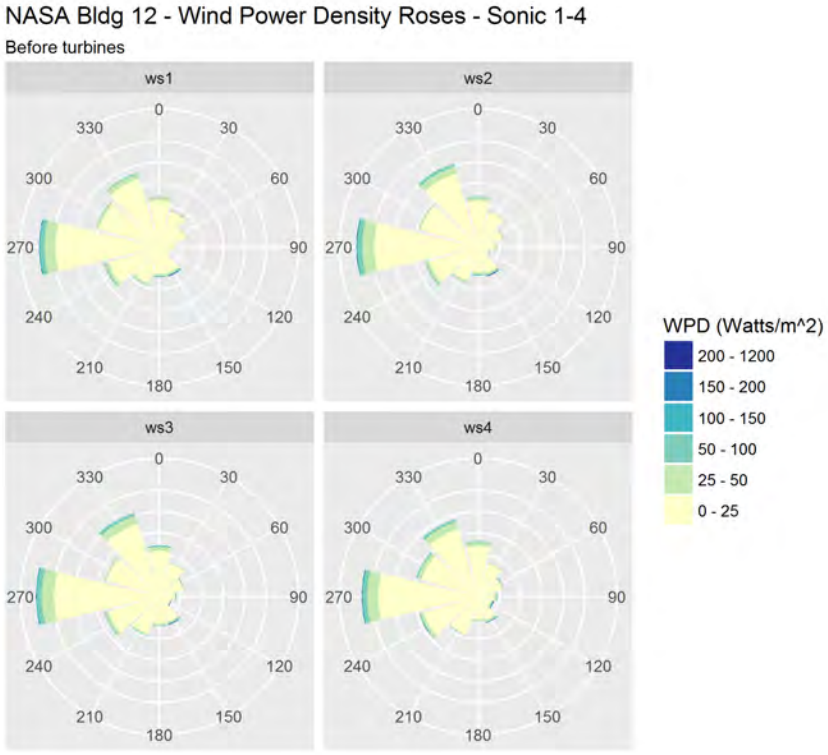

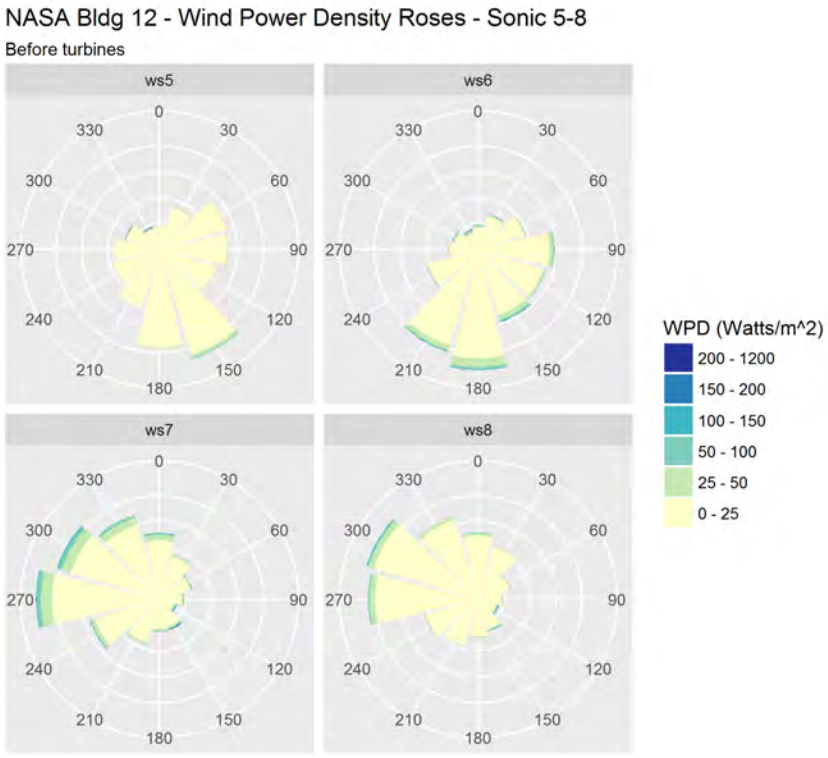

1.12.1.7 Wind speed frequency distribution

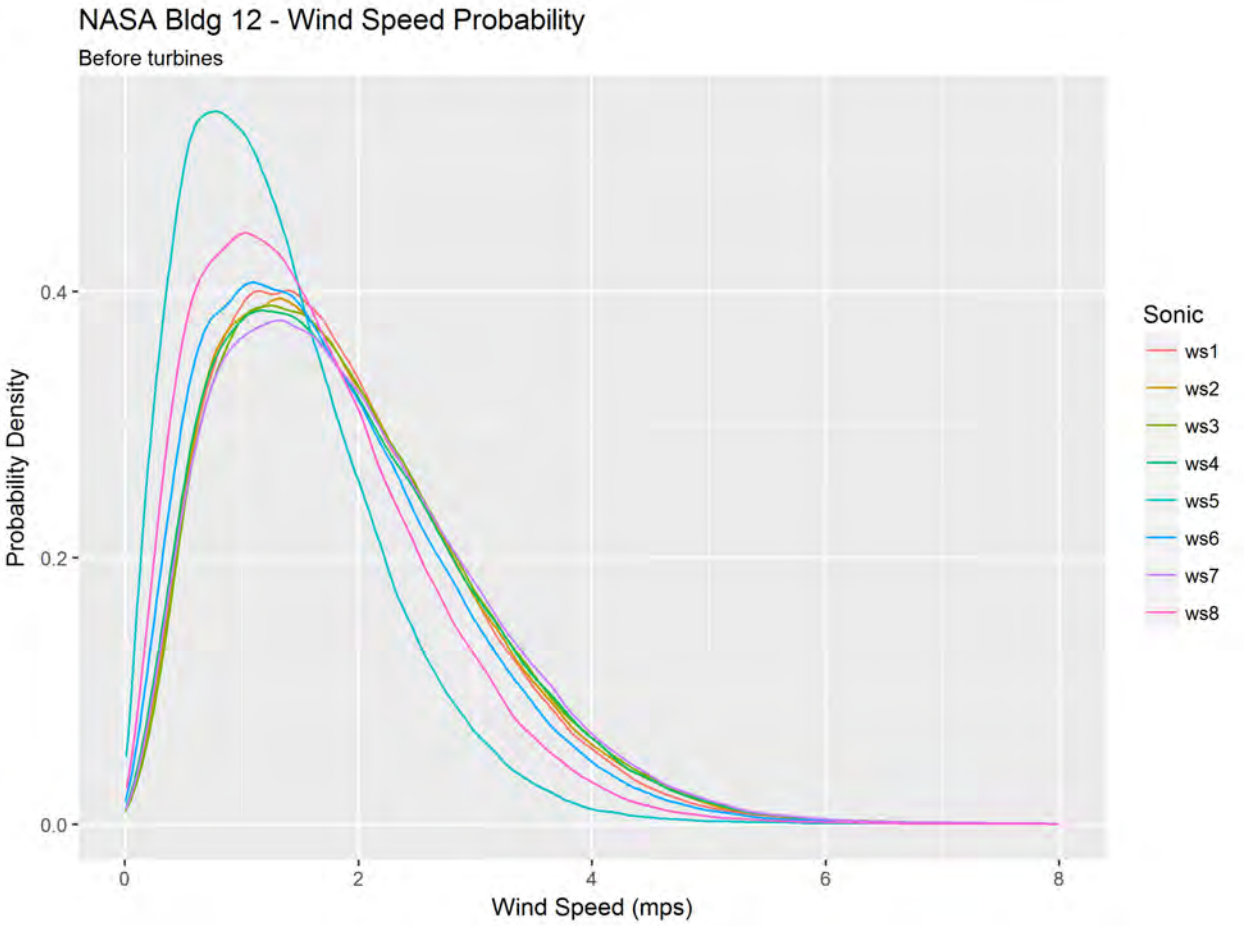

1.12.1.8 Off-site/reference wind measurement description

Two reference sites were found near to the project location. They were two local airports – Ellington Field and Clover Field. In Figure 52 and Figure 53 below, site 722427 refers to Clover Field Airport, site 722436 refers to Ellington Field Airport.

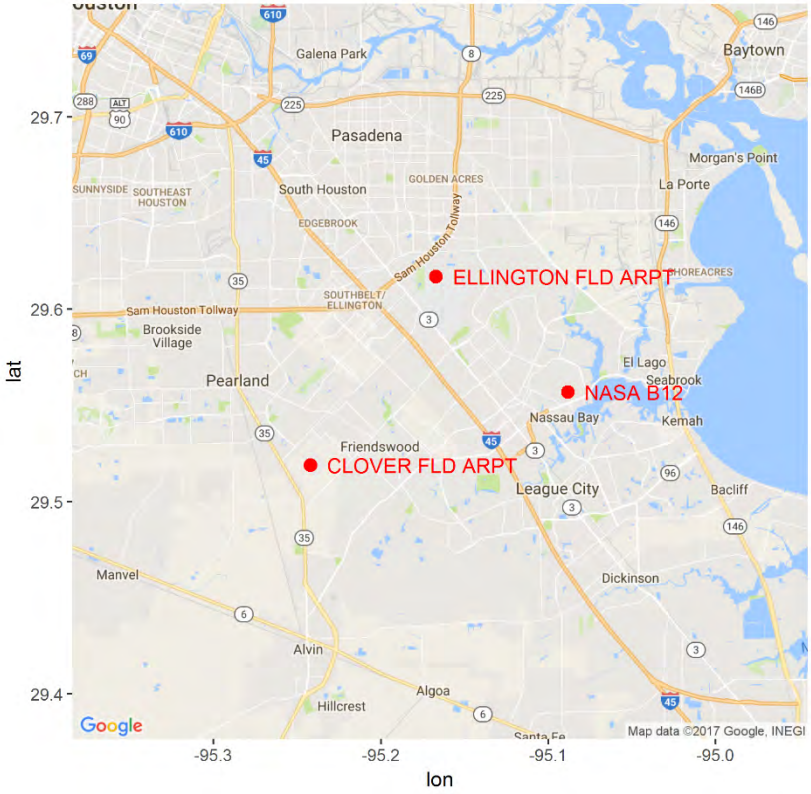

Figure 51: Map of offsite long-term reference sites.

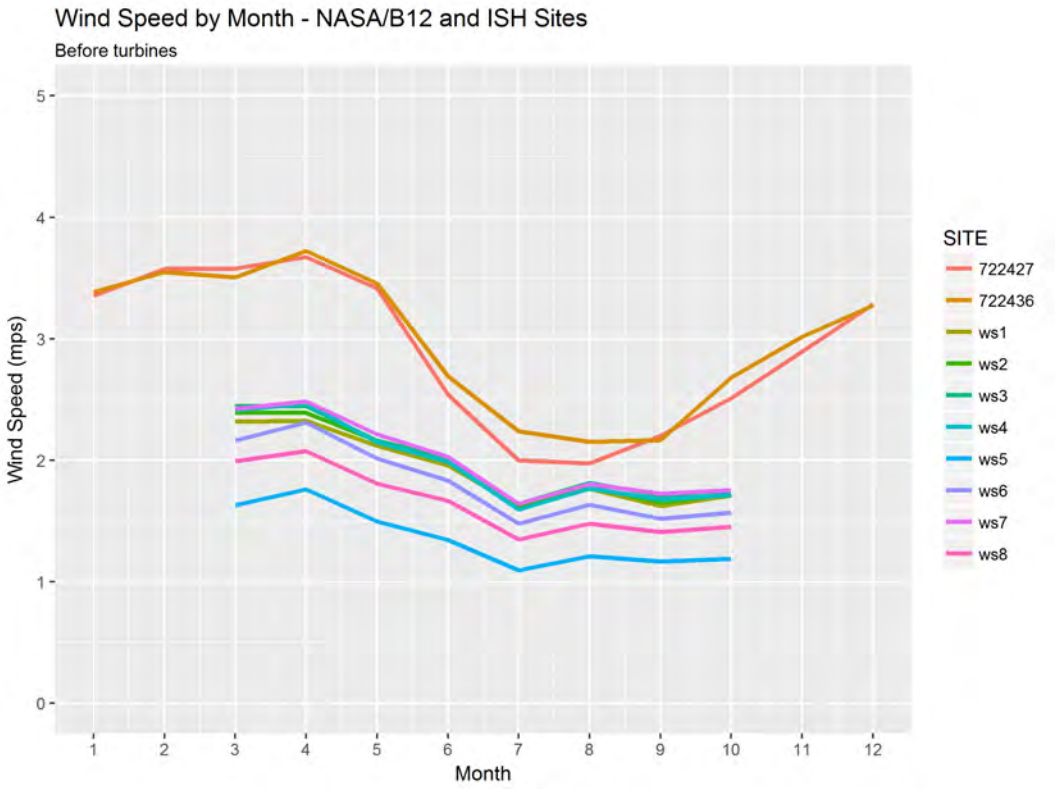

Figure 52: Wind Speed by Month for Reference Airport Weather Stations and Sonic Anemometers

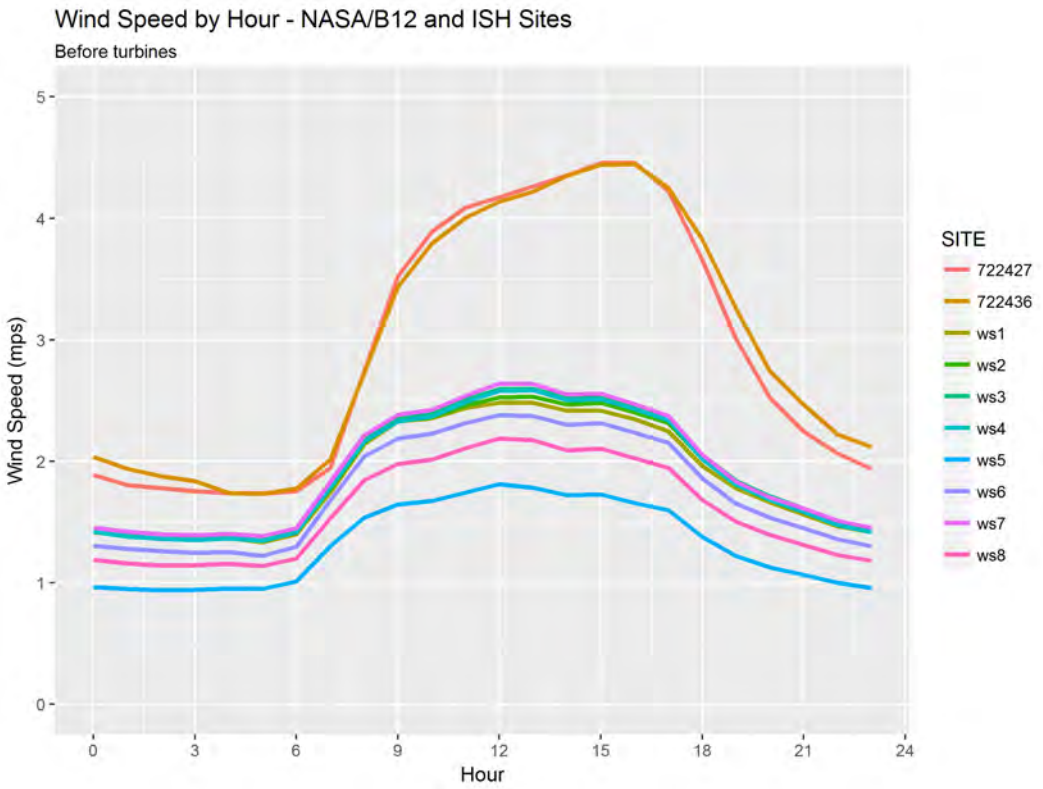

Figure 53: Wind Speed by Hour for Reference Airport Weather Stations and Sonic Anemometers

1.12.1.9 Data Acquisition Approach

The data acquisition system was designed to capture high frequency wind and atmospheric measurements. This data is envisioned to help test the hypothesis that rooftop deployments experience higher turbulence and potentially more damaging winds. At the time of this experiment there was a dearth of empirical measurements for building mounted wind turbines. These measurements will help us to understand the characteristics of built environment deployments.

The measurements for phase 1 of the NASA Building 12 deployment were placed on the rooftop to test the exact locations for future wind turbines but also to test the spatial variability of the resource. WS1 through WS4 were placed on the turbine pad mounts to measure wind speed at the future turbine locations. WS5 and WS6 were leading edge measurements of the building itself. WS7 and WS8 measurements were placed on a stand-alone tower to measure the effects of wind shear as well as horizontal spatial variability. You can find detailed instrument details and measurements heights in Table 1 below.

Figure 54: Wind speeds 1 & 2 (wind speeds 3 & 4 are similarly installed)

Figure 55: Wind speeds 5 & 6

Figure 56: Wind speeds 7 & 8

1.12.1.10 Instrumentation

Table 6 details the type of wind speed instruments used, height they were installed (above the roof), and sampling rate, and Table 7 details other instruments used, including: temperature, pressure, wind direction, humidity. All measurements were collected during an 8-month onsite resource assessment campaign conducted between February 21, 2014 through October 31, 2014.

Table 6: NASA Building 12 Wind Speed Instruments

Instrument	Type	Model	Height (m above roof)	Sampling Rate
Wind speed 1-4	3-D sonic	Gill WindMaster 1590-PK-020	4.572	20Hz
Wind speed 5	3-D sonic	Gill WindMaster 1590-PK-020	0 (roof leading edge)	20Hz
Wind speed 6	3-D sonic	Gill WindMaster 1590-PK-020	3.048	20Hz
Wind speed 7	3-D sonic	Gill WindMaster 1590-PK-020	4.724	20Hz
Wind speed 8	3-D sonic	Gill WindMaster 1590-PK-020	1.981	20Hz

Table 7: NASA Building 12 Resource Measurement Instrumentation

Instrument	Type	Model	Height (m above roof)	Record Rate
MetPak	2-D sonic, Temp, BP, RH, Dewpoint	Gill MetPak	1.676	15 min
Solar irradiance	Pyronometer	LiCOR LI200	1.448	15 min
Photosynthetically active radiation	Quantum PAR	LiCOR LI190	1.448	15 min
Rain Gage	Tipping bucket	TE525-L25		

1.12.1.11 Dataloggers:

- Campbell Scientific CR3000 and CR1000
- 4G-LTE cellular modem

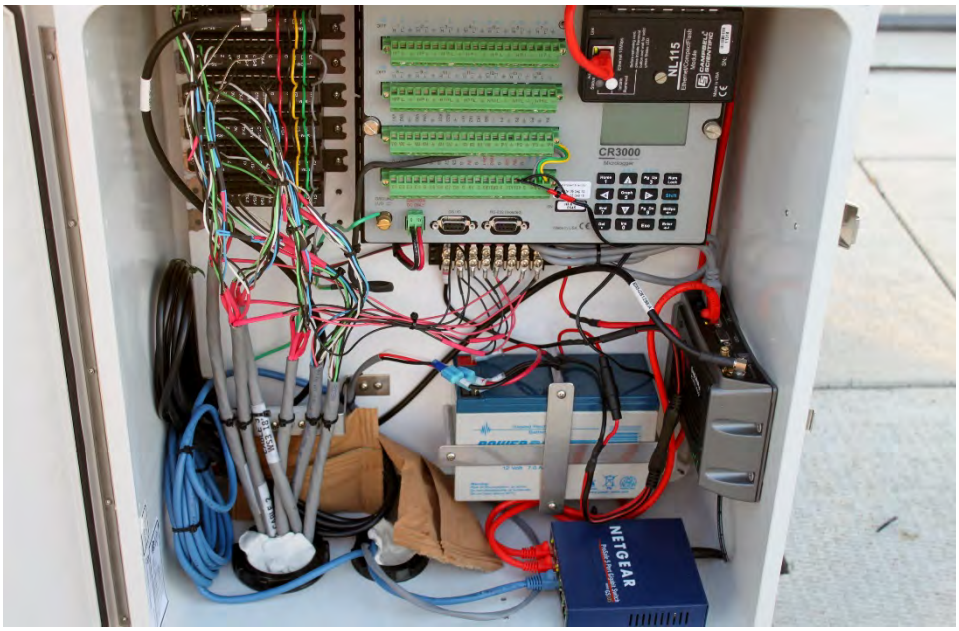

Figure 57: CR3000 Datalogger

Measurement location

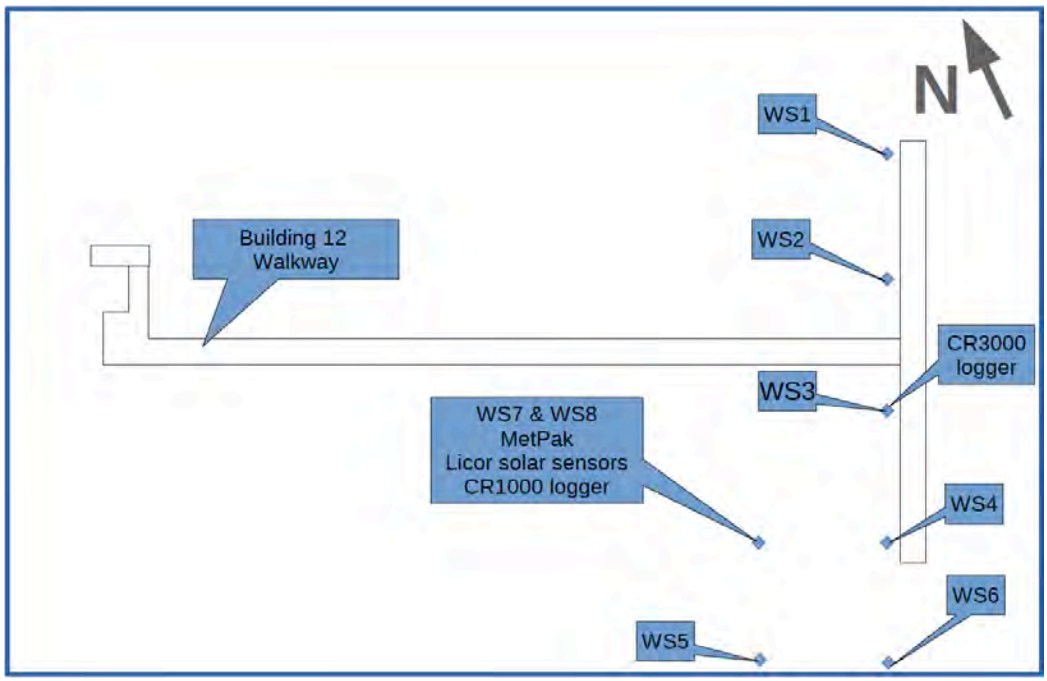

Figure 58: Schematic of instrument locations (not drawn to scale).

Sonics 1 through 4 are located on the turbine pads, 5 is on a boom hanging over the edge of the roof, 6 is on a tower at the edge of the roof, and 7 and 8 are on a small met tower.

1.12.1.12 Duration and results of data collection efforts

1.12.1.12.1 u*, Richardson Number

The fluctuating structural loads created by turbulent flow across the turbine rotor blades are one of the most important sources of both cyclic and impulsive stresses in the mechanical components of the turbine. A combination of cyclic stresses and random occurring, short period impulsive loadings cumulatively induce component fatigue damage that continues to increase

until failure. Short period, impulsive stress loads are particularly damaging and conditions which induce them must be included in any certification testing procedure.
20 Hz u and v components are averaged over one second intervals, and a resultant WS is computed for each second. Then 600 wind speed and temperature values are used to compute u* and Richardson number (Ri) for each 10-minute interval, where the temperatures are in Kelvins.

$$u* = 0.4\frac{[(U2 - U1)]}{\ln(z2/z1)}$$

$$Ri = \frac{9.8 \cdot [\bar{T}2 - \bar{T}1] \cdot (z2 - z1)}{0.5 \cdot [\bar{T}2 + \bar{T}1] \cdot (\bar{U}2 - \bar{U}1)2}$$

Samples

		Stability (class, Ri range)					
		STC01	STC02	STC03	STC04	STC05	STC06
WS (class, range)		(-20,-1)	(-1,0.01)	(0.01,0.05)	(0.05,0.1)	(0.1,0.25)	(0.25,20)
WSC00	(-1,1)	1434	357	17	14	75	2112
WSC01	(1,3)	3237	3179	182	176	673	10009
WSC02	(3,5)	459	1522	89	123	518	2146
WSC03	(5,7)	4	98	2	12	21	5
WSC04	(7,9)	0	20	0	0	0	0
WSC05	(9,11)	0	0	0	0	0	0
WSC06	(11,13)	0	0	0	0	0	0
WSC07	(13,15)	0	0	0	0	0	0
WSC08	(15,17)	0	0	0	0	0	0
WSC09	(17,99)	0	0	0	0	0	0

u*

		Stability (class, Ri range)					
		STC01	STC02	STC03	STC04	STC05	STC06
WS (class, range)		(-20,-1)	(-1,0.01)	(0.01,0.05)	(0.05,0.1)	(0.1,0.25)	(0.25,20)
WSC00	(-1,1)	0.02	0.03	0.04	0.03	0.03	0.03
WSC01	(1,3)	0.04	0.06	0.06	0.06	0.06	0.05
WSC02	(3,5)	0.07	0.1	0.1	0.11	0.1	0.09
WSC03	(5,7)	0.1	0.14	0.12	0.16	0.15	0.07
WSC04	(7,9)	NA	0.19	NA	NA	NA	NA
WSC05-09	(9,99)	NA	NA	NA	NA	NA	NA

Ri number		STC01 (-20,-1)	STC02 (-1,0.01)	STC03 (0.01,0.05)	STC04 (0.05,0.1)	STC05 (0.1,0.25)	STC06 (0.25,20)
WSC00	(-1,1)	-8.22	-0.47	0.03	0.07	0.17	3.84
WSC01	(1,3)	-3.21	-0.42	0.03	0.07	0.18	1.54
WSC02	(3,5)	-1.72	-0.36	0.03	0.08	0.18	0.6
WSC03	(5,7)	-1.2	-0.22	0.04	0.08	0.14	0.6
WSC04	(7,9)	NA	-0.08	NA	NA	NA	NA
WSC05-09	(9,99)	NA	NA	NA	NA	NA	NA

1.12.1.13 Data processing strategy, quality assurance methods

For the met data, simple data processing strategies were used to clean data that was obviously false such as flat line periods of data where the signal was likely non-reporting.

Data processing for the u* and Richardson numbers was more complex. Samples where the two sonic wind speeds are very close may have very large values of Ri. Large negative values of Ri are caused by negative temperature differences (t2 < t1) and small wind speed differences. Large positive values of Ri are caused by positive temperature differences (t2 > t1) and small wind speed differences. For convenience, we set these Ri values to ± 20. Negative u* values occur when the lower speed is greater than the upper speed, which happens in 151 records. Sonic anemometer 7 has many records where the U component is exactly 3.00 or 7.00 and the V component is usually NaN. If we find more than 400 such values in a 10-minute record, we remove it.

1.12.1.14 Conclusion of results

Plots of TI

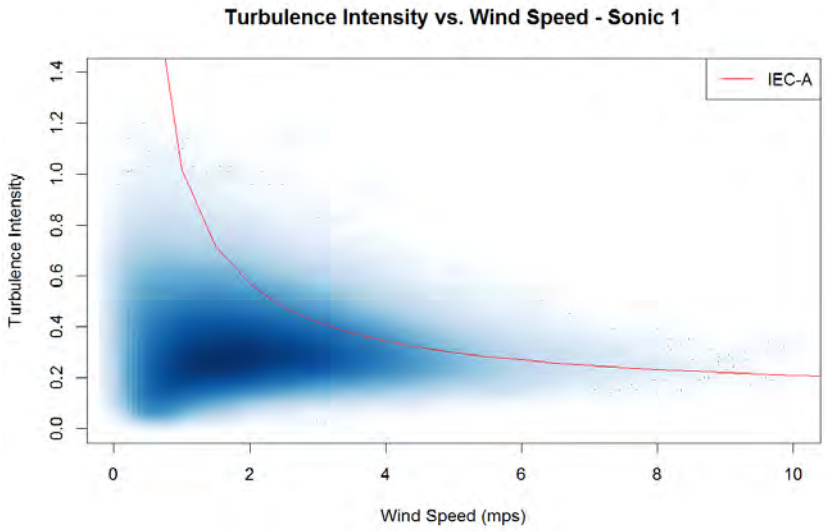

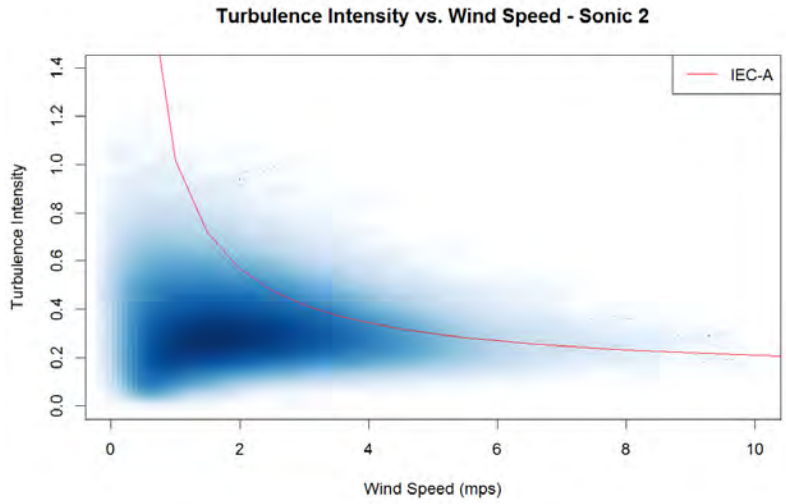
Turbulence Intensity vs. Wind Speed - Sonic 2
IEC-A
Turbulence Intensity
0.0
0.2
0.4
0.6
0.8
1.0
1.2
1.4
0
2
4
6
8
10
Wind Speed (mps)

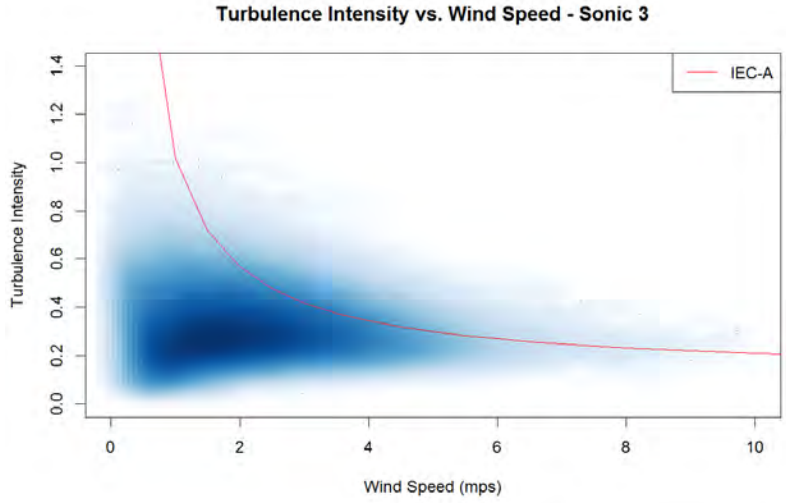
Turbulence Intensity vs. Wind Speed - Sonic 3
IEC-A
Turbulence Intensity
0.0
0.2
0.4
0.6
0.8
1.0
1.2
1.4
0
2
4
6
8
10
Wind Speed (mps)

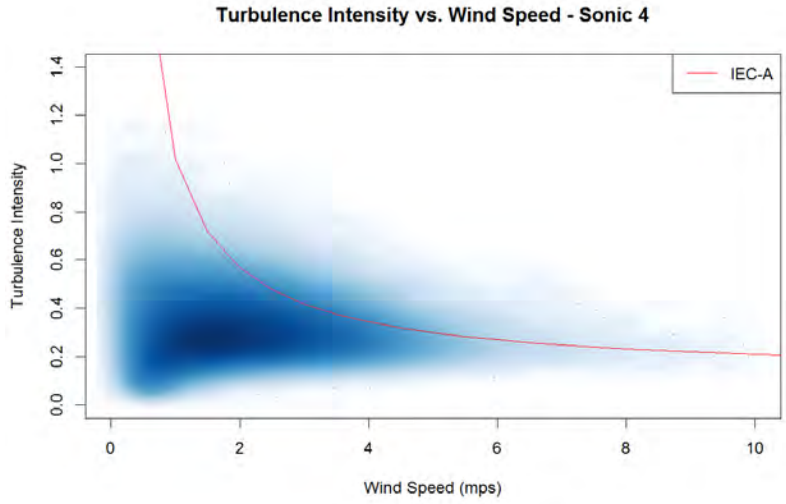
Turbulence Intensity vs. Wind Speed - Sonic 4
IEC-A
Turbulence Intensity
0.0
0.2
0.4
0.6
0.8
1.0
1.2
1.4
0
2
4
6
8
10
Wind Speed (mps)

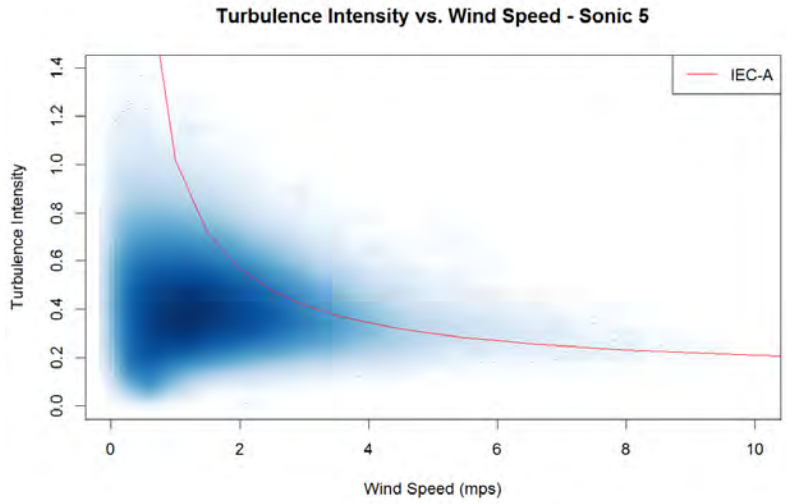
Turbulence Intensity vs. Wind Speed - Sonic 5
IEC-A
Turbulence Intensity
0.0
0.2
0.4
0.6
0.8
1.0
1.2
1.4
0
2
4
6
8
10
Wind Speed (mps)

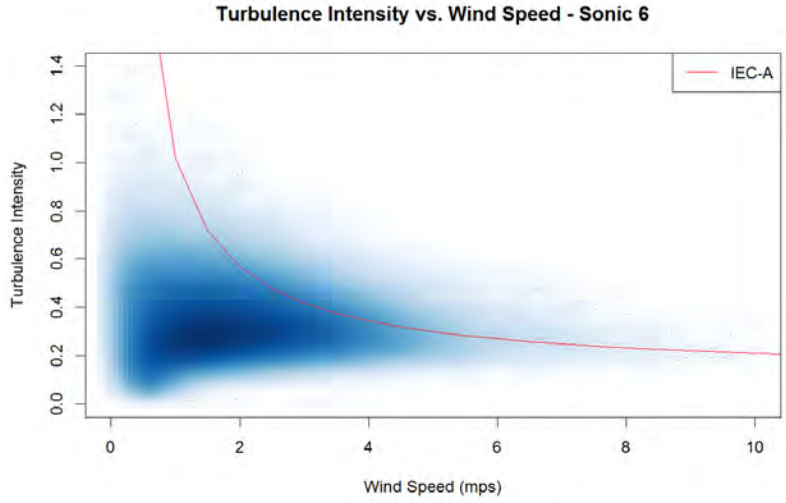
Turbulence Intensity vs. Wind Speed - Sonic 6
IEC-A
Turbulence Intensity
0.0
0.2
0.4
0.6
0.8
1.0
1.2
1.4
0
2
4
6
8
10
Wind Speed (mps)

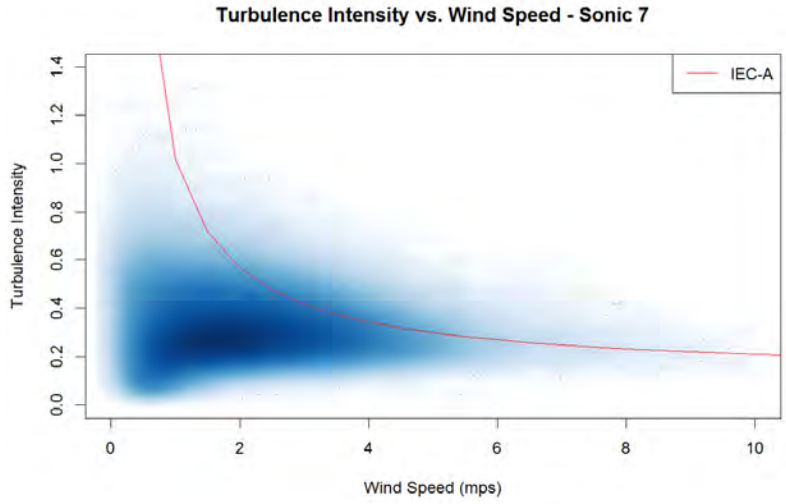
Turbulence Intensity vs. Wind Speed - Sonic 7
IEC-A
Turbulence Intensity
0.0
0.2
0.4
0.6
0.8
1.0
1.2
1.4
0
2
4
6
8
10
Wind Speed (mps)

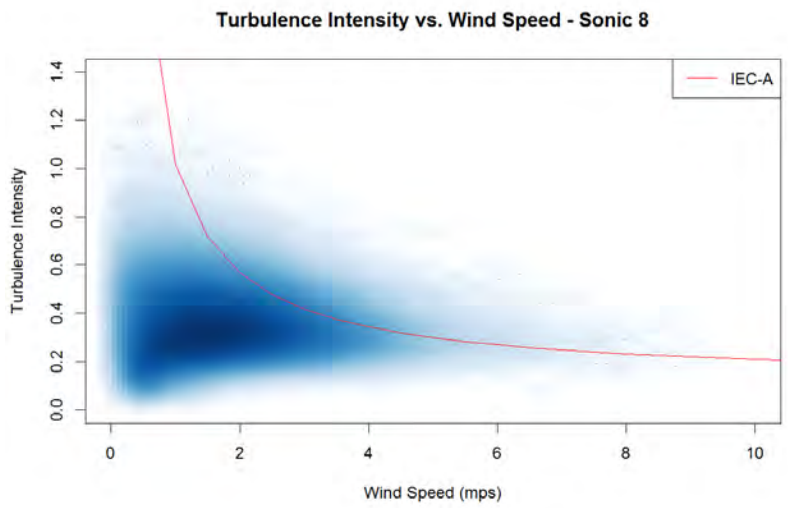

1.12.1.15 Wind resource characterization

Table 8: 8-month average wind speed and maximum 3 second gust

Sensor	WS1	WS2	WS3	WS4	WS5	WS6	WS7	WS8
WS (m/s)	1.871	1.901	1.932	1.905	1.321	1.761	1.946	1.603
3-s gust	n/a	n/a	n/a	n/a	n/a	n/a	n/a	n/a

Table 9: 8-month average wind speed and maximum 3 second gust for off-site reference towers

Sensor	Ellington Field	Clover Field
WS (m/s)	2.92	3.07
3-s gust	n/a	n/a

1.12.1.15.1 Monthly wind speed

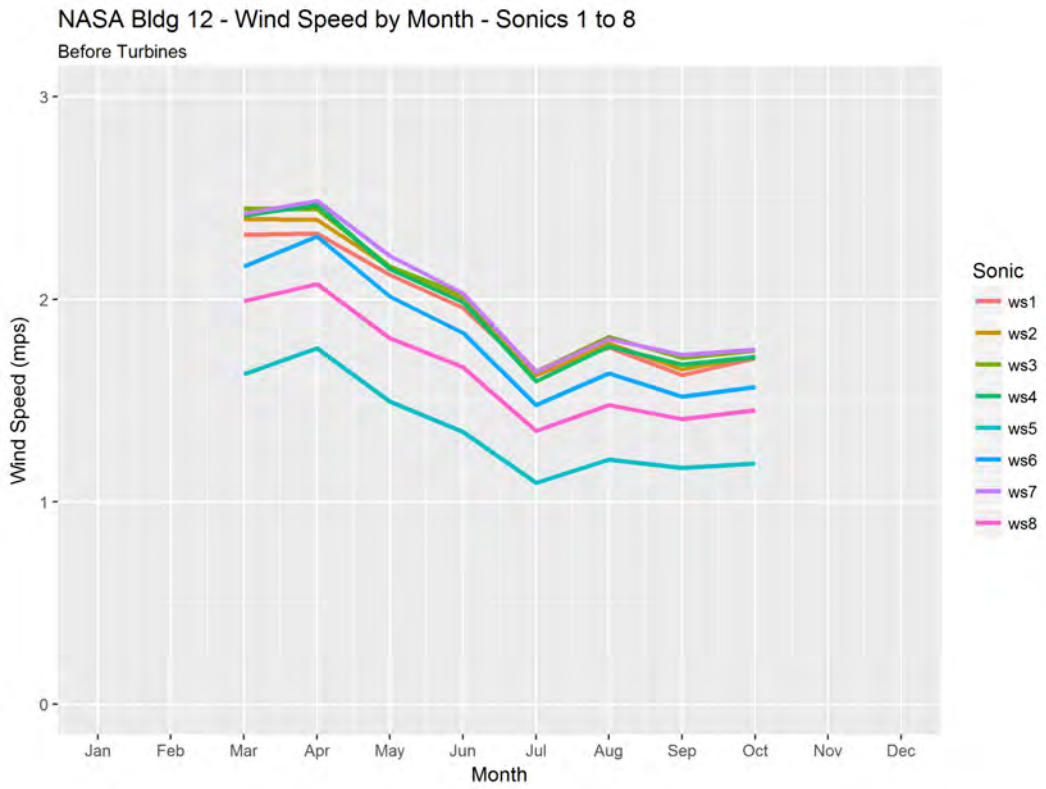

1.12.1.15.2 Diurnal wind speed

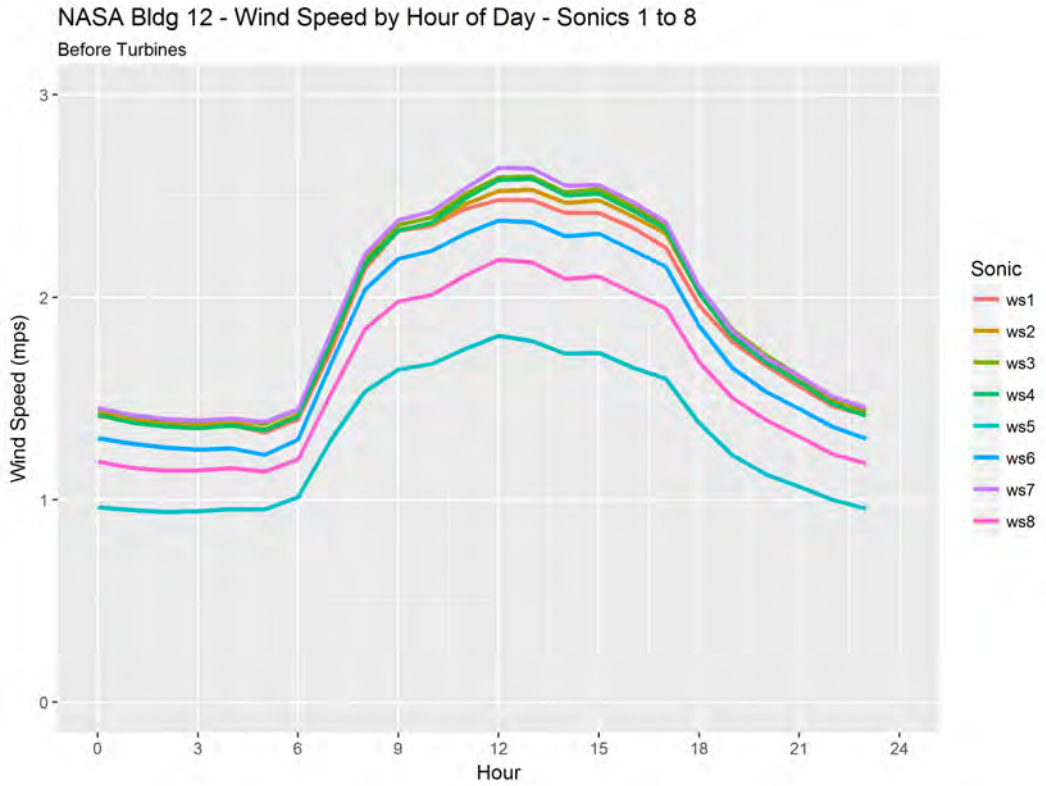

1.12.1.16 Summary of your findings

The measurement program had 8 months of measured wind speed data at multiple sites atop the roof of NASA building 12 all with averages below 2 m/s. Ground based reference sites were compared to the NASA measurements and as such they exhibited similar diurnal and monthly profiles but with the offsite ground-based references being generally higher in absolute wind

speed magnitude. There were some events embedded in the time series that reflect higher wind speed events such as storm or frontal passages. Those events while not focused on as part of this analysis could be good validation cases for CFD simulations or standards discussions.
Wind Direction measurements generally agree with both models and offsite references and show that the predominate wind direction is from the south-southwest.
The distribution for ultrasonic anemometer number 5 is noticeably lower than the others. Sonic 5 is mounted on a boom that hangs over the edge of the roof and is not on a tower like rest of the sonics.

1.12.1.17 Conclusions

The results of the Phase 1 measurement program at NASA Building 12 demonstrated very low wind speeds for wind energy production applications. Generally, an annual average wind resource of at least 5 m/s would be required for even a minimal amount of energy to be produced. At this low wind speed there is not likely enough energy in the wind to activate any current commercial machines. Additionally, this low wind speed makes it hard to draw broader inferences about turbulence and long-term resource in urban environments. There are however several instances of higher wind speed events such as storm or frontal passages that can be extracted for more detailed investigations.
Although it is hard to draw more general conclusions from this dataset we do see several important trends. First, we note that the leading-edge measurement (Sonic 5) reports lower wind speeds than the other measurement systems. This leads us to believe that trying to exploit leading edge building aerodynamics and accelerations is likely much harder than a typical small wind project developer might believe. Further the relationship between building measurements and offsite references shows similar diurnal and monthly patterns but reduced magnitude for building mounted measurements. This generally supports the intuition that urban areas disrupt the flow resulting in reduced wind speeds and available energy for wind production.

1.12.2 Deployment of Wind Turbines in Built Environment: Risks, Lessons, and Recommended Practices

Appendix A: Case Studies Twelve West Location: Portland, OR
Turbine type: Skystream 3.7

Number of turbines: 4

Installation date: 2009 Building integrated: Roof mounted (23-story building, mounted on 45-foot poles, blades at an elevation of 82 meters)

Estimated production: ~9,000 kWh yearly, or ~1% of the building's electricity Actual production: ~5,500 kWh per year

Cost: $20K per turbine; $240,000 for entire installation (mounting pads, engineering, etc.)

Incentives: 30% federal Investment Tax Credit in cash at project completion Payback: ~40 years Maintenance record: Have had issues with Turbine #3 (does not spin on occasion and must be restarted). This is under control with building management. What was the primary project objective? Raise awareness about renewable energy. Elevate the visibility of the building. Underscore the building's sustainability commitment. Did the installation meet those goals?

Rooftop wind in urban environments is challenging and has not evolved as much as we had hoped; however, all other objectives were met, and we consider this installation a success. Given your experience and the lessons you've learned, what suggestions would you give to another organization determined to develop a similar project? Take advantage of and leverage as many resources as you can. Make sure the turbine project is a good fit for your site; a token array that never spins will be detrimental when it comes to public opinion. Pay careful attention to turbine siting. A prominent wind specialist from the Netherlands advised us on Figure 8.

Twelve West wind turbine installation in Portland, OR. Photo from Flickr 4852149002 34

turbine placement based on the wind patterns in the area. Research the products well, and get comfortable with the fact that the manufacturer may go out of business (many of these companies are start-ups), which makes replacement/repair and warranty enforcement difficult.

Additional Notes Turbine choice: Due to the limited data regarding built environment wind installations, project developers didn't know what to anticipate in terms of turbine selection. None of the turbines researched had long track records for this type of installation, so the group conducted a significant investigation to identify what turbines would be best to use. Project developers conducted in-depth research during their turbine selection process, visiting multiple vendors and installations prior to selecting Southwest Windpower Inc. as the turbine supplier. One factor that influenced the selection was the company's compliance with European certification standards (Greeson 2010).

Development process: The wind turbines were part of a larger project: the design and construction of a 23-story LEED Platinum-certified mixed-use apartment and office building. Project developers decided to utilize solar and wind energy to help reach their LEED goal. The turbines were integrated into the building design early in the process, allowing the building's developers time to consult with experienced wind energy professionals to properly assess the site prior to installation. During this period, the developers conducted a thorough site assessment that included flow pattern simulations conducted at the Oregon State University's Aero Engineering Lab. The project developers also had to engage in discussions to address Federal Aviation Administration concerns related to the combined height of the building and project.

Public interest: Project developers believe the installation's visibility and the attention it has created for renewable energy and sustainability have been phenomenal. The installation has helped the building become a unique and recognizable feature in the city of Portland. Sound impacts: Since the project is located directly above the building's penthouse units, special consideration had to be given to reducing the potential sound impacts of the installation. This increased costs but was essential to overall project success.

Appendix A: Belgian Case Study

VRIJE
UNIVERSITEIT
BRUSSEL

Country case study Belgium:

Performance of a small wind turbine on an agricultural site

Mark Runacres

27 September 2018

Introduction

The present case study describes the performance of a small wind turbine on a farm in Diksmuide, in the West of Belgium. The report was prepared in the framework of a master thesis in the Faculty of Engineering at the Vrije Universiteit Brussel, by student Pierre Tordeur.

After a brief and general introduction, the work describes the layout of the site and wind measurements performed.

The energy production of the small wind turbine is compared with the energy consumption and with the production of a PV system on the same site. The economic feasibility of the small wind turbine project is analysed.

The actual energy production is compared with estimates of the energy production, and the level of agreement is discussed.

Chapter 1

Basics about wind energy

This chapter focuses on the theoretical background related to wind resource assessment aspects that will be used along this master's thesis.

The elements of theory about wind energy are mainly taken from the course of wind energy taught at the VUB by Pr. Mark Runacres (Runacres 2014).

Energy harvested from the wind is sustainable and renewable. Indeed, producing electricity from wind does not emit greenhouse gases during the operation and wind is a natural meteorological phenomenon. Wind turbines convert kinetic energy from the wind into mechanical energy. This mechanical energy is used to produce electricity by means of a generator. However, wind does not blow all the time and its occurrence is very difficult to predict. Challenges linked to intermittency and reliable prediction of energy production are real when using wind as an energy resource.

1.1 Wind energy fundamentals

The amount of energy flowing through a surface per unit time, i.e. the power available in wind, can be expressed as

$$P_w = \frac{1}{2}\rho V^3 A \qquad \text{(W)} \tag{1.1}$$

where ρ is the air density, V is the wind speed and A is the rotor swept area. The strong dependence between the available power and the wind speed emphasizes the imperative of having accurate wind speed data in order to have reliable energy production predictions.

Only a fraction of the available energy in the wind can be extracted by the rotor. The power coefficient at the rotor level, C_p, is the ratio of the power extracted by the rotor of the wind turbine, P, to the power available in the wind flowing through the swept area, P_w.

$$C_p = \frac{P}{P_w} \tag{1.2}$$

The one-dimensional momentum theory developed independently by Betz and Joukowski sets an upper limit on the energy that can be recovered by a wind turbine from the wind, i.e. on the efficiency of a wind turbine. By assuming a control volume, an homogeneous, incompressible, steady state fluid flow, no frictional drag, uniform thrust over the rotor area, unconstrained flow through the disc, non rotating wake and far up- and down-stream static pressure equal to the undisturbed ambient static pressure and by applying the conservation of linear momentum and the Bernoulli equation to this control volume, it is demonstrated that the maximum theoretical possible value for C_p is $16/27 \approx 59\%$. In practice, big wind turbines can reach power coefficients around 0.5. Small wind turbines have much lower C_p. Typical performance of various types of wind devices compared to the Betz limit as a function of the tip-speed ratio (the ratio between the speed of the tip of the blade and the wind speed) is shown in figure 1.1 (Berg 2007). It emphazises the fact that horizontal axis wind turbine are the most performing devices.

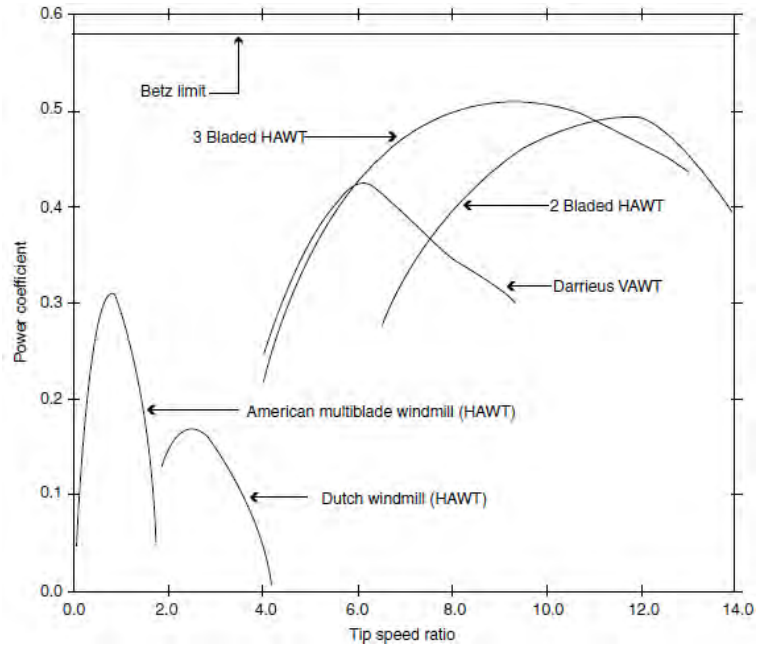

Figure 1.1: Typical performance of various types of wind turbines from Berg (2007).

The graph showing the power output of the wind turbine as a function of the wind speed is known as the power curve. The minimum wind speed at which the wind turbine starts to deliver useful power is the "cut-in wind speed". The maximum wind speed supported by the wind turbine is the "cut-out wind speed". The wind speed at which the rated power of the device is delivered is the "rated wind speed". A typical power curve is shown in the figure 1.2. The type of control of the power output (stall- or pitch-regulated) can lead to different power curve outputs around the rated power.

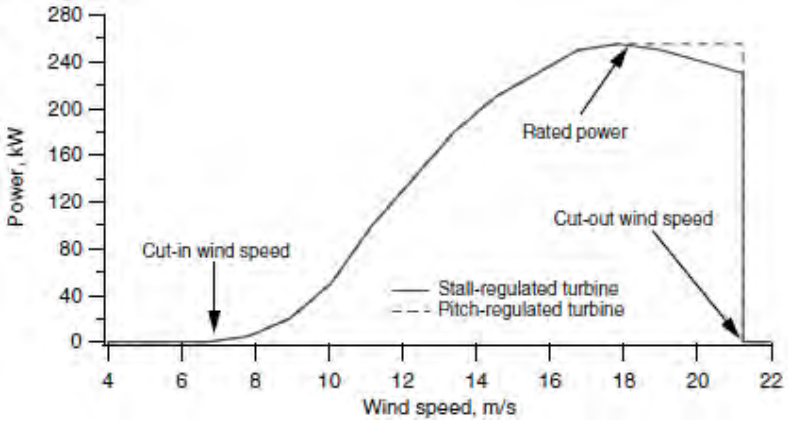

Figure 1.2: Typical power curve of a wind turbine, showing the power as a function of wind speed. Figure reproduced from Manwell et al. (2009).

1.2 Wind shear

Wind shear is the variation of wind speed with height. In turn, it has a direct consequence on the power available in the wind at a certain hub height but also influences the cyclic loading on the turbine blades

Knowing accurately the relation between elevation and wind speed is essential for wind power developers to extrapolate wind speed when wind measurement setups are not available at hub heights. It also allows to quantify the effects of terrain such as forests and hills. However, the task is not straightforward since additional factors influence the behavior of the wind such as the nature of the terrain, the atmospheric stability and the stochastic turbulent flows that result from it (Ray et al. 2006).

Two methods are generally used to estimate the wind shear: the log law and the power law.

1.2.1 Log law

The log law describing the relation between wind speed and elevation can be expressed as:

$$V(z) = \frac{V^*}{\mathrm{K}} \ln\left(\frac{z}{z_0}\right) \qquad (\mathrm{m/s}) \tag{1.3}$$

where $V(z)$ is the wind speed at height z, V^* is the friction velocity, $\mathrm{K} = 0.41$ is the von Karman constant and z_0 is the roughness height (i.e. the height above the ground at which the wind speed is theoretically zero).

It is worth noting that the log law is not suited to deal with wind speeds decreasing with height but also if the wind speeds at two different heights are the same.

1.2.2 Power law

For completeness, the power law model is also widely used for wind speed extrapolation. This wind shear model is an empirically developed relationship expressed as:

$$\frac{V(z)}{V(z_r)} = \left(\frac{z}{z_r}\right)^{\alpha} \tag{1.4}$$

with z_r a reference height and α the power law exponent.

Parameters characterizing the roughness of the terrain of both laws, i.e. z_0, V^* and α can be computed from the wind data available for the site of interest and compared to values available in the literature.

1.3 Statistical analysis

Once a great number of wind data has been monitored, there are ways to treat them in such a way to estimate the wind resource or wind power production potential on a particular site.

1.3.1 Direct methods

A number, N, of observations of data, X_i (wind speed, power, ...) will be monitored. Each measure is averaged over the time interval Δt. Basic properties can be directly computed from these data.

- The average of a serie of data over the monitoring period, $\overline{X}$

$$\overline{X} = \frac{1}{N}\sum_{i=1}^{N} X_i \tag{1.5}$$

- The standard deviation of the data set, σ_X

$$\sigma_X = \sqrt{\frac{1}{N-1}\sum_{i=1}^{N}(X_i - \overline{X})^2} \tag{1.6}$$

1.3.2 Probability density function

The Weibull and the Rayleigh probability distributions are commonly used in wind data analysis.

The **Weibull** probability density function allows to describe the wind speed distribution on a site with two parameters

- The shape factor, *k*
- The scale factor, *c*

Its probability density function is given by:

$$\varphi_W(V) = \frac{k}{c}\left(\frac{V}{c}\right)^{k-1} \exp\left[-\left(\frac{V}{c}\right)^{k}\right] \tag{1.7}$$

where V is the wind speed.

Based on the moment method, the parameters of the Weibull probability density function can be approximated by the following expressions:

$$k = \left(\frac{\sigma_V}{\overline{V}}\right)^{-1.086} \tag{1.8}$$

$$c = \frac{\overline{V}}{\Gamma(1+1/k)} \tag{1.9}$$

with Γ the gamma function.

The **Rayleigh** probability density function corresponds to a Weibull distribution with a fixed shape factor, k=2. It is thus a simpler probability distribution that depends only on one parameter: the mean wind speed. It can be expressed by the following expression:

$$\varphi_R(V) = \frac{\pi}{2}\left(\frac{V}{\overline{V^2}}\right) \exp\left[-\frac{\pi}{4}\left(\frac{V}{\overline{V}}\right)^{2}\right] \tag{1.10}$$

Probability density functions represent the probability that a certain wind speed occurs. Those functions are used to describe the wind conditions on the different sites. The advantage is that the wind conditions are represented with only one (i.e. Rayleigh) or two (i.e. Weibull) parameters.

1.3.3 Wind roses

A classical wind rose is a graphical tool that will show from where does the wind come from. It gives the relative frequency of each of the wind directions. By multiplying this wind rose by the mean wind speed in each direction, the wind rose of the average wind speed is obtained. It shows the contribution of each direction to the mean wind speed. Another adaptation of the wind rose consists in multiplying the frequency by the cube of the wind speed in each direction (as the energy content is proportional to the cube of the wind speed). This wind rose shows which sector contributes to the energy content of the wind at the site. Therefore, it is also the most relevant wind rose when doing resource assessment, as it indicates from which direction does the wind come with the most power.

1.4 Variation of wind speed with time

Wind is a very fluctuating parameter. Wind speed depends on a lot of factors such as location, height and time. This subsection focuses on the temporal variation of wind conditions at different time scales. A distinction can be made between short- and long-term fluctuations in wind speed and hence, in the power produced by the wind turbine.

Short-term fluctuations in wind power are caused by turbulence and gusts and are stochastic. However, for longer-term fluctuations, distinctive patterns exist. Longer-term fluctuations mean daily, seasonally and yearly fluctuations (Wan 2012).

A typical example of temporal variation of wind speed at different time-scales is shown in figure 1.3. The graph shows the power spectral density of the wind speed as a function of the frequency. It means that a high value indicates a considerable change in wind speed over the determined time-scale.

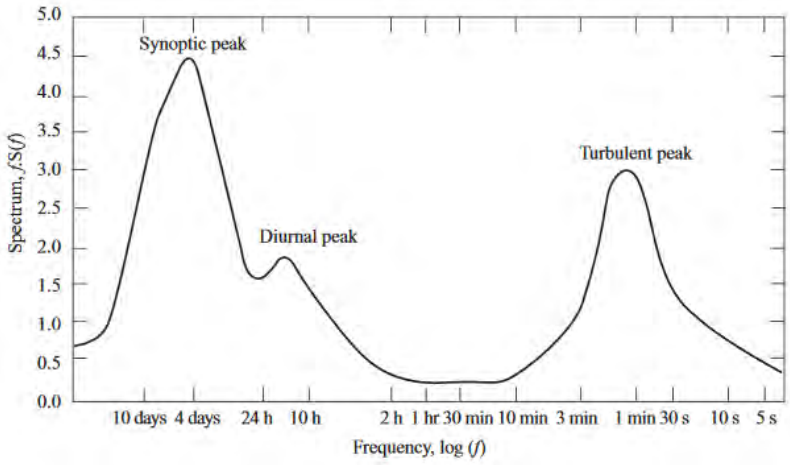

Figure 1.3: Power spectrum of wind speeds as a function of frequency of occurrence. From Burton et al. (2001).

Even if the graph is specific for a site, some trends can be generalized. The peaks on the left part of the graph (synoptic and diurnal) are variations on the macro-meteorological level, while peak on the right part of the graph (turbulent) is due to turbulence and gusts (Vermeir 2015).

1.5 Economic feasibility

The Levelized Cost of Energy (LCOE), the Net Present Value (NPV), the Internal Rate of Return (IRR) and Payback Period indicators (static and dynamic) (SPP/DPP) are widely used economic parameters to assess the economic feasibility of a renewable project (Karczewski et al. 2017, Vermeir 2015, Campoccia et al. 2009, Ayodele et al. 2013, Short et al. 1995).

LCOE (Short et al. 1995) The LCOE is an economical parameter allowing to compare alternative technologies with different scales of operation, investments and operating time periods. In turns, this parameter is used to rank different technologies. The LCOE is computed as follow:

$$\text{LCOE} = \frac{I_0 + \sum_{n=1}^{N} \frac{OM_n}{(1+d)^n}}{\sum_{n=1}^{N} \frac{\text{AEP}}{(1+d)^n}} \tag{1.11}$$

where I_0 is the investment cost,N is the lifetime of the wind turbine in years, OM_n are the operation and maintenance costs for year n, d is the discount rate and AEP is the annual energy production.

NPV (Short et al. 1995) The NPV is a way of examining the costs (cash outflows) and revenues (cash inflows) of a project. The difficulty when computing the NPV is to identify all these cash flows that need to be taken into account. For a project to be economically viable, the NPV should obviously be positive at the end of its lifetime. The discount rate allows to take the time value of money into account. The NPV is computed as follow:

$$\text{NPV} = \sum_{n=0}^{N} \frac{CF_n}{(1+d)^n} \tag{1.12}$$

where CF_n is the cash flow in year n.

IRR (Short et al. 1995) For an investment with a series of cash flows $(CF_0, ..., CF_N)$, the IRR is the rate for which the NPV=0.

SPP & DPP (Short et al. 1995) The SPP is the time (in years) to recover the cost of a project. As this parameter ignores the time value of money, the DPP is the number of years needed to recover the costs of the project while accounting for the time value of money.

Chapter 2

Wind measurement campaign

This chapter presents the wind and atmospheric conditions measurement setup used during the whole period of data acquisition and the type of data that were monitored.

The devices needed to gather wind and atmospheric data are the following:

- Anemometer to measure the wind speed
- Wind vane to measure the wind direction
- Thermometer to measure the air temperature
- Barometer to measure the air pressure
- Data logger to save the signals
- Memory card to store the data
- GPRS module to transmit the data

All the devices are mounted on a meteorological mast as indicated in the IEC 61400-12 (IEC 2005). Respecting the recommendations of the standard is important for minimizing flow distortions, influence of devices and, in turn, allowing accurate measurements.

The wind speed is measured with 3 cup anemometers. Two of them are mounted on top of the mast, at 15 m high, side-by-side with a required separation between them and between the tower in order to have relatively small flow distorsion. The primary cup anemometer (anemometer 1) is South-West oriented, i.e. the prevailing wind direction in Belgium (it will be shown in section 4.4 that the measured prevailing wind direction on site is West and not South-West), and measures wind speeds coming from directions East to North (i.e. range of 270°). The control anemometer (anemometer 3) is oriented North-East and is aimed to measure wind speeds coming from directions North to East (i.e. range of 90°). The remaining anemometer (anemometer 2) is placed at 10 m high. Measuring the wind speed at different heights is useful to characterize the vertical wind profile by computing wind shear parameters and in turn to extrapolate wind data up to higher heights.

The wind direction is measured with a wind vane mounted on the mast at 13.5m high and South-West oriented (again, prevailing wind direction in Belgium). The wind vane has to be situated as close to the anemometers as possible without distorting the flow.

The air temperature T and **air pressure** p are measured with respectively a thermometer and a barometer, placed at 12m high, in order to compute the air density ρ with the relation:

$$\rho = \frac{p}{R_0 T} \qquad (\text{kg/m}^3) \tag{2.1}$$

where R_0 is the gas constant of dry air (284 J/kgK).

The wind speed and direction are measured with a sample frequency of 1 Hz and per interval of 1, 10 or 60 minutes, the mean, minimum, maximum and standard deviation of the wind speed are registered. The air temperature and pressure are registered at the same intervals as the wind speed and direction (1,10 or 60 minutes). The datalogger setup was programmed to store only 10 minutes average data because, as it will be seen later, the power measurements were only available on (irregular) 5 minutes average. Faster sampling would only have been relevant to have a better grasp of the level of turbulence at the site.

Data are transmitted via a GPRS module.

The measurement setup is shown in Figure 2.1.

Figure 2.1: Clockwise starting from top left: Thies first class anemometer, Thies compact wind vane, Thies baro transmitter, Genpro 20e GSM/GPRS serial transmitter, Campbell Scientific CR 800 and Thies compact temperature sensor (Vermeir 2015).

Chapter 3

Test site and small wind turbine

As mentioned in the introduction, a small wind turbine and a wind measurement mast were installed on a farm in the municipality of Diksmuide, province of West Flanders, Belgium. This chapter highlights the layout of the terrain and of the electrical installation of the farm, the consumption needs and the renewable production potential, as well as the main characteristics of the wind turbine.

3.1 General layout

The farm considered in this Master's thesis is specialized in cattle breeding. The herd is made up of a few hundred of cattle. In turn, it is not the most energy consuming exploitation. However, the farmer is committed to take part in the electricity transition. Indeed, he installed photovoltaic (PV) panels (rated power: 6 kW) and a small wind turbine (rated power: 3.5 kW). As renewable resources are intermittent and that no batteries are installed, the farm is still connected to the grid. This configuration allows him to draw current from the grid when local production is not sufficient and to feed current into the grid when the PV-panels and wind turbine production exceeds the local energy needs.

An aerial view of the site is showed in figure 3.1. The picture is North oriented. The locations of the PV-panels, the wind turbine and the measurement mast are indicated. As a reminder, the primary anemometer is South-West oriented. The building "Hilleware Voeders" could be a cause of distortion of the wind flow since it is a tall building. Wind coming from West is highly distorted because of the buildings of the farm. In general, the site looks to be cleared.

A picture of the South-South-West direction is given in figure 3.2. The picture is not really well taken because a view of the West and South-West directions would have been more interesting as they are the prevailing wind directions. However, the picture shows the presence of trees and some buildings that can have an influence on the wind flow.

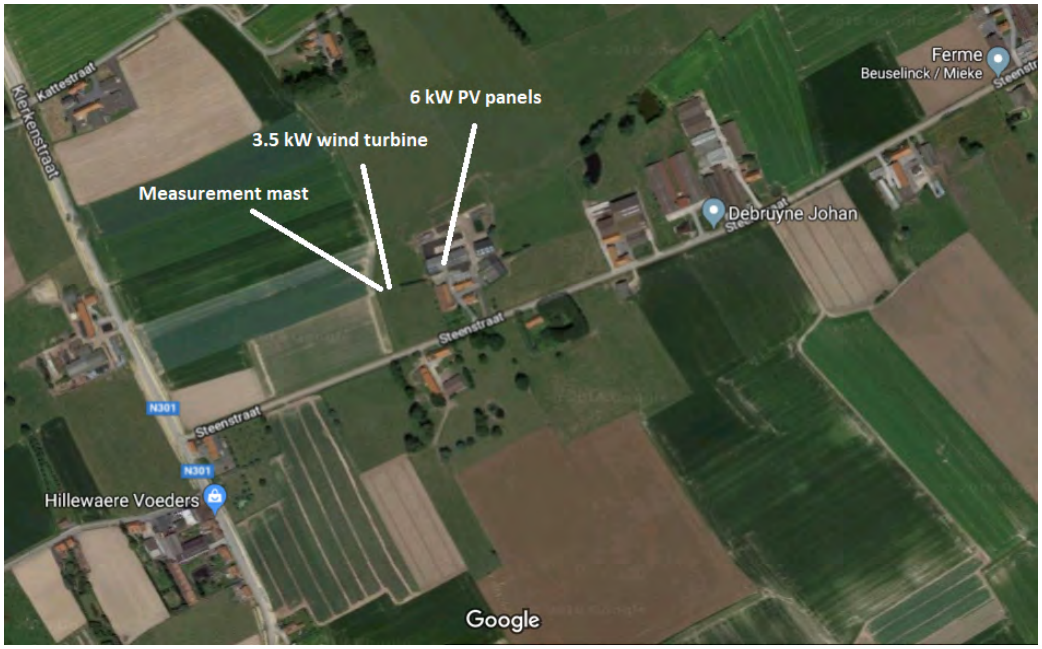

Figure 3.1: Aerial view of the farm in Diksmuide with the location of the PV-panels, wind turbine and measurement mast. The picture is North oriented.

Figure 3.2: South-South-West direction seen from the small wind turbine and measurement mast in Diksmuide.

A general and an electrical diagrams given by the manufacturer of the wind turbine, Enair, summarize the installation combining the PV panels, the wind turbine and the grid (see figures 3.3 and 3.4). For the PV-panels, an inverter is needed to convert DC current into AC current. AC/DC ("wind regulator" on figure 3.4) and DC/AC converters are needed to convert the variable frequency AC current produced by the wind turbine to an AC current with a fixed frequency of 50 Hz. A resistor can dissipate the current produced by the wind turbine in case of dysfunction of the power electronics or even to heat the maintenance room where those converters and resistor are placed. Downstream from the converters, produced electricity can be directly consumed by the farmer or fed into the grid.

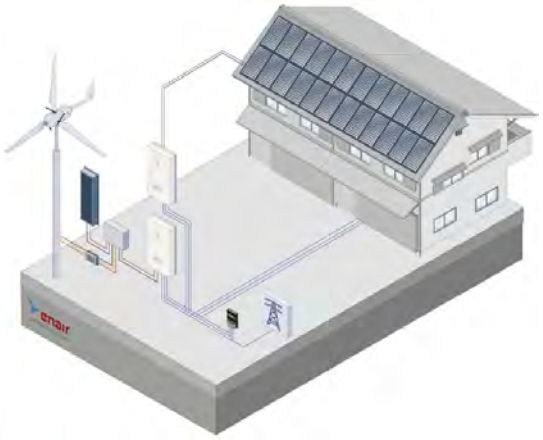

Figure 3.3: General diagram of the farm combining PV panels, wind turbine, grid and load given by Enair, the manufacturer of the wind turbine (Enair 2017*a*).

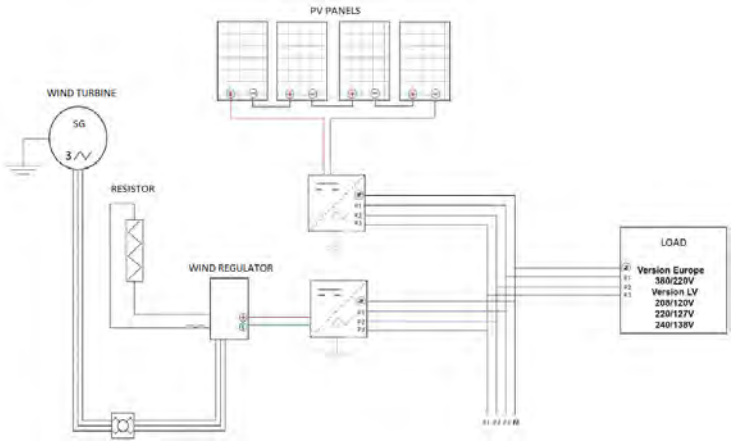

Figure 3.4: Electrical diagram of the farm combining PV panels, wind turbine, grid and load given by Enair, the manufacturer of the wind turbine (Enair 2017*a*).

3.2 Overview of the energy consumption and production

Figure 3.5 shows the electricity consumption and production of the farm for the year 2017. As mentioned in previous section, PV panels and a small wind turbine produce electricity.

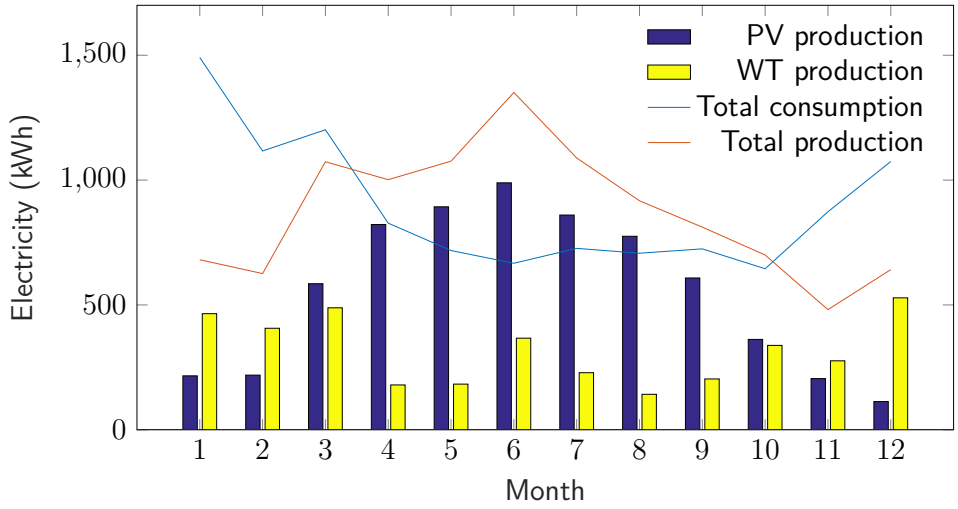

Figure 3.5: Monthly electricity production (solar, wind and total) and consumption of the farm in Diksmuide for the year 2017.

The annual electricity consumption of the farmer is roughly 11000 kWh. The electricity consumption of the farm fluctuates through the year. January 2017 was the month with the largest electricity consumption, around 1500 kWh. February, March and December 2017 also show a peak in electricity consumption, with more than 1000 kWh monthly consumed. On the contrary, June and October 2017 were the months with the lowest electricity consumption, with less than 700 kWh each month. During the rest of the year, the situation seems to be comparable in terms of electricity consumption with periods varying between 700-900 kWh per month.

The annual electricity production of the PV-panels is roughly 6650 kWh and the one of the wind turbine is estimated to be 3800 kWh for the period going from January 2017 to December 2017. In other words, the renewable electricity production from the PV-panels and from the wind turbine is similar to the energy consumption of the farmer. The total electricity production depends strongly of the period of the year. It can clearly be noticed that the peak of electricity produced happens during the summer (see June 2017 with a monthly electricity production around 1400 kWh). May, June and July 2017 are really profitable months on the electricity production point of view. On the contrary, November 2017 is the less profitable month on the energy production point of view. An important observation is that the total electricity production per month is greater than the electricity consumption from April to October 2017. The surplus of electricity is fed into the grid. As mentioned in section 3.1, without electricity storage system, the connection of the farm to the grid is unavoidable.

Furthermore, the main part of electricity is produced through the PV panels. The shape of the total electricity production is similar to the one of the electricity produced through PV

panels. It makes sense since the PV installation capacity is approximately two times more powerful than the one of the wind turbine. From May 2017 until August 2017, the amount of electricity produced through PV panels is even larger than the electricity consumed. Again, the peak of solar electricity is reached in June 2017. December 2017 is the worth month in terms of solar electricity. It can be mentioned that December 2017 was unique in terms of duration of sunshine since there was only 10 hours 29 minutes of sunshine during the whole month, where the normal value is 45 hours and 8 minutes. In fact, it is the month of December with the lower duration of sunshine since the IRM records data (IRM 2018).

Electricity produced through the wind turbine also strongly depends on the month of the year. The months of March 2017 and December 2017 were the most profitable on wind energy point of view respectively reaching around 490 kWh and 530 kWh of energy production. From April 2017 to September 2017, the wind energy is not really significant, except in June 2017.

Figure 3.6 shows the normalized electricity production of the 6 kW PV-panels and 3.5 kW wind turbine. The graph confirms that there is a lot of electricity produced from the sun from April 2017 until August 2017. Again, confirmation that April, May, July, August and September 2017 were months with little wind. Additionally to the figure 3.5, the figure 3.6 better highlights the fact that the wind turbine produces proportionally more energy than the PV-panels from January to March and from October to December. December 2017, with its low rate of sunshine, is the month that illustrates best this trends.

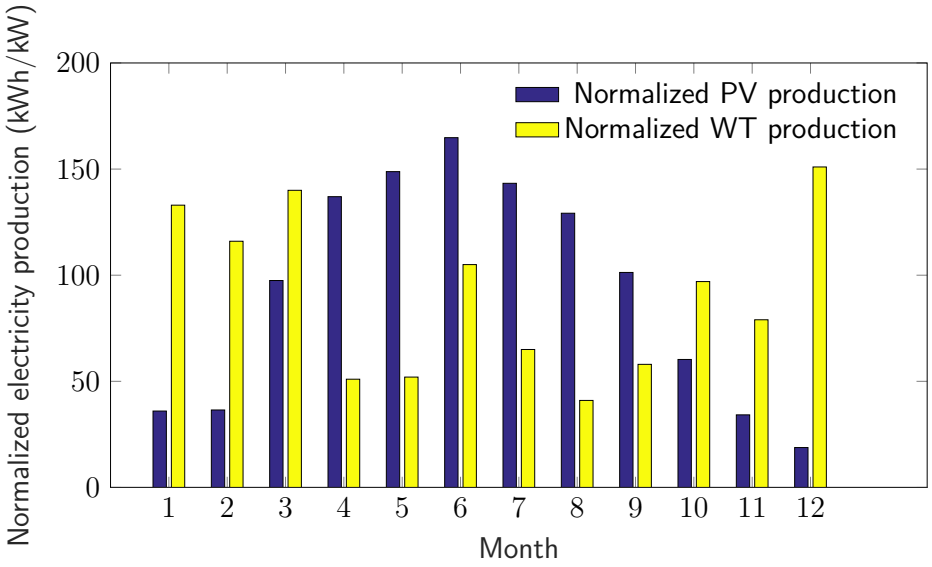

Figure 3.6: Monthly normalized electricity production from PV-panels (6 kW) and from the small wind turbine (3.5 kW) of the farm in Diksmuide for the year 2017.

3.3 Small wind turbine

The small wind turbine installed on the farm is the E70 PRO from the Spanish Enair company. [1] Their devices are developed according to the international standard IEC-61400 that regulates the small wind turbine sector. Their wind turbines are suited for installations connected to the network as well as for isolated power grid installations. Typical setups for different uses include telecommunication towers, small industries, greenhouses, houses, country hotels and farms.

The description and the dimensions of the E70 PRO can be seen in figures 3.7a and 3.8. Its main characteristics are gathered in the table 3.1. More information are available in appendix A (Enair 2017*b*).

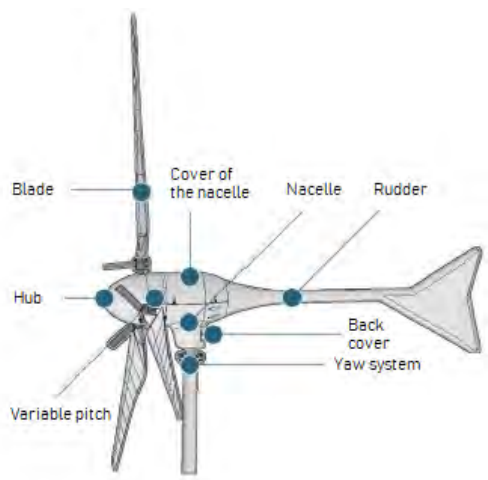

(a) Description of the small wind turbine E70 PRO from Enair (2017*a*).

(b) Picture of the small wind turbine E70 PRO from Enair (2017*a*).

Figure 3.7: Small wind turbine E70 PRO from Enair (2017*a*).

The wind data and power production on site were recorded during 1 year to draw the power curve and estimate the Annual Energy Production of the wind turbine. Therefore, a wind mast was also mounted on the farm, at approximately 10.75 m of the small wind turbine (2.5 times the rotor diameter (IEC 2005)). Direct measured and estimated long term data will be used for this purpose. A comparison analysis between the actual energy production of the wind turbine and the data provided by the manufacturer is interesting to see if the device is as efficient as the manufacturer claims.

[1] Enair (1970) activity focuses mainly on small to medium wind turbine with models ranging up to 50 kW.

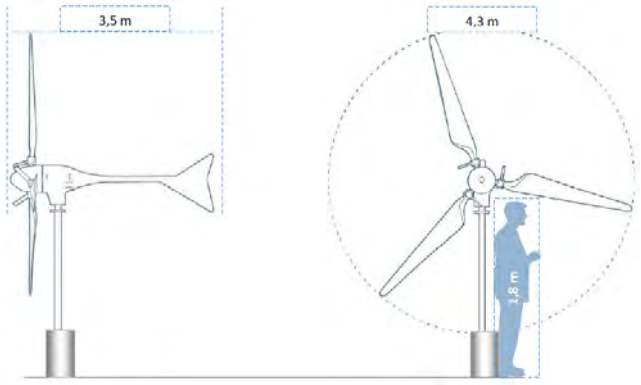

Figure 3.8: Dimensions of the small wind turbine E70 PRO from Enair (2017*a*).

Manufacturer	Enair
Model	E70 PRO
Type	Horizontal axis
Number of blades	3
Rotor diameter	4.3 m
Power control	Passive variable, centrifugal pitch system
Nominal power	3.5 kW
Nominal wind speed	11 m/s
Cut-in wind speed	2.8 m/s
Cut-out wind speed	>60 m/s
Converter	Efficiency 95%; MPPT algorithm
Height	15 m

Table 3.1: Main characteristics of the small wind turbine E70 PRO from Enair (2017*a*).

Chapter 4

On-site measurements

In this chapter, an analysis of the data of the measurement campaign conducted in Diksmuide is presented. The layout of the presentation is based on the data analysis of Runacres et al. (2014). The wind data were recorded from March 20th 2017 until March 7th 2018, so approximately during 1 year.

4.1 Preliminary work

At one moment, around December, the farmer noticed that the cables maintaining the mast were not under tension anymore. A stage of the telescopic mast had slipped down. The origin of this slipping seems to be cows rubbing against the mast combined to high wind speeds at this time of the year. As a consequence, the anemometers 1 and 3 were now at 13 m, the anemometer 2 at 8 m and the wind vane at 11.5 m. Having anemometers at 2 different heights, it was possible to extrapolate wind speed data up to 15 m.

The first point was to determine at what time did the mast slip down. An analysis of the wind data showed that from December 2nd 2017 until December 3rd 2017 the wind speed was 0 m/s (see figure 4.1). This is the only time during the whole measurement period that there was an uninterrupted period without wind at all during 24h. Furthermore, at the same time, a small amount of power was generated by the wind turbine. Therefore, it was decided to extrapolate data up to 15 m since December 2nd until the end of the measurement period.

As presented in section 1.2, 2 laws are often used to extrapolate wind speed data: the log- and power-law. Using the log law, 2 parameters, the roughness length, z_0, and the friction velocity, V^*, have to be determined. For the power law, only one parameter, the power law exponent, α, has to be computed. Their computation is presented in subsections 4.1.1 and 4.1.2.

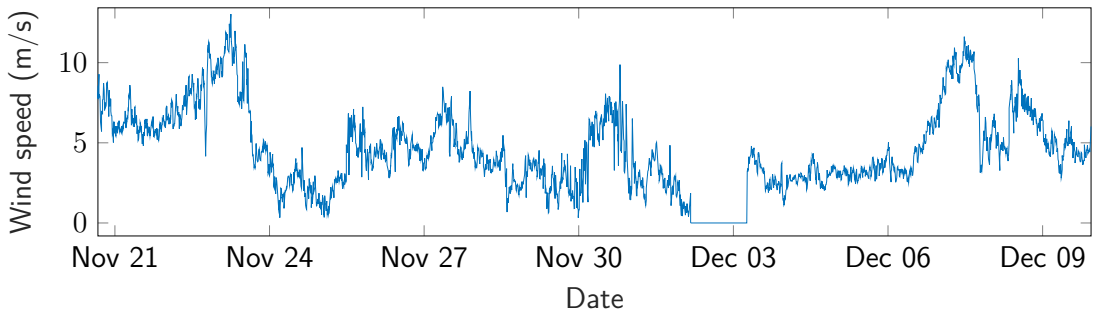

Figure 4.1: Wind speed as a function of time in November-December showing an abnormal 24h period of time with 0 m/s wind speed between December 2nd and December 3rd 2017.

4.1.1 Practical determination of roughness length and friction velocity

By applying equation 1.3 to the measured wind speeds at both heights the following expressions are obtained:

$$V_1 = V_1(z_1) = \frac{V^*}{\mathsf{K}} \ln\left(\frac{z_1}{z_0}\right) \qquad (\mathrm{m/s}) \tag{4.1}$$

$$V_2 = V_2(z_2) = \frac{V^*}{\mathsf{K}} \ln\left(\frac{z_2}{z_0}\right) \qquad (\mathrm{m/s}) \tag{4.2}$$

By dividing equation 4.1 by equation 4.2

$$\frac{\ln\left(\frac{z_1}{z_0}\right)}{\ln\left(\frac{z_2}{z_0}\right)} = \frac{V_1}{V_2} \tag{4.3}$$

From which the roughness length can be obtained

$$z_0 = \frac{z_1^{\frac{V_2}{V_2 - V_1}}}{z_2^{\frac{V_1}{V_2 - V_1}}} \qquad (\mathrm{m}) \tag{4.4}$$

The friction velocity can be computed with

$$V^* = \frac{\mathsf{K} V_1}{\ln\left(\frac{z_1}{z_0}\right)} = \frac{\mathsf{K} V_2}{\ln\left(\frac{z_2}{z_0}\right)} \qquad (\mathrm{m/s}) \tag{4.5}$$

To compute the wind speed at a certain height z, the following formula can be used

$$V(\mathsf{z}) = V_{\mathsf{ref}} \frac{\ln\left(\frac{\mathsf{z}}{\mathsf{z}_0}\right)}{\ln\left(\frac{\mathsf{z}_{\mathsf{ref}}}{\mathsf{z}_0}\right)} \qquad (\mathrm{m/s}) \tag{4.6}$$

4.1.2 Practical determination of power law exponent

By applying equation 1.4, the power law exponent can be determined with the following expression

$$\alpha = \frac{\ln\left(\frac{V_2}{V_1}\right)}{\ln\left(\frac{z_2}{z_1}\right)} \tag{4.7}$$

4.1.3 Selection of the law

The point here was to chose the law that could best describe the wind shear for the specific case of the site under test.

Ray et al. (2006) discussed the accuracy of both laws according to the layout of the terrain to determine the evolution of the wind speed as a function of the height. Furthermore, they used three approaches per law to determine the shear parameters, and hence to extrapolate hub height mean wind speed. The three approaches are the following ones:

- **Overall mean:** Use the mean wind speeds of both anemometers to compute an overall mean shear parameter. Hence, using 1.3 or 1.4, a mean wind speed can be computed at the desired height.
- **Parameter average:** Compute a 10-minute shear parameter for each of the 10-minute data. Then, average all these 10-minute shear parameters, resulting in an average 10-minute shear parameter. Hence, using 1.3 or 1.4, a mean wind speed can be computed at the desired height.
- **Extrapolated time series:** Use each 10-minute shear parameter to extrapolate a wind speed time series to the desired height.

The results obtained by Ray et al. (2006) showed that in general, wind shear estimation errors are likely to be large. However, the extrapolated time series approach used with the log law has shown good performance compared to the other approaches, specially for flat and forested terrains. That is why, for the present case study, the extrapolated time series approach was used with the log law to determine the wind shear. In turn, wind speeds from December 2nd 2017 until March 3rd 2018 were extrapolated from 8 and 13 m up to 10 and 15 m.

4.2 General results

The wind speed evolution as a function of time is shown in Figure 4.2. As explained in chapter 2, the wind speed was recorded by the primary cup anemometer - South-West oriented - for wind direction from East to North (270°) and by the control anemometer - North-East oriented - for wind direction from North to East (90°). By proceeding this way, the flow distortions are relatively small. The data showed in figure 4.2 were recorded at or extrapolated to 15 m (see section 4.1).

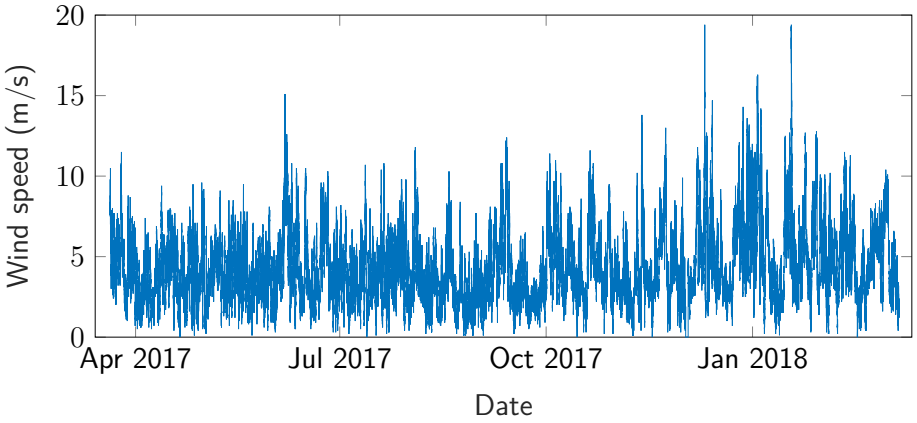

Figure 4.2: Wind speed as a function of time in Diksmuide at 15 m.

The mean wind speed, the dominant wind direction and the Weibull parameters at 10 and 15 m were computed using equations presented in sections 1.3.1 and 1.3.2. The coefficient of determination of the wind speed distribution, R^2, was also computed. This parameter, comprised between 0 and 1 describes the goodness of fit of the probability density function (PDF) (Carrillo et al. 2014). The higher R^2, the most suitable the PDF is to describe the wind speed data. The results are shown in the following table.

Parameter	Value at 10 m	Value at 15 m
Mean wind speed	3.92 m/s	4.25 m/s
Dominant wind direction	West	West
Shape factor k	1.8905	1.9713
Scale factor c	4.4183	4.7894
Coefficient of determination R^2	0.9624	0.9529

Table 4.1: Results of wind data measurement.

An histogram of the wind speed data in Diksmuide and its associated Weibull probability density function (PDF) are shown in figure 4.3. A 2 parameters PDF like the Weibull one does not fit perfectly with deformed and heterogeneous wind speed distributions. A problem highlighted by Takle & Brown (1977) is that the Weibull PDF can not cope with low or zero wind speeds probabilities. To include these calm periods into the probability distribution, a hybrid density function developed by Takle & Brown (1977) was used:

$$\varphi_W^H(V) = F_0\delta(V) + (1 - F_0)\varphi_W(V) \tag{4.8}$$

where F_0 is the probability of observing wind speed comprised between 0 and 0.25 m/s and $\delta(V)$ is the Dirac delta function.

The Weibull PDF in figure 4.3 may seem to over estimate the probability of wind speeds from 4.5 up to 8 m/s. However, the R^2=0.9529 is close to 1, meaning that the distribution fits well with the histogram data. To avoid the over estimation of this range of wind speeds,

the Weibull distribution could be shifted to the left. In this case, probability of lower wind speeds would be over estimated.

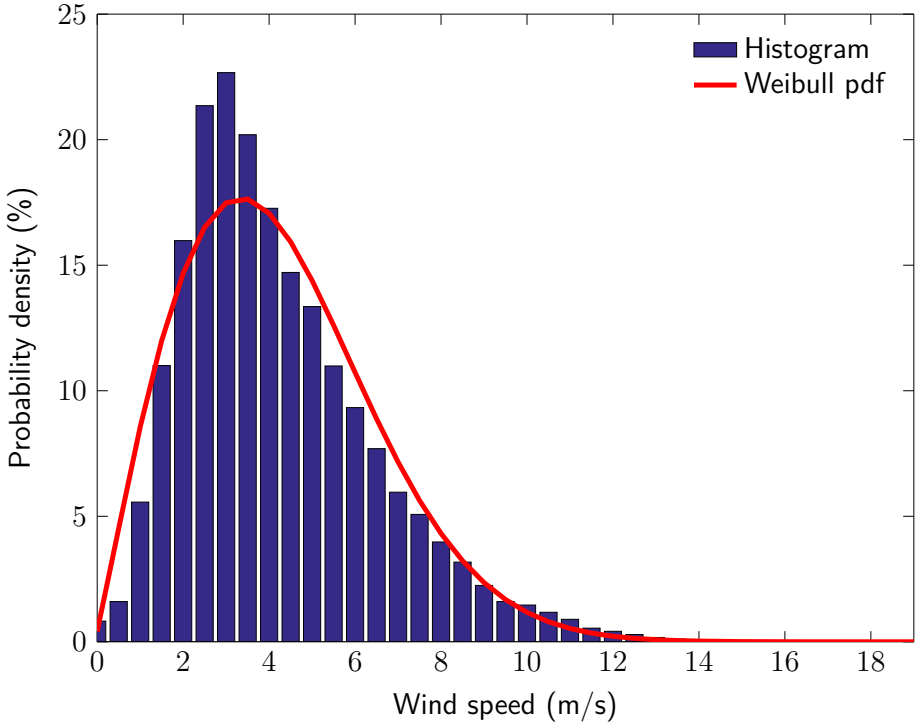

Figure 4.3: Histogram and Weibull probability density function of the wind speed in Diksmuide at 15 m.

4.3 Monthly results

The monthly results are shown in Tables 4.2 and 4.3. Data were available 100% of the time every month. January 2018 was the month with the highest mean wind speed over the whole measurement period, 5.46 m/s. The highest wind gust was recorded in December 2017 at 30.66 m/s.

Month	Mean wind speed at 10 m (m/s)	Mean wind speed at 15 m (m/s)	Max. wind speed at 15 m (m/s)	Data availability
April 2017	3.38	3.61	15.64	100%
May 2017	3.50	3.80	15.13	100%
June 2017	4.16	4.48	22.48	100%
July 2017	3.60	3.91	18.92	100%
August 2017	2.91	3.18	18.64	100%
September 2017	3.22	3.53	20.72	100%
October 2017	4.24	4.58	18.92	100%
November 2017	3.73	4.02	22.94	100%
December 2017	4.80	5.10	30.66	100%
January 2018	5.10	5.46	29.22	100%
February 2018	4.35	4.75	17.9	100%
Total	3.92	4.25	30.66	100%

Table 4.2: Monthly average and maximum wind speed and availability.

Month	Mean air pressure (hPa)	Mean air temperature (°C)	Mean air density (kg/m^3)
April 2017	1017.7	9.95	1.25
May 2017	1012.3	15.11	1.22
June 2017	1009.5	18.64	1.20
July 2017	1010.1	18.25	1.21
August 2017	1012.0	17.76	1.21
September 2017	1009.4	14.81	1.22
October 2017	1014.5	14.08	1.23
November 2017	1011.2	8.52	1.25
December 2017	1008.9	6.15	1.26
January 2018	1007.1	6.94	1.25
February 2018	1012.4	2.83	1.28
Total	1011.4	12.17	1.23

Table 4.3: Monthly mean air pressure, temperature and density.

4.4 Results per wind direction

In this section wind roses of the average wind speed as well as frequency and power density wind roses were computed for wind speeds at 15 and 22.5 m.

The dominant wind direction is West. Thanks to relatively high wind speeds coming from West, it is also the direction from where the wind contains the most energy.

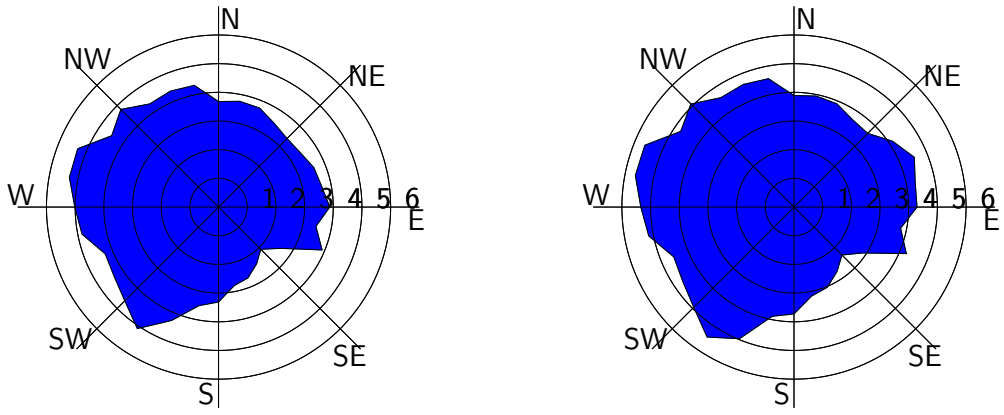

(a) 15 m (b) 22.5 m

Figure 4.4: Wind rose of the average wind speed (m/s) at 15 m and 22.5 m.

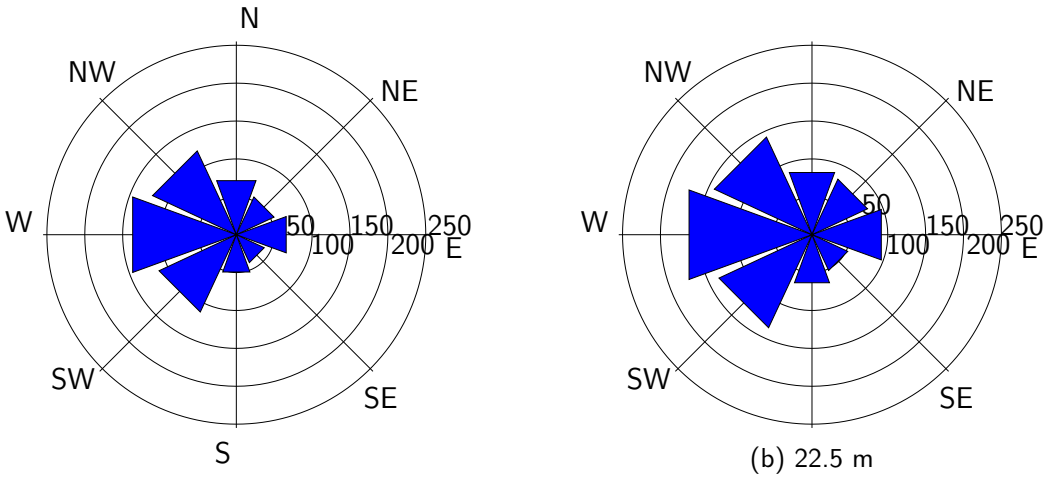

(a) 15 m (b) 22.5 m

Figure 4.5: Power density wind rose (W/m^2) at 15 m and 22.5 m.

The frequency wind rose in figure 4.6 indicates that wind comes from West 25% of the time and from South-West 23% of the time. The wind comes from the other wind directions less than 11% of the time.

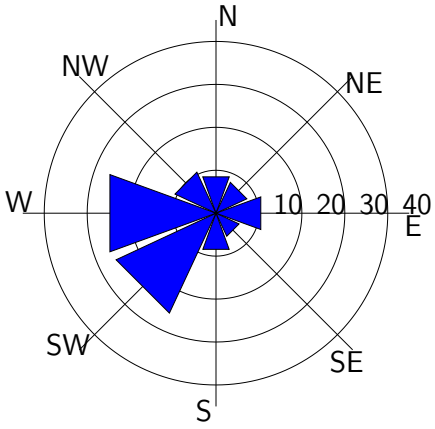

Figure 4.6: Frequency wind rose at 15 m (%).

Extrapolating wind data for higher heights increases the uncertainty level of the energy production predictions. There is a non written rule that says that in order for a wind project to be bankable (i.e. that banks are willing to invest in the project), the maximum height of extrapolation is 2/3 of the measurement height. In this case it corresponds to a height of 22.5 m. That is why it was decided to extrapolate wind speeds data up to 22.5 m and to compare the wind conditions to a height of 15 m.

The wind rose of the average wind speed and for the power density were drawn for 15 m (figures 4.4a and 4.5a) and for 22.5 m wind speed data (figures 4.4b and 4.5b). The interesting height is obviously 15 m as it is the hub height of the installed wind turbine and the maximum height for small wind turbines in Flanders on the legal point of view (Van Mechelen & Crevits 2009). However, having the data for 22.5 m allows to compare both heights. From figure 4.4a it can be seen that at 15 m the average wind speed for the North-West direction is 4.8 m/s, for the West direction is 5 m/s and for the South-West direction is 4.6 m/s. The higher mean wind speed comes from the West-North-West direction and is 5.3 m/s. If the data are extrapolated to 22.5 m, the mean wind speeds for the directions North-West, West, South-West and West-North-West are respectively 5.1 m/s, 5.3 m/s, 4.9 m/s and 5.6 m/s.

The average wind power density is computed as follow:

$$\frac{\overline{P}}{A} = \frac{1}{2}\rho\overline{V^3} \qquad (\mathrm{W/m^2}) \tag{4.9}$$

The power density wind rose 4.5 represents the power available in the wind per direction. At 15 m, see figure 4.5a, the power density in the North-West, West and South-West directions are respectively 115 W/m^2, 140 W/m^2 and 105 W/m^2. Wind coming from the West direction contains the most energy. The wind power density in the other wind directions is less than 100 W/m^2. At 22.5 m, in figure 4.5b, the power density from directions North-West, West and South-West are respectively 135 W/m^2, 160 W/m^2 and 130 W/m^2. Wind from the East direction has still a power density lower than 100 W/m^2. Increasing the height of 7.5 m can considerably increase the wind power density. Comparing the power density from the South-West direction, there is an increase of 24% with the increase of height.

4.5 Wind shear and terrain roughness

The wind shear profile of the site can be estimated using the log law. As measurements data are available at 2 heights, the variation of the wind speed with the height at the measurement site can be determined. Table 4.4 shows the roughness height, z_0, and the friction velocity, V^*, that were computed in Diksmuide based on equations 4.4 and 4.5 with wind speed data recorded at 2 heights, z_1 and z_2.

Site	z_1 (m)	z_2 (m)	z_0 (m)	V^* (m/s)
Diksmuide	10	15	0.42	0.33

Table 4.4: Wind speed measurements done at z_1 and z_2 allowed to compute the roughness height z_0 and the friction velocity V^* for Diksmuide.

The roughness height z_0=0.42 m fits well with what it said by the literature (see table 4.5). Trees and farm buildings located close to the wind mast can impact the flow of the wind. Furthermore, the presence of cattle during long periods of time just next the measurement mast could also be a cause of increased roughness height.

Terrain description	z_0 (m)
Very smooth, ice or mud	0.00001
Calm open sea	0.0002
Blown sea	0.0005
Snow surface	0.003
Lawn grass	0.008
Rough pasture	0.01
Fallow field	0.03
Crops	0.05
Few trees	0.1
Many trees, hedges, few buildings	0.25
Forest and woodlands	0.5
Suburbs	1.5
Centers of cities with tall buildings	3.0

Table 4.5: Surface roughness z_0 for various types of terrain (Manwell et al. 2009).

Based on the results of table 4.4 and using equation 4.6, the wind shear profile of the measurement site was computed. The result is presented in figure 4.7. According to the results presented in table 4.2, wind speed at 10 m is 3.9 m/s, at 15 m is 4.3 m/s and extrapolated to 22.5 m, the wind speed is 4.8 m/s.

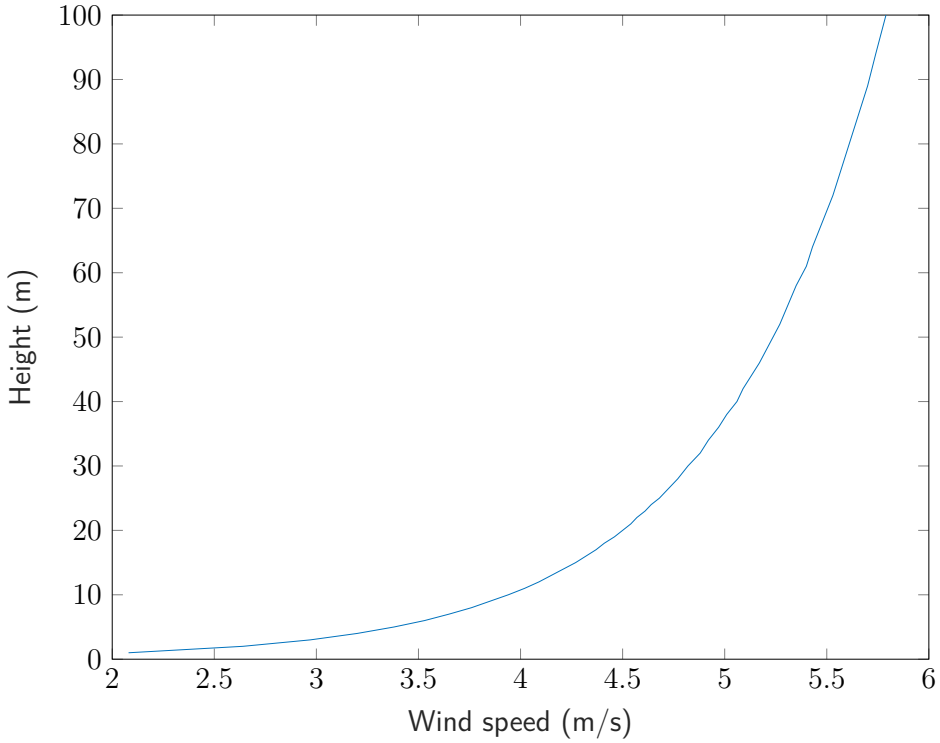

Figure 4.7: Wind shear profile for Diksmuide determined with the log law and the parameters of table 4.4.

4.6 Power Spectral Density

The fluctuations in the wind can be seen as a composition of sine waves with different frequencies and amplitudes. A function characterizing the power in a signal as a function of the frequency is known as the Power Spectral Density (PSD) (Mur-Amada & Bayord-Rujula 2010). As explained in section 1.4, the power spectral density function shows the strength of the variations in power as a function of the frequency. It shows at which frequencies strong and weak variations occur. Even if the sample of data seem to be stochastic, such as with wind speed data, a PSD analysis can be useful to know amplitudes and frequencies of oscillatory signals. The power spectral density function for the wind speed in Diksmuide is shown in figure 4.8.

The peak at 1 cycle per day (cpd) shows that a strong variation in wind speed occurs once a day. This peak represents typically the diurnal variation of the wind speed. On the left of this peak, no seasonal nor other macro-meteorological variation can be highlighted on this graph. On the right of the peak, 2 smaller peaks seem to appear at a frequency of 2 to 3 times per day. Further on the right, the turbulence do not carry a lot of energy as we can see that the PSD is decreasing with frequency. A more detailed analysis of daily energy production will be presented in section 6.4.2.

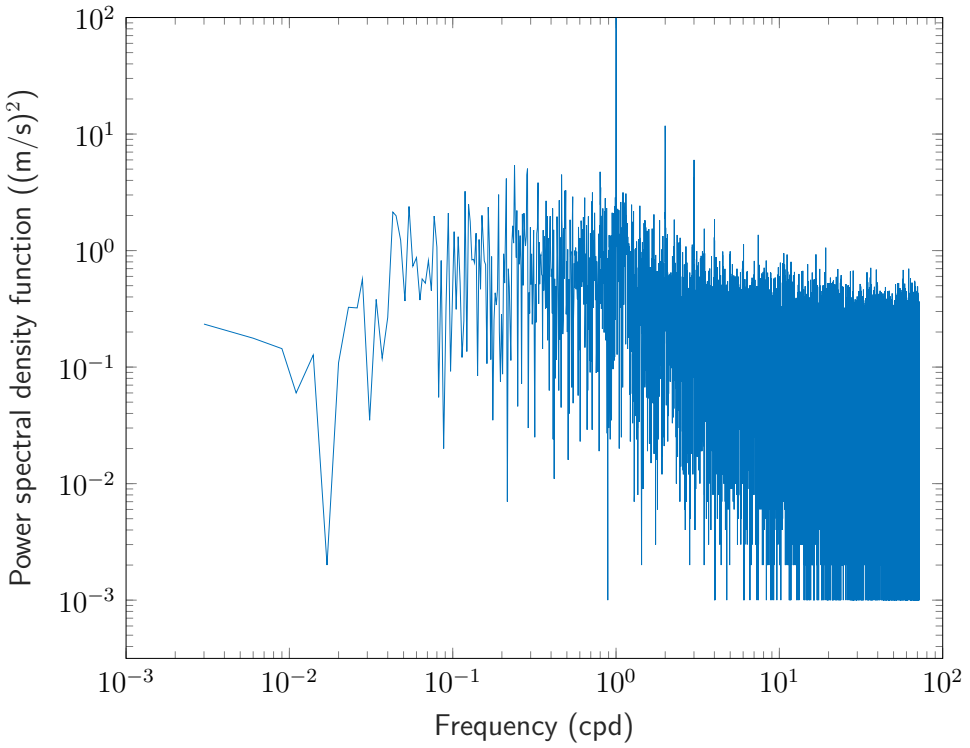

Figure 4.8: Power spectral density function of the wind speed expressed as $PSD(f) \cdot f$.

4.7 Measure Correlate Predict

The lifetime of the wind turbine is 25 years. On the other hand, wind conditions are recorded for 1 year. In turn, the seasonal variations on the site are recorded and this is what is recommended by the literature (Taylor & al. 2004). But wind conditions vary also between years. Therefore, measuring during a period of 1 year is not enough to cover the wind condition variations during the lifetime of the wind turbine. To avoid measuring data for multiple years, the Measure-Correlate-Predict (MCP) approaches are used.

The MCP is a statistical technique aimed at *predicting* long term wind conditions at a target site by *measuring* short term data at the target site and by *correlating* them to concurrent data at a reference site. The reference site should be a place where wind conditions have been recorded for a longer period of time. Practically, those reference sites are often meteorological stations. In these stations, wind data are usually available for more than 10 years.

The goal of the methods consists in finding parameters that describe the correlation between the target and the reference sites and to apply those parameters on the long-term wind data set, to predict wind conditions on a longer period at the target site (Vermeir 2015).

4.7.1 Determination of the reference site

As the wind data from Belgian meteorological stations are not freely available on the Internet, it was decided to use data from the Dutch national weather service, the Royal Netherlands Meteorological Institute (KNMI). The closest Dutch meteorological station, situated in Westdorpe, was chosen as the reference site. Diksmuide and Westdorpe are approximately 70 km apart (see figure 4.9). Wind data at 10 m height were compared since they were available at this height in both sites (Diksmuide and Westdorpe).

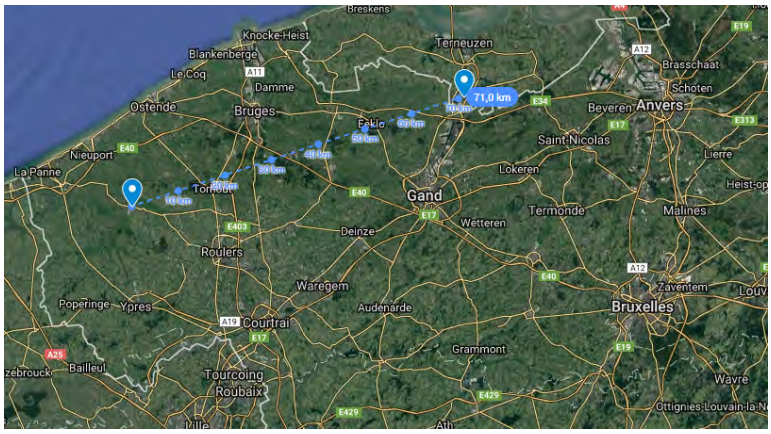

Figure 4.9: Maps and distance between Diksmuide (left) and Westdorpe (right).

4.7.2 Different MCP techniques

There exist different MCP techniques. Rogers et al. (2005) compared the performance of 4 of them, i.e. three linear regression techniques and the variance-ratio approach. Vermeir (2015) did it also. They both concluded that the variance-ratio technique was the most accurate approach. Rogers et al. (2005) also concluded that the most useful data length was about 9 months. As wind conditions were measured for 1 year, the measurement period is long enough and covers the seasonal variations. Therefore, it was decided to apply the variance-ratio MCP technique to predict the wind resource at target site (i.e. Diksmuide).

4.7.3 Presentation of the variance-ratio MCP approach

The relationship between the wind speed at the target site and the wind speed at the reference site can be expressed as

$$\widehat{V}_{\text{tar}} = \alpha V_{\text{ref}} + \beta \tag{4.10}$$

where $\widehat{V}_{\text{tar}}$ is the predicted wind speed at the target site (Diksmuide), V_{ref} is the wind speed at the reference site (Westdorpe), α and β are respectively the slope and the intercept. The variance ratio approach imposes to compute the parameters α and β as

$$\alpha = \frac{\sigma_{\text{tar}}}{\sigma_{\text{con}}} \tag{4.11}$$

$$\beta = \overline{V}_{\text{tar}} - \alpha \overline{V}_{\text{con}} \tag{4.12}$$

where σ_{tar} and σ_{con} are the standard deviation at the target and reference site for the concurrent measurement period.

Other MCP methods use linear regression. Linear regression is often used and well known. In turn, it can be easily implemented using available software and are accurate. In those linear regression techniques, the parameters α and β are determined in a least-squares way for the concurrent measurement period. Equation 4.10 is then used to predict the long-term wind conditions at the target site. Using those regression methods, the overall mean of the observed values at the target site, $\bar{V}_{\text{tar}}$, should be close to the overall mean of the predicted ones, $\widehat{V}_{\text{tar}}$. But the variance of the predicted wind speed will smaller than the one of the observed wind speeds. This can result in biased wind speed distribution predictions and in turn, impact the estimated AEP. That is why the variance ratio technique forces variance of the estimated wind speed at the target site to be equal to the measured variance at this same target site. Indeed, for a linear model of the form of 4.10, we have:

$$\sigma^2(\widehat{V}_{\text{tar}}) = \sigma^2(\alpha V_{\text{ref}} + \beta) = \alpha^2 \sigma^2(V_{\text{ref}}) \tag{4.13}$$

and therefore imposing 4.11 ensures

$$\sigma^2(\widehat{V}_{\text{tar}}) = \sigma^2(V_{\text{ref}}) \tag{4.14}$$

4.7.4 Long-term wind potential of the test site - Diksmuide

Long term wind data of the reference site, Westdorpe, were taken on 25 years (i.e. the lifetime of the wind turbine), from March 2003 until March 2018.

To estimate the long term wind speed at the target site (Diksmuide), the parameters α and β had to be computed for each of the 12 wind directions. For illustration, the scatter plot of the 1h averaged wind speeds of Diksmuide as a function of the concurrent 1h averaged wind speeds in Westdorpe is available in figure 4.10. The wind speeds in Westdorpe were only available rounded to unity. Equation 4.10 was then used to compute the long term wind speed in Diksmuide at 10 m height. Equation 4.6 was applied to compute the long term wind speed in Diksmuide extrapolated to 2 different hub heights: 15 and 22.5 m. The results are gathered in tables 4.6 and 4.7.

The mean wind speed in Diksmuide at 10 m during the measurement period was 3.92 m/s (see table 4.2). As the long term mean wind speed in Diksmuide at the same height is 3.66 m/s, it shows that the wind in Diksmuide during the period from March 2017 until March 2018 was stronger than it used to be on the last 25 years. The coefficient of correlation, r, a coefficient, comprised between -1 and 1 and measuring the degree of (linear) relation between 2 variables, was computed and is shown in table 4.6. The high value of r=0.8662 shows that wind speeds on both sites were strongly correlated during the measurement period.

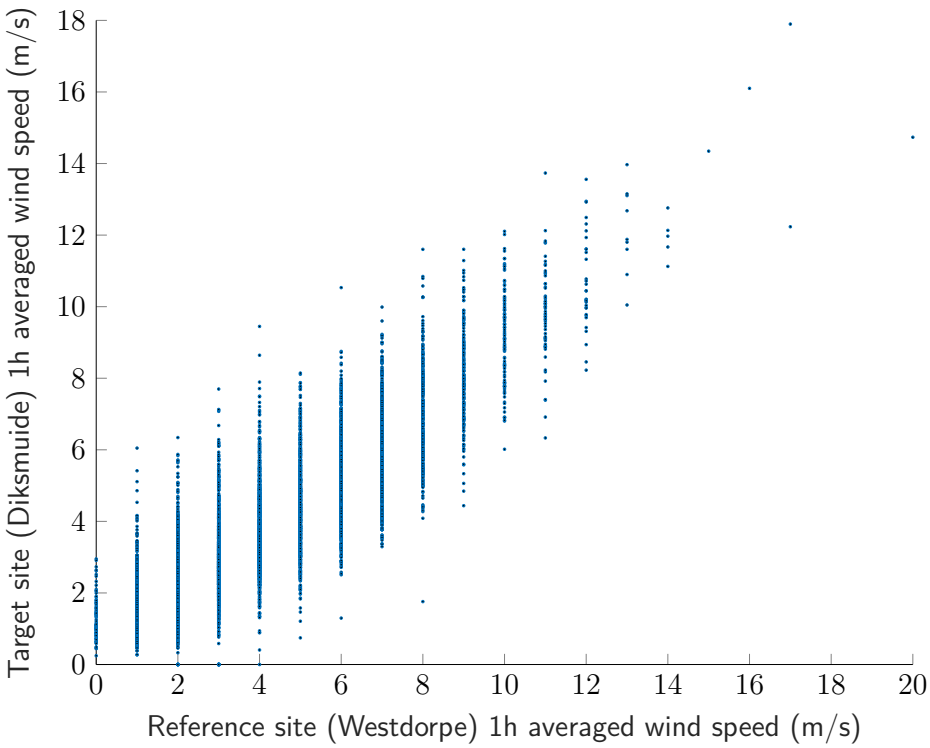

Figure 4.10: Scatter plot of the 1h averaged wind speeds at the target site (Diksmuide) as a function of the concurrent 1h averaged wind speeds at the reference site (Westdorpe).

Target site	Reference site	r	$\overline{V}_{\text{Measured}}$ (m/s)	$\overline{V}_{\text{Long-term}}$ (m/s)	Height (m)
Diksmuide	Westdorpe	0.8662	3.92	3.66	10

Table 4.6: Results of the variance ratio MCP method for the measurement site (Diksmuide).

Target site	z_0 (m)	$\overline{V}_{10}$ (m/s)	$\overline{V}_{15}$ (m/s)	$\overline{V}_{22.5}$ (m/s)
Diksmuide	0.42	3.66	4.13	4.60

Table 4.7: 25-year averaged wind speed extrapolated to 2 different hub heights.

Chapter 5

Estimation of the Annual Energy Production

Generally speaking, the market of small to medium wind turbine is still immature. It means that there is substantial discrepancies between turbine producers and that it is not rare that a small wind turbine, even in windy conditions, does not produce a significant amount of electricity (Simic et al. 2012, Vermeir 2015). The power curve and the Annual Energy Production (AEP) as a function of the mean wind speed of the small wind turbine Enair E70 installed on the site are available in the user manual of the manufacturer (Enair 2017*a*) (see appendix A). To check whether the device was producing the expected quantity of energy, it was decided to compute its actual power curve and the AEP. The AEP was evaluated first using directly power data, secondly following the instructions provided by IEC (2005), i.e. using the actual power curve and the Rayleigh probability density function. Comparison between actual and expected power performance and AEP was done. The Coefficient of Performance (C_p) as a function of the wind speed was also computed. Finally, some paths aimed to explain the mismatch between actual and manufacturer data are presented.

5.1 Basics about AEP prediction

The AEP can be computed with the following expression:

$$E = 8760\overline{P} \qquad \text{(J or Wh)} \tag{5.1}$$

The mean power, $\overline{P}$, can be determined by directly using available data, i.e. averaging all the power data over the total number of data.

$$\overline{P} = \frac{1}{N}\sum_{i=1}^{N} P(V_i) \qquad \text{(W)} \tag{5.2}$$

where $P(V_i)$ is the power produced by the wind turbine when the wind speed is V_i.

Having a reliable power curve of the wind turbine also allows to estimate the AEP. The IEC standard (IEC 2005) recommends to combine the detailed power curve of the wind turbine

and the hub height wind measurements at the given site. The mean power of the turbine is then computed as follow:

$$\overline{P} = \int_V P(V)\varphi(V)dV \tag{5.3}$$

with V the wind speed (m/s), $P(V)$ the power curve (kW) and $\varphi(V)$ the probability density function of the wind speed.

5.2 Different methods of AEP estimation

Different methods exist to estimate the AEP of a wind turbine on a site. Where too simplistic methods give a totally wrong estimation of the AEP compared to the direct use of data, some more sophisticated methods have shown more accuracy.

5.2.1 Example of an inaccurate AEP estimation method based on the rated power and a capacity factor

A simple method to estimate the mean power $\overline{P}$ of a wind turbine is to use a capacity factor, C_F:

$$\overline{P} = P_{\text{rat}} C_F \tag{5.4}$$

The capacity factor can be constant (Met Office & Entec 2008) or depend on the annual average wind speed of the specific site (Renewable Energy Research Laboratory 2002). Vermeir (2015) compared this method to a direct use of power data and concluded to a general underestimation of the AEP. It makes sense because the capacity factor takes into account only the mean wind speed on site and the individual performance of a wind turbine below rated power has no influence on the AEP estimation.

In general terms, the rated power is a bad indicator of the AEP. First because different definitions are used to define the rated power of a wind turbine. Where some standards define the rated power as a function of the rated speed (AWEA 2009), IEC (2005) defines it as a "quantity of power assigned, generally by a manufacturer, for a specified operating condition of a component, device or equipment". Secondly, the AEP depends on the power curve and on the wind distribution on the test site. Therefore, on a site with a high probability of low wind speed, a wind turbine with a high rated power will produce less electricity than a wind turbine with a lower rated power but with better performances at low wind speeds (see Vermeir (2015)).

5.2.2 AEP estimation based on the IEC standard

The standard IEC (2005) provides a method to determine the AEP for annual average wind speeds of 4, 5, 6, 7, 8, 9, 10 and 11 m/s and can be linearly interpolated for non-integer values of wind speed. The main assumption of the computation is that the wind speed is Rayleigh-distributed. The accuracy of this method was also compared to the direct use of

data for the AEP estimation by Vermeir (2015) and a good overall agreement was showed. The results pointed out that the AEP error was less than 10 % if the difference between the standard deviation of the measurement site, σ_{site}, and the standard deviation imposed by the Rayleigh distribution, σ_{ray}, (which is proportional to the mean wind speed: $\sigma_{\text{ray}} = 0.528\overline{V}$) was less than 10 %. For the case of Diksmuide, $\sigma_{\text{site}} = 2.2727$ and $\sigma_{\text{ray}} = 2.2417$, resulting in a deviation of 1.4%.

Therefore, this method was chosen to compute the AEP of the wind turbine in Diksmuide.

5.3 Derivation of the measured power curve

The method provided by the standard IEC (2005) to compute the AEP also provides the instructions to build the real life power curve of a wind turbine. These instructions will be followed in this section. However, some freedoms will sometimes be taken in order to produce the most representative power curve of the wind turbine on the measurement site of Diksmuide. These deviations from IEC (2005) will be clearly mentioned.

5.3.1 Gross data

To build the power curve, the simultaneous measurements of the wind speed and of the electrical power produced are needed. The net active electric power generation data from the wind turbine (i.e. "the wind turbine electric power output that is delivered to the electric power network" (IEC 2005)) [1] were available on irregular 5 minutes averages, not necessarily at the same instants than the wind speed. Therefore, power generation data were interpolated for every minute in order to be able to associate the 10 minutes wind speed averages. An example of the interpolation of the power as a function of time during 3 days in March 2017 is shown in the figure 5.1.

The figure 5.2 illustrates the concurrent measurements of the power generation and of the wind speed during 2 hours.

As a second step, to ensure non corrupted data and "that only data obtained during normal operation of the turbine were used" (IEC 2005), some measurements had to be rejected. Data for which the power produced by the wind turbine was zero and the wind speed was greater than 5 m/s were discarded. In this way, abnormal working conditions during which enough wind was available but where the wind turbine was not producing any electricity were not taken into account. No other data were rejected as it is assumed that the wind turbine was operating normally during the whole period of measurement. No specific report of the farmer indicated that the wind turbine was stopped or was in abnormal working conditions.

IEC (2005) also indicates that wind data coming from directions having significant obstacles (like buildings, trees, wind turbines) should be discarded as it can distort the wind flow. It was not done in this study because the goal of this site assessment is to have the most representative situation of the site, taking into account all the obstacles. Furthermore, the *Site Expérimental pour le Petit Eolien National* (SEPEN), the site for independent testing of

[1] The power data were available on the monitoring website of the wind turbine (Ginlong Technologies 2018).

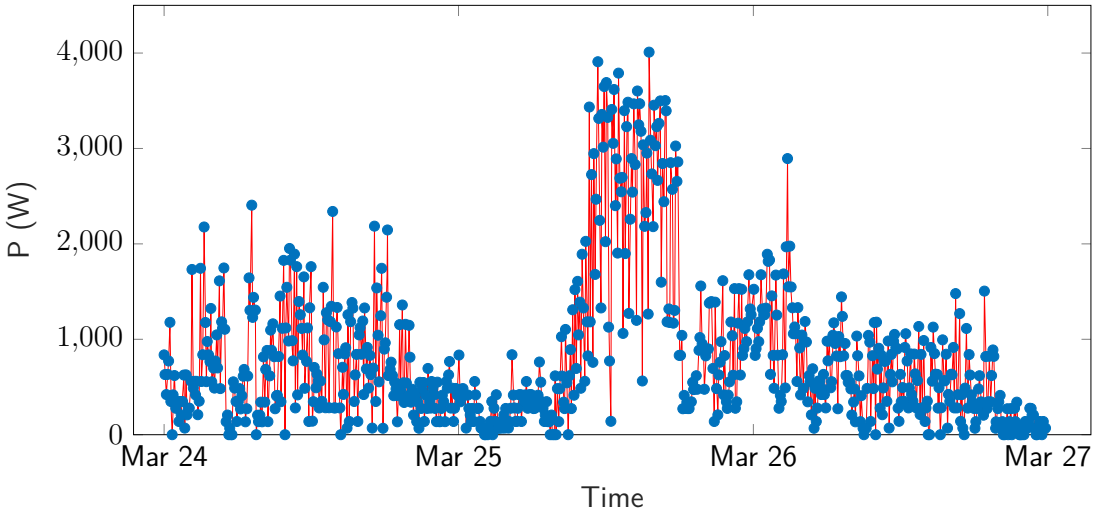

Figure 5.1: Power produced by the wind turbine during the 24th, 25th and 26th of March 2017. Blue points are measured data and red line represents the 1 minute interpolation.

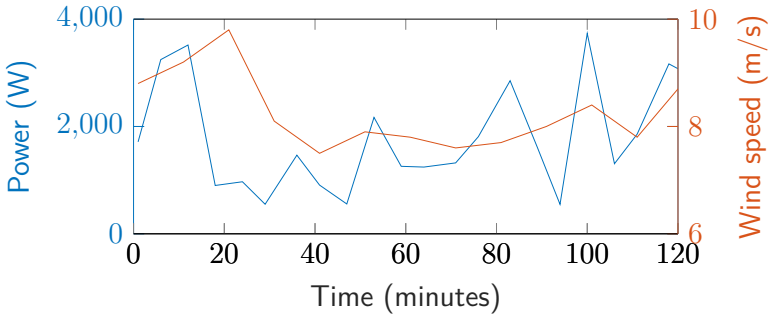

Figure 5.2: Simultaneous measurement of the power produced by the wind turbine and of the wind speed during 2 hours.

small wind turbines in France, usually takes into account only the influence of the neighboring wind turbines in a wind park (SEPEN 2010*c*, 2014*b*).

5.3.2 Data normalization

The third step consists in the normalization of the data. The selected data sets shall be normalized to the sea level air density, referring to ISO standard atmosphere (1.225 kg/m^3). The derived 10 minutes averaged air density can be computed as follow:

$$\rho_{10\text{min}} = \frac{p_{10\text{min}}}{R_0 T_{10\text{min}}} \tag{5.5}$$

with $\rho_{10\text{min}}$, the derived 10 minutes averaged air density, $p_{10\text{min}}$, the measured air pressure averaged over 10 minutes, R_0, the gas constant of dry air (287.05 J/(kgK)) and $T_{10\text{min}}$, the measured absolute air temperature averaged over 10 minutes.

Data normalization has to be applied as follow:

- For the power:

$$P_{\mathsf{n}} = P_{10\mathsf{min}} \frac{\rho_0}{\rho_{10\mathsf{min}}} \tag{5.6}$$

  where P_{n} is the normalized power output, $P_{10\mathsf{min}}$ is the measured power averaged over 10 minutes and ρ_0 is the reference air density (1.225 kg/m^3).

- For the wind speed:

$$V_{\mathsf{n}} = V_{10\mathsf{min}} \left(\frac{\rho_{10\mathsf{min}}}{\rho_0} \right)^{\frac{1}{3}} \tag{5.7}$$

  where V_{n} is the normalized wind speed and $V_{10\mathsf{min}}$ is the measured wind speed averaged over 10 minutes.

5.3.3 Determination of the measured power curve

To derive the measured power curve, the method of bins[2], using 0.5 m/s bins, centered on multiples of 0.5 m/s, has to be applied to the normalized data sets. The values of the wind speed and of the power output in each wind speed bin are computed as follow:

$$V_i = \frac{1}{N_i} \sum_{j=1}^{N_i} V_{\mathsf{n},i,j} \tag{5.8}$$

$$P_i = \frac{1}{N_i} \sum_{j=1}^{N_i} P_{\mathsf{n},i,j} \tag{5.9}$$

where V_i is the normalized and averaged wind speed in bin *i*, $V_{\mathsf{n},i,j}$ is the normalized wind speed of data set *j* in bin *i*, P_i is the normalized and averaged power output in bin *i*, $P_{\mathsf{n},i,j}$ is the normalized power output of data set *j* in bin *i* and N_i is the number of 10 minutes data sets in bin *i*.

5.3.4 Actual power curve

The measured power curve, called hereafter actual power curve, is shown in figure 5.3 as well as the number of data available per each wind speed bin. The error bars in blue are indicators of the dispersion of the measures. They show the limits towards plus and minus one standard deviation. The power curve provided by the manufacturer of the wind turbine Enair E70 is plotted on the same figure for a comparison.

The actual power curve, the manufacturer power curve and the number of data sets per bin are also available in table B.1. There, the bins that do not gather the minimum amount of data in order to be representative are highlighted in red: 16.5, 17 and 17.5 m/s. Bin centered

[2]The method of bins is defined by IEC (2005) as a "data reduction procedure that groups test data for a certain parameter into wind speed intervals (bins)."

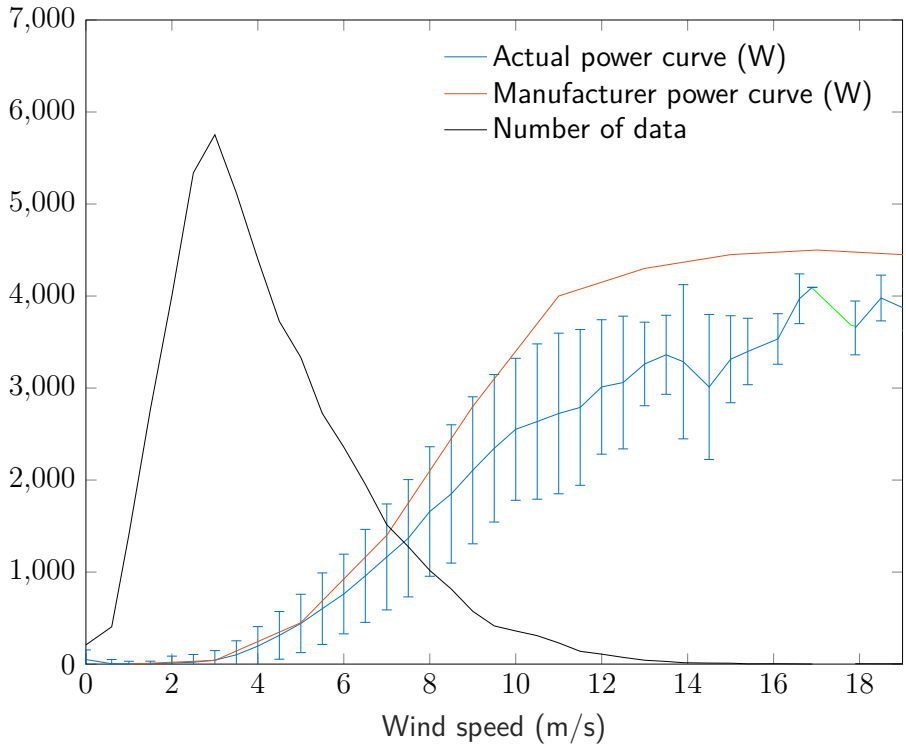

Figure 5.3: Comparison between the power curve of the manufacturer and the actual power curve with its error bars (corresponding to 1 standard deviation) of the Enair E70 small wind turbine in Diksmuide. Bins without data were interpolated in green.

around 17 and 17.5 contain respectively 1 and 0 data. That is why this section of the power curve on figure 5.3 is drawn in green and that no error bars are drawn. The value of the power output for wind speed of 17.5 m/s was linearly interpolated as advised in IEC (2005). The value of the manufacturer power curve are given in the last row of table B.1. The values in bold are the ones really given by the manufacturer. The other values in this last row were linearly interpolated. The deviations in percent given in the following paragraph are computed based on these values explicitly provided by the manufacturer.

Based on these results, 3 categories of wind speed in this comparison of power curves can be identified. Low wind speeds (3-5 m/s), medium wind speed (7-15 m/s) and large wind speeds (17-19 m/s). For low wind speeds, both power curves are matching with even an over production at 3 m/s of 6.5 % compared to the prediction of the manufacturer. For medium wind speeds the actual power curve is lacking what the manufacturer predicted. For these wind speeds, the actual performance of the wind turbine is between 17% (at 7 m/s) and 32% (at 11 m/s) below the performance ensured by the manufacturer. For large wind speed, the actual performance of the wind turbine is only between 9 and 11% below the prediction of the manufacturer.

It should be noted that IEC (2005) precises explicitly that for a bin to be representative, it should contain a minimum of 30 minutes of sampled data, which corresponds to a number

of 3 data sets of 10 minutes.

5.4 Annual Energy Production

This section presents the results of the AEP estimated in 2 different ways. First, the AEP from March 2017 until March 2018 was computed directly using power data. Secondly, the AEP for different mean wind speeds were estimated following the rules of IEC (2005). Finally, the results will be compared.

5.4.1 AEP estimation based on the direct use of data

The computation of the mean power can be done using equation 5.2. This simple method allows to have the most accurate estimation of the AEP on the specific site of Diksmuide. The result is shown in table 5.1.

Site	Height (m)	Mean wind speed (m/s)	Mean power (W)	AEP (kWh)
Diksmuide	15	4.25	444.88	3897

Table 5.1: AEP estimation based on the direct use of data (using equations 5.2 and 5.1) of the small wind turbine Enair E70 in Diksmuide during the measurement period.

For a mean wind speed of 4.25 m/s, the manufacturer of the wind turbine predicted an AEP of 4650 kWh (see table 5.2, by linearly interpolating data between 4 and 5 m/s). In other words, the wind turbine produced 16% less energy than expected between March 2017 and March 2018.

5.4.2 AEP estimation using statistical wind distributions

The AEP estimation method presented in section 5.4.1 is the most accurate and is taken as a reference to compare other AEP estimation techniques. IEC (2005) also provides a method to compute the AEP and its accuracy was already discussed previously (see section 5.2.2).

The measured power curve is applied to different wind speed frequency distributions. In this case, the Rayleigh distribution is used. Indeed, the Rayleigh distribution is identical to the Weibull distribution with a shape factor $k = 2$. By fixing the shape factor, the Rayleigh distribution is only a function of the scale factor c which, in turn, depends only on the mean wind speed (see equation 1.9). IEC (2005) specifies that the "AEP estimations shall be made for hub height annual average wind speeds of 4, 5, 6, 7, 8, 9, 10 and 11 m/s according to the equation:"

$$AEP = N_h \sum_{i=1}^{N} [\Phi(V_i) - \Phi(V_{i-1})] \left(\frac{P_{i-1} + P_i}{2} \right) \tag{5.10}$$

where AEP is the annual energy production (kWh), N_h is the number of hours in one year ($\approx$ 8760 (h)), N is the number of bins, V_i is the normalized and averaged wind speed in bin *i* and P_i is the normalized and averaged power output in bin *i*.

and

$$\Phi(V) = 1 - \exp\left(- \frac{\pi}{4} \left(\frac{V}{\overline{V}} \right)^2 \right) \tag{5.11}$$

where $\Phi(V)$ is the Rayleigh cumulative probability distribution function for wind speed, $\overline{V}$ is the annual average wind speed at hub height and V is the wind speed.

The results of the AEP estimation based on the method provided by IEC (2005) are shown in table 5.2.

Estimated Annual Energy Production			
Hub height annual average wind speed (m/s)	AEP based on the actual power curve (kWh)	AEP of the manufacturer (kWh)	Deviation (%)
4	3361	3900	13.8
5	5870	6900	14.9
6	8567	10000	14.3
7	11141	14300	22.1
8	13344	17700	24.6
9	15009	20000	25.0
10	16089	22500	28.5
11	16629	23700	29.8

Table 5.2: Table showing the comparison between the evolution of the AEP computed following the recommendations of IEC (2005), based on the actual power curve ('Actual AEP') with the mean wind speed, and the evolution of the AEP of the manufacturer with the mean wind speed. The deviation between both estimations is also given.

By linearly interpolating data from table 5.2, the AEP for a mean wind speed of 4.25 m/s is 3988 kWh. Compared to the AEP computed in section 5.4.1 with direct use of data, 3897 kWh, the deviation is only of 2.5 %. It shows that the AEP estimation method provided by the IEC (2005) is accurate and trustworthy compared to the AEP predictions of the manufacturer.

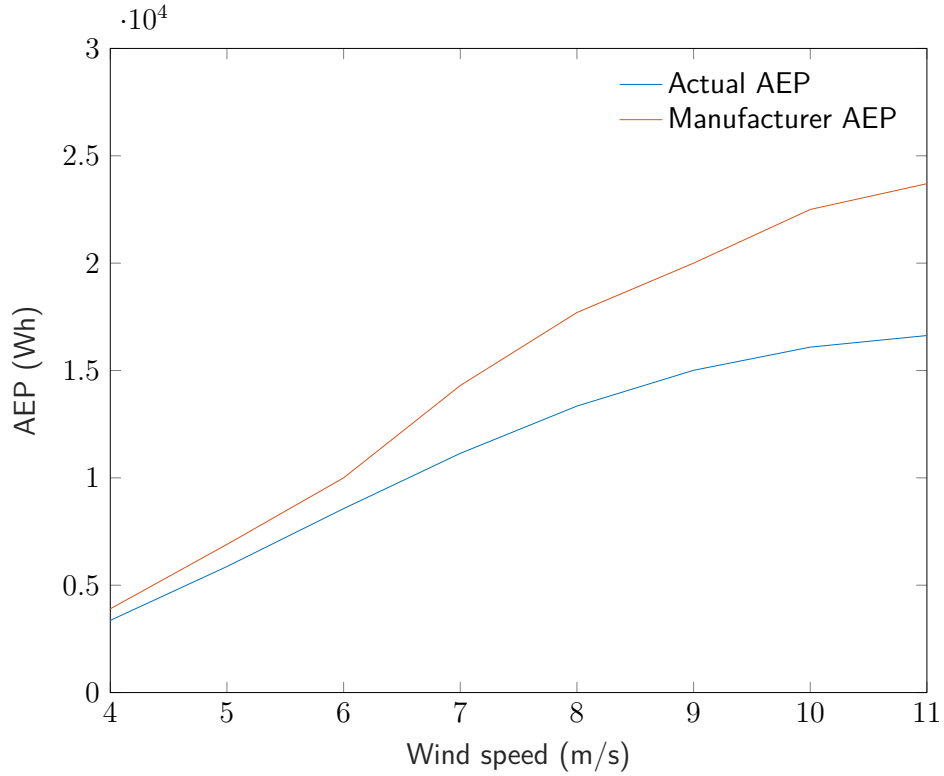

Figure 5.4: Plot showing the comparison between the evolution of the AEP computed following the recommendations of IEC (2005), based on the actual power curve ('Actual AEP') with the mean wind speed, and the evolution of the AEP of the manufacturer with the mean wind speed.

5.5 Coefficient of performance

The coefficient of performance, C_p, of the wind turbine in Diksmuide as a function of the wind speed is plot in figure 5.5 and is listed as function of the wind speed in table B.1. The value of the C_p for bins without data available, at 17.5 m/s, was interpolated and can be seen in green in figure 5.5. The C_p reaches its maximum value of 41% at 5.5 m/s and is above 25% from 3.5 to 10.5 m/s. Even if it does not reach the 50% mentioned in 1.1 (which is a C_p reachable for big wind turbines), 41% is a high value compared to other small wind turbines. When checking the reports of the SEPEN, small horizontal axis wind turbines (with a rater power up to 12 kW) have C_p ranging between 26.2% and 37.1% (SEPEN 2010*a*,*c*, 2011*a*,*b*, 2012, 2013*c*,*b*, 2014*b*,*a*, 2013*a*, 2010*b*). Small vertical axis devices (up to 10 kW) have smaller C_p ranging from 11% up to 26.3% (SEPEN 2009, 2011*c*, 2013*d*).

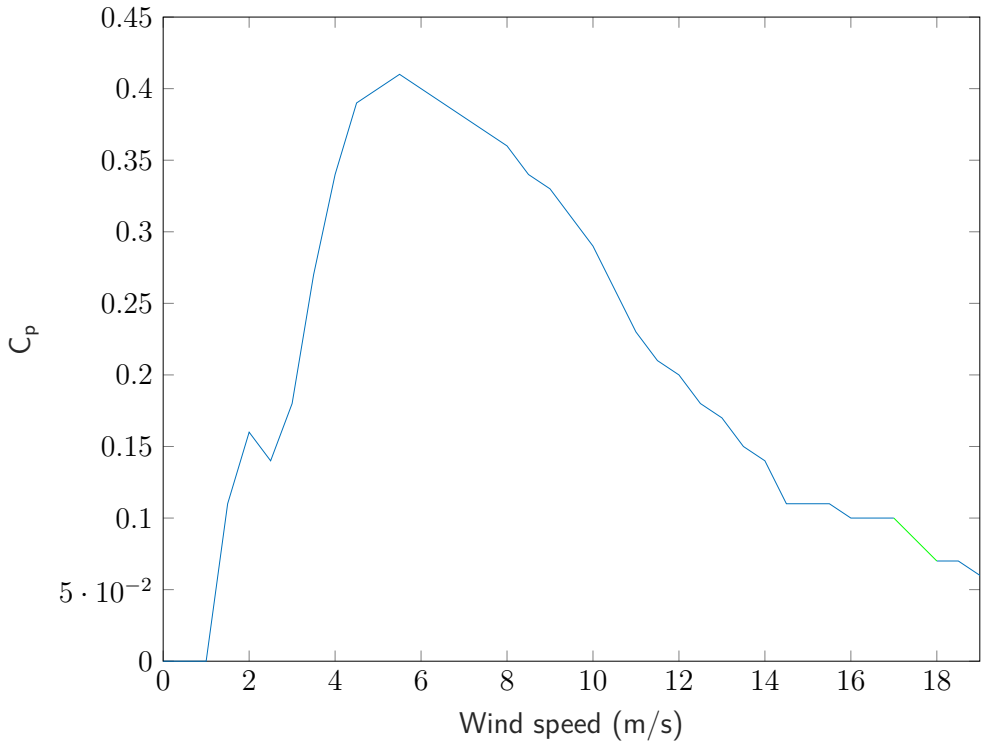

Figure 5.5: C_p at sea level air density 1.225 kg/m^3 as a function of the wind speed. Bins without data (17.5 and 20 m/s) were interpolated in green.

5.6 Investigations about the difference of performance between the actual production and the manufacturer one

It has to be noticed that the energy production of the wind turbine Enair E70 is not matching the energy production predicted by its manufacturer. For the AEP, the mismatch increases with the wind speed from 4 up to 11 m/s. The mismatch between the measured power curve and the one provided by the manufacturer showed already that the wind turbine was not producing what it was expected from it, according to the manufacturer. Some ideas to explain this difference of performance are presented below.

First element that could explain the difference between the measured and the manufacturer's power curve is the level at which power data were recorded. As mentioned in section 5.3.1, the net active electric power generation data from the wind turbine were recorded to draw the power curve. The manufacturer could possibly have measured power data just at the output of the wind turbine. Acting in this way, the power losses from the AC/DC and DC/AC converters are bypassed. Those converters have a certain efficiency (Blackledge et al. 2013) and convert an AC variable frequency voltage into a fixed AC voltage at 50 Hz. The electrical efficiency encompasses electric power losses at different levels: generator, converter, switches, controls and cables. For small wind turbines, the electrical efficiency ranges usually

between 60 and 70%. The larger the generator rating, the larger the electrical efficiency (de Vries 2008). This observation highlights the important role played by the power electronic technology in the integration of distributed and renewable energy sources into the electrical grid (Kumar et al. 2016).

Another type of explanations that could explain the performance differences between the manufacturer and the measured ones lies in the wind conditions. Performance assessments performed by the manufacturer could have been done in stable and optimal conditions. The wind turbine could have been placed and fixed in a wind tunnel with constant wind speed and direction, optimally oriented. These conditions are obviously not representative of real on-field conditions. Real conditions are characterized by a certain level of turbulence and wind gusts. Turbulence is known to impact power performance of small wind turbines. Furthermore, small wind turbine are more subjected to turbulence phenomenons since they are placed near buildings, trees and obstacles. In general, turbulence levels impact negatively the AEP. However, the effects of turbulence on power output is hard to generalize and in some cases it could even contribute to increase the power production of small wind turbine at certain wind speeds (Lubitz 2014). Using Computational Fluid Dynamics (CFD) could give insight about the behavior of air flows in the location of the wind turbine, the influence of the buildings, terrain and other obstacles. At the end, such an analysis could propose an optimized location to place the wind turbine.

Another effect linked to the level of turbulence is the orientation of the wind turbine towards the wind direction.The airflow inclination affects the performance of the wind turbine. For horizontal axis wind turbines the power output varies according to the $\cos^2$ of the relative wind angle (Pedersen 2004). Small wind turbines subjected to gusts and high level of turbulence are likely to be operating with the turbine not perfectly aligned with constantly changing wind directions. It highligts the important role of the rudder of the wind turbine (see figure 3.7a). This effect is not taken into account when the wind turbine is tested in stable and optimal conditions. Furthermore, a small inclination of the wind turbine, due for instance to a bad mounting of the device, can have significant impact on the power performance of the device.

As mentioned in section 4.1, due to the slip of the mast, wind speed had to be extrapolated from December 2017 to March 2018. Extrapolation induces a level of uncertainty in the data. It is possible that the extrapolated wind speeds of this period of the year contributed to a lowering of the performance assessment of the wind turbine. However, for an extrapolation of 2 m, the error will remain limited. In the same order of ideas, power data were interpolated in order to have concurrent power and wind data to draw the power curve (see figure 5.1). Uncertainty introduced by this interpolation could also have lead to errors in the assessment of the performance of the wind turbine.

Chapter 6

Economic feasibility of the small wind turbine on the test site

Investing in renewable energy sources should be profitable. As the market of small wind turbines is still young, the profitability of small wind projects is not yet demonstrated. Important parameters influencing the economic feasibility of small wind turbines projects are the prevailing wind speeds and the degree of urbanization (Grieser et al. 2015). It was proven for a long time that attractive net metering rules, high retail electricity rates and substantial buy-down program contributed to the shorten of the SPP and DPP. In turn, this could help speed the commercialization of grid-connected wind turbines (Forsyth et al. 1999).

With the long term wind speed in Diksmuide computed in section 4.7.4 and available in table 4.7 along with the estimation of the AEP as a function of the mean annual wind speed derived in section 5.4.2, the economic feasibility of the small wind turbine in Diksmuide was studied. As the economic assessment strongly depends on the mean wind speed but also on the incentives available in a geographical regions, this study is specific for Flanders.

Firstly, the cash flows and the economic parameters used in the computation of the LCOE, NPV, IRR, SPP and DPP were presented. After that, the results for farmers, SME and private users were presented and discussed. A sensitivity analysis about the sub mentioned parameters was conducted for the case of the farmer. A major assumption is that the electricity produced by the wind turbine is directly self-consumed by the farmer and not fed into the grid. Therefore, finally, investigations about the matching between electricity consumption and production on a monthly and then on a daily basis were conducted in order to check the pertinence of this assumption.

6.1 Economic parameters

6.1.1 Cash flows

Cash outflows

Investment The investment cost of the whole wind turbine project in Diksmuide was €15 000. This price comprises the purchase of the device but also the installation costs. The financial

situation of the farmer in Diksmuide is not known, but the assumption of an investment on its own account is made. Therefore, the buyer didn't apply for a loan generating interests. It should be noticed that the farmer acquired the mast separately from the turbine (at a lower price) and installed it himself. It lead to a lower investment compared to the situation in which the mast should be mounted by someone else. It is a real financial benefits since the costs for installation and foundation can reach up to one third of the entire investment for big on shore wind turbines (IRENA 2012).

Operation and Maintenance costs O&M for wind turbines are often estimated at 2% of the investment price per year (Chedid & Saliba 1996). This rate is considered to remain constant even if logic would recommend to increase it with time as the device is aging. The manufacturer ensures that the lifetime of the wind turbine is 25 years, where 20 years is customary used for small wind turbines (The European Wind Energy Association 2018, Vermeir 2015). However, 25 years will be considered for the lifetime of the project in this economic analysis as a longer period should allow to spread the costs and to give a better output for the economical analysis.

Taxes The tax rate is not the same for private users and for SME. Private users are subject to income taxes. A tax rate of 45% was chosen for private users and farmer. This tax rate takes into account the average income taxes as well as the potential municipality taxes (Mees 2017). SME are subject to corporate taxes (ISOC). The corporate taxes in Belgium have recently changed. Until 2017, the ISOC was 33.99%. The reform of the corporate taxes adopted in December 2017 imposes an ISOC of 29.58% for 2018 and 2019 and will continue to decrease to reach a level of 25% in 2020. SME will benefit of an ISOC of 20.4% for 2018 and 2019 and of 20% in 2020 on the 100,000 first euros (Mathieu 2018). To remain the most general possible, it was chosen to use a corporate tax rate of 33.99% for 2017, 29.58% for 2018 and 2019 and 25% from 2020 until the end of the lifetime of the wind turbine (2042). The taxes apply on the revenues generated by the sale of the green certificates and eventually by the sale of the surplus of electricity generated. However, as the monthly wind energy production is always lower than the monthly energy consumption (see figure 3.5), it was decided to consider that all the energy produced by the wind turbine is consumed in real time by the farmer (see section 6.4 for more information about this assumption).

Cash inflows

Energy not bought When producing its own energy, a user does not have to buy the electricity from the network. This represents a source of income for renewable projects (Mermuys 2010). It does not really consist in an income but it can be seen as money that does not need to be spent to buy energy. It is money saved compared to the situation without renewable energy source. This cash inflow will depend on the price of the electricity. For a private user, as the annual energy consumption of the farmer is roughly 11000 kWh, the electricity price for high consumer private users which is around €0.21/kWh (VREG 2016) will be considered. For SME, the average electricity price according to VREG (2017) is €0.22/kWh. In this economical analysis, it will be assumed that all the energy produced by the wind turbine is consumed in real time by the farmer (see section 6.4 for more information about this assumption).

Incentives Incentives received by farmers, SME and private users are not the same. The 3 of them can sell green certificates (which are taxable). Farmers can benefit from 'VLIF' and SME can, in some circumstances, request an increased investment deduction for renewable energy production.

- *Greencertificates (GC)* In Flanders, GC are used as a support for renewable energy technologies. Before January 2013, 1 GC was delivered for 1 MWh of green electricity produced. This incentive could be used for 10 years. Since January 2013, the GC can be used for 15 years and a banding factor was introduced to make distinction between technologies. This factor is recomputed every year and per technology. The banding factor from August 2016 to August 2017 for wind turbines was BF=0.743 (Vlaams Energieagentschap 2016). It means that 1 GC is delivered for 1.345 kWh. The minimum price for a GC is €93 (Agentschap Innoveren and Ondernemen 2018). A significant change in the GC policy happened recently. Since January 2018 wind turbines on land with a gross nominal power up to (and including) 10 kW are no longer eligible for GC (see appendix C and Agentschap Innoveren and Ondernemen (2018)). It is bad news for the sector of small wind turbines as the GC are a non negligible economic support. However, GC will remain for more powerful on land wind turbine and the support period will be increased to 20 years (Vlaams Energieagentschap 2018*a*).
- *VLIF* There is also VLIF investment support for farmers. A farmer can receive support for a wind turbine if a number of conditions are met. One of the conditions is that the investment should be minimum €15000. The amount of support depends on the extent to which the investments improve the sustainability of agricultural and horticultural production. For wind energy projects, the incentive reaches 30% of the investment. The upper limit of the support is €1000000 (Vlaamse overheid Departement landbouw & visserij 2018).
- *Support for SME* In certain circumstances a company can also claim the increased investment deduction for energy production on renewable energy. The amount of this deduction is 13.5% of the investment price, received at once (Vlaamse Energieagentschap 2018).

Other economic parameters

The other economic parameters were set in order to follow values frequently used in feasibility studies (Vermeir 2015, Mermuys 2010):

- Inflation of 2%
- Increase of the electricity price of 3.5% per year
- Discount rate of 4%

6.2 Results

The economic feasibility of installing a small wind turbine was done for farmers, SME and private users. The results are presented in this section.

Obviously, the economic profitability of a wind energy project strongly depends on the energy produced by the wind turbine and hence from the wind speed at hub height. Therefore, it was decided to consider an annual mean wind speed of 4.13 m/s as this was the long term wind speed computed for Diksmuide at 15 m high (see table 4.7). With this annual mean wind speed, the AEP of the wind turbine can be linearly interpolated from table 5.2 and an AEP of 3687.17 kWh/year was considered.

	Farmer	SME	Private
LCOE (€/kWh)	0.363	0.363	0.363
NPV (€)	3027	810	-1133
IRR (%)	6.0	4.5	3.4
SPP (years)	14	16	18
DPP (years)	19	24	>25

Table 6.1: Levelized Cost of Energy, Net Present Value, Internal Rate of Return, Static Payback Period and Dynamic Payback Period per category of users (farmer, SME and private) for a wind turbine project in Diksmuide with the wind turbine Enair E70.

The LCOE for this small wind turbine project is still high compared to the LCOE of other technologies. As a mean of comparison, in 2016 in Belgium, the LCOE of residential solar energy was comprised between 0.140-0.160 €/kWh and the one of on- and off-shore wind turbines was between 0.060-0.080 €/kWh (Meinke-Hubeny et al. 2017).

Table 6.1 shows that a wind turbine project like the one in Diksmuide is profitable for farmers and SME but not for private users. Under the stated conditions, the project can become profitable for the farmer after 19 years. SME should wait 24 years before earning money from the project and private users don't have financial interest to invest in a wind project under these conditions. Indeed, the IRR is smaller than the discount rate and therefore the dynamic payback period exceeds the lifetime of the wind turbine. What makes a substantial difference between these 3 cases is mainly the level of subsidy. Where a farmer can receive 30% of the investment as a financial support, there is no such financial help for private users. SME are in between these 2 extreme cases with a financial support of 13.5% of the investment price. With the end of GC for small wind turbine projects ($<$ 10 kW), the situation will even be worth.

6.3 Sensitivity analysis

Based on the case of the farmer, different economic parameters were varied to highlight their impact on the LCOE, NPV, IRR and payback periods. The results are presented in table 6.2. A variation of $\pm$ 10% was applied on the discount rate, inflation, electricity price, AEP, investment and O&M costs. As GC are coming to their end for small scale wind projects, the

situation without any GC was also analyzed. The situation with a constant electricity price was also investigated.

Economic parameter	Variation of the economic parameter	LCOE (€/kWh)	NPV (€)	IRR (%)	SPP (years)	DPP (years)
Discount rate	-10%	0.352	3747	6.0	14	19
	+10%	0.373	2353	6.0	14	20
Inflation	-10%	0.360	3164	6.1	14	20
	+10%	0.365	2887	6.0	14	20
Electricity price	-10%	0.363	1208	4.9	15	23
	+10%	0.363	4847	7.1	13	17
AEP	-10%	0.403	1052	4.7	15	23
	+10%	0.330	5002	7.2	12	17
Investment	-10%	0.326	4700	7.4	12	16
	+10%	0.399	1355	4.9	15	23
O&M	-10%	0.352	3616	6.4	13	19
	+10%	0.373	2439	5.7	14	20
No more GC	-100%	0.363	1469	5.0	16	23
Constant electricity price	-100%	0.363	-3069	0.9	22	>25

Table 6.2: Values of the LCOE, NPV, IRR and Payback periods for the case of the farmer when varying the discount rate, inflation, electricity price, AEP, investment and O&M costs by $\pm$ 10%, without any GC and with a constant electricity price.

From table 6.2 it can be seen that a variation of $\pm$ 10% of the AEP has a strong effect on the economic profitability of the small wind turbine project. If the AEP used to compute elements in table 6.1 was 10% underestimated, the project could become profitable after 17 years (instead of 19 years). On the contrary, if the AEP was 10% overestimated, the project will be profitable after 23 years (instead of 19 years). It leads also to the highest LCOE and to the second lowest NPV and IRR among all simulations.

Another parameter that influences a lot the economic feasibility of the project is the investment cost. With an investment lowered by 10%, the project could become profitable in 16 years, which is the shortest DPP among all simulations. Also the LCOE is the lowest one and the NPV and IRR are the largest one among all simulations done in table 6.2. This result shows the importance of a low investment price and also of financial support received at the beginning of the project (since it can be seen as a lowering of the investment).

Without any GC, the wind project would be profitable after 23 years instead of 19 years. In turn, it can be deduced that the situation for SME would not be economically viable. This result shows that GC are critical to allow small wind projects to be profitable.

As the evolution of the electricity price is difficult to estimate, a reference case considering constant electricity price during the life time of the wind turbine was considered. In this

case, the small wind turbine project is not profitable for the farmer. This simulation results in the worth results for the NPV, IRR and Payback periods among all simulations. This last case highlights the fact that such small wind projects can become economically interesting if increase of the electricity price is to be expected for the next years.

6.4 Further researches about the matching between consumption and production

A very general assumption done in this economical feasibility study is to consider that all the electricity produced by the wind turbine is instantaneously consumed and that no electricity is fed into the grid. Indeed, the energy production of renewable sources depends on the meteorological conditions and is therefore stochastic. Assuming that electricity is produced and available always when it is needed is not representing the reality. Furthermore, the PSD analysis conducted in section 4.6 with figure 4.8 showed that there was a substantial variation in power of the wind once a day. It should be verified that strong winds are available when energy consumption is significant. Therefore, it was decided to proceed in 2 steps, increasing in the granularity of the data. First, the monthly analysis of the daily and night energy consumption and wind energy production will be done. Increasing in precision, the second step consists in comparing the daily consumption needs and production possibilities through the wind turbine to see if both are matching or not.

6.4.1 Monthly comparison

The farmer has a two rate meter and read it every month. Therefore, the daily and night consumption per month were available. Daily consumption is considered for electricity consumed from Monday to Friday between 7:00 and 22:00. Night tarif applies for electricity consumed between 22:00 and 7:00 from Monday to Friday and the whole day during the week-ends (Infrax 2018). This is based on the tarif of the Distribution System Operator of the municipality of Diksmuide, Infrax. Power data on the monitoring website of the wind turbine (Ginlong Technologies 2018) allowed to compute the daily and night energy production of the wind turbine. Day production accounts for energy produced from 7:00 to 22:00 and night production for energy produced between 22:00 and 7:00 for every day (no distinction anymore between week and week end days). Therefore, there will be a small discrepancy between day and night consumption and production. The daily and night electricity consumption and wind production per month for the year 2017 are shown in figure 6.1.

The daily production considers the sum of the electricity produced by the wind turbine between 7:00 and 22:00 every day. The daily consumption is the sum of the electricity produced by the PV-panels, the wind turbine and the delta of electricity needed or in surplus indicated by the day meter (from Monday to Friday between 7:00 and 22:00). The night production represents the electricity produced by the wind turbine between 7:00 and 22:00 every day. The night consumption is the sum of the electricity produced by the wind turbine between 22:00 and 7:00 and of the value indicated by the night meter. This last value is a bit misleading since it takes into account the daily energy flows, including the PV-panels and wind turbine

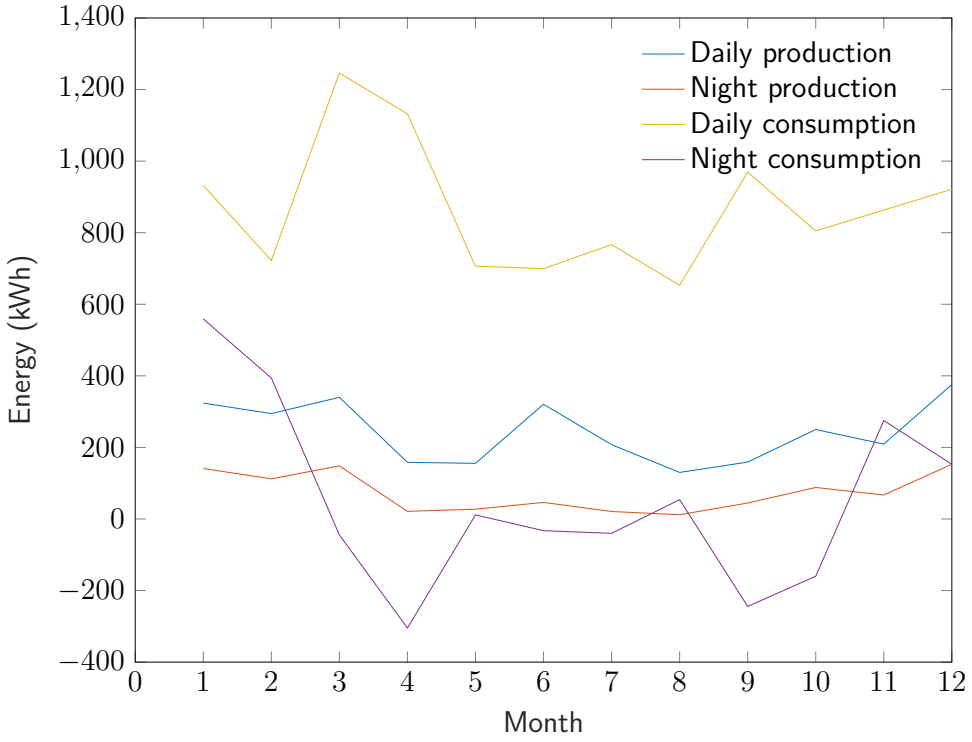

Figure 6.1: Daily and night electricity consumption of the farmer and production through the wind turbine per month for the year 2017.

production, during the week ends.

A first observation from figure 6.1 is that both day consumption and production are higher than respectively night consumption and production. In other words, consumption needs during the day are higher than the consumption needs during the night and wind is blowing faster during the day than during the night. Figure 6.1 shows on one hand that in average in 2017 the electricity consumed by the farmer during the day is much greater than the electricity daily produced by the wind turbine during the whole year. On the other hand, the graph also shows that night electricity production through wind is in average greater than the electricity consumed based on the night tariff. Three elements need to be highlighted before interpreting those 2 curves. First, the night consumption also takes into account the energy flows during the weekend (both production and consumption flows, see previous paragraph). The great amount of night consumption in January and November could be explained by a high consumption of electricity combined to a low renewable electricity production during the week ends of these 2 months (see the low total production in figure 3.5). On the contrary, the strong negative values of the night consumption in April and September could be explained by a rather low electricity consumption during the week ends combined to high rate of renewable energy production during the week ends (again, see the significant amount of total production in figure 3.5). Nevertheless, the night production and consumption curves seem to indicate that more electricity is produced through the wind turbine during the night than needed. Therefore, this electricity is not self-consumed by the farmer and has to be fed and sold to

the grid. This solution is less profitable since the price of electricity sold back to the network is close to 0.04 €/kWh where the price of electricity is 0.21-0.22 €/kWh (Mermuys 2010).

6.4.2 Daily comparison

Increasing in the granularity of the data, it was found interesting to know how the production of wind electricity matches (or mismatches) the electricity needs along the day. Precise consumption data of the farm were not available. Therefore, it was decided to use Synthetic Load Profiles (SLP) available on Synergrid (2018). SLP are typical load profiles which show the variation in the electrical load as a function of the time. The residential SLP was chosen as a reference for the consumption profile. The website provides an Excel file with the normalized load every quarter of hour. By knowing the annual energy consumption, the SLP in kW can be derived (Kremers 2012). Once the SLP in kW was available, the mean SLP per season as a function of the time of the day was computed based on the annual electricity consumption of the farm (11000 kWh, see 3.2) and compared to the mean power production of the wind turbine per season as a function of the time of the day and to its box plot. This comparison was done for data acquired during the whole year 2017 and are shown in figures 6.2, 6.3, 6.4, 6.5.

Different comments can be done for average values of consumption and production. First on the SLP. Whatever the season, 2 peaks of consumption can be identified. One in the morning around 10:00 or 11:00, where the load varies between 1.32 kW during summer up to 1.68 kW during winter. Another more important peak arises around 18:00 or 19:00 with loads between 1.45 kW and 2.11 kW for the same seasons. The lowest level of consumption happens at night around 03:00 or 04:00 and varies between 0.68 kW in spring and 0.74 kW in winter. On the production side, peaks of production happen in the afternoon between 13:00 (autumn) and 17:00 (spring) with values ranging from 0.56 kW (summer) up to 0.86 kW (winter). Off-peak production levels arise at night between 21:00 (winter) and 02:00 (summer) with a production varying from 0.09 kW (summer) up to 0.52 kW (winter).

The main observation is that wind production reaches its maximum level during the afternoon and the exact hour depends on the season. Same observation can be done for off-peak production levels during the night. On the contrary, peaks and off-peak consumption periods are much more precise in time through the year. Also, the maximum of electricity production through the wind happens during a local minimum in the consumption curve. Hence the importance of having right sized systems to not over produce electricity and be obliged to feed the electricity to the grid at a low price.

To have a feeling about the variability of the power data, the method of boxes indicating the median, the first and third quartiles as well as a maximum and minimum values (without being "outliers"). The outliers are values above or below 3 times the interquartile range from the third and first quartile. They were not plotted on the graph for clarity. For a normal distribution, the standard deviation is a an appropriate measure of variability (or spread) of the distribution. Indeed, if the distribution is known to be normal, knowing its mean and standard deviation are enough to characterize the normal distribution. But for skewed distributions, the standard deviation gives no information on the asymmetry. It is better to use the first and third quartiles, since these will give some sense of the asymmetry of the distribution. It should

be mentioned that the larger the boxes, the larger the variability of the data (University of Texas 2018).

In general, the third quartiles are lower than the load curve (except in winter at 02:00). But it is not rare that the maximum values of the power production are higher than the load demand. In winter, nearly all maximum values are higher than the average load curve. In spring, summer and autumn, the maximum values of power data are above the average load curve for the period of off-peak consumption in the afternoon. The greater size of the boxes also indicates a high degree of variability of the power data at this moment of the day. The small boxes at night in spring and summer (where even the maximum values without being outliers are 0) indicate that the wind turbine does not produce a significant amount of electricity during those periods. In spring and summer, boxes are greater from 07:00 until 20:00. In contrast, great boxes in winter and autumn are more evenly distributed through the day. But greater boxes are observed in the afternoon.

These graphs also highlight the importance of storage systems like batteries that could store the electricity produced during peak production periods to be able to use it later, during high load demand periods.

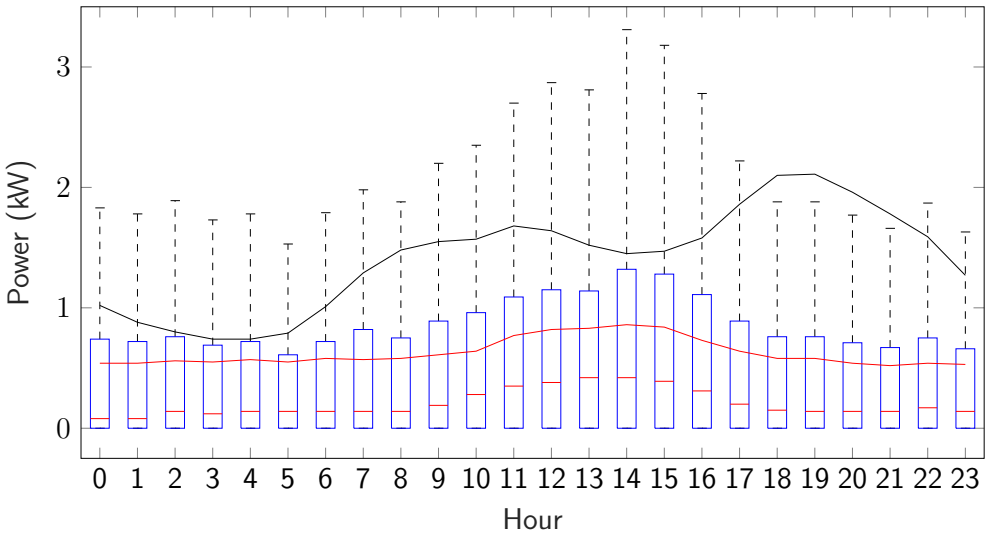

Figure 6.2: Winter 2017: Mean wind electricity production of the wind turbine Enair E70 in Diksmuide (red) and its box plot compared to the mean residential load (computed based on the SLP with an annual electricity consumption of 11000 kWh) (black) as a function of the time of the day.

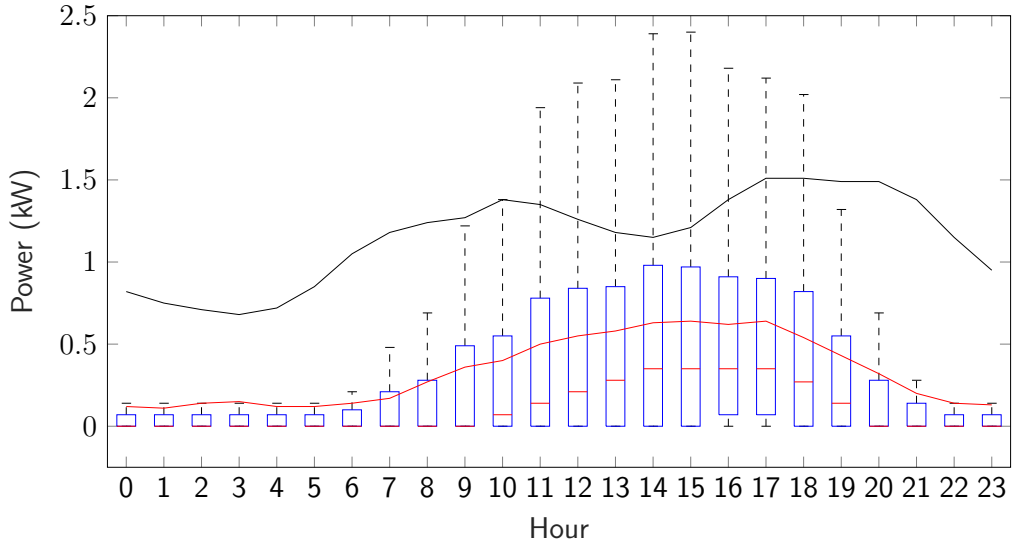

Figure 6.3: Spring 2017: Mean wind electricity production of the wind turbine Enair E70 in Diksmuide (red) and its box plot compared to the mean residential load (computed based on the SLP with an annual electricity consumption of 11000 kWh) (black) as a function of the time of the day.

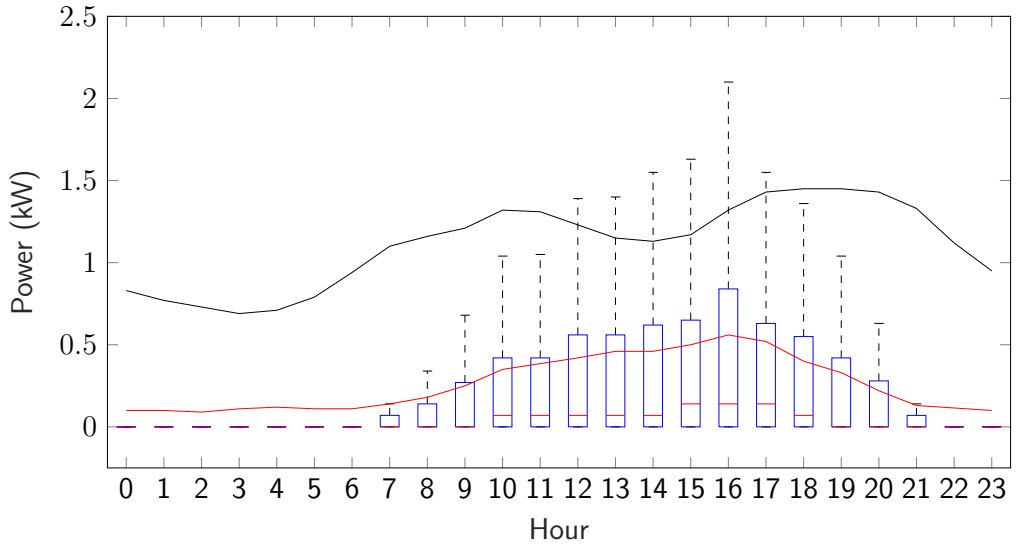

Figure 6.4: Summer 2017: Mean wind electricity production of the wind turbine Enair E70 in Diksmuide (red) and its box plot compared to the mean residential load (computed based on the SLP with an annual electricity consumption of 11000 kWh) (black) as a function of the time of the day.

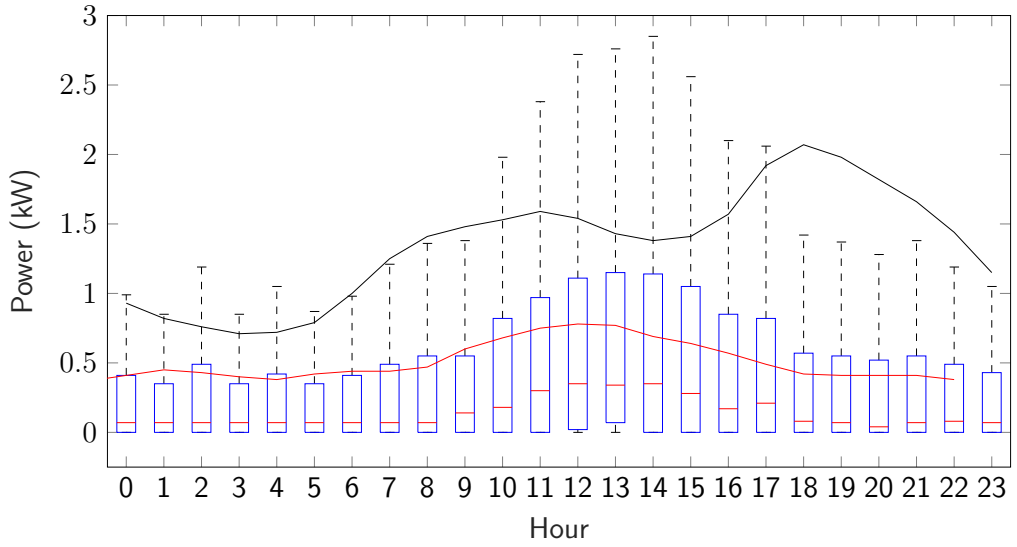

Figure 6.5: Autumn 2017: Mean wind electricity production of the wind turbine Enair E70 in Diksmuide (red) and its box plot compared to the mean residential load (computed based on the SLP with an annual electricity consumption of 11000 kWh) (black) as a function of the time of the day.

Chapter 7

Conclusion

The purpose of this renewable energy oriented Master's thesis was to assess and analyze in depth the wind potential in the municipality of Diksmuide, Belgium, the operation of a small wind turbine of 3.5 kW installed on a farm and finally the economic feasibility of such a project.

The context of the Master's thesis was developed as well as the necessary wind energy background. Fundamentals like power in the wind or coefficient of performance, wind shear, statistical analysis methods, variation of the wind speed with time and economic background were presented theoretically.

The measurement setup used for measuring wind and atmospheric data at 10 and 15 m high from March 2017 until March 2018 was presented.

The site on which the small wind turbine is installed was presented with aerial view, picture and diagrams of the installation. The monthly consumption and renewable production of energy of the farm for the year 2017 was presented. The annual energy consumption of the farmer (around 11000 kWh) is similar to the total annual electricity produced through the 6 kW PV-panels and the 3.5 kW small wind turbine. Peak of consumption arises during the winter. Peak of solar production happens during summer and peak of wind energy production happens during the winter. Because of a larger installation, the PV-panels are producing the largest share of electricity in average through the year. However, $1/3$ of the time, the wind electricity production was more important than the solar one. These results are much more nuanced when considering the normalized electricity production. In this case, the wind turbine produces proportionally more electricity than the PV-panels 50% of the year. The technical specifications of the small wind turbine were presented.

A specific analyze of the wind conditions data for the location of Diksmuide was conducted. The biased data, due to the slip of the mast during the measurement period, were extrapolated to 10 and 15 m using the extrapolated time series method. The dominant wind direction is West. The average wind speed is 3.92 m/s at 10 m and 4.25 m/s at 15 m for the measurement period. Weibull parameters, shape and scale factor, k and c, were computed using the moment method and the histogram and Weibull probability density function of the wind data at 15 m were drawn. Wind roses of the average wind speed and of the power density were plotted for heights of 15 m and 22.5 m. The roughness height, $z_0 = 0.42$ m, and the friction velocity, $V^* = 0.33$ m/s, were computed and the wind shear profile was plotted. The Power Spectral Density of the wind speed data was plotted and has showed that there is a clear variation

for the wind speed between night and day. The long term average wind speed in Diksmuide was determined using the Variance Ratio approach and 25-year data from the meteorological station of Westdorpe, Netherlands. The long term average wind speeds in Diksmuide at 10, 15 and 22.5 m are respectively 3.66, 4.13 and 4.60 m/s. These values show that the measurement period was a period of stronger wind conditions than what it used to be in Diksmuide.

After focusing on the wind conditions, the actual performance of the wind turbine was assessed. The actual power curve was computed following the method of the standard IEC (2005) and compared to the power curve provided by the manufacturer. Good agreement between both power curves was found for low and high wind speeds, with even an over performance of 6% for a wind speed of 3 m/s. For medium wind speeds, the power curve of the wind turbine is down to 32% lower than the one of the manufacturer. The AEP was computed using 2 different methods. First using directly the power data, the AEP for a mean wind speed of 4.25 m/s was computed to be 3897 kWh. The AEP was also computed following the recommendations of IEC (2005) for wind speeds comprised between 4-11 m/s. Compared to the first AEP estimation method, it overestimated the AEP of only 2.5%. The power coefficient of the wind turbine was computed and peaked at 41% for a wind speed of 5.5 m/s. Some explanations based on the electrical efficiency of the wind turbine, the level of turbulence and the uncertainty of the data were presented to understand the deviation between the actual performance and the manufacturer predicted one of the wind turbine.

The economic feasibility of the small wind project was investigated. A LCOE of 0.363 €/kWh, a NPV of 3027 €, a IRR of 6.0% and a dynamic payback period of 19 years showed that the project was profitable for the farmer. For SME and private users, the results are more nuanced. A sensitivity analysis was performed and has shown that the AEP, the investment costs, the GC and the increase of the electricity price were economic parameters having a strong impact on the profitability of such a project.

Finally, monthly and daily consumption needs and production of wind energy availabilities were compared to investigate if energy was produced through wind when there was a demand of electricity. The monthly results have shown that both energy consumption and production were higher during the day compared to the night. It was also highlighted that the night production exceeded the night consumption of electricity. But these were biased results since the night meter also recorded energy flows (net consumption) during week end days. The daily consumption and production curves were compared per season. The graphs highlighted that wind energy production reached a peak in the afternoon when the consumption needs reached a local minimum.

Further improvements

This Master's thesis contributed to have a better view and understanding about wind conditions in Flanders at a low height, typically at 15 m high. It also provided a real case independent assessment of the performance of a small wind project as well as the economic feasibility of the project. All of this gathered in one document. Even if an attempt to explain the low performance of the small wind turbine Enair E70 was presented, no real proposition for improving the performance of the wind turbine was provided. This could be done through for instance micro-siting and the use of Computational Fluid Dynamic to understand and quantify the behaviour of the complex flow patterns of the wind on the specific site. This could enable to suggest to place the wind turbine in a better location and in turn improving its performance.

Furthermore, this document could serve as a basis for a layout for generating automated wind resources and assessment reports for potential buyers of small wind turbines.

Another point highlighted in this Master's thesis was the matching between the consumption needs and the wind production availabilities. It was pointed out that night production could exceed night consumption and that peak of production happened during a local minimum of consumption. It could lead in turn to the need of feed the surplus of electricity to the network, which is not economically interesting. Furthermore, in this special case, PV-panels also produced more electricity than needed. The complete study of an hybrid renewable energy system including both renewable sources of energy, the PV-panels and the wind turbine, could be conducted. The introduction of storage systems like batteries could reveal economically interesting. Indeed, it could allow to benefit from periods of high production and low consumption at a time of high consumption needs and low production.

Appendix A

Small wind turbine ENAIR E70 PRO datasheet

E70 PRO
Wind Turbine

DATA SHEET

With an average wind speed of 11m/s the model Enair 70PRO is capable of generating more than 70kWh/day

TECHNICAL, ELECTRICAL AND OPERATIONAL FEATURES

Number of Blades	3
Blades material	Fibreglass with flex resins and polyurethane core
Generator	250rpm | neodymium magnets
Power	5500W
Rated power	4000W (Acording to IEC 61400-2)
Voltage	24 / 48 / 220V
Wind class	CLASS II -IEC 61400-2/NVN I - A
Diameter	4,3m
Turning sense	Clockwise
Swept area	14,5m²
Weight	165kg
Applications	Isolated connection batteries, electric grid connection
Wind to start	2m/s
Rated speed	11m/s
Speed regulation of pitch	12m/s
Survival speed	60 m/s
Efficient generation range	From 2 to 60 m/s
Type	Upwind horizontal rotor
Orientation	Rudder passive yaw system
Power control	Variable passive centrifugal pitch system with 2 actuation speeds
Transmission	Direct
Brake	Electric by short and aerodynamic by variable pitch
Controller	Grid connection and battery charging
Inverter	Efficiency 97%; MPPT algorithm
Noise	48db | Reduction to a minimum: due to the design of the blades and the low revolutions. 1% more than ambient wind noise
Anti corrosive protection	Airtight, hight-temperature bake-drying epoxy paint, generating a plastic coating
Tower	Lattice, clip, tubular. Variable height axles can be folded according to conditions

CLASS II Wind Turbine
IEC 61400-2/NVN I - A

POWER CURVE

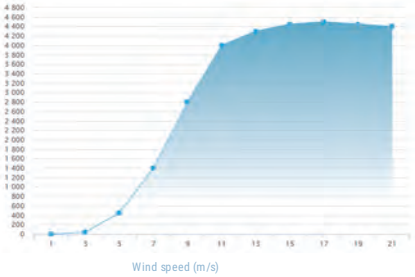

ANNUAL PRODUCTION

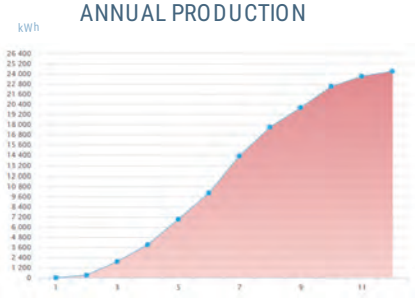

Avenida Ibi, 44 – P.O. 182 C.P. 03420 | Castalla (Alicante), Spain
+34 96 556 00 18 info@enair.es

www.enair.es

E70PRO Wind Turbine
TECHNICAL PROFILE

PASSIVE VARIABLE PITCH

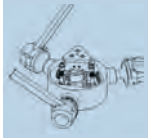

Patented technology to maximize energy production

It is a mechanical system due to what the blades angle of attack is modified to obtain the maximum energy in each case and never exceeds its rotor rpms

It achieves:

- Less noise
- More ability to absorb high winds
- More consistency in the generation
- More energy with less wind

ELECTRONIC CONTROL

System of intelligent energy management

Batteries connection:

7 types of programmable batteries (lithium, lead, gel, etc.)
Charging shunt resistor pulses if overload. The excess which can't be charged is derived to protect the batteries

Grid connection:

Through the MPPT inverters, which are programmed by the wind power curve which maximises energy production
Compatible with triphasic grids, monophasic and European and American systems

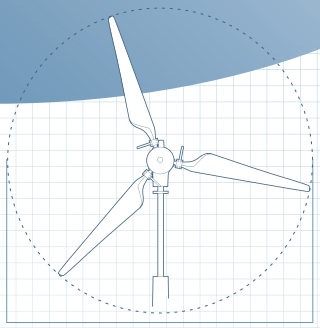

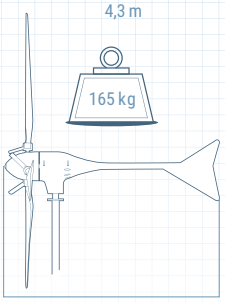

MORE EFFICIENCY

A PMG with more powerful magnets and a rotor fully integrated in the magnetic sheet, with improved airfoiles of the blades makes us with less wind to be more efficient

MORE STURDINESS

The whole design has been developed based on a centre of gravity positioned in the yaw axis for balance tension and improve the loads

MORE SECURITY

By incorporating new materials like carbon fiber and the integration of the resins with steel, the safety factors increase reaching Fs= 9

MORE ENERGY

Making all these improvements and applying the computational fluid dynamics we improve up to 15% at the energy production

Minimum noise
The noise is around 1% above ambient noise, being invaluable to our ears

Maximum efficiency
It works with a simple breeze of 2m/s and continues running at more than 40m/s

Anticorrosive
Epoxy painting, which becomes a covering anticorrosive and perfect for salt on islands and coasts

Hermetic
Hermetically sealed alltogether, to avoid microparticles, humidity air entering and prevents damage to coastal or desert areas which have a lot of sand

Sturdiness
To withstand strong winds and offer a long operating life all equipment parts are oversized

PREMIO A LA INNOVACIÓN EMPRESARIAL 2014

GARANTIA 5 AÑOS

CO2 FREE

IN CERTIFICATION PROCESS...

AWEA MCS Intertek

Avenida Ibi, 44 – P.O. 182 C.P. 03420 | Castalla (Alicante), Spain
+34 96 556 00 18 info@enair.es

www.enair.es

Appendix B

Measured power curve

Measured power curve					
Reference air density: 1.225 kg/m^3					
Bin no.	Hub height wind speed (m/s)	Actual power output (W)	C_p	No. of data sets (10 min. avg.)	Manufacturer power output (W)
4	2.1	11.7	0.16	4002	20.0
5	2.5	20.2	0.14	5339	30.0
6	3.0	42.6	0.18	5753	**40.0**
7	3.5	101.0	0.27	5121	142.5
8	4.0	195.4	0.34	4401	245.0
9	4.5	312.2	0.39	3725	347.5
10	5.0	442.0	0.40	3333	**450.0**
11	5.5	602.2	0.41	2724	687.5
12	6.0	761.7	0.40	2358	925.0
13	6.5	958.8	0.39	1955	1162.5
14	7.0	1164.6	0.38	1515	**1400.0**
15	7.5	1367.8	0.37	1276	1750.0
16	8.0	1658.2	0.36	1018	2100.0
17	8.5	1849.3	0.34	816	2450.0
18	9.0	2106.0	0.33	574	**2800.0**
19	9.5	2345.2	0.31	415	3100.0
20	10.0	2551.9	0.29	360	3400.0
21	10.5	2636.1	0.26	309	3700.0
22	11.0	2723.7	0.23	230	**4000.0**
23	11.5	2789.6	0.21	139	4075.0
24	12.0	3011.9	0.20	108	4150.0
25	12.5	3060.2	0.18	73	4225.0
26	13.0	3261.7	0.17	42	**4300.0**
27	13.5	3361.5	0.16	29	4337.5
28	14.0	3285.8	0.13	15	4375.0
29	14.5	3011.6	0.11	11	4412.5
30	15.0	3313.1	0.11	10	**4450**
31	15.5	3397.6	0.11	3	4462.5
32	16.0	3533.5	0.10	4	4475.0
33	16.5	3970.4	0.10	2	4487.5
34	17.0	4094.4	0.10	1	**4500.0**
35	17.5	**3817.7**	**0.08**	**0**	4487.5
36	18.0	3653.6	0.07	4	4475.0
37	18.5	3978.6	0.07	3	4462.5
38	19.0	3853.8	0.06	4	**4450.0**

Table B.1: Presentation of the actual power curve of the Enair E70 small wind turbine, coefficient of performance, number of data per bin as a function of the wind speed and comparison to the manufacturer power output. The values given by the manufacturer are in bold in the last row. The other values were linearly interpolated.

Appendix C

Mail exchange with the Vlaams Energieagentschap, April 2018

Pierre Tordeur original message - 17/04/2018 at 15:38:30:

"Geachte,

Ik ben een student in Master 2 aan de ULB in burgelijk ingenieur richting electro-mechanica en ik doe mijn master thesis op the installatie van kleine wind molent (15 m hoog, $<$10 kW) in Diksmuide, West Vlaanderen. Daarvoor moet ik een financiele analysis uitvoeren. Ik heb op de website "www.energiesparen.be" gesurft maar ik heb moeijlijkheden om alle informatie die ik nodig heb te vinden.

Ik zou graag informatie krijgen over de volgende items voor de plaatsing van kleine wind molen(s) zowel bij particulieren en voor KMO's in Vlaanderen:

- Wat zijn de fiscale voordelen voor eigenaars van zo een kleine wind molen zowel voor particulieren dan voor KMO's in Vlaanderen (Diksmuide)?
- Wat zijn de subsidies die beschikbaar zijn zowel voor particulieren dan voor KMO's in Vlaanderen (Diksmuide)?
- Zijn er andere financiële voordelen voor de plaatsing van kleine wind molen zowel voor particulieren dan voor KMO's in Vlaanderen (Diksmuide)?
- Bestaan er ook andere financiele/fiscale hulp of federaal niveau?

Met dank bij vorbaat en vriendelijke groeten,
Pierre Tordeur"

Answer from the Vlaams Energieagentschap - 23/04/2018 at 13:41:00:

"Geachte,

Als antwoord op uw bericht van 17-04-2018 gegeven wij graag het volgende mee:

Tot vorig jaar (2017) kwamen ook kleine windturbines in aanmerking voor groenestroomcertificaten. Hierover kan u informatie terugvinden in het Onrendabele Toppen rapport voor nieuwe projecten dat jaarlijks de benodigde steun berekent voor groene stroom en WKK technologieën.

Zie: http://www.energiesparen.be/monitoring-en-evaluatie

Sinds 1 januari 2018 komen windturbines op land met een bruto nominaal vermogen kleiner dan en tot en met 10 kW niet meer in aanmerking voor GSC.

Momenteel is er een investeringssteunprogramma in opmaak om een subsidie toe te kennen voor kleine en middelgrote windturbines. Aangezien het wetgevend kader nog in opmaak is voor deze nieuwe steunregeling kan ik hierover nog geen verdere informatie geven.

Er bestaat ook VLIF-investeringssteun voor land- en tuinbouwers. Een land- of tuinbouwer kan hier steun krijgen voor een windturbine indien aan een aantal voorwaarden voldaan is.

Voor meer informatie kan u terecht op: https://lv.vlaanderen.be/nl/subsidies/vlif-steun/vlif-investeringssteun-voor-land-en-tuinbouwers

In bepaalde omstandigheden kan een bedrijf ook aanspraak maken op de verhoogde investeringsaftrek voor energieproductie o.b.v. hernieuwbare energie: http://www.energiesparen.be/verhoogdeinvesteringsaftrek (Informatiedocument, categorie 11).

Met vriendelijke groeten,

Vlaams Energieagentschap"

Appendix D

On Field

At the beginning of the Master's thesis, I participated to the wiring and the coding of a data logger to get started with the subject. These data logger is aimed to record data in Brussels on a rooftop. The figures D.1 and D.2 shows the layout of a typical box with a data logger CR800, a Thies baro transmitter, a GSM/GPRS serial transmitter and a module for the connection of a battery. Figures D.3 and D.4 show the operations of dismantlement in Diksmuide and the re-mounting of the measurement mast in an other farm in Brugge. The code for programming a data logger is also shown.

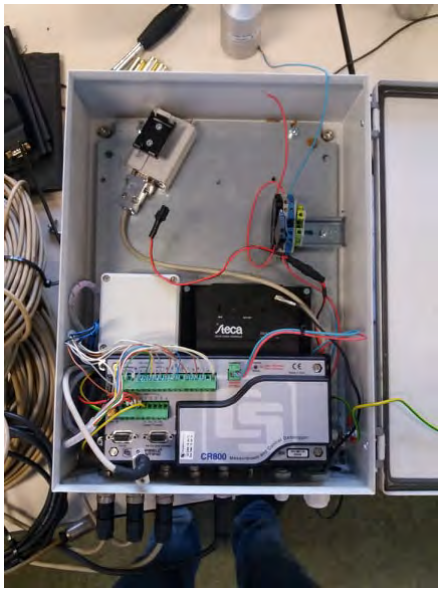

Figure D.1: Typical measurement box containing the GSM/GPRS data trasnmitter (up left), the baro transmitter (middle left) and the data logger Campbell Scientific CR800 (bottom). The wire connection in the bottom are connected to the wind vane, anemometers and temperature sensor.

On March 7th 2018, Tim De Troyer, Quentin Deltenre, Marta Castana and myself went on site in Diksmuide to dismantle the measurement mast and to mount it on another place in

Figure D.2: Box installed on the measurement mast in Diksmuide. The only difference compared to D.1 is the presence of the battery (up left).

Brugge. Here are some pictures of the operations.

(a) Picture of the installation in Diksmuide with the small wind turbine (left) and the measurement mast (right).

(b) Picture at the beginning of the dismantlement with Quentin Deltenre (in front) and the farmer, Johan Debruyne (in the back).

Figure D.3: Pictures taken during the dismantelment of the measurement mast in Diksmuide.

Figure D.4: Picture taken during the mounting of the measurement mast in Brugge.

```
' CR800 Series Datalogger
' Client      : BRUXELLES ENVIRONMENT
'   Supplier    : INENSUS GmbH
'   Programming   :   pierretordeur
' Date      :   2017.11.21

' Sensor connections:
' Signal        Colour external   Colour internal   Datalogger

' Socket 1: Anemometer 1 (5-pin M12)
' GND           brown             brown             GND (adjacent to P1)
' V+            white             white             +5V
' heating +       green             blue              not connected
' heating -       yellow              black             not connected
' frequency       gray              gray              P1

' Socket 2: Unused (5-pin M12)
' GND           brown             brown             GND (adjacent to P2)
' V+            white             white             +5V
' heating +       green             blue              not connected
' heating -       yellow              black             not connected
' frequency       gray              gray              P2

' Socket 3: Wind direction (5-pin M12)
' GND + GND       brown             brown             GND (adjacent to SE2)
' V+            white             white             12V
' heating +       green             blue              not connected
' heating -       yellow              black             not connected
' analog          gray              gray              SE2

' Socket 4: Reserved (5-pin M12)
' GND           -               brown             GND
' V+            -               white             12V
' analog          -               blue              Disconnected
' reference       -               black             Vx2
' frequency       -               gray              C4

' Socket 5: Temperature and humidity (8-pin M12)
' V+            #5                white             +5V
' GND           #6                brown             GND
' H+            #1                green             Disconnected
' GND           #2                yellow              Disconnected (
   adjacent to SE4)
' T1            #7                blue              GND (adcacent to Vx1)
' T1            #8                gray              DIFF3L
' T2            #9                pink              DIFF3H
' T2            #10               red               Vx1 with 100 ohm (0.1%)
    in series

' External PV to battery charger (3-pin M8)
' solar +         white             black
' solar -         brown             brown
'                 blue
```

```
52
53 ' Air pressure
54 ' GND           #3              brown           GND (adjacent to C1)
55 ' V+            #2              red             12V
56 ' Frequency         #4              gray            C1 (with 1k to C2)
57 ' SHUTDOWN          #1              purple            C2
58
59 ' GSM/GPRS modem supply
60 ' V+                           red             SW12
61 ' GND                          black           GND (adjecent to SW12)
62
63 ' Ultrasonic Anemometer (Cable)
64 ' V+                           red             SW12
65 ' GND                          black           GND (adjecent to SW12)
66 ' Vx                             Grey            SE1
67 ' Vy                             white           SE3
68 ' Vz                             Pink            SE4
69 ' ref                            Green/Yellow                GND (
   adjecent to SE4)
70
71
72 ' Declaration of public variables
73
74
75 Public t_internal         ' Temperature inside datalogger
76 Units t_internal = degC
77 Public v_supply           ' Datalogger supply voltage
78 Units v_supply = V
79 Public wind_s1            ' Windspeed anemometer 1 # 01125856
80 Units wind_s1 = m/s
81 'Public wind_s2           ' Windspeed anemometer 1 # 01125856
82 'Units wind_s2 = m/s
83 Public wind_sx            ' Windspeed anemometer 1 # 01125856
84 Units wind_sx = m/s
85 Public wind_sy            ' Windspeed anemometer 1 # 01125856
86 Units wind_sy = m/s
87 Public wind_sz            ' Windspeed anemometer 1 # 01125856
88 Units wind_sz = m/s
89 Public temperatureUltrasonic ' Temperqture ultrasonic anemometer
90 Units temperatureUltrasonic = degC
91 Public wind_d             ' wind direction
92 Units wind_d = deg
93 Public pressure           ' local air pressure
94 Units pressure = hPa
95 Public temperature        ' air temperature
96 Units temperature = degC
97 Public humidity             ' relative humidity
98 Units humidity = RH
99
100 Public RTclock(9)
101 Alias RTclock(1) = year
102 Alias RTclock(2) = month
103 Alias RTclock(3) = day_of_month
```

```
Alias RTclock(4) = hour
Alias RTclock(5) = minute
Alias RTclock(6) = seconds
Alias RTclock(7) = u_second
Alias RTclock(8) = day_of_week
Alias RTclock(9) = day_in_year


' Declaration of internal variables
Dim temp
Public temp_pressure

' Definition of data tables - 10 minute-interval
DataTable (table_seconds,1,50400)
  DataInterval (0,1,Sec,10)
  TableFile ("USB:table_seconds",8,-2,0,120,Min,0,0))


  ' Ultrasonic Anemometer
  Sample (1,wind_sx,FP2)
  Sample (1,wind_sy,FP2)
  Sample (1,wind_sz,FP2)
  Sample (1,wind_s1,FP2)
  Sample (1,temperatureUltrasonic,FP2)
  'Sample (1,wind_s2,FP2)
  Sample (1,wind_d,FP2)
  Sample (1,temperature,FP2)
  Sample (1,pressure,FP2)

EndTable

' Definition of data tables - 10 minute-interval
DataTable (table_10minutes,1,-1)
  DataInterval (0,10,Min,10)

  ' wind direction and anemometer 1
  WindVector (1,wind_s1,wind_d,FP2,False,0,0,0)
  Minimum (1,wind_s1,FP2,False,False)
  Maximum (1,wind_s1,FP2,False,False)
  StdDev (1,wind_s1,FP2,False)
  'WindVector (1,wind_s2,wind_d,FP2,False,0,0,0)
  'Minimum (1,wind_s2,FP2,False,False)
  'Maximum (1,wind_s2,FP2,False,False)
  'StdDev (1,wind_s2,FP2,False)

  ' Ultrasonic Anemometer x Direction
  Average (1,wind_sx,FP2,False)
  Minimum (1,wind_sx,FP2,False,False)
  Maximum (1,wind_sx,FP2,False,False)
  StdDev (1,wind_sx,FP2,False)
  ' Temperature ultrasonic anemometer
  Average (1,temperatureUltrasonic,FP2,False)
  Minimum (1,temperatureUltrasonic,FP2,False,False)
```

```
  Maximum (1,temperatureUltrasonic,FP2,False,False)
  StdDev (1,temperatureUltrasonic,FP2,False)


  ' temperature
  Average (1,temperature,FP2,False)
  Minimum (1,temperature,FP2,False,False)
  Maximum (1,temperature,FP2,False,False)
  StdDev (1,temperature,FP2,False)

  ' humidity
  Average (1,humidity,FP2,False)

  ' Pressure
  Average (1,pressure,FP2,False)
EndTable



' Definition of data tables - 1 hour
DataTable (table_hour,1,-1)
  DataInterval (0,1,Hr,10)

  ' air pressure
  Sample (1,pressure,FP2)
  Average (1,humidity,FP2,False)

  ' wind speed
  Average (1,wind_s1,FP2,False)
  'Average (1,wind_s2,FP2,False)
  Average (1,wind_sx,FP2,False)

  ' supply voltage and data logger internal temperature
  Average (1,t_internal,FP2,False)
  Minimum (1,v_supply,FP2,False,True)

EndTable


' Main program
BeginProg


  PulseCountReset

  Scan (1,Sec,0,0)    ' 1 second program interval

    ' internal measurements
    PanelTemp (t_internal,250)
    Battery (v_supply)
    RealTime (RTclock())

    ' measure wind speed
```

```
210     PulseCount (wind_s1,1,1,0,1,0.0456,0.2725)
211     If wind_s1 = 0.2725 Then wind_s1 = 0      ' suppress offset
212     ' measure wind speed
213     'PulseCount (wind_s2,1,2,0,1,0.0456,0.2725)
214     'If wind_s2 = 0.2725 Then wind_s2 = 0     ' suppress offset
215
216
217     ' measure wind direction
218     VoltSe (wind_d,1,mV5000,3,1,0,_50Hz,360/5000,0)
219
220     ' suppress possible over range
221     If wind_d >=360 Then wind_d = 0
222     If wind_d < 0 Then wind_d = 0
223
224     ' measure wind speed ultrasonic
225     VoltSe (wind_sx,1,mV5000,9,False,0,250,50/2500,-50.85)
226     VoltSe (wind_sy,1,mV5000,10,False,0,250,1/50,-50.85)
227     VoltSe (wind_sz,1,mV5000,11,False,0,250,1/50,-50.85)
228
229
230     ' measure ultrasonic temperature
231     VoltSe (temperatureUltrasonic,1,mv5000,12,False,0,250,1/50,-50)
232
233     ' relative humidity
234     VoltSe (humidity,1,mV2500,4,1,0,_50Hz,0.1,0)
235
236     ' temperature
237     ExciteV (Vx1,430,0)
238     VoltDiff (temp,1,mV250,3,True ,0,_50Hz,1.0,0)
239     ' 100R + 3R in series and 430mV exitation
240     temperature = 0.01745299*temp*temp - 5.17199243*temp + 307.43171387
241
242     ' air pressure
243     ' VoltSe (pressure,1,mV5000,1,1,0,_50Hz,260/5000,800)
244     ' Note that this is a continuous measurement; it should be modified
        into switchable power
245     ' air pressure
246     If (v_supply) > 11.5 Then
247     ''  If ( (minute = 1) OR (minute = 2) ) Then
248         PortSet (1,1)    ' switch on sensor (and sensor heater)
249         'PulseCount (pressure,1,2,1,1,1.0,0)
250       ''EndIf
251 '     If (minute = 2 ) AND (seconds = 50)
252         VoltSe (pressure,1,mV5000,1,1,0,_50Hz,260/5000,800)
253 '     EndIf
254     Else
255       PortSet (1,0)    ' switch off sensor (and sensor heater)
256       pressure = NaN
257     EndIf
258
259     ' switch modem (activated only on Thursday and Friday from 13:00 ...
        14:59)
260     If (v_supply) > 11.5 Then
```

```
'       If ( (day_of_week = 5) OR (day_of_week = 6) ) AND ( (Hour = 16) OR (
    Hour = 17) ) Then
'         SW12 (1)
'       Else
          SW12 (1)
'       EndIf
     Else
       SW12 (0)
     EndIf

     ' call data tables for processing of measurements
     CallTable table_seconds
     CallTable table_10minutes
     CallTable table_hour
  NextScan
EndProg
```

Bibliography

Agentschap Innoveren and Ondernemen (2018), '*Vlaamse groenestroomcertificaten (GSC)*', https://www.vlaio.be/nl/subsidies-financiering/subsidiedatabank/vlaamse-groenestroomcertificaten-gsc.

AWEA (2009), '*9.1-2009: Small wind turbine performance and safety standard*', 9.1.

Ayodele, T., Jimoh, A., Munda, J., Agee, J. & M'boungui, G. (2013), '*Economic analysis of a small scale wind turbine for power generation in Johannesburg*', IEEE 2013 pp. 1728-1732.

Berg, D. E. (2007), '*Handbook of energy efficiency and renewable energy - Chapter 22: Wind energy conversion*', CRC Press.

Blackledge, J., Coyle, E., Kearney, D. & Murphy, E. (2013), '*Inverter performance for small wind turbines when connected in paralled with the low-voltage distribution system*', i-manager's Journal on Embedded Systems, Vol. 1, No.4 pp.9-16.

Burton, T., Sharpe, D., Jenkins, N. & Bossanyi, E. (2001), '*Wind energy handbook*', John Wiley & Sons.

Campoccia, A., Dusonchet, L., Telaretti, E. & Zizzo, G. (2009), '*Comparative analysis of different supporting measures for the production of electrical energy by solar PV and wind systems: four representative European cases*', Solar Energy 83, pp. 287-297.

Carrillo, C., Cidras, J., Diaz-Dorado, E. & Obando-Montano, A. F. (2014), '*An approach to determine the Weibull parameters for wind energy analysis: the case of Galicia (Spain)*', Energies 7, pp. 2676-2700.

Chedid, R. & Saliba, Y. (1996), '*Optimization and control of autonomous renewable energy systems*', International Journal of Energy Research, Vol. 20, 609-624.

de Vries, E. (2008), '*Small wind turbines: driving performance*', https://www.renewableenergyworld.com/articles/print/volume-11/issue-3/wind-power/small-wind-turbines-driving-performance-52701.html.

Enair (2017*a*), '*E70 Pro Wind Turbine - User manual*'.

Enair (2017*b*), '*Small Wind Turbine Enair 70PRO*', https://www.enair.es/en/small-wind-turbines/e70pro.

Forsyth, T., Tu, P. & Gilbert, J. (1999), '*Optimization and control of autonomous renewable energy systems*', AWEA WindPower '99 Conference Burlington, Vermont.

Ginlong Technologies (2018), ' ', http://www.ginlongmonitoring.com/l.

Grieser, B., Sunak, Y. & Madlener, R. (2015), '*Economics of small wind turbines in urban settings: an empirical investigation for Germany*', Renewable Energy 78 pp. 334-350.

IEC (2005), *61400-12-1:2005: Wind turbines - Part 12-1: Power performance measurements of electricity producing wind turbines*, International standard, IEC 61400-12-1.

IEC (2013), *61400-2:2013: Design requirements for small wind turbines*, International standard, IEC 61400-2.

Infrax (2018), '*Uren van het dag-en nachttarief*', https://www.infrax.be/nl/Aansluitingen/tarieven/uren-dag-nachttarief.

IRENA (2012), '*Renewable energy technologies: costs analysis series - Wind Power*', International Renewable Energy Agency working paper, Vol.1: Power sector - Issue 5/5.

IRM (2018), '*Bilan climatique mensuel: décembre 2017*', https://www.meteo.be/meteo/view/fr/35424281-Decembre+2017.html.

Karczewski, M., Baszczynski, P., Wiklak, P., Sobczak, K. & Jozwik, K. (2017), '*Economic analysis of small wind turbines*', Journal of Machine Engineering, Vol. 17, No. 3.

Kremers, E. (2012), '*Modelling and simulation of electrical energy systems through a complex systems approach using agent-based models*', KIT Scientific Publishing.

Kumar, V., Panday, A. & Sinha, S. (2016), '*Grid integration and power quality issues of wind and solar energy system: a review*', International Conference on Emerging Trends in Electrical, Electronics and Sustainable Energy Systems.

Lubitz, W. (2014), '*Impact of ambiant turbulence on performance of a small wind turbine*', Renewable Energy 61 pp. 69-73.

Manwell, F., McGowan, J. & Rogers, A. (2009), '*Wind Energy Explained*', John Wiley & Sons.

Mathieu, B. (2018), '*Place à la consolidation fiscale*', https://www.lecho.be/economie-politique/belgique-federal/Place-a-la-consolidation-fiscale/10000699.

Mees, K. (2017), '*Le fisc publie les montants indexés en matière d'impôts sur les revenus de l'exercice d'imposition 2018*', Wolters Kluwer.

Meinke-Hubeny, F., de Oliveira, L. P. & Duerinck, J. (2017), '*Energy transition in Belgium - Choices and costs*', EnergyVille.

Mermuys, K. (2010), '*Windenergie in land- en tuinbouw*', Tech. rep. Privinciall onderzoeks- en voorlichtingscentrum voor land- en tuinbouw.

Met Office & Entec (2008), '*Small-scale wind energy: Policy insights and practical guidance*', The carbon trust.

Mur-Amada, J. & Bayord-Rujula, A. (2010), '*Variability of wind and wind power*', Zaragoza University.

Pedersen, T. (2004), '*On wind turbine power performance measurements at inclined airflow*', Wind Energy, No.7 pp. 163-176.

Ray, M., Rogers, A. & McGowan, J. (2006), '*Analysis of wind shear models and trends in different terrains*', AWEA conference proceedings.

REN21 (2018), '*Renewables 2017 Global status report - Chapter 1 Global overview*', http://www.ren21.net/gsr-2017/chapters/chapter_01/chapter_01/.

Renewable Energy Research Laboratory (2002), '*Wind power performance, economics and integration*', Tech. rep. University of Massachusetts.

Rogers, A., Rogers, J. & Manwell, J. (2005), '*Comparison of the performance of four Measure-Correlate-Predict algorithms*', Journal of Wind Engineering and Industrial Aerodynamics 93, pp.243-264.

Runacres, M. (2014), '*Wind Energy*', Vrije Universiteit Brussels Lecture.

Runacres, M., Vermeir, J. & De Troyer, T. (2014), '*Eindrapport BIM E11-359: Identificatie sites, opzetten windmetingscampagnes en uitvoering van haalbaarheidsstudies in het Brussels Hoffdstedelijk Gewest*', Leefmilieu Brussel.

SEPEN (2009), '*Eolienne windspire connectée réseau*', Tech. rep. No. 16.2.

SEPEN (2010*a*), '*Eolienne AirDolphin Z-1000-250*', Tech. rep. No. 18.5.

SEPEN (2010*b*), '*Eolienne Skystream connectée réseau*', Tech. rep. No. 15.4.

SEPEN (2010*c*), '*Eolienne Sonkyo Energy Windspot 3.5 kW*', Tech. rep. No. 19.2.

SEPEN (2011*a*), '*Eolienne Arrow Solar Energy - Black 600*', Tech. rep. No. 23.2.

SEPEN (2011*b*), '*Eolienne Southwest Windpower - Air Breeze 24 V*', Tech. rep. No. 24.1.

SEPEN (2011*c*), '*Eolienne Windela - Windela 600*', Tech. rep. No. 22.2.

SEPEN (2012), '*Eolienne Sonkyo - Windspot 7.5 kW version beta*', Tech. rep. No. 28.5.

SEPEN (2013*a*), '*Eolienne - Eole System - ES 10 - 10.0 kW*', Tech. rep. No. 29.6.

SEPEN (2013*b*), '*Eolienne auto construite Piggott - 1.7 kW*', Tech. rep. No. 32.6.

SEPEN (2013*c*), '*Eolienne Eolys - Métronome - 12.0 kW*', Tech. rep. No. 30.5.

SEPEN (2013*d*), '*Eolienne Fairwind - F64.10 - 10.0 kW*', Tech. rep. No. 31.4.

SEPEN (2014*a*), '*Eolienne - Eole System H3 - 3 kW*', Tech. rep. No. 38.1.

SEPEN (2014*b*), '*Eolienne Anelion SW 3.5-GT - 3.5 kW*', Tech. rep. No. 37.4.

Short, W., Packey, D. J. & Holt, T. (1995), '*A manual for the economic evaluation of the energy efficiency and renewable energy technologies*', National Renewable Energy Laboratory.

Simic, Z., Havelka, J. G. & Bozicevic, V. M. (2012), '*Small wind turbines - A unique segment of the wind power market*', Renewable Energy 50, pp. 1027-1036.

Synergrid (2018), '*Synthetic Load Profiles (SLP)*', http://www.synergrid.be/index.cfm?PageID=16896.

Takle, E. & Brown, J. (1977), '*Note on the use of Weibull statistics to characterize wind-speed data*', Iowa Agriculture and Home Economics Experiment Station 8941, pp. 556-559.

Taylor, M. & al. (2004), '*An analysis of wind resource uncertainty in energy production estimates*', Proceedings of the European Wind Energy Association Conference.

The European Wind Energy Association (2018), '*The cost of energy generated by wind power*', https://www.wind-energy-the-facts.org/the-cost-of-energy-generated-by-wind-power.html.

University of Texas (2018), '*Summary statistics for skewed distributions*', https://www.ma.utexas.edu/users/mks/statmistakes/skeweddistributions.html#Example.

Van Mechelen, D. & Crevits, H. (2009), '*Beoordelingskader voor de inplanting van kleine en middelgrote windturbines*', Omzendbrief LNE/2009/01 - RO/2009/01. Vlaamse Regering.

Vermeir, J. (2015), '*Feasibility and performance assessment of small and medium-sized windturbines*', VUB Press.

Vlaams Energieagentschap (2016), '*Rapport 2016 - Deel 2: Actualisaties OT/Bf* ', https://www.energiesparen.be/sites/default/files/atoms/files/20160630-Rapport2016-Deel2-Actualisaties.pdf.

Vlaams Energieagentschap (2018*a*), '*Groene energie and WKK: Steunperiode*', https://www.energiesparen.be/steunperiode.

Vlaams Energieagentschap (2018*b*), '*Infografiek groene energie in Vlaanderen 2016*', https://www.energiesparen.be/sites/default/files/atoms/files/Infografiek_groene_energie_2016.pdf.

Vlaamse Energieagentschap (2018), '*Verhoogde investeringsaftre voor energiebesparende investeringen*', https://www.energiesparen.be/verhoogdeinvesteringsaftrek.

Vlaamse overheid Departement landbouw & visserij (2018), '*VLIF-steun*', https://lv.vlaanderen.be/nl/subsidies/vlif-steun/vlif-investeringssteun-voor-land-en-tuinbouwers.

VREG (2016), '*Evolutie van de totale elektriciteitsprijzen (incl. btw) voor huishoudelijke afnemers*', http://www.vreg.be/sites/default/files/statistieken/evolutie_prijzen_hh_juli_2016.pdf.

VREG (2017), '*Marktmonitor 2017*', http://www.vreg.be/sites/default/files/document/rapp-2017-14.pdf.

Wan, Y. (2012), '*Long-term wind power variability*', National Renewable Energy Laboratory.